2015

A Molecular-Level View of the Physical Stability of Amorphous Solid Dispersions

Xiaoda Yuan
University of Kentucky, xyuan3@gmail.com

STUDENT AGREEMENT:

I represent that my thesis or dissertation and abstract are my original work. Proper attribution has been given to all outside sources. I understand that I am solely responsible for obtaining any needed copyright permissions. I have obtained needed written permission statement(s) from the owner(s) of each third-party copyrighted matter to be included in my work, allowing electronic distribution (if such use is not permitted by the fair use doctrine) which will be submitted to UKnowledge as Additional File.

I hereby grant to The University of Kentucky and its agents the irrevocable, non-exclusive, and royalty-free license to archive and make accessible my work in whole or in part in all forms of media, now or hereafter known. I agree that the document mentioned above may be made available immediately for worldwide access unless an embargo applies.

I retain all other ownership rights to the copyright of my work. I also retain the right to use in future works (such as articles or books) all or part of my work. I understand that I am free to register the copyright to my work.

REVIEW, APPROVAL AND ACCEPTANCE

The document mentioned above has been reviewed and accepted by the student's advisor, on behalf of the advisory committee, and by the Director of Graduate Studies (DGS), on behalf of the program; we verify that this is the final, approved version of the student's thesis including all changes required by the advisory committee. The undersigned agree to abide by the statements above.

Xiaoda Yuan, Student

Dr. Eric J. Munson, Major Professor

Dr. Jim R. Pauly, Director of Graduate Studies

A MOLECULAR-LEVEL VIEW OF THE PHYSICAL STABILITY OF AMORPHOUS SOLID DISPERSIONS

DISSERTATION

A dissertation submitted in partial fulfillment of the
requirements for the degree of Doctor of Philosophy in the
College of Pharmacy
at the University of Kentucky

By
Xiaoda Yuan
Lexington, Kentucky

Director: Dr. Eric J. Munson, Professor of Pharmaceutical Sciences
University of Kentucky, Lexington, Kentucky

2015

ABSTRACT OF DISSERTATION

A MOLECULAR-LEVEL VIEW OF THE PHYSICAL STABILITY OF AMORPHOUS SOLID DISPERSIONS

Many pharmaceutical compounds being developed in recent years are poorly soluble in water. This has led to insufficient oral bioavailability of many compounds *in vitro*. The amorphous formulation is one of the promising techniques to increase the oral bioavailability of these poorly water-soluble compounds. However, an amorphous drug substance is inherently unstable because it is a high energy form. In order to increase the physical stability, the amorphous drug is often formulated with a suitable polymer to form an amorphous solid dispersion. Previous research has suggested that the formation of an intimately mixed drug-polymer mixture contributes to the stabilization of the amorphous drug compound. The goal of this research is to better understand the role of miscibility, molecular interactions and mobility on the physical stability of amorphous solid dispersions. Methods were developed to detect different degrees of miscibility on nanometer scale and to quantify the extent of hydrogen-bonding interactions between the drug and the polymer. Miscibility, hydrogen-bonding interactions and molecular mobility were correlated with physical stability during a six-month period using three model systems. Overall, this research provides molecular-level insights into many factors that govern the physical stability of amorphous solid dispersions which can lead to a more effective design of stable amorphous formulations.

KEYWORDS: amorphous; solid dispersion; miscibility; hydrogen bond; mobility; solid-state NMR

Xiaoda Yuan
Student's Signature

Sep 14, 2015
Date

A MOLECULAR-LEVEL VIEW OF THE PHYSICAL STABILITY OF AMORPHOUS SOLID DISPERSIONS

By
Xiaoda Yuan

Eric J. Munson, Ph.D.
Director of Dissertation

Jim R. Pauly, Ph.D.
Director of Graduate Studies

Sep 14, 2015
Date

To my parents

Acknowledgements

First and foremost, I would like to express my gratitude to my advisor, Dr. Eric Munson, for his guidance and support for the past five years at the University of Kentucky. I feel very fortunate to have him as my mentor. Despite having amassed a vast amount of knowledge, he is still willing to listen to new ideas. He has given me the freedom to explore my scientific interest and has always wanted the best for his student. For his genuine care and support, I cannot thank him enough.

I would like to thank Dr. Brad Anderson, Dr. Dan Pack and Dr. Anne-Frances Miller for taking time out of their busy schedule to serve on my dissertation committee. I am especially grateful to Dr. Anderson for his insights and suggestions for my work involving hydrogen bonding. I must also thank him for reading and correcting my dissertation in its entirety and providing excellent feedback. This dissertation would not be the same without his input. I want to acknowledge Dr. Miller for her participation in my committee from the very beginning and giving advice from a different perspective. I would also like to thank Dr. Paul Bummer who recently passed for his help and support throughout my time at University of Kentucky. His kindness will always be remembered. In addition, I am indebted to Dr. Shelly Schmidt, my Master's thesis advisor, for her trainings years ago. Many of her teachings have proved to be relevant till this day.

I would also like to thank all past and present members of the Munson group: Dr. Diana Sperger, Dr. Matt Nethercott, Dr. Elodie Dempah, Dr. Sarah Pyszczynski, Dr. Sean Delaney, Ashley Lay and Kanika Sarpal. I would like to thank Diana for training me on

the solid-state NMR instrument when I first joined the lab. Many thanks to Matt for serving as a tremendous source of help in the lab and providing the friendship over the years. Our fun-filled trip from San Antonio to Atlanta was a travel highlight, made complete by multi-day baggage delays and clothes shopping in the middle of the night. Thank you Sean for the help and friendship in my last year of graduate school. You made the time go by fast and the dissertation writing process less daunting. In addition, I would like to thank our summer undergrad Jonathan Gerszberg for the help in developing a MATLAB code that I used in analyzing the stability data. Besides the members of the Munson lab, fellow graduate students Dr. Xiaojian Li and Nico Setiawan in Dr. Bummer's lab have been wonderful colleagues and friends over the past few years. Thank you Xiaojian for being my "lunch buddy" and sharing my joys and frustrations as a graduate student. Thank you Nico for teaching me how to use the μDiss apparatus and your willingness to help whenever needed.

Many thanks to Catina Rossoll and Tonya Vance for their assistance that made my life as a graduate student easier. Catina has been extremely helpful in making sure that everything is on track and every piece of document is turned in on time. Tonya has provided excellent assistance to make travel plans and place lab orders. The conversations we shared from Frida Kahlo to women's soccer served as nice breaks from the experiments and writing.

My wonderful friends at the University of Kentucky have made my time here more enjoyable. In addition to the previously mentioned Munson and Bummer lab members, I would like to thank the following people for their friendship: Dr. Wenlong Cai, Dr. Ling Zou, Dr. Liu Xue, Dr. Xiaodong Liu, Zheng Cui, Dr. Ying Wu, Zhengyi

Zhao, Hui Li, Shaoying Wang, Dr. Halide Tuna, Dr. Alessandra Mattei, Dr. Christin Hollis, Dr. Lisha Wu, Dr. Bei Zhang and Jingyi Zhang.

Above all, I must thank my parents for their love and support throughout my life. Dad, thank you for instilling in me a sense of curiosity. Mom, thank you for teaching me how to become a strong and independent woman. Grandma, thank you for being my biggest fan. We might be living half a globe away, you all always remain closest to my heart.

Table of Contents

Acknowledgements iii

Table of Contents vi

List of Tables xii

List of Figures xiv

Chapter 1. Introduction 1

1.1 Pharmaceutical Solids 1

1.2 Crystalline vs. Amorphous Solids 2

1.2.1 The Crystalline State 2

1.2.2 Polymorphism 2

1.2.3 The Amorphous State 5

1.3 Crystallization from the Amorphous State 8

1.3.1 Nucleation Theory 8

1.3.2 Crystal Growth Theory 15

1.3.3 Factors Influencing the Tendency to Crystallize 18

1.4 Amorphous Solid Dispersions to Increase Physical Stability 19

1.4.1 Glass Transition Temperature and Mobility 19

1.4.2 Miscibility of Drug and Polymer 20

1.4.3 Specific Interactions 20

1.4.4 Effect of Water 21

1.5 Overview of Research 22

Chapter 2. Solid-State NMR Spectroscopy of Pharmaceuticals 24

2.1 Introduction 24

2.2 Basics of NMR Spectroscopy 24

2.3 Solid-state NMR Spectroscopy 26

2.3.1 Chemical Shift Anisotropy and Magic Angle Spinning 26

2.3.2 Dipolar Coupling and High-power Proton Decoupling 27

2.3.3 Low Sensitivity and Cross Polarization 28

2.4 Solid-state NMR Techniques for Amorphous Solid Dispersions 29

2.4.1 Miscibility and ^{1}H Relaxation Times 29

2.4.2 Molecular Mobility and Dynamics 32

Chapter 3. Miscibility of Amorphous Solid Dispersions 45

3.1 Introduction 45

3.2 Materials and Matheods 48

3.2.1 Materials 48

3.2.2 Preparation of Amorphous Nifedipine 48

3.2.3 Preparation of Physical Mixture 49

3.2.4 Preparation of Amorphous Solid Dispersions 49

3.2.5 Modulated DSC 51

3.2.6 Solid-State NMR ^{1}H T_1 and $T_{1\rho}$ Relaxation Measurements 51

3.3 Results 53

3.3.1 Modulated DSC 53

3.3.2 Solid-State ^{13}C NMR of Nifedipine 57

3.3.3 Miscibility by SSNMR of Samples Prepared by Melt quenching in the Lab Setting 59

3.3.4 Miscibility by SSNMR of Samples Prepared by Other Methods . 65

3.4 Discussion 66

3.4.1 Miscibility of Nifedipine and PVP 66

3.4.2 Effect of Preparation Methods on Miscibility 69

3.5 Conclusions 70

Chapter 4. Hydrogen Bonding Interactions of Amorphous Indomethacin and its Amorphous Solid Dispersions 71

4.1 Introduction 71

4.2 Materials and Methods 73

4.2.1 Materials 73

4.2.2 Preparation of Amorphous Indomethacin 75

4.2.3 Preparation of Amorphous Solid Dispersions 75

4.2.4 Solid-State NMR Experiments 76

4.3 Results and Discussion 78

4.3.1 ^{13}C Solid-State NMR of Indomethacin 78

4.3.2 Hydrogen Bonding Interactions of Amorphous Indomethacin 82

4.3.3 Hydrogen Bonding Interactions in Indomethacin Amorphous Solid Dispersions with PVP and PVP/VA 94

4.3.4 Investigating Hydrogen Bonds in Amorphous Indomethacin 101

4.3.5 Investigating the Carboxylic Acid-Amide Hydrogen Bond 104

4.3.6 Thermodynamics of Amorphous Indomethacin Dimerization in a Dilute System 105

4.3.7 Hydrogen Bonding Effects on Miscibility and Physical Stability of Amorphous Solid Dispersions 109

4.3.8 Comparison of Experimental Data with MD Simulation Results in the Literature 111

4.4 Conclusions 112

Chapter 5. Molecular Mobility of Amorphous Solid Dispersions near the Glass Transition Temperature 114

5.1 Introduction 114

5.2 Materials and Methods 117

5.2.1 Materials 117

5.2.2 Preparation of Amorphous Solid Dispersions 118

5.2.3 Modulated DSC 119

5.2.4 Solid-State NMR Experiments 119

5.3 Results and Discussion 121

5.3.1 Molecular Mobility of Amorphous Indomethacin 121

5.3.2 Molecular Mobility of Amorphous Indomethacin in Amorphous Solid Dispersions with PVP 124

5.3.3 Molecular Mobility of Amorphous Indomethacin in a Dilute System 129

Chapter 6. Impact of Miscibility, Hydrogen Bonding, and Mobility on Physical Stability of Amorphous Solid Dispersions 137

6.1 Introduction 137

6.2 Materials and Methods 139

6.2.1 Materials 139

6.2.2 Synthesis of Indomethacin Methyl Ester 141

6.2.3 Preparation of Amorphous Solid Dispersions 141

6.2.4 Stability Studies 142

6.2.5 Powder X-ray Diffraction 143

6.2.6 Microscopic and Spectroscopic Characterization 143

6.2.7 Thermal Characterization 144

6.2.8 Solid-State NMR Spectroscopy 145

6.2.9 Dissolution Studies 147

6.3 Results 148

6.3.1 Characterization of Indomethacin Methyl Ester 148

6.3.2 Analysis of Stability Samples by Various Techniques 154

6.3.3 Analysis of Stability Samples by Solid-State NMR Spectroscopy 188

6.3.4 Dissolution Studies..... 213

6.3.5 Implications of Miscibility, Hydrogen Bonding and Mobility on Physical Stability 216

6.4 Conclusions..... 218

Chapter 7. Conclusions and Future Directions 220

Appendix A. Investigate the Effects of Water on Hydrogen Bonding Interactions of Indomethacin-Poly(Vinylpyrrolidone) Amorphous Solid Dispersions 225

A.1 Introduction..... 225

A.2 Materials and Methods..... 226

A.2.1 Materials..... 226

A.2.2 Preparation of Amorphous Samples with Different Water Contents 226

A.2.3 Solid-State NMR Experiments..... 227

A.3 Results and Discussion..... 228

A.4 Conclusions..... 235

References..... 236

Vita..... 254

List of Tables

Table 3.1. ^{1}H T_1 and $T_{1\rho}$ relaxation times of different forms of NIF, PVP and the 50:50 NIF:PVP physical mixture (PM). 64

Table 3.2. Comparison of the measured ^{1}H T_1 and $T_{1\rho}$ values for NIF:PVP amorphous solid dispersions made by melt quenching in the lab setting. 64

Table 3.3. Comparison of the measured ^{1}H T_1 and $T_{1\rho}$ values for 90:10 NIF:PVP amorphous solid dispersions made by melt quenching in the lab setting (MQ), spray drying (SD) and melt quenching in the NMR rotor while spinning (MIR). 66

Table 3.4. Chemical shift of the carbonyl carbon of PVP in various NIF:PVP amorphous solid dispersions of different compositions. 68

Table 4.1. The fitting parameters for the deconvolution of ^{13}C SSNMR spectrum of amorphous indomethacin. 93

Table 4.2. The fitting parameters of CPMAS ^{13}C spectra of IMC carboxylic acid carbon in IMC-PVP and IMC-PVP/VA amorphous solid dispersions. 97

Table 4.3. Principal components of the CSA tensors of the amorphous IMC carboxylic acid carbon that participates in various hydrogen bonding states. 103

Table 4.4. Principal components of the CSA tensor of the IMC carboxylic acid carbon in a 1% IMC amorphous solid dispersion with polystyrene. 103

Table 4.5. Principal components of the chemical shift tensor of the IMC carboxyl carbon that participates in the carboxyl-amide hydrogen bond. 110

Table 5.1. ^{1}H $T_{1\rho}$ relaxation times of different species in the IMC-PS amorphous solid dispersion with 1% IMC. 135

Table 6.1. Glass transition temperatures of 70-30 IMC methyl ester-PVP amorphous solid dispersions stored at 4 °C/0% RH at different time points. 184

Table 6.2. Glass transition temperatures of 70-30 IMC-PVP amorphous solid dispersions stored at various conditions at different time points. 184

Table 6.3. Glass transition temperatures of 70-30 NIF-PVP amorphous solid dispersions stored at various conditions at different time points. 185

Table 6.4. Water content of 70-30 IMC methyl ester-PVP amorphous solid dispersion at various time points. 187

Table 6.5. Water contents of 70-30 IMC-PVP amorphous solid dispersions stored at different conditions at various time points 187

Table 6.6. Water contents of 70-30 NIF-PVP amorphous solid dispersions stored at different conditions at various time points 187

List of Figures

Figure 1.1. Free energy diagrams of (a) a monotropic and (b) an enantiotropic system. .. 4

Figure 1.2. Illustration of the enthalpy relationship between the liquid, the amorphous and the crystalline state as a function of temperature. 7

Figure 1.3. The relationship between free energy and nucleus size. 9

Figure 1.4. Effects of temperature on the size and free energy of forming a critical nucleus. 13

Figure 1.5. Comparison between the homogeneous nucleation and the heterogeneous nucleation. 14

Figure 2.1. Solid-state NMR pulse sequences of (a) ^{1}H T_1 and (b) ^{1}H $T_{1\rho}$ with ^{13}C detection. 30

Figure 2.2. ^{1}H $T_{1\rho}$ relaxation times of nifedipine (NIF) and PVP in the 50-50 NIF-PVP amorphous solid dispersion as a function of temperature. 34

Figure 2.3. Pulse sequence of the ^{13}C 2D exchange experiment to study molecular motions 37

Figure 2.4. Illustration of a processed ^{13}C 2D exchange spectrum. 38

Figure 2.5. Evolution of peak area as a function of contact time of a naltrexone crystalline solvate form and the amorphous form 42

Figure 3.1. Chemical structures of (a) nifedipine and (b) PVP 49

Figure 3.2. MDSC of (a) NIF, PVP and NIF:PVP amorphous solid dispersions of various weight ratios and (b) 90:10 NIF:PVP amorphous solid dispersions prepared by three different methods. 55

Figure 3.3. Glass transition temperatures of NIF:PVP amorphous solid dispersions. 56

Figure 3.4. ^{13}C SSNMR spectra of (a) α crystalline nifedipine, (b) β crystalline nifedipine and (c) amorphous nifedipine. 58

Figure 3.5. ^{13}C SSNMR spectra of NIF-PVP amorphous solid dispersions prepared by melt quenching in the lab setting containing 0, 5, 10, 25, 40, 50 and 100% PVP (from top to bottom). 62

Figure 3.6. (a) ^{1}H T_1 and (b) $T_{1\rho}$ differential between nifedipine and PVP in the amorphous solid dispersions prepared by melt quenching in the lab setting as a function of PVP content. 63

Figure 4.1. Chemical structures of (a) indomethacin, (b) PVP, (c) PVP/VA, and (d) polystyrene. 74

Figure 4.2. ^{13}C SSNMR spectra of (a) γ crystalline indomethacin, (b) α crystalline indomethacin, and (c) amorphous indomethacin. 80

Figure 4.3. Carbonyl region of ^{13}C SSNMR spectra of (a) γ crystalline indomethacin, (b) α crystalline indomethacin, and (c) amorphous indomethacin. 81

Figure 4.4. ^{13}C SSNMR spectra of (a) ^{13}C labeled amorphous indomethacin, (b) natural abundance amorphous indomethacin, and (c) carboxyl carbon of amorphous indomethacin. 83

Figure 4.5. CPMAS ^{13}C spectrum of the carboxylic acid of amorphous indomethacin. . 85

Figure 4.6. ^{13}C CPMAS spectrum of the carboxylic acid region of 1% indomethacin in polystyrene. 88

Figure 4.7. ^{13}C CPMAS spectra of the carboxylic acid region of (a) 5% indomethacin, (b) 2% indomethacin, (c) 1% indomethacin, and (d) 0.2% indomethacin in amorphous solid dispersions with polystyrene. 89

Figure 4.8. ^{13}C spectra of the carboxylic acid carbon of 1% amorphous indomethacin in polystyrene at (a) 20 °C, (b) 30 °C, (c) 40 °C, (d) 50 °C, (e) 60 °C, (f) 70 °C, (g) 80 °C, (h) 110 °C, (i) 140 °C, and (j) 160 °C. 90

Figure 4.9. Peak area ratio between the carboxylic acid dimer and the free carboxylic acid as a function of temperature. 91

Figure 4.10. Deconvolution of the CPMAS ^{13}C spectrum of the carboxylic acid carbon of amorphous indomethacin. 93

Figure 4.11. CPMAS ^{13}C spectrum of IMC carboxylic acid carbon in (a) IMC-PVP and (b) IMC-PVP/VA amorphous solid dispersions. 96

Figure 4.12. Fraction of IMC carboxylic acid participating in various hydrogen-bonding interactions in the amorphous solid dispersion with (a) PVP and (b) PVP/VA as a function of polymer concentration. 100

Figure 5.1. 2D exchange ^{13}C MAS NMR spectra of the carbonyl region of amorphous indomethacin at (a) 20 °C, (b) 40 °C, and (c) 50 °C. 123

Figure 5.2. 2D exchange ^{13}C MAS NMR spectra of the carbonyl region of 90-10 IMC-PVP amorphous solid dispersions at (a) 40 °C, (b) 50 °C and (c) 60 °C. 126

Figure 5.3. 2D exchange ^{13}C MAS NMR spectra of the carbonyl region of 80-20 IMC-PVP amorphous solid dispersions at (a) 50 °C, (b) 60 °C and (c) 70 °C. 127

Figure 5.4. 2D exchange ^{13}C MAS NMR spectra of the carbonyl region of 70-30 IMC-PVP amorphous solid dispersions at (a) 70 °C, and (b) 80 °C. 128

Figure 5.5. 2D exchange ^{13}C MAS NMR spectra of the carbonyl region of 1% IMC in polystyrene at (a) 40 °C, and (b) 50 °C. 132

Figure 5.6. ^{13}C spectra of the carboxylic acid carbon of 1% amorphous indomethacin in polystyrene at (a) 20 °C, (b) 30 °C, (c) 40 °C, (d) 50 °C, (e) 60 °C, (f) 70 °C, (g) 80 °C, (h) 110 °C, (i) 140 °C, and (j) 160 °C. 133

Figure 5.7. Temperature dependence of ^{13}C SSNMR linewidth of the non-protonated phenyl carbon of polystyrene in the IMC-polystyrene amorphous solid dispersion. 134

Figure 6.1. Chemical structures of (a) indomethacin, (b) nifedipine, (c) indomethacin methyl ester, and (d) PVP. 140

Figure 6.2. ^{1}H NMR spectrum of indomethacin methyl ester in $CDCl_3$..... 149

Figure 6.3. Polarized light microscopy image of indomethacin methyl ester..... 150

Figure 6.4. DSC thermogram of indomethacin methyl ester. 151

Figure 6.5. TGA of indomethacin methyl ester. 151

Figure 6.6. Powder X-ray diffractogram of indomethacin methyl ester compared with simulated pattern from solved structure..... 152

Figure 6.7. ^{13}C CPMAS spectra of (a) indomethacin methyl ester, (b) γ-indomethacin, and (c) α-indomethacin. 153

Figure 6.8. PXRD patterns of 70-30 IMC methyl ester-PVP amorphous solid dispersions stored at 4 °C/0% RH..... 155

Figure 6.9. PXRD patterns of 70-30 IMC-PVP amorphous solid dispersions stored at 50 °C/0% RH. 156

Figure 6.10. PXRD patterns of 70-30 IMC-PVP amorphous solid dispersions stored at 40 °C/57%RH. 157

Figure 6.11. PXRD patterns of 70-30 IMC-PVP amorphous solid dispersions stored at 40 °C/75%RH. 158

Figure 6.12. PXRD patterns of 70-30 NIF-PVP amorphous solid dispersions stored at 50 °C/0% RH. 159

Figure 6.13. PXRD patterns of 70-30 NIF-PVP amorphous solid dispersions stored at 40 °C/57%RH. 160

Figure 6.14. PXRD patterns of 70-30 NIF-PVP amorphous solid dispersions stored at 40 °C/75%RH. 161

Figure 6.15. (a) Raman spectra and (b) the carbonyl region of the Raman spectra of 70-30 IMC methyl ester-PVP amorphous solid dispersion stored at 4 °C/0% RH..... 163

Figure 6.16. (a) Raman spectra and (b) the carbonyl region of the Raman spectra of 70-30 IMC-PVP amorphous solid dispersion stored at 50 °C/0% RH. 164

Figure 6.18. (a) Raman spectra and (b) the carbonyl region of the Raman spectra of 70-30 IMC-PVP amorphous solid dispersion stored at 40 °C/75% RH. 166

Figure 6.19. (a) Raman spectra and (b) the carbonyl region of the Raman spectra of 70-30 NIF-PVP amorphous solid dispersion stored at 50 °C/0% RH. 167

Figure 6.20. (a) Raman spectra and (b) the carbonyl region of the Raman spectra of 70-30 NIF-PVP amorphous solid dispersion stored at 40 °C/57% RH. 168

Figure 6.21. (a) Raman spectra and (b) the carbonyl region of the Raman spectra of 70-30 NIF-PVP amorphous solid dispersion stored at 40 °C/75% RH. 169

Figure 6.22. Polarized light microscopy image of 70-30 IMC methyl ester-PVP amorphous solid dispersion stored at 4 °C/0% RH at (a) time 0, (b) 1 week, (c) 2 weeks, (d) 1 month, (e) 2 months, and (f) 6 months of storage. 171

Figure 6.23. Polarized light microscopy image of 70-30 IMC-PVP amorphous solid dispersion stored at 50 °C/0% RH at (a) time 0, (b) 1 week, (c) 2 weeks, (d) 1 month, (e) 2 months, and (f) 6 months of storage. 172

Figure 6.24. Polarized light microscopy image of 70-30 IMC-PVP amorphous solid dispersion stored at 40 °C/57% RH at (a) time 0, (b) 1 week, (c) 2 weeks, (d) 1 month, (e) 2 months, and (f) 6 months of storage. 173

Figure 6.25. Polarized light microscopy image of 70-30 IMC-PVP amorphous solid dispersion stored at 40 °C/75% RH at (a) time 0, (b) 1 week, (c) 2 weeks, (d) 1 month, (e) 2 months, and (f) 6 months of storage. 174

Figure 6.26. Polarized light microscopy image of 70-30 NIF-PVP amorphous solid dispersion stored at 50 °C/0% RH at (a) time 0, (b) 1 week, (c) 2 weeks, (d) 1 month, (e) 2 months, and (f) 6 months of storage. 175

Figure 6.27. Polarized light microscopy image of 70-30 NIF-PVP amorphous solid dispersion stored at 40 °C/57% RH at (a) time 0, (b) 1 week, (c) 2 weeks, (d) 1 month, (e) 2 months, and (f) 6 months of storage. 176

Figure 6.28. Polarized light microscopy image of 70-30 NIF-PVP amorphous solid dispersion stored at 40 °C/75% RH at (a) time 0, (b) 1 week, (c) 2 weeks, (d) 1 month, (e) 2 months, and (f) 6 months of storage. 177

Figure 6.29. MDSC of 70-30 IMC methyl ester-PVP amorphous solid dispersions stored at 4 °C/0% RH. 180

Figure 6.30. MDSC of 70-30 IMC-PVP amorphous solid dispersions stored at 50 °C/0% RH. 180

Figure 6.31. MDSC of 70-30 IMC-PVP amorphous solid dispersions stored at 40 °C/57%RH. 181

Figure 6.32. MDSC of 70-30 IMC-PVP amorphous solid dispersions stored at 40 °C/75%RH. 181

Figure 6.33. MDSC of 70-30 NIF-PVP amorphous solid dispersions stored at 50 °C/0% RH. 182

Figure 6.34. MDSC of 70-30 NIF-PVP amorphous solid dispersions stored at 40 °C/57%RH. 182

Figure 6.35. MDSC of 70-30 NIF-PVP amorphous solid dispersions stored at 40 °C/75%RH. 183

Figure 6.36. ^{13}C CPMAS spectra of 70-30 IMC methyl ester-PVP amorphous solid dispersion stored at 4 °C/0% RH at (a) time 0, (b) 1 week, (c) 2 weeks, (d) 1 month, (e) 2 months, and (f) 6 months of storage. 193

Figure 6.37. ^{13}C CPMAS spectra of 70-30 IMC-PVP amorphous solid dispersion stored at 50 °C/0% RH at (a) time 0, (b) 1 week, (c) 2 weeks, (d) 1 month, (e) 2 months, and (f) 6 months of storage. 194

Figure 6.38. ^{13}C CPMAS spectra of 70-30 IMC-PVP amorphous solid dispersion stored at 40 °C/57% RH at (a) time 0, (b) 1 week, (c) 2 weeks, (d) 1 month, (e) 2 months, and (f) 6 months of storage. 195

Figure 6.39. ^{13}C CPMAS spectra of 70-30 IMC-PVP amorphous solid dispersion stored at 40 °C/75% RH at (a) time 0, (b) 1 week, (c) 2 weeks, (d) 1 month, (e) 2 months, and (f) 6 months of storage. 196

Figure 6.40. ^{13}C CPMAS spectra of 70-30 NIF-PVP amorphous solid dispersion stored at 50 °C/0% RH at (a) time 0, (b) 1 week, (c) 2 weeks, (d) 1 month, (e) 2 months, and (f) 6 months of storage. 197

Figure 6.41. ^{13}C CPMAS spectra of 70-30 NIF-PVP amorphous solid dispersion stored at 40 °C/57% RH at (a) time 0, (b) 1 week, (c) 2 weeks, (d) 1 month, (e) 2 months, and (f) 6 months of storage. 198

Figure 6.42. ^{13}C CPMAS spectra of 70-30 NIF-PVP amorphous solid dispersion stored at 40 °C/75% RH at (a) time 0, (b) 1 week, (c) 2 weeks, (d) 1 month, (e) 2 months, and (f) 6 months of storage. 199

Figure 6.43. ^{13}C CPMAS spectra of (a) 70-30 IMC-PVP amorphous solid dispersion stored at 40 °C/57% RH for 6 months, (b)) 70-30 IMC-PVP amorphous solid dispersion stored at 40 °C/57% RH for 6 months collected with a 40 ms ^{1}H $T_{1\rho}$ filter, (c) γ-indomethacin, and (d) α-indomethacin. 200

Figure 6.44. ^{13}C CPMAS spectra of (a) 70-30 IMC-PVP amorphous solid dispersion stored at 40 °C/75% RH for 1 month, (b)) 70-30 IMC-PVP amorphous solid dispersion stored at 40 °C/75% RH for 1 month collected with a 40 ms ^{1}H $T_{1\rho}$ filter, (c) γ-indomethacin, and (d) α-indomethacin. 201

Figure 6.45. ^{13}C CPMAS spectra of (a) 70-30 NIF-PVP amorphous solid dispersion stored at 40 °C/75% RH for 1 month, (b)) 70-30 NIF-PVP amorphous solid dispersion stored at 40 °C/75% RH for 1 month collected with a 40 ms ^{1}H $T_{1\rho}$ filter, (c) α-nifedipine, (d) β-nifedipine, and (e) carbonyl region of (b). 202

Figure 6.46. ^{13}C CPMAS spectrum of the carbonyl region of 70-30 NIF-PVP amorphous solid dispersion stored at 40 °C/75% RH after 1 week. 203

Figure 6.47. Crystallization of amorphous NIF in the 70-30 NIF-PVP amorphous solid dispersion stored at 40 °C/75% RH as a function of time. 204

Figure 6.48. Normalized differences of (a) ^{1}H T_1 and (b) ^{1}H $T_{1\rho}$ relaxation times between IMC methyl ester and PVP in the 70-30 IMC methyl ester-PVP amorphous solid dispersion a function of storage time at 4 °C/0% RH. 205

Figure 6.49. Normalized differences of (a) ^{1}H T_1 and (b) ^{1}H $T_{1\rho}$ relaxation times between IMC and PVP in the 70-30 IMC-PVP amorphous solid dispersion a function of storage time at 50 °C/0% RH. 206

Figure 6.50. Normalized differences of (a) ^{1}H T_1 and (b) ^{1}H $T_{1\rho}$ relaxation times between IMC and PVP in the 70-30 IMC-PVP amorphous solid dispersion a function of storage time at 40 °C/57% RH. 207

Figure 6.51. Normalized differences of (a) ^{1}H T_1 and (b) ^{1}H $T_{1\rho}$ relaxation times between IMC and PVP in the 70-30 IMC-PVP amorphous solid dispersion a function of storage time at 40 °C/75% RH. 208

Figure 6.52. Normalized differences of (a) ^{1}H T_1 and (b) ^{1}H $T_{1\rho}$ relaxation times between NIF and PVP in the 70-30 NIF-PVP amorphous solid dispersion a function of storage time at 50 °C/0% RH. 209

Figure 6.53. Differences of (a) ^{1}H T_1 and (b) ^{1}H $T_{1\rho}$ relaxation times between NIF and PVP in the 70-30 NIF-PVP amorphous solid dispersion a function of storage time at 40 °C/57% RH. 210

Figure 6.54. Differences of (a) ^{1}H T_1 and (b) ^{1}H $T_{1\rho}$ relaxation times between NIF and PVP in the 70-30 NIF-PVP amorphous solid dispersion a function of storage time at 40 °C/75% RH. 211

Figure 6.55. Dependence of (a) ^{1}H $T_{1\rho}$ relaxation time, and (b) ^{1}H T_1 relaxation time on water content for the 70-30 IMC-PVP amorphous solid dispersion. 212

Figure 4.56. Dissolution profiles of 70-30 IMC-PVP amorphous solid dispersion at time 0 and after storage for 6 months. 214

Figure 6.57. Dissolution profiles of 70-30NIF-PVP amorphous solid dispersion at time 0 and after storage for 6 months. 215

Figure A.1. Chemical structures of (a) indomethacin and (b) PVP. 226

Figure A.2. CPMASS ^{13}C spectrum of IMC carboxylic acid carbon in a 80-20 IMC-PVP amorphous solid dispersion with (a) 0.2 % water, (b) 1.2 % water and (c) 1.6% water (wt %)..... 231

Figure A.3. CPMASS ^{13}C spectrum of IMC carboxylic acid carbon in a 70-30 IMC-PVP amorphous solid dispersion with (a) ~0% water, (b) 0.7% water, (c) 1.7% water, (d) 2.5% water and (e) 3.6% water (wt %). 232

Figure A.4. Illustrations of (a) carboxylic acid-amide-water (Type I) and (b) carboxylic acid-water (Type II) interactions. 233

Figure A.5. Fraction of IMC carboxylic acid participating in various hydrogen-bonding interactions in the (a) 80-20 IMC-PVP and (b) 70-30 IMC-PVP amorphous solid dispersion as a function of water content. 234

Chapter 1. Introduction

1.1 Pharmaceutical Solids

Solid-state pharmaceuticals have traditionally been the backbone of pharmaceutical products since the inception of the modern pharmaceutical industry. The first synthetic drug, chloral hydrate, a simple organic solid, was introduced in 1869 as a sedative. The first blockbuster drug, aspirin, was launched in 1899 and is still used today. Penicillin, first commercially produced in 1942, saved hundreds of thousands of lives among the allied forces in WWII. All of these drugs were marketed as solid-state pharmaceuticals. The widespread usage of solid dosage forms can be attributed to several factors such as a longer shelf life, a lower cost of production and the ease of transport and handling.

In recent years, however, there has been a challenge in the pharmaceutical industry. More and more molecules being discovered nowadays belong to Class II of the Biopharmaceutics Classification System (BCS), characterized by low aqueous solubility. Poor solubility often leads to low oral bioavailability and inadequate efficacy. Thus, the effort to increase oral bioavailability has been a focus of research in pharmaceutics in recent years.

There are many different ways to potentially increase the oral bioavailability of an active pharmaceutical ingredient, or API, in a solid dosage form, such as micronizatinon, the use of salts or co-crystals, or the use of amorphous solid dispersions. This research is focused on amorphous solid dispersions. The following sections introduce the concept of

crystalline versus amorphous materials and various aspects of amorphous solid dispersions.

1.2 Crystalline vs. Amorphous Solids

1.2.1 The Crystalline State

Crystalline solids are the most commonly-encountered solid forms for pharmaceuticals. A crystal is a solid in which molecules are arranged in a highly ordered fashion, with both short range and long range orders. In an organic crystal, the molecules are held together by non-covalent interactions. Of these non-covalent forces, hydrogen bonding is probably the most important.[1]

1.2.2 Polymorphism

Oftentimes, compounds of the same chemical composition can have different crystal structures, giving rise to the phenomenon called polymorphism. Polymorphism is defined by McCrone as the ability of any compound "to crystallize as more than one distinct crystal species."[2] Due to the differences in molecular packing, polymorphs may exhibit very different physical and chemical properties. Polymorphs can differ in their solubility, density, hardness, and crystal shape.[1] The most common example is carbon, with three polymorphs (i.e. diamond, graphite, and fullerenes) all exhibiting different properties because of their different internal structures. The most well-known example of the importance of polymorph control in pharmaceutics is probably the incident involving Ritonavir. This anti-HIV drug was marketed in 1996 as a semi-solid formulation. In 1998,

a previously unknown, thermodynamically more stable, and much less soluble crystalline form (Form II) emerged in production.[3] Due to the extremely low solubility of Form II, the batches produced with this polymorph failed the dissolution test. The inability to consistently produce Form I finally led to a withdrawal of the product. The drug was subsequently reformulated into an oral solution. Thus, the control of polymorphism is very important for pharmaceutical development to avoid changing in dissolution rate, bioavailability and stability.

A survey of 245 organic compounds showed that 50% exhibited polymorphism.[4] Regardless of the statistical number, the prevalence of polymorphism among drug substances is very high. The often-quoted statement from McCrone says that the number of polymorphs discovered for each compound is proportional to the time and effort spent in research on that compound,[2] which offers quite some insight on the subject.

At a given temperature and pressure, only one polymorph will have the lowest free energy and is the most stable polymorph. All other polymorphs are referred to as the metastable forms. Metastable forms could convert to the most stable form given enough time or other suitable conditions. Depending on the relationship between thermodynamic stability and temperature, two polymorphs can be classified as either being monotropic or enantiotropic. Two polymorphs are said to be monotropic if one form is more stable than the other form at all temperatures below the melting temperatures of each form. The two polymorphs are enantiotropic if their relative stability is dependent on temperature. Figure 1.1 illustrates the energy-temperature relationship of these two systems.

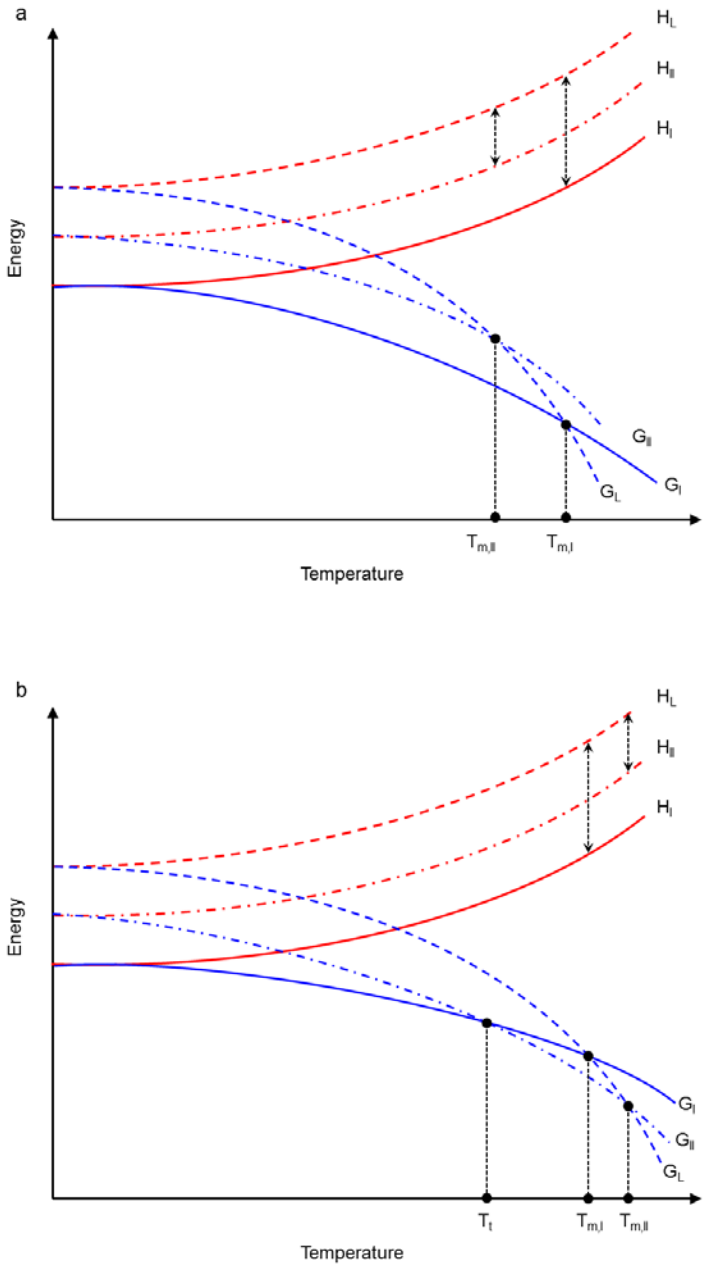

Figure 1.1. Free energy diagrams of (a) a monotropic and (b) an enantiotropic system. H denotes enthalpy, G denotes the Gibbs free energy, and T denotes the temperature. Subscripts I, II and L denote polymorph I, polymorph II, and the liquid phase, respectively. Adapted from Burger and Ramberger.5

1.2.3 The Amorphous State

The word “amorphous” is derived from the Greek term “αορφος”, meaning “shapeless”.[6] Amorphous materials are highly disordered and lack the long-range molecular order that is typical for crystalline materials. They do, however, possess the short-range order over a few Ångstroms. The short-range order could be similar to that found in its crystalline counterpart, such as that due to hydrogen bonding.[1]

The amorphous state is a thermodynamically metastable state compared to the crystalline state. Given sufficient time, an amorphous material can transform to the crystalline for. In fact, the amorphous state can be viewed as an extension of the liquid phase to temperatures below the melting point of the crystalline solid phase. Figure 1.2 illustrates the thermodynamic relationship between a liquid, an amorphous and a crystalline state. When a liquid is cooled to below its melting temperature fast enough and the timescale does not allow adequate rearrangement of the molecules, the material will fall out of equilibrium and become a supercooled liquid. As temperature continues to cool and viscosity increases, the material is kinetically “frozen” to form a glass.

An amorphous material exists in the rubbery state above a temperature range called the glass transition temperature, T_g, whereas it exists in the glassy state below T_g. As a result of the pseudo second-order phase transition, the glass transition is directly related to the properties of the material, such as the specific heat, enthalpy, free volume, viscosity, etc. In the rubbery state, the amorphous material has high molecular mobility, high free volume and low viscosity, and behaves like a liquid. In the glassy state, the material has low molecular mobility, low free volume and high viscosity, and behaves like a solid.

With the higher free energy, organic compounds in the amorphous state have higher dissolution rates and exhibit higher apparent solubilities compared to their crystalline counterparts. For this reason, using APIs in the amorphous state has become an effective strategy to increase the bioavailability of BCS class II compounds. However, to date, there are only a few amorphous formulations on the market.[7] One of the major concerns is the stability. Spontaneous crystallization from the amorphous state during storage can greatly reduce the bioavailability and render the drug product ineffective. The following sections of this chapter will examine the theories of crystallization from the amorphous state and the stabilization of amorphous APIs in solid dispersions.

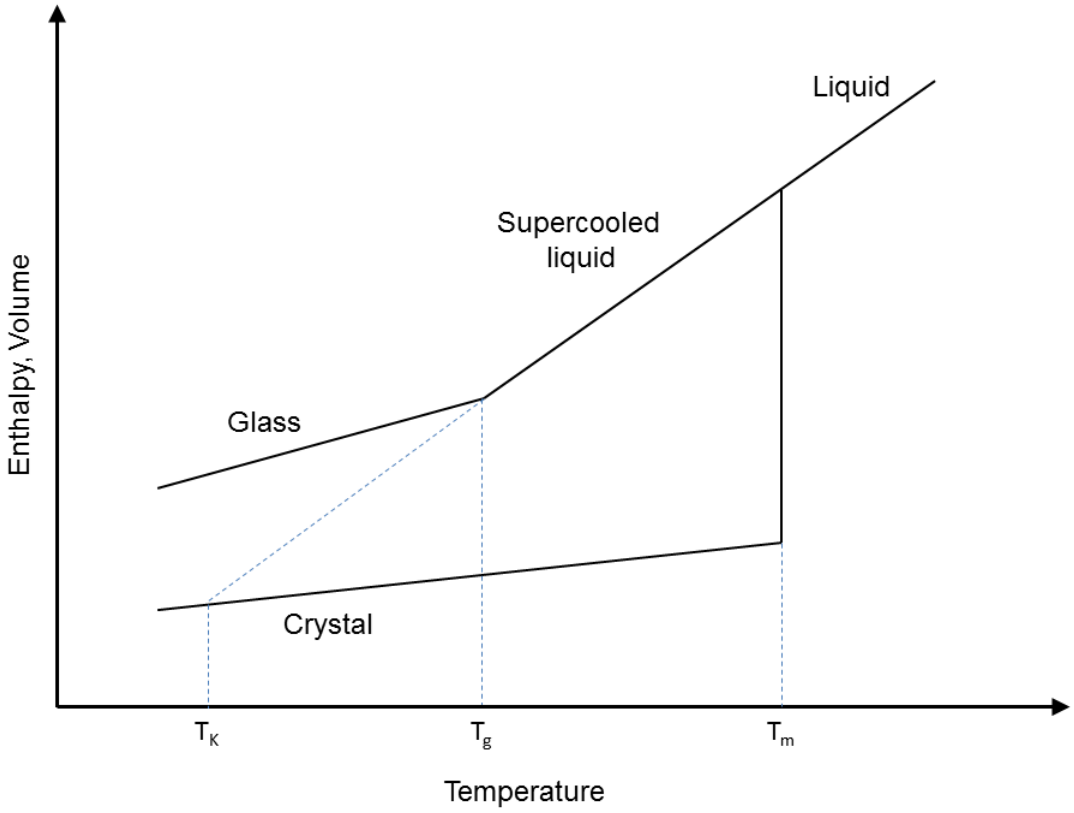

Figure 1.2. Illustration of the enthalpy relationship between the liquid, the amorphous and the crystalline state as a function of temperature. Adapted from Hancock et al.[8]

1.3 Crystallization from the Amorphous State

1.3.1 Nucleation Theory

As mentioned in the previous section, the amorphous state is intrinsically metastable, and will crystallize given sufficient time. Similar to crystallization from solution, crystallization from the amorphous state involves nucleation and crystal growth. According to classical nucleation theory, the free energy change for nucleation includes two terms, the free energy change to create a surface (ΔG_S), and the free energy change from the amorphous to the crystalline state (ΔG_V).[9] The relationship can be described as follows:

$$\Delta G = \Delta G_S + \Delta G_V = 4\pi r^2\gamma + \frac{4}{3}\pi r^3 \Delta G_v \qquad (1.1)$$

where r is the radius of the nucleus, γ is interfacial tension, and ΔG_v is the free energy change of the transformation per unit volume. Since creating new surfaces is energetically unfavorable, ΔG_S bears a positive sign. On the other hand, the free energy change from the amorphous to the crystalline state (ΔG_V) is energetically favorable, and bears a negative sign. It is easy to see that the overall free energy change of nucleation reflects a competition between the energy penalty for creating new surfaces and the energy gain from forming crystals. As seen in the equation, the energy penalty for creating new surfaces is a function of r^2, whereas the energy gain from crystal formation is a function of r^3. When a nucleus is formed with a very small radius, it will have a high energy penalty and tend to be unstable. As illustrated in Figure 1.3, when the nucleus increases to a sufficiently large size as characterized by the critical radius r_c, any further increase in the size of the crystal will reduce the overall free energy, ΔG. Under this condition, the further increase of nucleus size becomes energetically favorable and a

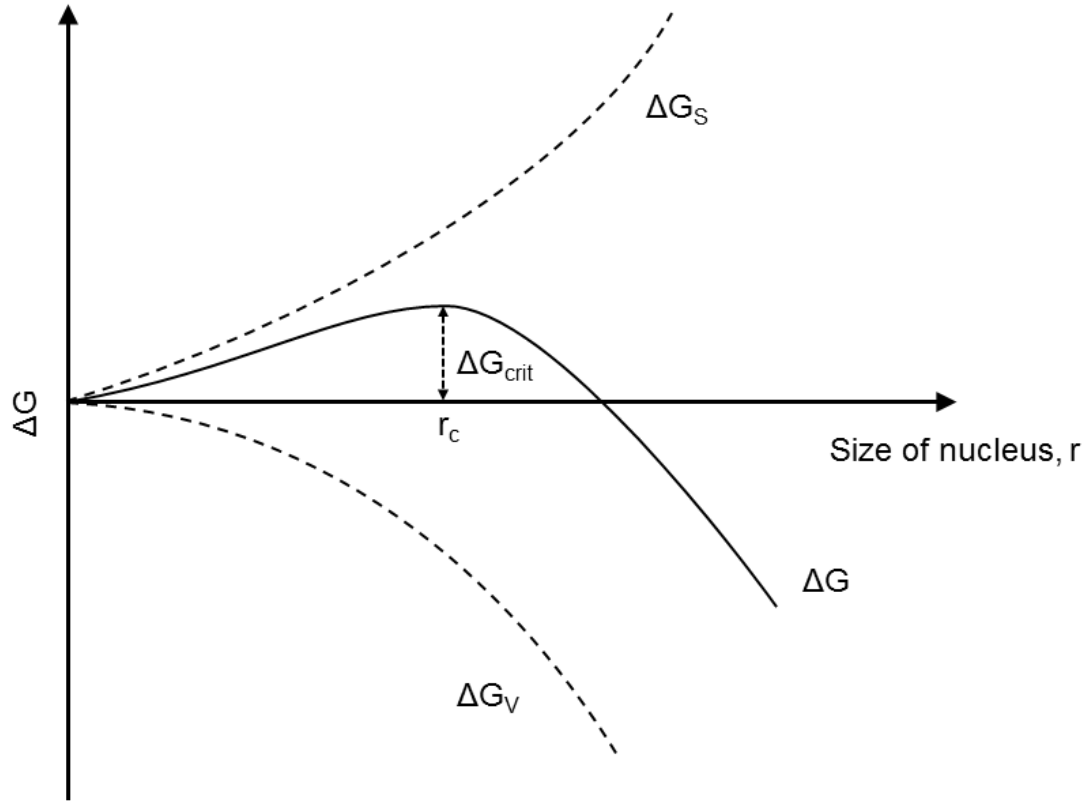

Figure 1.3. The relationship between free energy and nucleus size. Adapted from Mullin.9

stable nucleus can be formed. The free energy change at this radius r_c is the activation barrier of nucleation (ΔG_{crit}).

The energy barrier ΔG_{crit} can be mathematically obtained by taking the derivative of the free energy and setting it to zero as shown in the following expression:

$$\frac{d\Delta G}{dr} = 8\pi r\gamma + 4\pi r^2 \Delta G_v = 0 \quad (1.2)$$

Therefore,

$$r_c = \frac{-2\gamma}{\Delta G_v} \quad (1.3)$$

From Equation 1.1 and Equation 1.3, we get

$$\Delta G_{crit} = \frac{16\pi\gamma^3}{3(\Delta G_v)^2} \quad (1.4)$$

The volume free energy is often estimated by[9]

$$\Delta G_v = \frac{\Delta H_f (T_m - T)}{Tm} \quad (1.5)$$

assuming T is close to T_m, and the enthalpy and entropy changes are independent of temperature and equal to ΔH_f and $\Delta H_f/T_m$, respectively. From Equations 1.3, 1.4 and 1.5, one can see that

$$r_c \propto (T_m - T)^{-1} \quad (1.6)$$

and

$$\Delta G_{crit} \propto (T_m - T)^{-2} \quad (1.7)$$

The above expressions suggest that both the size of the critical nucleus and the energy barrier decrease with decreasing temperature. This relationship is illustrated in Figure 1.4.

The rate of nucleation *J* can be expressed in an Arrhenius form[9]:

$$J = Aexp(-\Delta G_{crit}/kT) \qquad (1.8)$$

where *A* is a pre-exponential constant and *k* is the Boltzmann constant.

Combining Equations 1.4, 1.5 and 1.8, we can obtain the rate of nucleation in the form:

$$J = Aexp\left[-\frac{16\pi\gamma^3 {T_m}^2}{3kT\Delta {H_f}^2 (T_m - T)^2}\right] \qquad (1.9)$$

Equation 1.9 seems to suggest that the rate of nucleation should increase indefinitely as the degree of supercooling increases and the temperature decreases from T_m. Experiments, however, often find that the nucleation rate reaches a maximum as the supercooling increases and further increases in supercooling cause the rate to decrease. This behavior was postulated to be caused by the sharp increase in viscosity in the vicinity of the glass transition temperature.[9] Thus the nucleation rate was modified to include a "viscosity" term in the following expression:

$$J = Aexp\left[-\frac{16\pi\gamma^3 {T_m}^2}{3kT\Delta {H_f}^2 (T_m - T)^2} + \frac{\Delta G\prime}{kT}\right] \qquad (1.10)$$

where $\Delta G'$ describes the activation energy for molecular motion within the matrix. As can be seen from the above expression, nucleation reflects a balance between the thermodynamic driving force and the kinetic motion, where each is favored by different

temperature regimes. The optimum temperature for nucleation is typically somewhere above the glass transition temperature.[10]

The classical nucleation theory describes the process of homogeneous nucleation, which assumes that there are no foreign particles in the system. In reality, this is rarely the case. In fact, it is generally accepted that homogenous nucleation is not a common event.[9] Most of the time, heterogeneous nucleation is what is observed in practice. In heterogeneous nucleation, the activation energy is reduced due to the reduction of interfacial energy, which depends on the affinity between the crystalline phase and the foreign solid. The higher the affinity between the two solid phases, the lower the activation energy. Figure 1.5 shows the schematic of the free energy versus nucleus size for heterogeneous nucleation in comparison to homogeneous nucleation. In solution, atmospheric dust or walls of the container often provide the surface of heterogeneous nucleation. In the case of crystallization from the amorphous state, cracks in the glass can serve as sites for nucleation. A substantial increase in nucleation rate was observed in amorphous RS ibuprofen when cracks were intentionally produced in the glassy state.[11] The authors pointed out that the crack formation in the glassy state was able to promote heterogeneous nucleation in a temperature regime (i.e. lower than glass transition temperature) in which it was difficult to achieve homogeneous nucleation due to the slow mobility.[11]

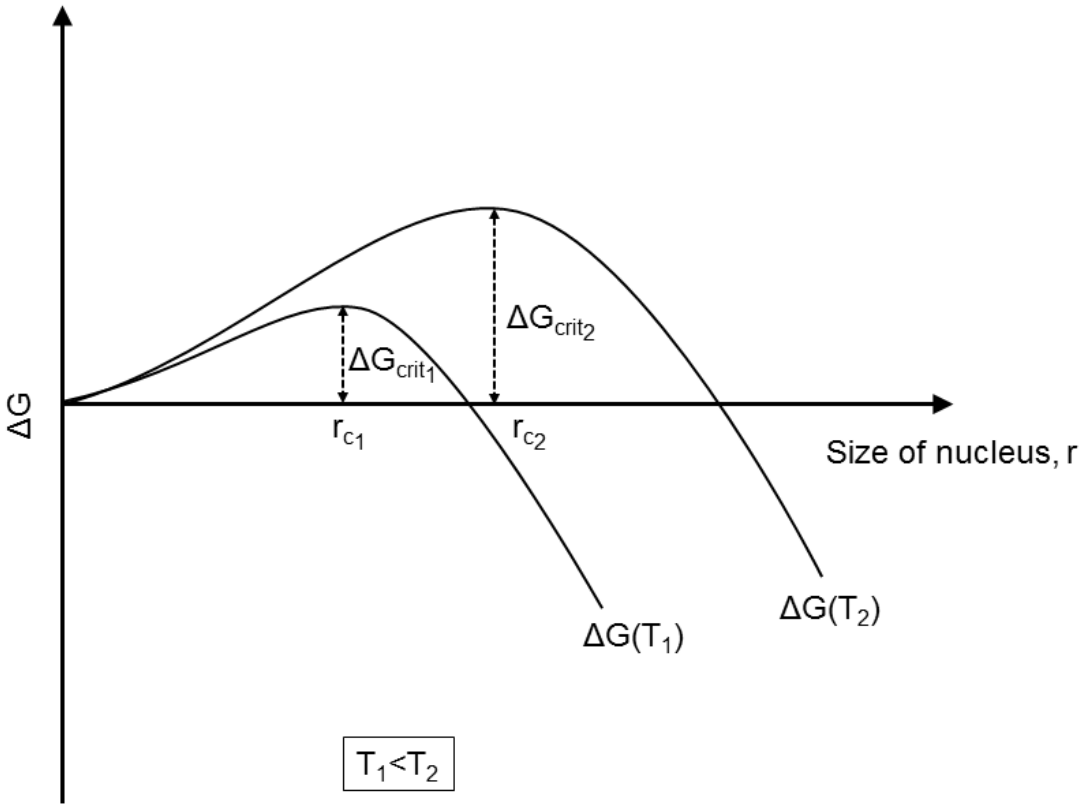

Figure 1.4. Effects of temperature on the size and free energy of forming a critical nucleus. Adapted from Mullin.[9]

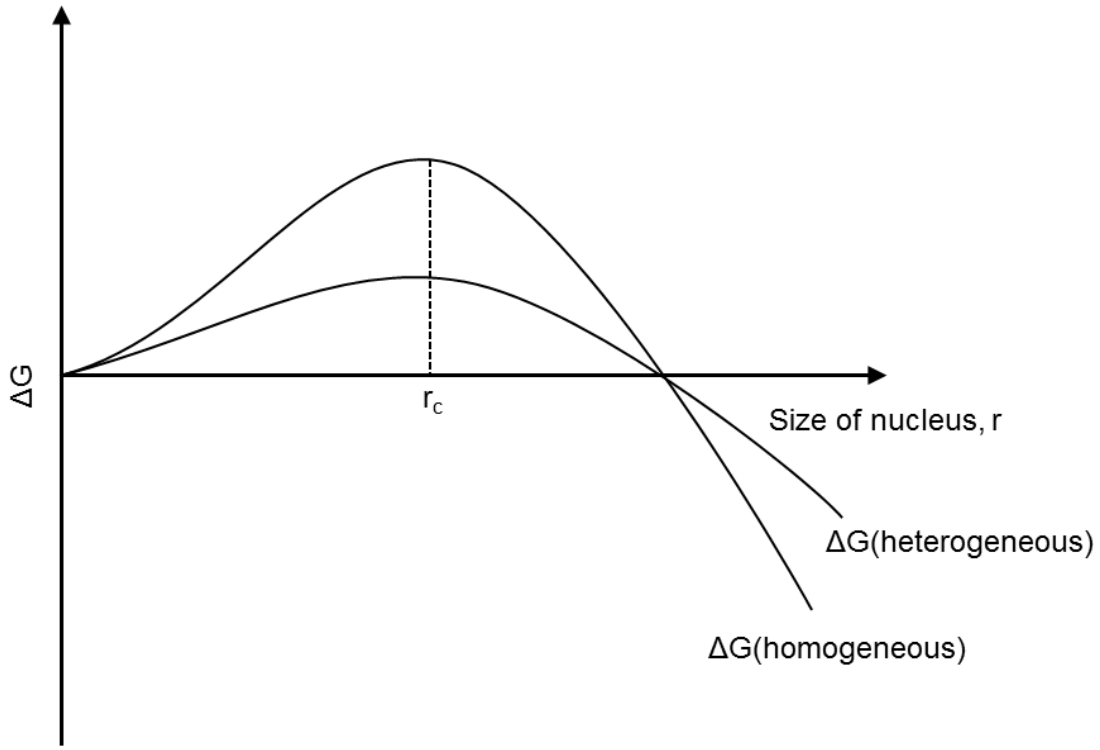

Figure 1.5. Comparison between the homogeneous nucleation and the heterogeneous nucleation. The free energy for heterogeneous nucleation is substantially lower than that for homogeneous nucleation. Adapted from Ragone.[12]

1.3.2 Crystal Growth Theory

Once stable nuclei are formed, they start growing into crystals. Similar to nucleation, crystal growth is also governed by two competing mechanisms. At low degrees of supercooling, the growth rate increases with supercooling as the free energy difference increases. At high degrees of supercooling, the growth rate decreases with supercooling as the mobility in the system decreases. The maximum growth rate is situated in between the glass transition temperature and the melting temperature, and is typically much higher than the temperature where the maximum rate of nucleation is found.[13] Figure 1.5 shows the schematic of the temperature dependence of these two processes.

A different mode of fast crystal growth in the glassy state was first noticed by Greet and Turnbull.[14] O-terphenyl crystals were found to grow three to four orders of magnitude faster than what was expected from the calculations of viscosity near the glass transition temperature.[14] This fast growth phenomenon was studied by Oguni and coworkers[15, 16] and later by Lian Yu's research group.[17-20] The sudden activation of this growth mode near the glass transition temperature is not limited by molecular diffusion in the bulk liquid and is termed glass-crystal (GC) growth. Not all organic compounds, and sometimes not all polymorphs of a given molecular compound are subjected to GC growth. Sun et al. studied seven polymorphs of 5-methyl-2-[(2-nitrophenyl)amino]-3-thiophenecarbonitrile (ROY) and observed four polymorphs showing the fast growth mode.[18] The polymorphs exhibiting the fast growth mode showed changing morphologies with temperature, from faceted crystals at high temperature, to fiber-like crystals near T_g, and to compact spherulites in the fast growth mode.[18] The polymorphs exhibiting fast

growth mode also had higher densities and more isotropic crystal packing, which suggests that the fast growth may occur if there are sufficient similarities in crystalline packing between the liquid and the crystalline state.[21] Current evidence seems to suggest that this type of growth mode stems from the solid-state transformations enabled from local molecular motions native to the glassy state.[18]

Besides the fast crystal growth in certain organic glasses, a different type of crystallization at the surface was observed and studied by Yu and coworkers. [22-24] The crystal growth of indomethacin at the surface was observed to be orders of magnitude faster than the growth in the bulk.[22] In the case of nifedipine, which exhibited the fast growth mode in the glass, the surface growth rate is even faster than the fast growth mode in the bulk.[23] This type of fast surface growth is postulated to be related to the much faster surface diffusion compared to that in the bulk[21, 25] and high surface mobility.[20, 24]

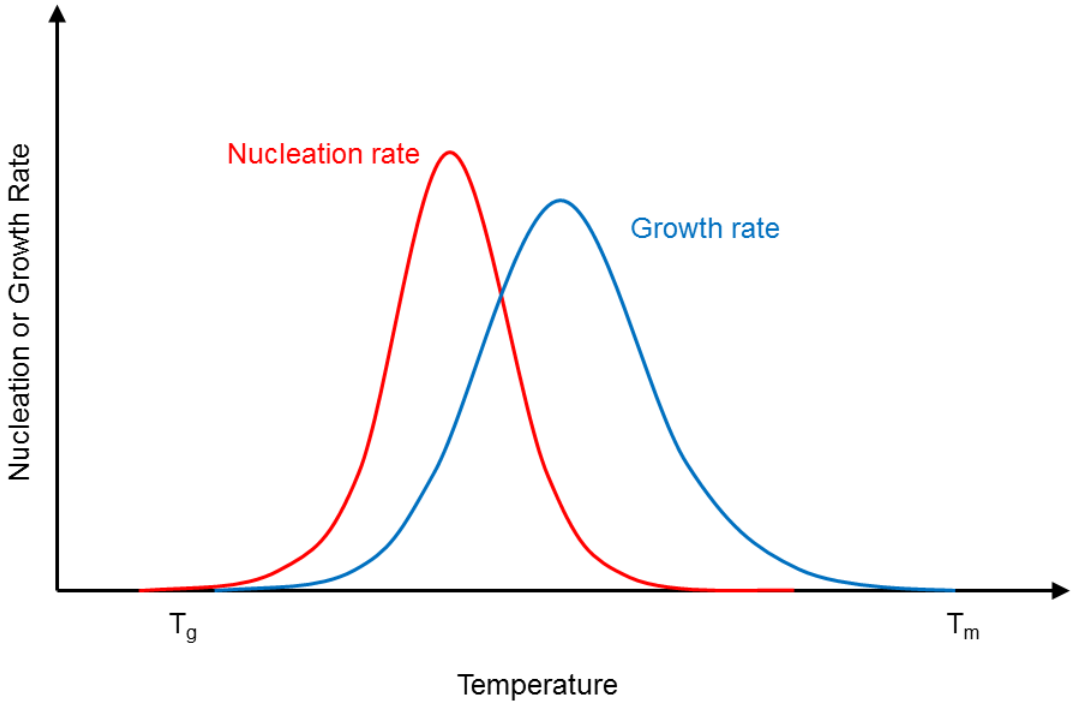

Figure 1.5. Temperature dependence of nucleation and crystal growth. Adapted from Gutzow.[10]

1.3.3 Factors Influencing the Tendency to Crystallize

As described before, the crystallization process strongly depends on temperature because both nucleation and crystal growth are temperature dependent events. This temperature dependency is often coupled with the temperature dependence of molecular mobility. It is generally accepted that mass transport is one of the most critical factors in nucleation and growth from the amorphous state.[26] Most organic compounds crystallize at a much faster rate above the glass transition temperature than below the glass transition temperature, due to the restricted molecular mobility below T_g.

It has been observed that different compounds have shown different crystallization behaviors, some of which cannot be fully explained by molecular mobility alone.[26] Zhou *et al.* studied five pharmaceutical compounds and found that the crystallization tendencies of acetaminophen, sucrose, fenofibrate, ABT-229 and ritonavir are related to both molecular mobility and configurational entropy.[26] Configurational entropy describes the spatial disposition of particles, rather than the quantum states of them. Qualitatively, the higher the configurational entropy for a system, the more orientations the molecules can assume, and the harder it is for them to pack into a specific crystalline form. The cited work showed that molecules with lower configurational entropies require less mobility for spontaneous crystallization. Since configurational entropy is inversely related to the probability that molecules will have the proper orientation and conformation for crystal formation and the mobility is related to the number of molecular collisions in a given period of time, both quantities are equally important to the physical stability of amorphous compounds.[26]

1.4 Amorphous Solid Dispersions to Increase Physical Stability

1.4.1 Glass Transition Temperature and Mobility

As discussed earlier in this chapter, the amorphous state is a thermodynamically meta-stable state and is prone to crystallization. Thus, effective ways to increase the physical stability and prevent crystallization from occurring are crucial in making amorphous drugs viable for the market. Most commonly, the amorphous API is mixed with a suitable polymer to form an amorphous solid dispersion. Typically, the polymer has a high glass transition temperature and would have an antiplasticization effect on the drug compound. For an ideally mixed binary mixture, the glass transition temperature can be estimated by the Gordon-Taylor equation:[27]

$$T_g = \frac{w_1 T_{g1} + k w_2 T_{g2}}{w_1 + k w_2} \quad (1.11)$$

where w_1 and w_2 are the weight fractions of each component, and T_{g1} and T_{g2} are the glass transition temperatures of each component. The value k can be estimated as follows,

$$k \approx \frac{\rho_1 T_{g1}}{\rho_2 T_{g2}} \quad (1.12)$$

where ρ_1 and ρ_2 are the densities of each component. If there are very strong interactions between the drug and polymer, there will be a positive deviation from the predicted T_g values. Conversely, if the drug and polymer interaction is less than that their self interactions, there will be a negative deviation from the predicted values.

As implied earlier, an amorphous solid dispersion usually has a higher glass transition temperature than the drug compound by itself. The increase in the glass transition temperature of the amorphous system can often result in the amorphous system

being in the glassy state at room temperature. This effectively reduces the molecular mobility of the system and the crystallization rate.

1.4.2 Miscibility of Drug and Polymer

To form a more stable amorphous solid dispersion, the amorphous drug and polymer have to be intimately mixed. Partial miscibility can lead to phase separation of the system, where drug rich regions exist and could be sites for crystallization. One of the most common methods to determine whether the drug and polymer are miscible is by measuring the glass transition temperature of the mixture using differential scanning calorimetry (DSC). A miscible system is characterized by a single glass transition temperature intermediate to those of the API and polymer, as opposed to two separate glass transition temperatures in a phase-separated system. However, it has been recognized that a single T_g is not an infallible indicator of miscibility.[28, 29] Thus, there is a need to development better understandings and methods to measure phase homogeneity of these amorphous solid dispersions.

1.4.3 Specific Interactions

Besides molecular mobility, specific interactions between the drug and polymer play an important role in stabilizing amorphous drugs. Hydrogen bonding is one of the most important drug-polymer specific interactions in creating stable amorphous solid dispersions. It has been observed that the stabilization of amorphous indomethacin by polymers cannot be attributed to the antiplasticizing effect (increase of T_g) alone, and is

likely to be related to the ability of the drug to hydrogen bond to the polymer.[30, 31] An example by Khougaz and Clas showed delayed onset of crystallization of MK-0951 in dispersions with PVP, even in dispersions where the T_g values were lower than that of the drug by itself.[32] The authors ascribed the stabilization effect to ion-dipole interactions between COO^-Na^+ of the drug and the cyclic amide group of PVP. Despite the importance, most of the studies of specific interactions such as hydrogen bonding interactions are qualitative. Quantitative information pertaining to hydrogen bonding interactions in amorphous systems has been lacking, mainly due to the limitations of infrared (IR) or Raman spectroscopy.

1.4.4 Effect of Water

It has been well established that water absorbed by an amorphous solid will act as a plasticizer and lower the T_g.[33] Consequently, sorbed water has been observed to increase the crystallization rate of amorphous compounds, presumably due to the increase of molecular mobility.[34] The role of water has also been investigated in amorphous solid dispersions of a hydrophobic drug and a hydrophilic polymer.[35, 36] In these studies, water was thought to form a "cosolvent" with the hydrophilic polymer and decrease the solubility of the drug in the "cosolvent" system, leading to phase separation. However, it was noted that some drug-polymer systems remained in one phase even at high relative humidity, while others phase separated.[36] Stronger hydrogen bonding interactions between the drug and polymer were found in systems that remained in one phase after the water absorption. The favorable interactions between the drug and polymer were thought to reduce the mixing enthalpy and help to keep the dispersions in one phase. A caveat of

this study was that the conclusion was based upon the detection of hydrogen bonding between the drug and the polymer after the water was removed from the samples. Thus, it would be interesting to see how sorbed water affects the miscibility of amorphous solid dispersions in the “as is” condition and, how the physical stability is affected by sorbed water.

1.5 Overview of Research

This chapter has provided some background on pharmaceutical solids, the reason to employ amorphous solid as a formulation strategy, and the challenges associated with it. Some of the issues and gaps in the current literature are identified, including the need for better measurements of drug-polymer miscibility and quantitative information on hydrogen bonding interactions in amorphous solid dispersions. Chapter 2 highlights the fundamentals of solid-state NMR (SSNMR) spectroscopy, with an emphasis on the experiments and techniques that are pertinent to the study of amorphous systems. Chapter 3 develops a method to determine the miscibility of amorphous solid dispersions using nifedipine as a model compound and PVP as a polymer. The method employs SSNMR relaxation time measurements and allows the detection of phase homogeneity on the order of a few nanometers. In Chapter 4, hydrogen bonding interactions in amorphous indomethacin and its amorphous solid dispersions are discussed, which involved the identification and quantitation of various hydrogen bonding species. Chapter 5 focuses on how molecular mobility and dynamics change in amorphous solid dispersions as a function of temperature. Dynamics of amorphous systems are examined by two-dimensional (2D) exchange NMR spectroscopy. Chapter 6 describes physical stability

studies of three different amorphous solid dispersions with varying hydrogen bonding capabilities under different relative humidity conditions. Correlations with miscibility and the strength of hydrogen bonding are attempted to explain the differences observed in crystallization behaviors.

Chapter 2. Solid-State NMR Spectroscopy of Pharmaceuticals

2.1 Introduction

Nuclear magnetic resonance was first independently observed in 1945 by Purcell and others at Harvard and Bloch and others at Stanford.[37, 38] For this discovery, the two were jointly awarded the Nobel Prize for physics in 1952. Since then, solution NMR spectroscopy has developed into one of the most powerful techniques for the structural elucidation of organic molecules. In recent years, solid-state NMR spectroscopy has become a powerful technique in solid-state characterization, and is finding more and more applications in the analysis of pharmaceuticals. However, there are a few challenges in producing high-resolution solid-state NMR (SSNMR) spectra due to the unique characteristics of solids. Many of the challenges have been overcome through techniques such as magic-angle spinning (MAS), cross polarization and high power ^{1}H decoupling. This chapter provides an overview of the basic theory of SSNMR spectroscopy and its applications to the analysis of amorphous pharmaceuticals. For a comprehensive review of SSNMR theory and its applications to pharmaceuticals, the reader is directed to other sources.[39-41]

2.2 Basics of NMR Spectroscopy

The phenomenon of NMR has to do with the nuclei of atoms. All nuclei have a nuclear spin quantum number *I*, which takes the values of 0, ½, 1, 3/2, etc. with the units of $h/2\pi$, where *h* is the Planck's constant. Nuclei such as ^{12}C and ^{16}O have a spin quantum

number of zero and are not NMR active. Any nuclei with a non-zero spin quantum number possesses angular momentum and will generate a magnetic field, which is called the magnetic moment, μ, as given by Equation 2.1,

$$\mu = \frac{\gamma I h}{2\pi} \tag{2.1}$$

where γ is the gyromagnetic ratio, a constant for the particular nucleus.

When nuclei with magnetic moments are placed in an outside magnetic field (B_0), the magnetic moments will orient themselves to certain quantum mechanical states. For a spin ½ nucleus, such as ^{1}H or ^{13}C, there are two possible orientations, one aligned with (α state) and one against (β state) the static magnetic field B_0, with the β state being the higher energy state. The population ratio of the two states is governed by the Boltzmann distribution,

$$\frac{N_\beta}{N_\alpha} = e^{-\Delta E/k_B T} \tag{2.2}$$

where k_B is the Boltzmann constant and T is the temperature. ΔE is the energy difference between the two states and is given by

$$\Delta E = \frac{\gamma h B_0}{2\pi} \tag{2.3}$$

Since $\Delta E = h\nu$, resonance can be achieved when the following condition is met,

$$\nu = \frac{\gamma B_0}{2\pi} \tag{2.4}$$

where ν is the resonance frequency and is often referred to as the *Larmor* frequency. The NMR signal originates from the population difference of the two spin states. Calculating from the above equations, the population difference for ^{1}H nuclei in 7.1 Tesla magnetic

field is only on the order of 1 in 10^5. This is the reason why NMR has low sensitivity compared to IR and UV spectroscopy. We can also easily see from Equations 2.2 and 2.3 that the NMR signal can be boosted at lower temperatures or with higher magnetic fields.

NMR spectroscopy uses a radio frequency (RF) pulse to excite the nuclei of interest and detect the signal, or free induction decay (FID), when the spins come back to equilibrium. When placed in a magnetic field B_0, electrons circulate and generate an induced magnetic field in the opposite direction of B_0. Thus the effective field experienced by the nucleus is affected by the local electronic environment. This causes different nuclei to resonate at slightly different frequencies. Despite changes on the order of parts per million (ppm), this difference is detectable and is the basis of the NMR chemical shift.

2.3 Solid-state NMR Spectroscopy

2.3.1 Chemical Shift Anisotropy and Magic Angle Spinning

For a nucleus with a non-spherical electron density, the magnetic field it experiences will vary with its orientation with respect to the static magnetic field.[42] This is not a problem in solution NMR because the rapid tumbling of the molecules in solution averages out the effect and the chemical shift is an isotropic value. In solids, however, molecules are generally not free to move in space and the different orientations that molecules reside in with respect to the static field result in a distribution of chemical shifts, known as the chemical shift anisotropy (CSA). This orientation dependence of chemical shift can be described in terms of the chemical shielding tensor, σ, the

directionality component of the chemical shift anisotropy. σ can be written in terms of two components, the isotropic component and the anisotropic component, as in Equation 2.5.

$$\sigma = \sigma_{iso} + (3cos^2\theta - 1)\sigma_{aniso} \quad (2.5)$$

As can be seen from the equation, the anisotropic component includes a term ($3cos^2\theta - 1$). The anisotropic component can be effectively eliminated if the sample is spun at an angle θ such that ($3cos^2\theta - 1) = 0$. This angle is 54.75° with respect to the static field, and is called the magic angle.[43]

If the sample is spun at a rate less than the width of CSA, spinning side bands will occur at intervals equal to the spinning speed. When high speed is not feasible with some spinning systems, one remedy is to use a pulse sequence called total suppression of spinning sideband (TOSS) to eliminate the spinning sidebands.[44]

2.3.2 Dipolar Coupling and High-power Proton Decoupling

Dipolar coupling is the through-space interaction between the magnetic moments of two nuclei. This spin interaction is analogous to the interaction of two bar magnets. ^{1}H-^{1}H homonuclear coupling is much stronger in solids than in liquids, due to the lack of molecular tumbling in solids. This makes the ^{1}H spectrum of a compound in the solid state very broad, and generally the spectrum yields little useful information. For this reason, ^{13}C is the more commonly detected nucleus for solid-state NMR. Since the natural abundance of ^{13}C only accounts for about 1.1% of the carbon isotopes, homonuclear ^{13}C-^{13}C coupling is very weak in unlabeled samples due to the low

probability of two ^{13}C nuclei being spatially close to each other. However, heteronuclear ^{1}H-^{13}C coupling is still a significant interaction in solids. This interaction is removed by applying a high decoupling field at the ^{1}H Larmor frequency to rapidly flip the ^{1}H spins between the α and the β states so that the dipolar interaction is averaged to zero.

2.3.3 Low Sensitivity and Cross Polarization

Since the ^{13}C isotope only accounts for about 1.1% of naturally occurring carbon isotopes, most of the carbon nuclei in a sample do not yield any NMR signal, which leads to extremely low sensitivity of ^{13}C NMR spectra. To mitigate this problem, a technique called cross polarization (CP) is often implemented.[45] In a CP experiment, bulk magnetization is transferred from the abundant spins (^{1}H) to the dilute spins (^{13}C) and results in an approximately four-fold signal enhancement. This enhancement ratio is related to the gyromagnetic ratios of the two spins by a relation of γ_H/γ_X, which is approximately 4/1 for $^{1}H/^{13}C$. Another benefit of the CP experiment is that the relaxation time for the spins to come back to equilibrium before the next acquisition is governed by the ^{1}H relaxation time instead of ^{13}C. Since ^{13}C nuclei have notoriously long relaxation times compared to ^{1}H nuclei, this technique allows for significantly more acquisitions in a given period, greatly enhancing the signal to noise ratio and decreasing the amount of time needed for a high-quality ^{13}C spectrum.

2.4 Solid-state NMR Techniques for Amorphous Solid Dispersions

2.4.1 Miscibility and ^{1}H Relaxation Times

Among the various techniques in SSNMR spectroscopy to study amorphous solid dispersions, relaxation time measurements are one of the most useful techniques and is also very easy to implement. Generally, the relaxation process in SSNMR describes the restoration of spins to equilibrium after a perturbation by an RF pulse. The relaxation process described by the spin-lattice relaxation time T_1 or the spin-lattice relaxation time in the rotating frame $T_{1\rho}$ is achieved through interactions between the spins and their surroundings. The RF timing and acquisition sequences, which are called pulse sequences, for measuring ^{1}H T_1 and ^{1}H $_{1\rho}$ used in this work are shown in Figure 2.1

Due to strong dipolar coupling of ^{1}H spins and spin diffusion in the solid state, the spin-lattice relaxation times of all the ^{1}H spins in the same molecule are usually the same. The ^{1}H spin-lattice relaxation times of a mixture, on the other hand, are dependent on the degree of mixing and the spin diffusion length scale. If the length scale of mixing is shorter than the length scale of spin diffusion, then the magnetization transfer from the slower to the faster relaxing component is very efficient, and the relaxation times of both components are equal to the weighted average of the values of the individual component. If the length scale of mixing is longer than the length scale of spin diffusion, the relaxation times are those of the individual components. In the case of partial mixing of the components, the relaxation process may exhibit more complex, multidimensional decay.[46]

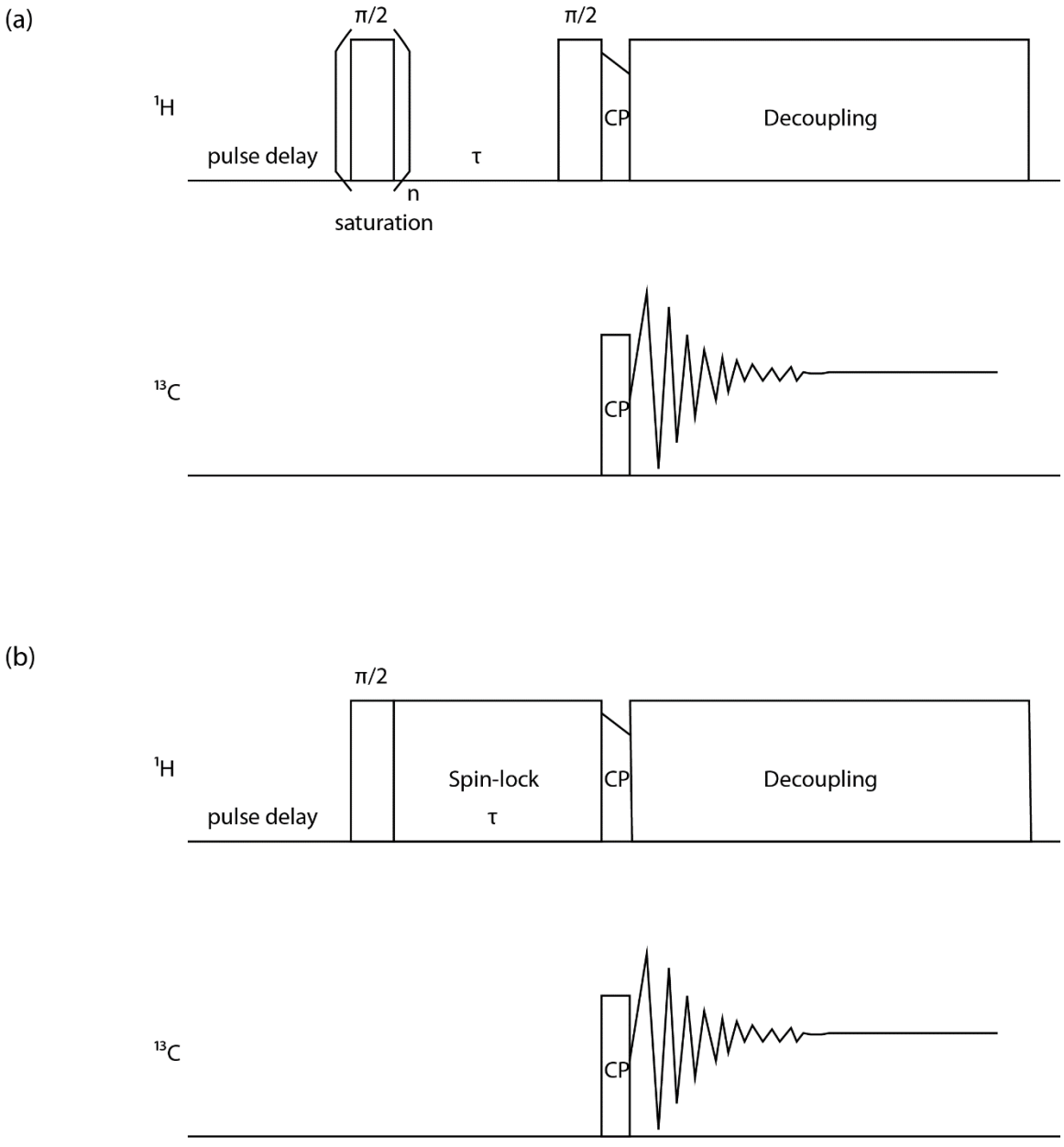

Figure 2.1. Solid-state NMR pulse sequences of (a) ^{1}H T_1 and (b) ^{1}H $T_{1\rho}$ with ^{13}C detection. The ^{1}H T_1 pulse sequence utilizes the saturation recovery method.

The length scale of spin diffusion *L* is dependent on the relaxation time *t* and spin diffusion coefficient *D,* and is given by

$$\langle L \rangle = \sqrt{6Dt} \qquad (2.6)$$

Commonly D is assumed to be 10^{-12} cm^2/s for organic molecules.[46] For a typical ^1H T_1 value of 5 s, the length scale of the spin diffusion is approximately 50 nm. For a typical ^1H $T_{1\rho}$ value of 50 ms, the length scale of the spin diffusion is approximately 5 nm.

Based on the principal of ^1H spin diffusion, ^1H T_1 and ^1H $T_{1\rho}$ relaxation time measurements can be used to determine the miscibility of an amorphous solid dispersion.[47] Depending on the miscibility and domain size, the following three scenarios can be differentiated for an amorphous solid dispersion: 1) If the API and the polymer in a dispersion are miscible on the order of ca. 5 nm (domain size smaller than 5 nm), common ^1H $T_{1\rho}$ and ^1H T_1 values would be obtained from the API and polymer; 2) If the components in a dispersion are miscible on the order of 50 nm but not on the order of 5 nm (i.e. the domain size is between ca. 5 nm and 50 nm), the ^1H $T_{1\rho}$ values will be different for each component but the ^1H T_1 will still be the same; 3) If the components in a dispersion are not miscible on the order of 50 nm (domain size larger than ca. 50 nm), both ^1H $T_{1\rho}$ and ^1H T_1 values will be different for each component.

The ^1H T_1 and ^1H $T_{1\rho}$ relaxation time measurements for amorphous solid dispersions are very important because of the unique ability to probe miscibility on a small scale. When miscibility is determined by differential scanning calorimetry (DSC), the detection limit is usually assumed to be 30 nm.[48-50] Nano-scale phase separation smaller than 30 nm can not be distinguished by DSC, but can be distinguished by SSNMR ^1H T_1 relaxation measurements.

2.4.2 Molecular Mobility and Dynamics

2.4.2.1 Variable-Temperature (VT) Relaxation Time Measurement

SSNMR relaxation times can be used to detect motional processes occurring over a very broad timescale, depending on the nuclei being studied and the types of relaxation times being measured. ^{1}H relaxation times provide "global" information on molecular motion, as the strong ^{1}H spin dipolar interactions result in all of the protons having a common relaxation time.[39] On the contrary, relaxation times of ^{13}C provide the "local" information since ^{13}C nuclei are sparse and are thus relatively unaffected by homonuclear dipolar interactions. In this dissertation work, the majority of relaxation times measured were on ^{1}H nuclei.

The spin-lattice relaxation T_1 is sensitive to motions in the MHz region and usually detects faster motions such as methyl group rotations.[42] The rotating frame spin-lattice relaxation time $T_{1\rho}$ is sensitive to motions in the kHz region and detects slower motions such as intermolecular interactions and phase structure. Lubach et al. measured the ^{1}H T_1 relaxation time of crystalline lactose before and after processing.[51] Crystalline lactose α-monohydrate had a ^{1}H T_1 relaxation time of 243 s, while compaction reduced the relaxation time to 79 s with little change in the spectrum. The reduction of ^{1}H T_1 relaxation time is an indication of higher mobility resulted from increasing high-energy sites (crystal defects).

Molecular mobility is affected by temperature and SSNMR relaxation times can be studied as a function of temperature. Figure 2.2 shows the ^{1}H $T_{1\rho}$ relaxation times of nifedipine (NIF) and PVP in a 50-50 NIF-PVP amorphous solid dispersion.[47] There are slight decreases in the relaxation times of both compounds as temperature increases from

room temperature. As the temperature continues to increase, the decreases in relaxation times become pronounced. The decrease in relaxation time indicates an increase in molecular mobility. The large increase of ^{1}H $T_{1\rho}$ relaxation time at temperatures above 60 °C suggests a higher degree of mobility near the glass transition temperature range. This example highlights the potential of using SSNMR relaxation time to probe molecular mobility of pharmaceutical solids.

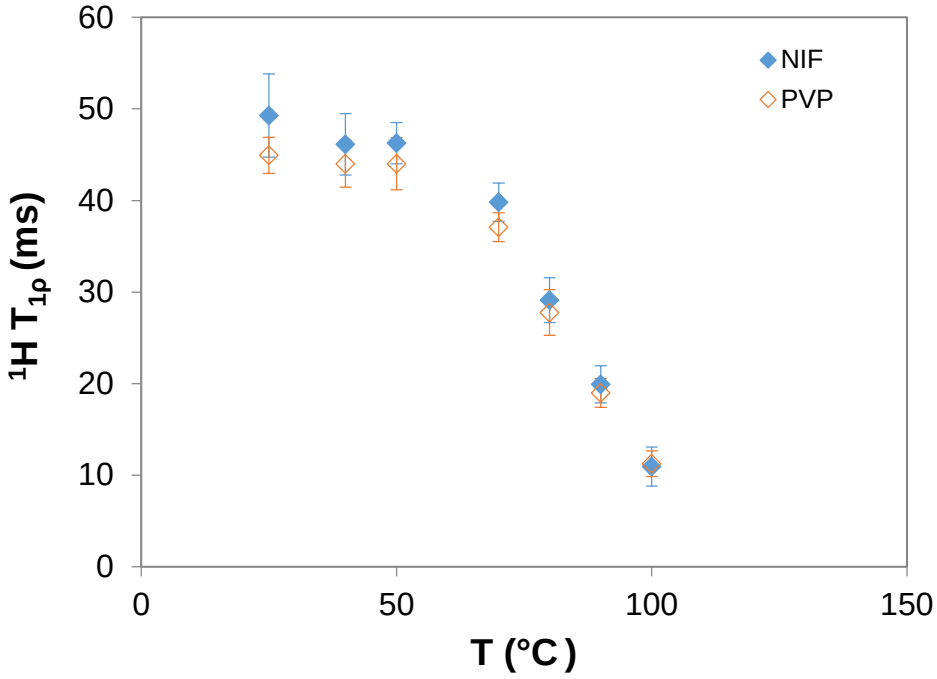

Figure 2.2. ^{1}H $T_{1\rho}$ relaxation times of nifedipine (NIF) and PVP in the 50-50 NIF-PVP amorphous solid dispersion as a function of temperature. The error bar indicates 95% confidence interval of the fit. Adapted from reference. [47]

2.4.2.2 Two-Dimensional Exchange NMR

Besides relaxation time measurements, two-dimensional (2D) exchange NMR is another powerful technique for the study of mobility and dynamics, especially for slow molecular motions. Chemical exchange refers to the dynamic process during which the magnetization is exposed to two different chemical environments during a specified period of time.

The basic form of any 2D experiment includes four stages: preparation, evolution, mixing and detection. The pulse sequence of a 2D ^{13}C exchange experiment is shown in Figure 2.3. During the preparation stage, transverse magnetization of ^{13}C is created by cross polarization. The magnetization is then allowed to evolve under its characteristic frequency ω_1 during t_1. This characteristic frequency arises from the nuclear spin interaction during t_1. At the end of t_1, the magnetization is restored to the z direction by a 90° pulse on ^{13}C. During the mixing time, molecules may change orientations or experience different environments. Last, the magnetization is returned to the observable transverse plane by another 90° pulse and evolves under the frequency ω_2. This evolution is recorded as a FID during t_2. [52]

By repeating the experiment for successive values of t_1, we can obtain a two-dimensional dataset, which, after processing, correlates changes of the molecular environment during the mixing time. If a change in the molecular environment has occurred during the mixing time, the frequency after the mixing time ω_2 will be different from the initial frequency ω_1 and the 2D spectrum will contain an off-diagonal intensity at (ω_1, ω_2). If there is no change in the molecular environment, ω_2 will remain the same as ω_1, and the intensity will lie on the diagonal. Since the analysis relies on there being no

molecular motions during the t_1 and t_2 periods, the exchange experiment is only suitable for studying slow molecular motions (approximately 10 ms – 5 s), where $t_{mix} >> t_1, t_2$. [52]

Figure 2.4 is an illustration of a processed 2D exchange spectrum. The off-diagonal peaks AB and BA suggest that the molecular environment has changed during the mixing time. The lack of off-diagonal peaks of frequency C suggests that this frequency has no change in the molecular environment during the mixing time.

2D exchange NMR can be used in combination with the variable temperature technique to probe molecular dynamics at different temperatures. Chapter 6 will provide some examples of using this approach to study molecular dynamics of amorphous solid dispersions.

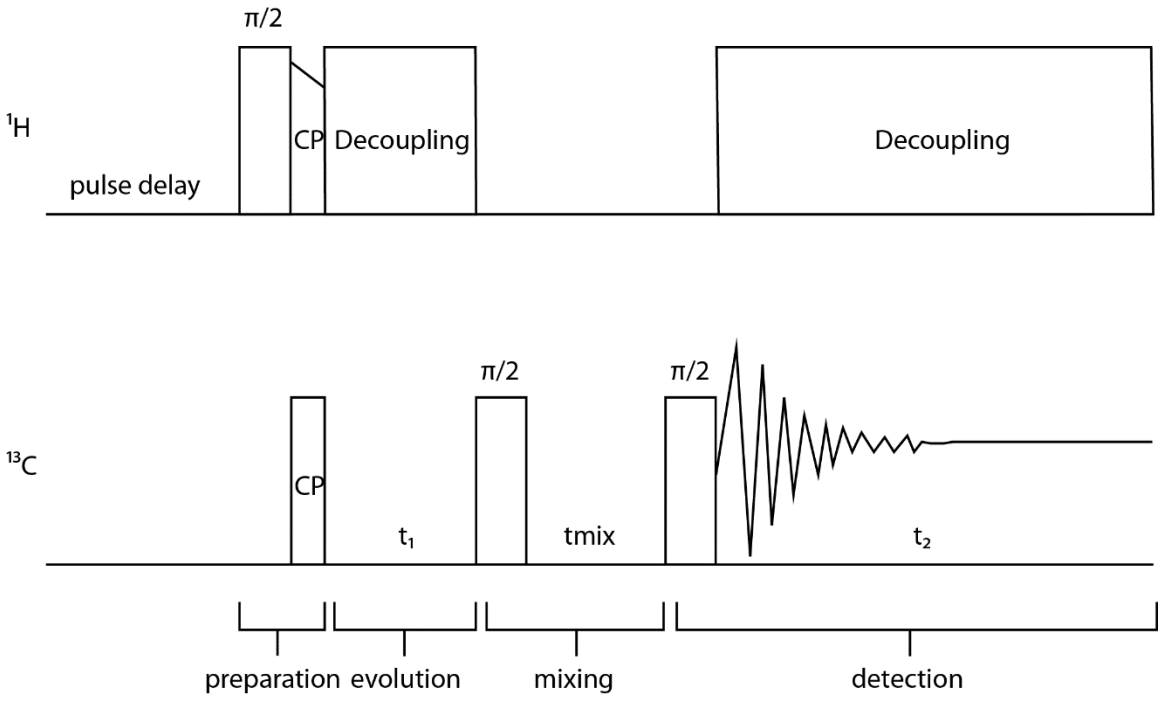

Figure 2.3. Pulse sequence of the ^{13}C 2D exchange experiment to study molecular motions. The four stages of a 2D experiment are labeled underneath.

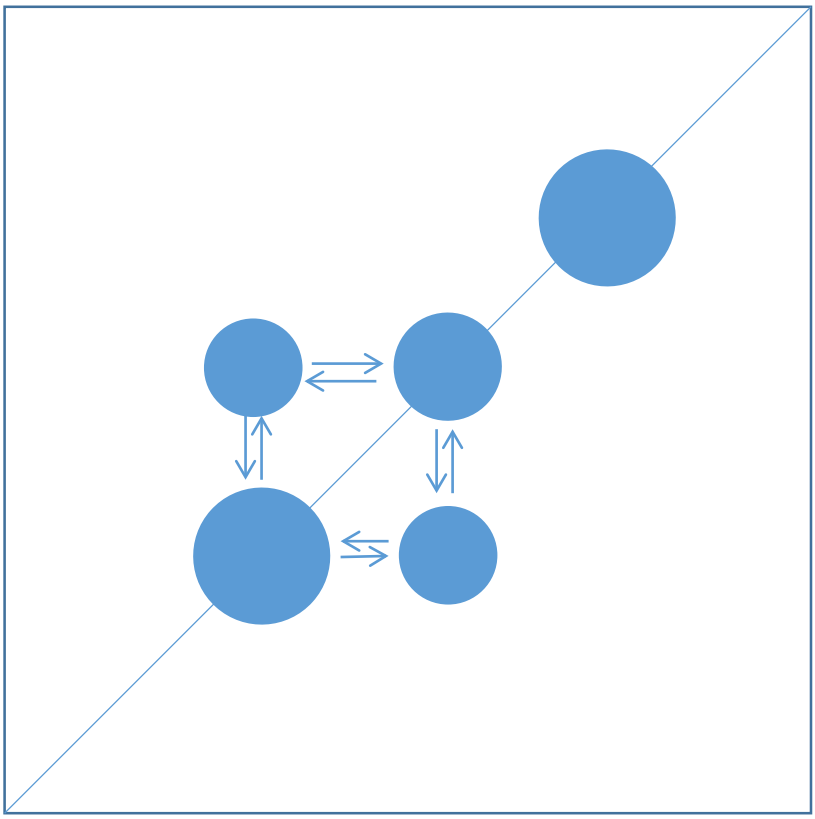

Figure 2.4. Illustration of a processed ^{13}C 2D exchange spectrum. Frequency A and B has exchange between each other while frequency C has no exchange with either A or B.

2.5 Quantitation

NMR spectroscopy is an inherently quantitative technique, as the amount of signal observed is directly proportional to the number of nuclei resonating at a given frequency. There are a number of examples in the literature wherein solid-state NMR has been used in quantitation. Gao quantified binary mixtures of delavirdine mesylate crystalline forms using ^{13}C CPMAS.[53] Offerdahl and others successfully quantified different forms of neotame including the amorphous forms.[54] However, a number of factors have to be considered before a quantitative analysis can be achieved from a SSNMR spectrum. The considerations mainly involve cross polarization in the solid state, T_1 relaxation and the total sideband suppression (TOSS) sequence prevalently used in SSNMR.

2.5.1 Cross Polarization Dynamics

Cross polarization (CP) is a widely used technique in SSNMR spectroscopy to increase the sensitivity of ^{13}C signals. As discussed in a previous section, a rare nucleus such as ^{13}C has very low sensitivity due to its low natural abundance and long relaxation time. During a CP process, magnetization is transferred from an abundant spin (^{1}H) to a rare spin (^{13}C), offering a four-fold increase in sensitivity and fast relaxation time.[45] However, the transfer of magnetization generally does not occur at a uniform rate for each carbon and thus the signal is no longer directly proportional to the number of each nucleus. So it is generally assumed that the spectra collected with CP are not quantitative [54].

The CP transfer process is determined by two rate constants, T_{CH} and $T_{1\rho H}$. The former determines the rate of increase in the ^{13}C magnetization, while the latter determines the rate of decay. The CP dynamic is described in Equation 2.7.

$$I(\tau) = \frac{M_0\left(\frac{\gamma_H}{\gamma_C}\right)\left[\exp\left(-\frac{\tau}{T_{1\rho H}}\right) - exp\left(-\frac{\tau}{T_{CH}}\right)\right]}{1-\left(\frac{T_{CH}}{T_{1\rho H}}\right)} \tag{2.7}$$

where $I(\tau)$ is the intensity or peak area at each contact time τ, M_0 is the thermal equilibrium value of ^{13}C magnetization, and γ_H/γ_C is the gyromagnetic ratio between ^{1}H and ^{13}C which takes the value of 4.

Figure 2.5 shows the CP dynamics of two forms of naltrexone. The crystalline form shows slower buildup and longer decay compared to the amorphous form. From Equation 2.7 one can see that the signal intensity difference between the two forms can be written as,

$$F_{A/B} = \frac{\left(1-\frac{T^A_{CH}}{T^A_{1\rho H}}\right)\left[\exp\left(-\frac{\tau}{T^B_{1\rho H}}\right) - exp\left(-\frac{\tau}{T^B_{CH}}\right)\right]}{\left(1-\frac{T^B_{CH}}{T^B_{1\rho H}}\right)\left[\exp\left(-\frac{\tau}{T^A_{1\rho H}}\right) - exp\left(-\frac{\tau}{T^A_{CH}}\right)\right]} \tag{2.8}$$

where $F_{A/B}$ is the intensity ratio between the two forms (A=crystalline and B=amorphous) and all the other parameters are defined the same as in Equation 2.7. For a chosen contact time of 2 ms, $F_{A/B}$ is calculated to be 1.179. Thus, this value can be used to account for the signal differences resulted from the CP dynamics of the two forms.

Sometimes, if the species to be quantified come from the same form of a same molecule, T_{CH} and $T_{1\rho H}$ can easily be assumed to be the same for all the species. This is the case in quantifying the hydrogen-bonding interactions of amorphous indomethacin

(Chapter 4). The species to be quantified is the carboxylic acid carbon of amorphous indomethacin in different hydrogen-bonded states. Since all the species to be compared come from the amorphous form of indomethacin, the CP dynamics can be safely assumed to be very similar in the analysis.

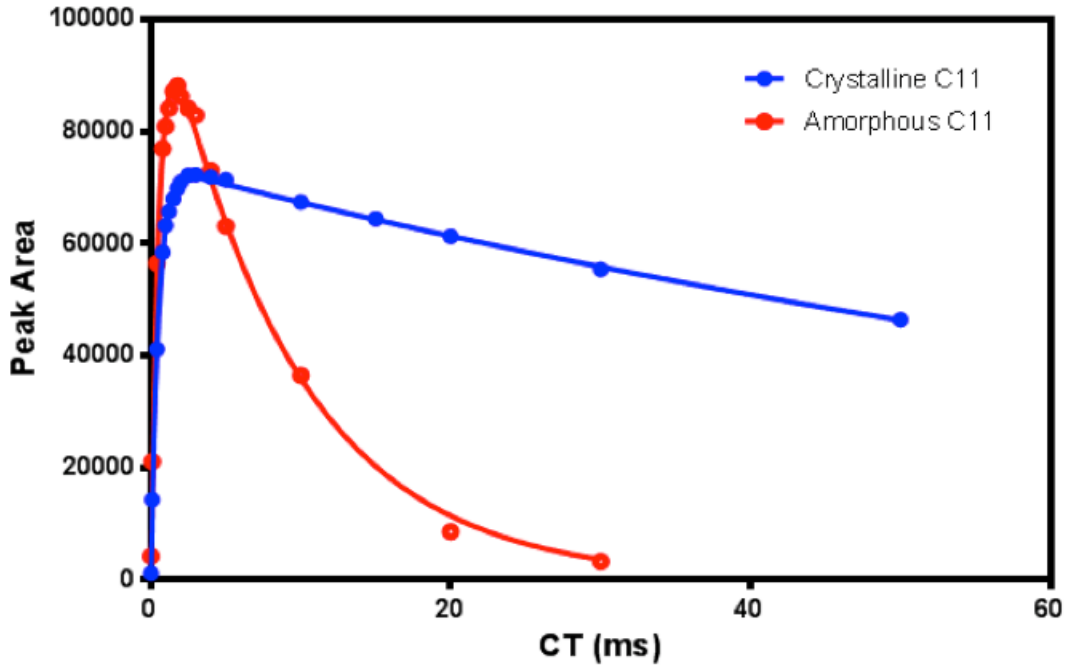

Figure 2.5. Evolution of peak area as a function of contact time of a naltrexone crystalline solvate form and the amorphous form. Carbon 11 is the chosen carbon to be analyzed. The lines are fitted to Equation 2.7.

2.5.2 T_1 Relaxation Time

In theory, to acquire a quantitative spectrum, signal saturation should be avoided. Saturation occurs when spins are not allowed enough time to fully relax to equilibrium. This relaxation process is T_1 relaxation. Typically, a pulse delay of at least five times the T_1 of the slowest relaxing species of interest is needed to allow all species to reach equilibrium. For direct polarization of ^{13}C, this could mean minutes and even hours of relaxation delay between each RF pulse, which is usually not feasible. Luckily, with the CP experiment, the T_1 relaxation time of ^{13}C is no longer relevant. The ^1H T_1 relaxation (T_{1H}) is the governing relaxation mechanism. Since T_{1H} is typically on the order of seconds to minutes, the experimental time is greatly reduced for quantitation.

Sometimes, if the species to be quantified have the same T_{1H}, then it is not necessary to wait five times T_{1H} because the species of interests can not be discriminated on the basis of their relaxation behavior. A pulse delay of 1.5-2 times of T_{1H} can be chosen to maximize the signal to noise ratio. The T_{1H} used in Chapter 4 was chosen based on this idea.

2.5.3 Effect of Sidebands

Magic angle spinning (MAS) is an essential component in modern SSNMR spectroscopy. In order to get rid of the chemical shift anisotropy and obtain isotropic chemical shifts, MAS is utilized to split the powder pattern into a series of peaks separated by spinning speed. When MAS speed is sufficiently high, spinning sidebands can be eliminated. However, the typical spinning speed of 4 kHz for a 7.5 mm rotor is not high enough to eliminate all the sidebands, and TOSS[44] is often utilized to suppress these

sidebands for a cleaner spectrum. If we are only concerned qualitatively about the signal of a nucleus, the isotropic chemical shift has enough information; if we are concerned quantitatively about a nucleus, the spinning sidebands also contain a certain portion of the total signal. When the sidebands are artificially suppressed, this portion of the signal is lost. The distribution of SSNMR signal in the center band (i.e. isotropic peak) and sidebands is influenced by the local environment of each nucleus. Therefore, different nuclei can lead to differences in how much of the total signal resides in the center bands. Thus, it is sometimes useful to not only compare the center bands but also the center bands to total signal ratio when performing quantitative analyses. Luckily, in many cases, the difference of the center band to total signal ratio is negligible among different species when the spectrum was acquired with a high spinning speed.

Chapter 3. Miscibility of Amorphous Solid Dispersions

3.1 Introduction

Formulation of oral solid dosage forms using the amorphous form of the active pharmaceutical ingredient (API) is a strategy used to enhance the oral bioavailability of poorly water-soluble compounds, as the amorphous API has higher apparent solubility and faster dissolution rate than its crystalline counterpart.[8, 55] However, amorphous materials possess higher free energies and have the risk of converting to the crystalline state, which is thermodynamically more stable. To overcome physical instability, a polymer can be mixed with the amorphous API to form an amorphous solid dispersion, which has been shown to significantly delay the onset of crystallization.[30, 56, 57] The two main processes that are commonly used to commercially prepare amorphous solid dispersions are spray drying and hot-melt extrusion. These two methods use different approaches to prepare stable amorphous dispersions and are most closely mimicked on a laboratory scale using a mini spray dryer or a melt-quenching approach.

There have been extensive discussions in the literature about the mechanisms of physical stabilization, including reduction in the thermodynamic driving force towards crystallization, increase in crystallization energy barrier, disruption/formation of molecular interactions, and combinations of these factors.[58] Regardless of the specific mechanism, it is generally agreed that molecular-level miscibility is necessary to achieve maximum stabilization.[59, 60] Immiscibility between the drug and polymer has been reported to have led to increased crystallization rates of amorphous drugs.[61, 62] Herein, the

---

This chapter is adapted with permission from Yuan, X.; Sperger, D.; Munson, E. J. Investigating miscibility and molecular mobility of nifedipine-PVP amorphous solid dispersions using solid-state NMR spectroscopy *Mol. Pharmaceutics* 2014, 11, 329– 337.

term miscibility describes a single-phase amorphous system in which the API is supersaturated in the polymer and the components are intimately mixed at the molecular level. The API is not necessarily at its equilibrium solubility in the polymer.[62]

Currently, the most common method to determine whether the API and polymer are miscible is by measuring the glass transition temperature (T_g) of the mixture using differential scanning calorimetry (DSC). A miscible system is characterized by a single glass transition temperature intermediate between those of the API and polymer, as opposed to two separate glass transition temperatures in a phase-separated system. However, it has been reported in the literature that it is possible to observe a single T_g in a phase-separated system [28, 29] and vice versa.[63] In addition, Raman mapping has been used to access phase homogeneity of amorphous solid dispersions.[29] The method, however, is limited by the low spatial resolution as the step size is typically on the micron scale. Thus, a mixture that appears to be homogeneous using one technique may be found heterogeneous using another technique with a finer detection limit. For example, when T_g is used to assess miscibility, a detection limit of about 20 to 30 nm is generally assumed and domain sizes smaller than that are indistinguishable by DSC.[48-50] Thus, a method to accurately measure the miscibility between the API and polymer at smaller domain sizes is of great importance to advance our understanding of drug-polymer mixing.

There are many examples in the literature of polymer blends where the length scale of polymer mixing can be measured via solid-state NMR (SSNMR) ^1H T_1 and $T_{1\rho}$ relaxation times.[64, 65] If the polymer chains are closer to each other than the length scale of proton spin diffusion, magnetization transfer from the slower to the faster relaxing chains is very effective, and the relaxation times of both chains are equal to a weighted

average of the values of the individual chains.[46] The length scale of spin diffusion L is given by

$$\langle L \rangle = \sqrt{6Dt} \qquad (3.1)$$

where D is the spin diffusion coefficient and t is the relaxation time. Typically, D is assumed to be 10^{-12} cm^2/s.[46, 66] For a typical spin-lattice relaxation time T_1 value between 1 and 5 s, the length scale of spin diffusion corresponds to ca. 20 to 50 nm. For a typical $T_{1\rho}$ value between 5 and 50 ms, the length scale corresponds to ca. 2 to 5 nm. Depending on the domain size, the following three scenarios can be expected: 1) If the domain size is smaller than 2-5 nm, a common ^1H $T_{1\rho}$ and T_1 values should be obtained from the API and polymer; 2) If the domain size is between the 5 nm and 20 nm range, the $T_{1\rho}$ values will be different for API and polymer but the T_1 will still be the same; 3) If the domain size is larger than 20-50 nm, both $T_{1\rho}$ and T_1 values will be different for API and polymer.

In recent years, SSNMR has been used to study miscibility of drug and polymer in amorphous solid dispersions. Aso and coworkers studied miscibility of nifedipine and PVP using ^1H NMR relaxation measurements and found that all three tested compositions (3:7, 5:5 and 7:3 by weight) were miscible based on the free induction decay (FID) pattern of $T_{1\rho}$ measurements [66] Vogt and coworkers studied several amorphous solid dispersion systems using 2D SSNMR heteronuclear correlation (HETCOR) experiments and demonstrated the feasibility of using SSNMR techniques to detect phase separation and molecular interactions in amorphous solid dispersions.[67] Very recently, Van den Mooter and coworkers studied a hot melt-extruded miconazole and PEG-g-PVA mixture and found that miconazole (10 wt%) was molecularly dispersed in PEG-g-PVA with an

average cluster size of 1.6 nm.[68] However, in-depth research on miscibility of drugs and polymers across a large composition range is still lacking and is the focus of this study.

Nifedipine, a dihydropyridine calcium channel blocker is often used as a model compound to study the stability of amorphous drugs.[69, 70] Polyvinylpyrrolidone (PVP), a common pharmaceutical excipient has been used to form amorphous solid dispersions with nifedipine.[66, 71, 72] It has been reported that nifedipine and PVP formed molecular level dispersions based on the detection of hydrogen bonding between the drug and the polymer.[72] In this study, we used ^{13}C SSNMR to evaluate the miscibility of nifedipine-PVP amorphous solid dispersions of different compositions. The effect of different preparation methods on miscibility was also investigated.

3.2 Materials and Matheods

3.2.1 Materials

Nifedipine (NIF, minimum purity 98.0 %) was purchased from TCI America (Portland, OR) and was protected from light whenever possible. Poly(vinylpyrrolidone), (PVP, Kollidon 25, M_w=28-34 kg/mole) was obtained from BASF (Edison, NJ). PVP was vacuum dried at 70 °C over night and stored over Drierite™ at all times. The chemical structures of nifedipine and PVP are shown in Figure 3.1.

3.2.2 Preparation of Amorphous Nifedipine

Amorphous nifedipine was prepared by melting the drug in a Teflon beaker in an oven at 180 °C for 10 minutes. The melt was then quench-cooled on a piece of cold metal block. The resulting sample was lightly ground in a mortar and pestle.

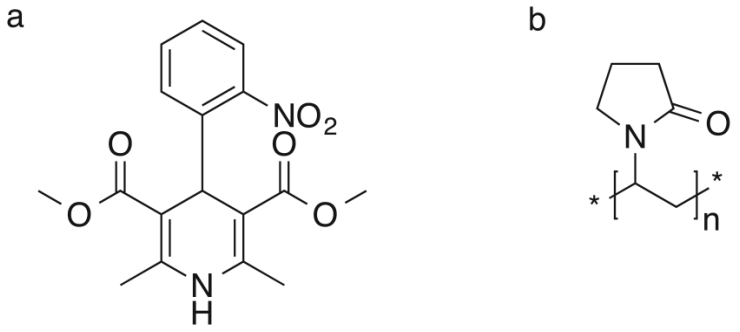

Figure 3.1. Chemical structures of (a) nifedipine and (b) PVP.

3.2.3 Preparation of Physical Mixture

A physical mixture of amorphous nifedipine (prepared by melt quenching as described above) and PVP was prepared at a 50:50 ratio (w:w) by mixing in a Turbula Shaker-Mixer (Glen Mills Inc, Clifton, NJ) at 49 rpm for 30 minutes.

3.2.4 Preparation of Amorphous Solid Dispersions

Amorphous solid dispersions of nifedipine and PVP were prepared in three different ways: melt quenching in the lab setting, spray drying, and melt quenching in an NMR rotor while spinning. Amorphous dispersions at ratios of 95:5, 90:10, 75:25, 60:40 and 50:50 nifedipine:PVP (w:w) were prepared by melt quenching in the lab setting. To prepare the amorphous dispersions via this method, mixtures of drug and polymer were ball milled for 10 minutes to obtain optimum mixing. The ball-milled mixtures were then transferred into an oven and heated at 180 °C for 30 minutes. The melted mixtures were

then quench-cooled on a piece of cold metal block to solidify. The solid dispersions were vacuum dried at room temperature over night to minimize residual moisture. All solid dispersions were confirmed amorphous by polarized light microscopy. No chemical degradation of nifedipine was observed by ^{1}H NMR in solutions of DMSO-d_6.

A 90:10 (w:w) nifedipine:PVP amorphous dispersion was prepared by melt quenching in an NMR rotor while spinning. To prepare amorphous dispersions via this method, an appropriate mixture of drug and polymer was ball milled for 10 minutes to obtain optimum mixing. The ball-milled mixture was then transferred into a 7.5 mm zirconia NMR rotor with Teflon end caps. The rotor was heated in the NMR probe equipped with a variable-temperature accessory stack (Varian, Palo Alto, CA) at 180 °C for 30 minutes while spinning at 4000 Hz. The rotor was then rapidly cooled to room temperature, resulting in the amorphous dispersion.

A 90:10 (w:w) nifedipine:PVP amorphous dispersion was also prepared by spray drying using a Büchi Mini Spray Dryer B-290 (Büchi, Switzerland) equipped with a 0.7 mm nozzle. Compressed nitrogen gas was used for atomization at a flow rate of 10 L/min. The drug and polymer were dissolved in methanol to form a solution with a total solid concentration of 13 mg/mL. The feed rate was set at 22.5 mL/min. The inlet temperature was set at 120 °C and the corresponding outlet temperature was 49 °C. All amorphous dispersions were stored in glass vials over Drierite™ in the freezer when not being analyzed.

3.2.5 Modulated DSC

The glass transition temperature (T_g) of nifedipine–PVP solid dispersions was determined by modulated DSC (MDSC) using a Q2000 differential scanning calorimeter equipped with an RCS90 refrigerated cooling system (TA Instruments, Newcastle, DE). Nitrogen gas was used as the purge gas at a flow rate of 50 mL/min. Temperature and enthalpy were calibrated using indium. Samples (2-5 mg) prepared by melt quenching as described above were placed in TZero™aluminum pans and sealed with TZero™aluminum hermetic lids with one pinhole (TA Instruments, New Castle, DE). Samples were equilibrated at 0°C, and then heated at 1°C/min to 200°C with an amplitude of ±0.5 °C and a modulation period of 60 s. The glass transition was separated into the reversing heat flow signal and was determined by half height at midpoint using the Universal Analysis software (TA Instruments, Newcastle, DE).

3.2.6 Solid-State NMR ^{1}H T_1 and $T_{1\rho}$ Relaxation Measurements

All solid-state NMR spectra were acquired using a Tecmag Redstone HF3 2RX spectrometer (Tecmag, Inc., Houston, TX) operating at 75.48 MHz for ^{13}C (7 Tesla static magnetic field). Samples were packed into 7.5 mm zirconia rotors and sealed with Teflon or Kel-F end caps (Revolution NMR, LLC, Fort Collins, CO). Experiments were performed using a 7.5 mm double-resonance MAS probe (Varian, Palo Alto, CA). All ^{13}C spectra were acquired under magic angle spinning (MAS) [43] at 4 kHz, using ramped-amplitude CP,[45] total sideband suppression (TOSS) [44] and SPINAL64 decoupling [73] with a ^{1}H decoupling field of about 62 kHz. A 2 ms contact time was used in all experiments. 3-Methylglutaric acid was used to optimize spectrometer settings and as an external

standard, with the methyl peak referenced to 18.84 ppm.[74] All experiments were conducted at room temperature if not otherwise specified.

^{1}H T_1 relaxation values were measured using the saturation-recovery experiment through ^{13}C observation. The reason to observe ^{13}C is to provide information on the relaxation behavior of the protons that belong to each of the individual compounds. A 90° pulse width of about 4 μs was used in the experiment. In the Fourier-transformed spectrum, the peak of interest was integrated and plotted against recovery delay times and the values were fitted to the following equation using GraphPad Prism (GraphPad Software, Inc., La Jolla, CA)

$$M = M_0 \cdot (1 - e^{-\frac{\tau}{T_1}}) \quad (3.2)$$

where M is the integrated signal intensity and τ is the recovery delay time. M_0 is an amplitude parameter obtained from the fit and T_1 is the obtained spin-lattice relaxation time.

^{1}H $T_{1\rho}$ relaxation times were measured by varying the spin-lock duration time following a 90° pulse. A recycle delay of about 1.5 – 2 times the measured T_1 was used to maximize the signal to noise ratio. A frequency field of about 65 KHz was used for the spin-lock field. The peak of interest was integrated and plotted against the spin-lock duration times and the values were fitted to the following equation using GraphPad Prism (GraphPad Software, Inc., La Jolla, CA)

$$M = M_0 \cdot e^{-\frac{\tau}{T_{1\rho}}} \quad (3.3)$$

where M is the integrated signal intensity and τ is the spin-lock duration time. M_0 is an amplitude parameter obtained from the fit and $T_{1\rho}$ is the obtained spin-lattice relaxation time in the rotating frame.

3.3 Results

3.3.1 Modulated DSC

Figure 3.2a shows the MDSC thermograms of NIF, PVP and five compositions of NIF:PVP amorphous solid dispersions (95:5, 90:10, 75:25, 60:40, 50:50) made by melt quenching in the lab setting. Only the reversing heat flow is plotted to show the glass transition event. NIF showed a T_g at 42 °C and a recrystallization event at 78 °C, followed by melting at 172 °C. The 95:5 and 90:10 dispersions showed similar thermal events, with T_g, recrystallization and melting all being observed. The thermogram of the 75:25 dispersion was different from the previous three thermograms in that there was no observable change in the heat capacity above T_g. A small melting peak was observed at 168 °C. The 60:40 and 50:50 dispersions showed no change of heat capacity or melting peaks above T_g. All five compositions showed single T_g values which was in agreement with previous reports.[72] Figure 3.2b shows the MDSC reversing signal of 90:10 NIF:PVP (w:w) dispersions prepared by all three methods (spray drying, melt quenching in the NMR rotor during spinning, and melt quenching in the lab). A single T_g was observed in all three samples and the thermal events were consistent with each other. As expected, two separate T_g events were observed for the 50:50 NIF:PVP physical mixture, corresponding to the respective glass transition temperatures of the drug and the polymer (data not shown).

The Gordon-Taylor equation can be used to estimate the T_g of an ideal binary mixture,[27]

$$T_g = \frac{w_1 T_{g1} + k w_2 T_{g2}}{w_1 + k w_2} \quad (3.4)$$

where w_1 and w_2 are the weight fractions of each component, and T_{g1} and T_{g2} are the glass transition temperatures of each component. The value k can be estimated by Equation 3.5,

$$k \approx \frac{\rho_1 T_{g1}}{\rho_2 T_{g2}} \tag{3.5}$$

where ρ_1 and ρ_2 are the densities of each component. The predicted T_g values are plotted with the experimental T_g values in Figure 3.3. Also shown in Figure 3.3 are the T_g values obtained by two other preparation methods at the 90:10 NIF:PVP (w:w) ratio. As shown in the figure, the experimental T_g values agree reasonably well with the Gordon-Taylor prediction. The small deviation may be due to the presence of a small amount of water or less than ideal mixing between the two components.

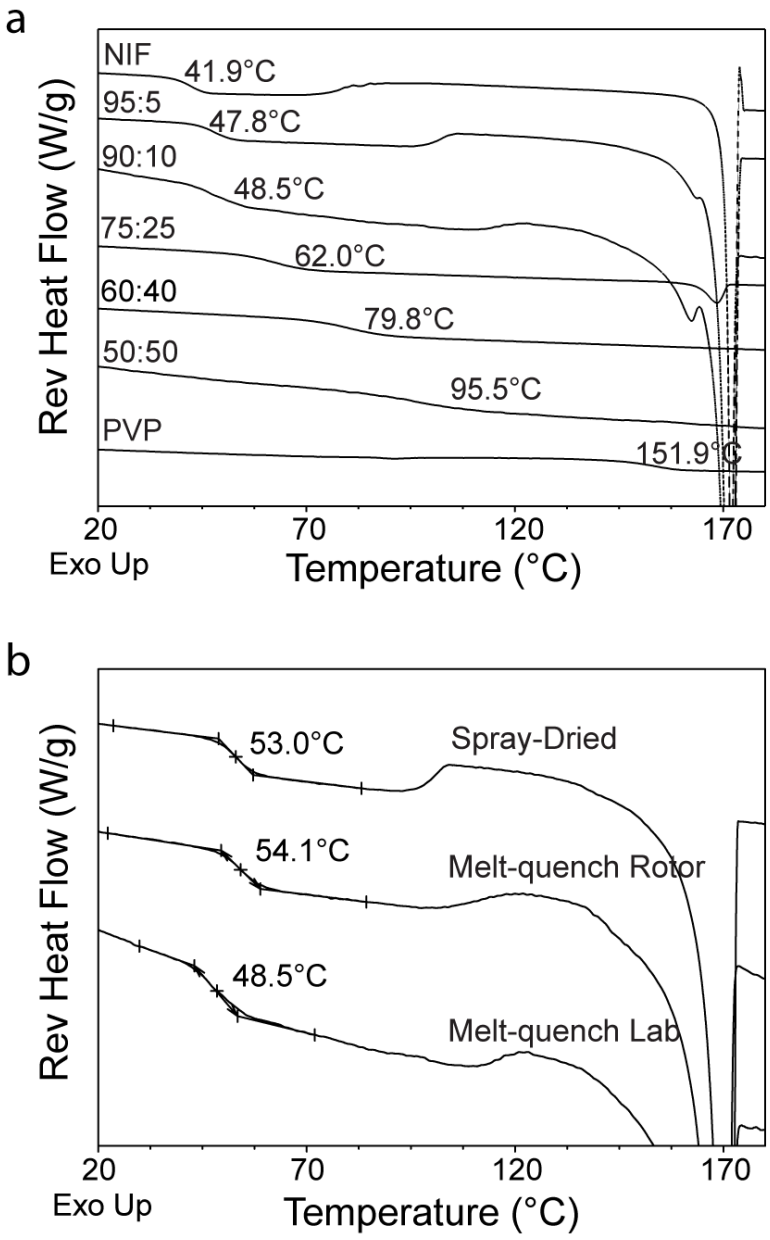

Figure 3.2. MDSC of (a) NIF, PVP and NIF:PVP amorphous solid dispersions of various weight ratios and (b) 90:10 NIF:PVP amorphous solid dispersions prepared by three different methods. The T_g values represent the half-height midpoint values.

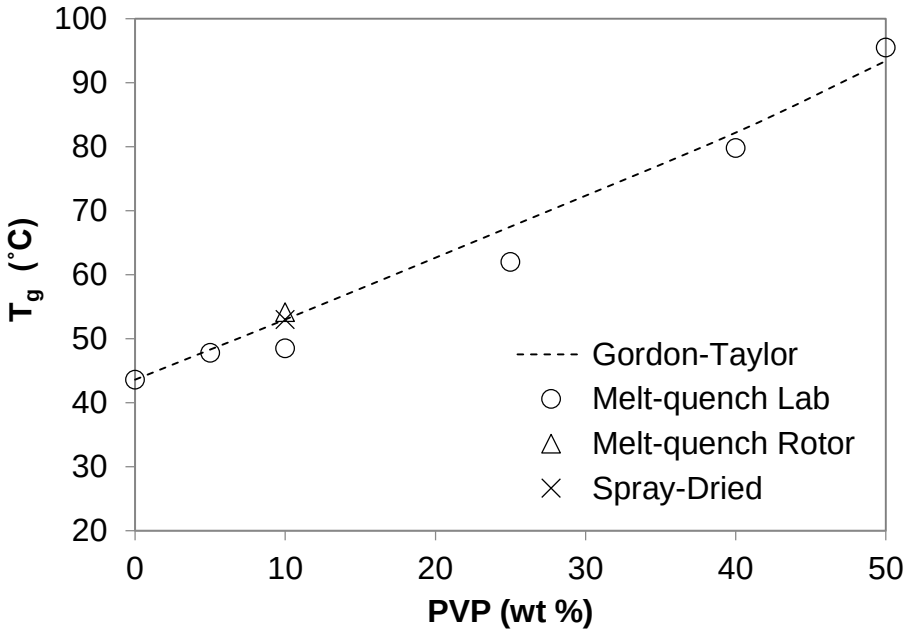

Figure 3.3. Glass transition temperatures of NIF:PVP amorphous solid dispersions. The circles represent the samples made by melt quenching in the lab setting; the triangle represents the sample made by melt quenching in the NMR rotor; the cross represents the sample made by spray drying; the dashed line represents the prediction from the Gordon-Taylor equation. All experimental T_g values are half-height midpoint T_g values.

3.3.2 Solid-State ^{13}C NMR of Nifedipine

^{13}C CPMAS NMR spectra of two crystalline forms, α and β, and the amorphous form of nifedipine are shown in Figure 3.4. The spectrum of the α form shows narrow peaks ($\Delta\nu_{1/2}$ = 28 Hz). There is one peak for each carbon indicating there is one molecule in each asymmetric unit in the crystalline structure. The peaks between 144 and 150 ppm showed splitting due to coupling to ^{14}N. The peaks have been previously assigned by Apperley et al.[75] The spectrum of the β form showed two peaks for most carbons, indicating there are two molecules in an asymmetric crystalline unit. This agrees with the crystalline structure of β nifedipine recently solved by Yu and co-workers.[76] The line width of β nifedipine was larger than α ($\Delta\nu_{1/2}$ ~ 60 Hz). Amorphous nifedipine had much broader peaks than both crystalline forms ($\Delta\nu_{1/2}$ ~ 215 Hz). The broader lines are the result of a wide range of molecular conformations that exist in the amorphous state. Amorphous nifedipine crystallizes to the β form at temperatures below 42 °C.[76] The β form shown in Figure 4b was obtained by storing the sample over Drierite^{TM} at 40 °C for four days. However, a minute amount of α form was also present, indicated by the shoulders around 19.7 and 170.5 ppm. For all three spectra, the crystalline peaks overlapped to a large degree with the amorphous peaks, making the identification of crystalline and amorphous fractions difficult.

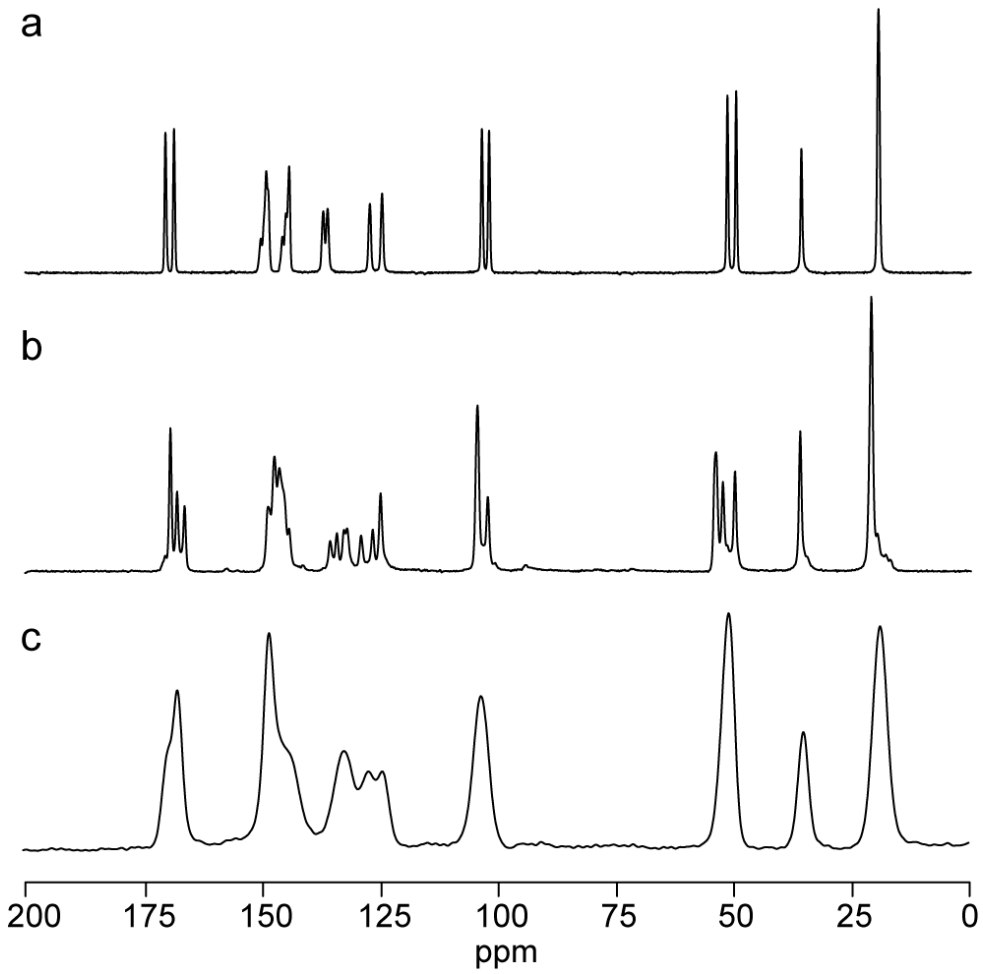

Figure 3.4. ^{13}C SSNMR spectra of (a) α crystalline nifedipine, (b) β crystalline nifedipine and (c) amorphous nifedipine.

3.3.3 Miscibility by SSNMR of Samples Prepared by Melt quenching in the Lab Setting

The ^{1}H T_1 and $T_{1\rho}$ relaxation times of the α and β forms of crystalline nifedipine and amorphous nifedipine are shown in Table 3.1. As seen in the table, the α form had the longest T_1 and $T_{1\rho}$ relaxation times. The β form had shorter relaxation times than the α form, while the amorphous form had the shortest relaxation times of all the nifedipine samples. SSNMR relaxation times are usually a reflection of mobility in the solid state and are generally influenced by structural rigidity, the number of existing 'relaxation sinks' (i.e. methyl or ethyl groups), and the presence of moisture.[77, 78] Since both crystalline forms of nifedipine are packed into crystal lattices with fixed structures, they are much more rigid than the amorphous form, which can adopt a range of molecular conformations. As a result, amorphous nifedipine exhibited the shortest relaxation times, as expected. Among the two crystalline forms of nifedipine, the α form has been shown to be the stable polymorph,[76, 79] which in this case coincided with the relaxation time measurements.

Also shown in Table 3.1 are the relaxation times of the two components present in the 50:50 NIF:PVP physical mixture in the amorphous state. As evident in the table, nifedipine had different relaxation times than PVP in both ^{1}H T_1 and $T_{1\rho}$ measurements. The relaxation times of nifedipine and PVP in the physical mixture were similar to the values measured in their pure forms. These results showed that the physical mixture of nifedipine and PVP was not homogeneous on the molecular level.

Because the relaxation times are very sensitive to small changes in water content, the differences in the relaxation times between nifedipine and PVP were compared, rather

than their absolute values. Ideally, relaxation time is a weighted arithmetic mean of the two components in a miscible system. However, water is known to decrease the relaxation time if present in a system.[78]

^{13}C SSNMR spectra of NIF-PVP amorphous solid dispersions prepared by melt quenching in the lab setting are shown in Figure 3.5. All the spectra had broad peaks, consistent with the amorphous nature of the samples. For pure amorphous nifedipine (or PVP), a single proton relaxation time (T_1 and $T_{1\rho}$) was observed regardless of the resonances used for the integration, as expected due to rapid proton spin diffusion in the solid state. Thus, any peak from one component that does not overlap with peaks from the other component can be used to calculate the relaxation times of the component of interest in the solid dispersion. Thus, the peaks around 175 and 43 ppm were chosen to calculate the relaxation times of PVP because there was no interference from nifedipine peaks in the same region. Likewise, the peaks at approximately 167, 148 and 103 ppm were chosen for nifedipine because they do not overlap with peaks from PVP.

The ^1H T_1 and $T_{1\rho}$ relaxation times of nifedipine and PVP in the amorphous solid dispersions prepared by melt quenching in the lab setting are shown in Table 3.2, and the differences of the relaxation times between nifedipine and PVP are plotted in Figure 3.6. There were no obvious differences in ^1H T_1 values between nifedipine and PVP in the amorphous solid dispersions except for the 95:5 NIF:PVP composition. As shown in Figure 3.6a, no obvious trend could be seen in the plot of ^1H T_1 differentials. The similar ^1H T_1 relaxation times indicated that nifedipine and PVP were miscible on the 20-50 nm length scale. This was consistent with modulated DSC measurements that showed single T_g values for these samples, since DSC generally assumes a distinguishable domain size

of 30 nm.[28] The 95:5 and 90:10 NIF:PVP compositions were on the borderline of being miscible as the confidence intervals did not or barely touched the zero horizontal line. It is interesting that the 95:5 and 90:10 compositions were the two that showed the large recrystallization peaks in the DSC.

^{1}H $T_{1\rho}$ relaxation times, on the other hand, were different for the drug and polymer for the 95:5 and 90:10 compositions. There was also a clear trend of decreasing differentials with increasing PVP content, as shown in Figure 3.6b. The ^{1}H $T_{1\rho}$ relaxation times indicated that the compositions with 25%, 40% and 50% PVP were miscible on the 2-5 nm length scale. The combination of ^{1}H T_1 and ^{1}H $T_{1\rho}$ relaxation times indicated that the two compositions with higher drug loadings were immiscible on the 2-5 nm length scale and might be borderline miscible on the 20-50 nm length scale. The three compositions with lower drug loadings were miscible on the 2-5 nm length scale. The biggest domain size was estimated to be 4.5 nm for those three miscible compositions using Equation 3.1 with a ^{1}H $T_{1\rho}$ value of 35 ms. D was assumed to be 10^{-12} cm^2/s.[46]

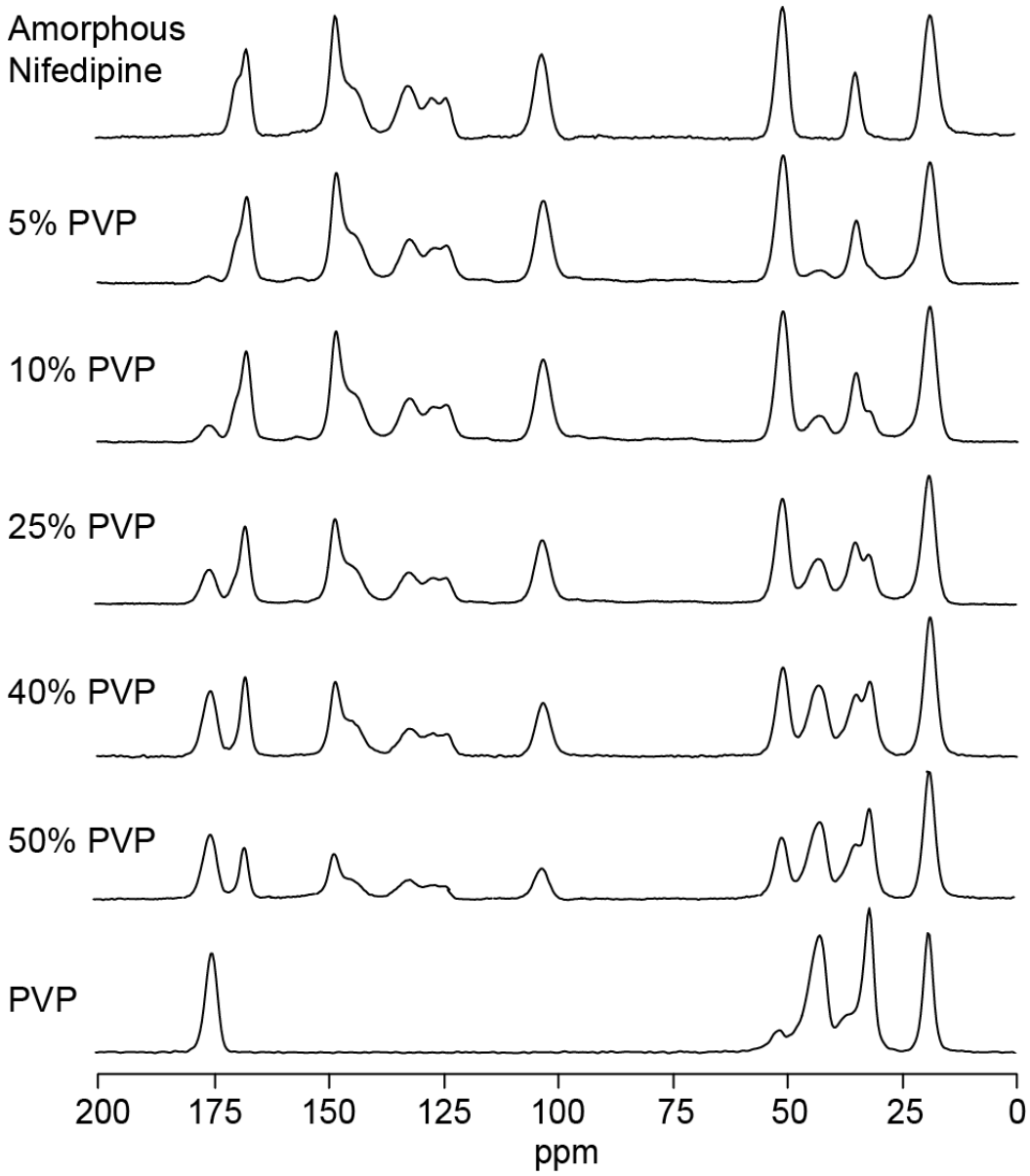

Figure 3.5. ^{13}C SSNMR spectra of NIF-PVP amorphous solid dispersions prepared by melt quenching in the lab setting containing 0, 5, 10, 25, 40, 50 and 100% PVP (from top to bottom).

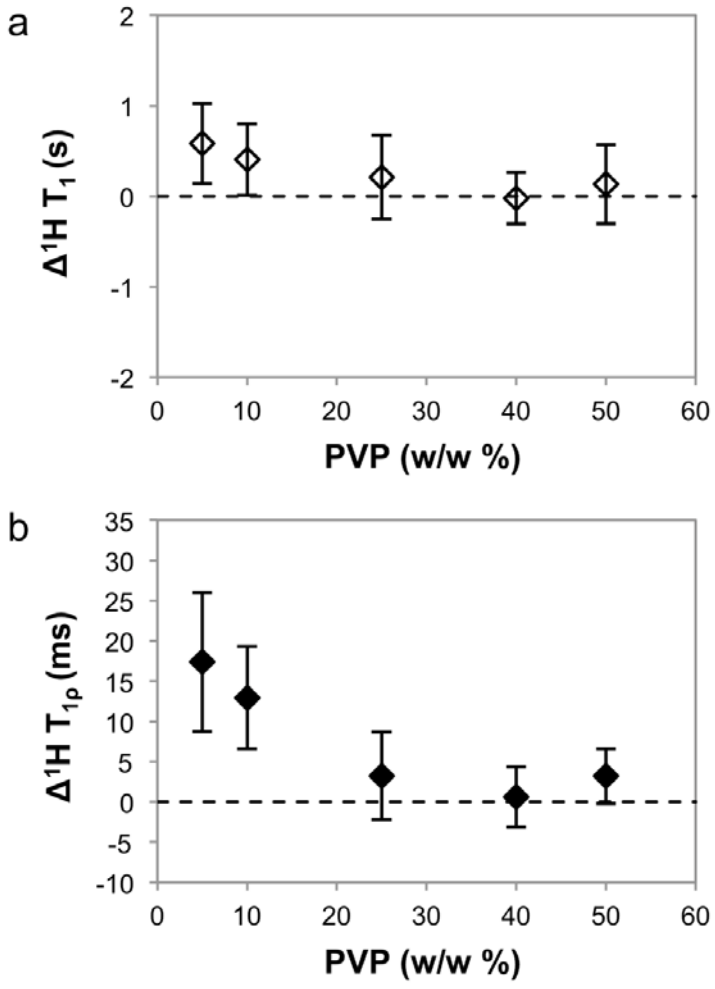

Figure 3.6. (a) ^{1}H T_1 and (b) $T_{1\rho}$ differential between nifedipine and PVP in the amorphous solid dispersions prepared by melt quenching in the lab setting as a function of PVP content. The error bars represent 95% confidence intervals associated with the fit. Dashed lines represent the zero value.

Table 3.1. ^{1}H T_1 and $T_{1\rho}$ relaxation times of different forms of NIF, PVP and the 50:50 NIF:PVP physical mixture (PM). The numbers in parentheses indicate the standard errors associated with the fits.

	Nifedipine			PVP	50:50 NIF:PVP PM	
	α	β	Amorphous		NIF	PVP
^{1}H T_1 (s)	32.4 (0.5)	13.0 (0.4)	4.2 (0.1)	2.1 (0.04)	3.6 (0.07)	2.1 (0.04)
^{1}H $T_{1\rho}$ (ms)	287 (6)	190 (6)	79.3 (0.1)	27.3 (0.3)	88 (3.5)	16.0 (0.4)

Table 3.2. Comparison of the measured ^{1}H T_1 and $T_{1\rho}$ values for NIF:PVP amorphous solid dispersions made by melt quenching in the lab setting. The numbers in parentheses indicate the standard errors associated with the fits.

		NIF:PVP Amorphous Solid Dispersions				
		95:5	90:10	75:25	60:40	50:50
^{1}H T_1 (s)	Nifedipine	4.4 (0.03)	4.4 (0.05)	4.3 (0.2)	4.0 (0.08)	3.7 (0.2)
	PVP	3.8 (0.2)	4.0 (0.2)	4.2 (0.2)	4.0 (0.09)	3.6 (0.2)
^{1}H $T_{1\rho}$ (ms)	Nifedipine	94 (2.0)	65 (1.6)	80 (3.1)	42 (0.7)	37 (0.8)
	PVP	77 (3.1)	52 (2.3)	73 (1.9)	41 (1.5)	34 (1.2)

3.3.4 Miscibility by SSNMR of Samples Prepared by Other Methods

^{1}H T_1 and $T_{1\rho}$ values were also obtained for the 90:10 NIF:PVP amorphous solid dispersions prepared by two other methods: spray drying, and melt quenching in the NMR rotor while spinning. The results are shown in Table 3.3. The ^{1}H $T_{1\rho}$ values suggested that the dispersions made by spray drying and melt quenching in the NMR rotor during spinning were miscible while the dispersion made by simple melt quenching in the lab setting was not. The ^{1}H $T_{1\rho}$ values of the dispersion made by melt quenching in the NMR rotor were large compared to the values of the other two dispersions. This is due to the dryness of the sample prepared in this method as the sample was heated to high temperatures while being subjected to a dry environment due to the spinning gas (dewpoint of -40 ° C). Likewise, the short relaxation times observed for the spray-dried sample were attributed to residual solvent acting as relaxation sinks which led to short relaxation times.

Table 3.3. Comparison of the measured ^{1}H T_1 and $T_{1\rho}$ values for 90:10 NIF:PVP amorphous solid dispersions made by melt quenching in the lab setting (MQ), spray drying (SD) and melt quenching in the NMR rotor while spinning (MIR). The numbers in parentheses indicate the standard errors associated with fits.

	90:10 NIF:PVP Amorphous Solid Dispersions			
		MQ	SD	MIR
^{1}H T_1 (s)	Nifedipine	4.4 (0.05)	3.4 (0.07)	4.5 (0.06)
	PVP	4.0 (0.2)	3.4 (0.2)	4.3 (0.1)
^{1}H $T_{1\rho}$ (ms)	Nifedipine	65 (1.6)	34 (0.3)	123 (5.4)
	PVP	52 (2.3)	31 (1.6)	123 (5.4)

3.4 Discussion

3.4.1 Miscibility of Nifedipine and PVP

Taylor and co-workers reported that spin-coated films of nifedipine and PVP can form molecular level dispersions over all compositions based on IR detection of drug-polymer hydrogen bonding involving the nifedipine NH moiety.[72] Taylor and coworkers have also calculated the interaction parameter (χ) between nifedipine and PVP (K12) to be -3.8 using a melting point depression method.[59] The fairly large negative value indicated mixing was favored; however, the result obtained through this method only applied to temperatures close to the melting temperature of the drug. This has apparently limited its practical usage, as storage temperatures are typically much lower than the

melting point of the drug and the phase behavior of the drug-polymer mixture could be different at different temperatures.

Hydrogen bonding between nifedipine and PVP has also been studied by Aso and Yoshioka using ^{13}C NMR spin-lattice (T_1) relaxation times.[71] It was found that the T_1 of both PVP (carbonyl carbon) and nifedipine (dihydropyridine ring carbon adjacent to nitrogen) increased in the solid dispersion compared to the polymer or drug alone. The result suggested reduced motions of these functional groups, which were ascribed to hydrogen bonding between the PVP carbonyl and nifedipine NH. Interestingly, the increase of T_1 for nifedipine carbons plateaued at about 40% (w:w) PVP, coinciding with the level of PVP necessary to make miscible dispersions in the present work. It was also found that the chemical shift of PVP carbonyl carbon increased by about 1 ppm as the drug content increased,[71] which is usually an indication of hydrogen bond formation. In the present SSNMR spectra, we also observed about a 1 ppm downfield chemical shift change of the carbonyl carbon of PVP between neat PVP (175.1 ppm) and the dispersion with up to 95% nifedipine (175.9 ppm) (Table 3.4). The similar chemical shift change observed in this study indicates that the extent of hydrogen bonding interactions in these dispersion samples was similar to the samples prepared by Aso and Yoshioka, which in turn suggests that the existence of hydrogen bonds alone was not enough to demonstrate complete miscibility. It is likely that in the high drug content dispersions, some population of the drug was hydrogen bonded with PVP, thus being molecularly dispersed, while the rest of the drug formed small clusters of roughly 5-20 nm in size.

Table 3.4. Chemical shift of the carbonyl carbon of PVP in various NIF:PVP amorphous solid dispersions of different compositions.

NIF:PVP Dispersion	ppm
Neat PVP	175.1
50:50	175.4
60:40	175.6
75:25	175.7
90:10	175.8
95:5	175.9

Hydrogen bonding at the nifedipine NH was also probed using ^{15}N solid-state NMR CPMAS. However, no significant change in chemical shift was found among crystalline NIF, amorphous NIF and the dispersions. It has been reported in the case of acetaminophen-PVP amorphous dispersions that ^{14}N SSNMR showed differences in chemical shift between neat drug and dispersions, while ^{15}N SSNMR did not show any difference in chemical shift.[80] This finding suggests that ^{14}N chemical shift is more sensitive to hydrogen bonding interactions than ^{15}N in some cases and that same ^{15}N chemical shifts may be the same for different hydrogen bonding interactions. Since ^{14}N is a quadrupolar nucleus with complicated lineshapes, we are currently exploring the feasibility of performing ^{14}N SSNMR on these systems.

3.4.2 Effect of Preparation Methods on Miscibility

In this study the main focus was to investigate the melt-quench mixtures prepared as might be done in a laboratory setting. Because the melting point of crystalline nifedipine was 173 °C and the T_g of PVP was around 160 °C, it was determined that heating a ball milled mixture of crystalline nifedipine and PVP to 180 °C for 30 minutes would result in a uniformly mixed melt. Because PVP was still very viscous at 180 °C, the concern at higher PVP concentrations was that the drug would not adequately diffuse into PVP, and so a low limit of 50% drug was used for this study.

It was found in this study that 95:5 and 90:10 NIF:PVP dispersions prepared by melt quenching in the lab setting were not intimately mixed at the molecular level. However, 90:10 NIF:PVP dispersions prepared by the other two methods, spray drying and melt quenching in the NMR rotor during spinning, produced miscible systems as indicated by the common ^1H $T_{1\rho}$ relaxation times. The DSC thermograms of both dispersions showed recrystallization peaks between 100-115 °C, similar to the recrystallization behavior of the 90:10 dispersion made by melt quenching in the lab setting.

It is known that preparation methods affect the crystallization tendency of amorphous state materials. Strachan and coworkers compared amorphous indomethacin prepared by melt quenching, spray drying, ball-milling and cryo-milling and found differences in the recrystallization rates among the samples.[81] Our study demonstrated that on a molecular level, the ability to form a miscible amorphous solid dispersion depended on the preparation method. It is likely that the 90:10 solid dispersion made by

melt quenching in the lab setting will phase separate and thus crystallize over time faster than the other two dispersions of the same composition but prepared differently.

3.5 Conclusions

NIF and PVP amorphous solid dispersions prepared by three different methods were studied using SSNMR ^{1}H relaxation time measurements. The 95:5 and 90:10 NIF:PVP dispersions prepared by melt quenching in the typical lab setting were found to be immiscible on the molecular level. Contrary to previous reports that NIF and PVP can form miscible solid dispersions at all compositions, only the 75:25, 60:40 and 50:50 dispersions were shown to be homogeneous with a domain size of about 4.5 nm using the above-mentioned preparation method. 90:10 NIF:PVP amorphous dispersions prepared by spray drying and melt quenching in the NMR rotor with spinning appeared to be miscible by relaxation measurements. These results demonstrated that different preparation methods could lead to amorphous systems with different phase homogeneities undetected by common techniques such as DSC.

Chapter 4. Hydrogen Bonding Interactions of Amorphous Indomethacin and its Amorphous Solid Dispersions

4.1 Introduction

The amorphous form of an active pharmaceutical ingredient (API) has been used as a strategy to enhance the oral bioavailability of poorly water-soluble compounds, as the amorphous API has a higher apparent solubility and faster dissolution rate than its crystalline counterpart.[8, 55] However, the amorphous API also has a higher free energy and could convert to the thermodynamically more stable crystalline state. To minimize the possibility of crystallization, a polymer is usually mixed with the amorphous API to form an amorphous solid dispersion, which has been shown to significantly delay the onset of crystallization.[30, 56, 57] Hydrogen bond (HB) formation between the API and the polymer is often thought to play a significant role in reducing the tendency of amorphous drugs to crystallize.[31, 82]

The predominant technique used to identify the existence of hydrogen bonds between the API and the polymer has been FT-IR.[31, 72, 82, 83] Taylor and Zografi detected the interaction between the carboxylic acid moiety of indomethacin and PVP using FT-IR.[82] With the same technique, Marsac and others identified the presence of hydrogen bonds between the drugs nifedipine, felodipine and the polymer PVP in amorphous solid dispersions.[72]

High resolution ^{13}C solid-state NMR has also been used to investigate hydrogen bonding interactions in the solid state.[84] Miyoshi and others found three types of

carboxylic acid groups in blends of poly(acrylic acid) (PAA) and poly(ethylene oxide) (PEO). They were assigned to: 1) those forming interpolymer hydrogen bonds between PAA and PEO, 2) those forming hydrogen bonded PAA dimers, and 3) those not forming hydrogen bonds.[85, 86]

In addition to experimental methods, molecular dynamics (MD) simulations have been used to study hydrogen bonding interactions in amorphous systems.[87, 88] Xiang and Anderson probed the structural properties of amorphous drug indomethacin (IMC) using MD simulations.[87] They reported that approximately 79% of simulated IMC formed at least one hydrogen bond and 21% was hydrogen bond free.[87] The authors also performed MD simulations on amorphous IMC-PVP glasses and found that the overall hydrogen bonding capability of IMC was not substantially altered in the presence of PVP.[88] HBs between IMC molecules decreased with the addition of PVP and the loss of HBs between IMC molecules was compensated by the formation of HBs between IMC and PVP.[88]

Despite the vast number of reports on hydrogen bonding interactions between amorphous drugs and polymers studied using IR spectroscopy, no experiments, to the best of our knowledge, have successfully dealt with the question of how *much* of an amorphous drug is hydrogen bonded with a polymer excipient at a given composition. In this chapter, a novel approach is described to identify and quantify the various hydrogen bonding interactions in the amorphous drug indomethacin and in its amorphous solid dispersions with PVP and PVP/VA using ^{13}C solid-state NMR spectroscopy. The method employed single-site ^{13}C isotopic labeling and spectral subtraction. The quantitative information obtained from this study was compared with results from MD simulations reported in the literature. These experiments for the first time quantified hydrogen

bonding interactions in amorphous indomethacin systems. This approach may be useful in understanding the role of intermolecular drug-excipient interactions on the physical stability of amorphous formulations.

4.2 Materials and Methods

4.2.1 Materials

Indomethacin (γ form, minimum purity 99%) was purchased from Sigma-Aldrich (St Louis, MO). ^{13}C isotopically labeled indomethacin (99% ^{13}C at the carboxylic acid carbon) was custom synthesized by Chemtos (Austin, TX). Indomethacin α form was prepared by precipitation from ethanol solution using deionized water as described by Kaneniwa et al.[89] Polystyrene (average M_w=35 kg/mole) was purchased from Sigma-Aldrich (St Louis, MO). PVP (Kollidon® 25, M_w=28-34 kg/mole) and PVP/VA (Kollidon® VA 64, Mw=45-70 kg/mole) were obtained from BASF (Edison, NJ). PVP and PVP/VA were vacuum dried at 70 °C overnight and stored over Drierite™ at all times. The chemical structure of indomethacin, PVP, PVP/VA and polystyrene are shown in Figure 4.1.

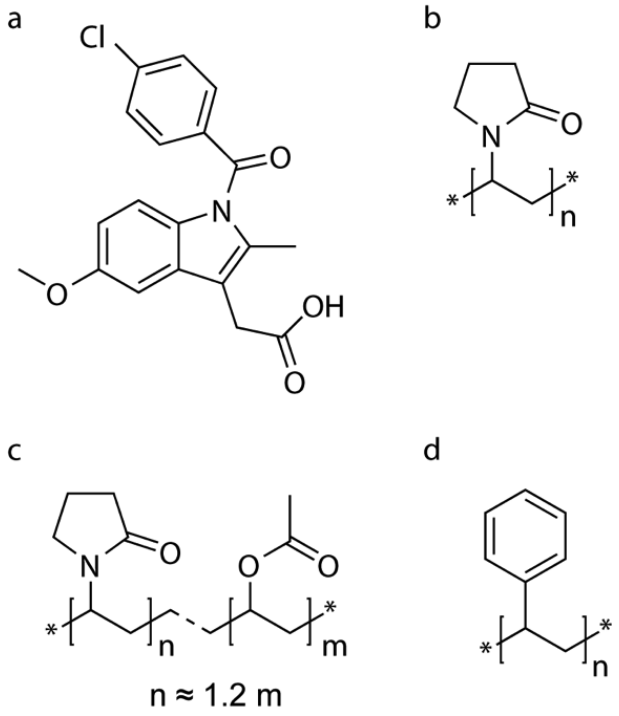

Figure 4.1. Chemical structures of (a) indomethacin, (b) PVP, (c) PVP/VA, and (d) polystyrene.

4.2.2 Preparation of Amorphous Indomethacin

Amorphous indomethacin samples were prepared by *in situ* melt quenching in the spinning NMR rotor. Both natural abundance and ^{13}C isotopically enriched indomethacin (5% wt ^{13}C-labeled and 95% wt unlabeled) samples were prepared. Samples were packed into 7.5 mm zirconia NMR rotors with Teflon or Kel-F end caps (Revolution NMR, LLC, For Collins, CO). The rotors were heated in the NMR probe equipped with a variable-temperature accessory stack (Varian, Palo Alto, CA) at 170 °C for approximately 10 minutes while spinning at 4 kHz. The rotors were then rapidly cooled to room temperature (over approximately 10 min), resulting in the solidified glasses.

4.2.3 Preparation of Amorphous Solid Dispersions

IMC-PVP and IMC-PVP/VA amorphous solid dispersions were prepared by cryomilling followed by *in situ* melt quenching in spinning NMR rotors. Samples of both natural abundance and ^{13}C isotopically enriched indomethacin (3% wt ^{13}C-labeled and 97% wt unlabeled at the carboxylic acid carbon) were prepared. One gram samples at drug:polymer weight ratios ranging from 9:1 to 1:1 were cryomilled at 10 Hz (SPEX SamplePrep 6770 Freezer/Mill, SPEX SamplePrep LLC., Metuchen, NJ) for five cycles, each consisting of 2 minutes of milling and 2 minutes of cooling. Liquid nitrogen was used as a coolant. The cryomilling procedure was used to ensure optimum mixing of the drug and polymer prior to melting. The mixtures were then transferred into 7.5 mm zirconia NMR rotors with Teflon or Kel-F end caps (Revolution NMR, LLC, Fort Collins, CO). The top end cap had a small hole to allow moisture to evaporate during heating. The rotors were heated in the NMR probe at 170 °C for approximately 10

minutes while spinning at 4 kHz and then rapidly cooled to room temperature, resulting in the amorphous solid dispersions.

IMC-polystyrene amorphous solid dispersions were also prepared with low percentages of IMC (0.2%, 1%, 2% and 5%) that was ^{13}C labeled at the carboxylic acid carbon. These amorphous solid dispersions were made by solvent evaporation using a Büchi Rotavapor R-215 (Büchi, Switzerland). The drug and polymer were dissolved in methylene chloride and the solvent was rotary evaporated at 35 °C. The obtained solids were subsequently vacuum dried at room temperature overnight to remove residual solvent.

4.2.4 Solid-State NMR Experiments

All solid-state NMR spectra were acquired using a Tecmag Redstone HF3 2RX spectrometer (Tecmag, Inc., Houston, TX) operating at 75.48 MHz for ^{13}C. Experiments were performed using a 7.5 mm double-resonance MAS probe (Varian, Palo Alto, CA). All ^{13}C spectra were acquired under magic angle spinning (MAS)[43] at 4 kHz if not otherwise specified, using ramped-amplitude cross polarization,[45] total sideband suppression (TOSS)[44] and SPINAL64 decoupling[73] with a ^{1}H decoupling field of about 62 kHz. A 2 ms contact time and a pulse delay of 5 s were used in all experiments. A total of 512 points were acquired with a spectral width of 15 kHz. 3-Methylglutaric acid was used to optimize spectrometer settings and as an external standard, with the methyl peak referenced to 18.84 ppm.[74] All experiments were conducted at 20 °C if not otherwise specified. The data were zero-filled to 4096 points with no line-broadening. Spectra in the region of 160-190 ppm were fitted by Gaussian functions using MATLAB

(MathWorks, Natick, MA). The details of the fitting procedure are explained in the results section.

The spectra of IMC-polystyrene (PS) amorphous solid dispersions were acquired using MAS of 5.2 kHz to avoid residual spinning sideband overlap. The spectra of an amorphous solid dispersion of 1% IMC in PS were also collected as a function of temperature using a variable-temperature accessory stack (Varian, Palo Alto, CA). Lead nitrate was used to calibrate the temperature and a linear slope of 0.73 was obtained for the plot of the chemical shift change versus temperature in the range between -30 and 200 °C, agreeing well with values reported in the literature.[90] Samples were equilibrated at each temperature for at least 15 min before data acquisition. At temperatures above 100 °C, direct polarization was used to acquire the spectra because cross-polarization efficiency was greatly reduced in the highly mobile environment.

For chemical shift anisotropy tensor analysis, the samples were spun at a low speed of 1.5 kHz to generate spinning sideband patterns. Both natural abundance and ^{13}C labeled samples of each composition were used and spectral subtraction was applied to obtain the signal of the carboxylic acid carbon. The subtracted spectra were deconvoluted using TNMR (Tecmag, Inc., Houston, TX) and the peaks of interest were analyzed using the Herzfeld-Berger approach[91] with the software HBA.[92] For the IMC-PS amorphous solid dispersion, a dipolar-decoupled sequence was used to suppress polystyrene aromatic and -CH_2 peaks. Since the carboxylic acid peaks in the spectrum did not overlap, the intensity was used to calculate the tensor elements.

4.3 Results and Discussion

4.3.1 ^{13}C Solid-State NMR of Indomethacin

^{13}C CPMAS spectra of two crystalline forms, γ and α, and the amorphous form of indomethacin are shown in Figure 4.2. The spectrum of the γ polymorph shows narrow peaks ($\Delta\nu_{1/2}$ = 80 Hz for the methyl carbon). There is one peak for each carbon, indicating there is one molecule in an asymmetric crystalline unit, which is consistent with the solved structure of the γ polymorph.[93] The spectrum of the α polymorph shows three peaks for most carbons, indicating there are three molecules in an asymmetric crystalline unit. This also agrees with the crystalline structure of the α polymorph solved by Chen and others.[94] The line width of the methyl carbon is approximately 40 Hz for the α polymorph. The peaks of both polymorphs have been previously assigned.[75, 95] Amorphous indomethacin has much broader peaks than both crystalline forms ($\Delta\nu_{1/2}$ = 400 Hz for the methyl carbon).

Figure 4.3 shows the carbonyl region of the three different forms of indomethacin. γ indomethacin (Figure 4.3a) consists of cyclic dimers between carboxylic acid groups of two indomethacin molecules.[93] The most downfield peak at 179.2 ppm corresponds to the hydrogen-bonded carboxylic acid carbon. The peak at 167.6 ppm corresponds to the amide carbon, which is not involved in hydrogen bonding. α indomethacin (Figure 4.3b) consists of two types of hydrogen bonds, with three crystallographically inequivalent molecules per unit cell.[94] This gives rise to three peaks for each carbonyl carbon and a total of six peaks in the carbonyl region. The peaks at 181.4 and 179.9 ppm correspond to the carboxylic acid groups of two of the three molecules that form hydrogen bonded dimers, similar to what exists in γ indomethacin. The peak at 172.3 ppm corresponds to

the carboxylic acid of the third molecule that is hydrogen bonded to one of the amide carbonyls of the dimer. This assignment was confirmed by an experiment using α indomethacin that was ^{13}C isotopically labeled at the carboxylic acid carbon. The peak at 170.9 ppm probably corresponds to the aforementioned amide carbonyl in the dimer that is hydrogen bonded to the carboxylic acid group. Finally, the two peaks at 166.6 and 167.1 ppm probably correspond to the two non-hydrogen bonded amide carbonyls. The peak at 167.1 ppm appears as a shoulder which is presumably due to imperfect crystallization. It was seen as a more defined peak in another report.[96] Amorphous indomethacin (Figure 4.3c) shows very broad peaks in the carbonyl region and the peak locations seem to be a combination of γ and α forms. However, the exact correlation between the peaks and carbons is not obvious. A potential mixture of different carboxyl species might exist due to hydrogen bonding interactions,[85, 86] which complicates the spectrum.

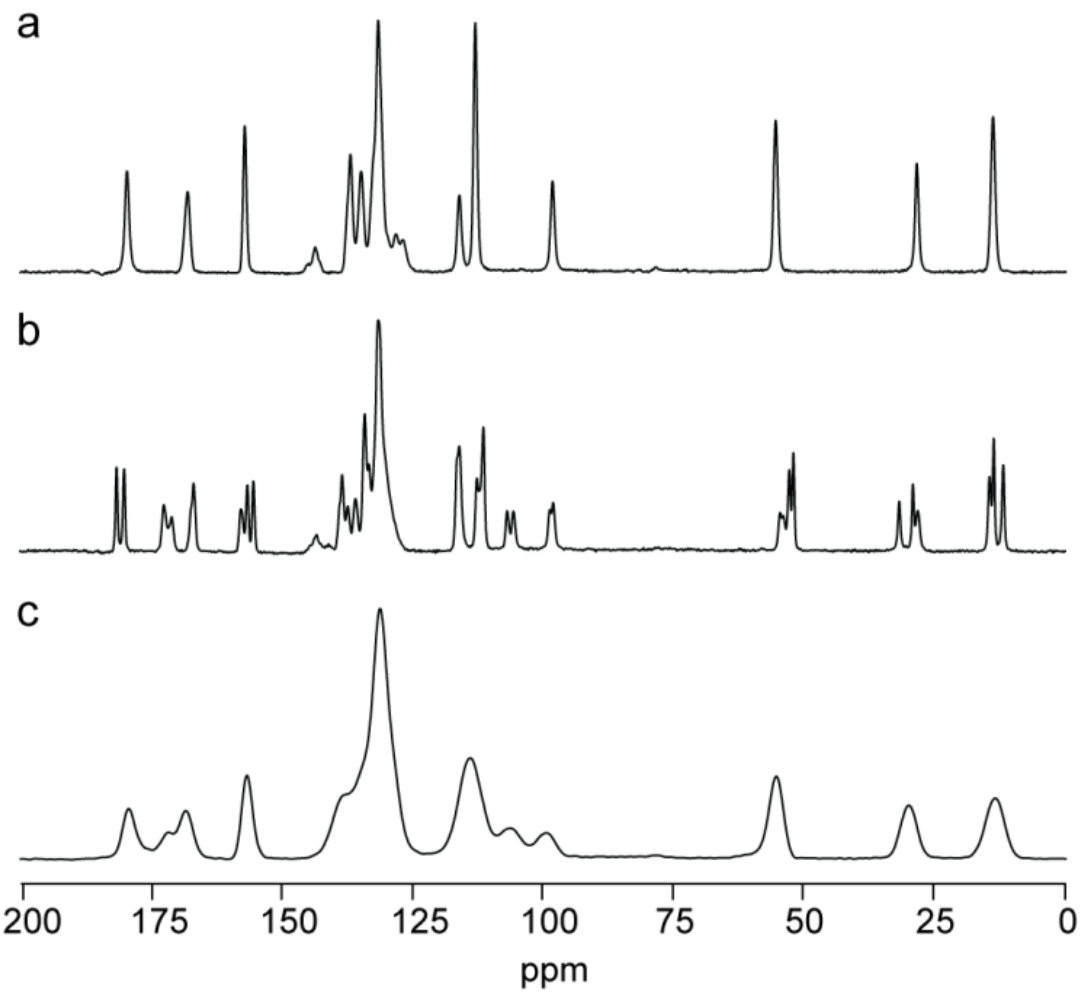

Figure 4.2. ^{13}C SSNMR spectra of (a) γ crystalline indomethacin, (b) α crystalline indomethacin, and (c) amorphous indomethacin.

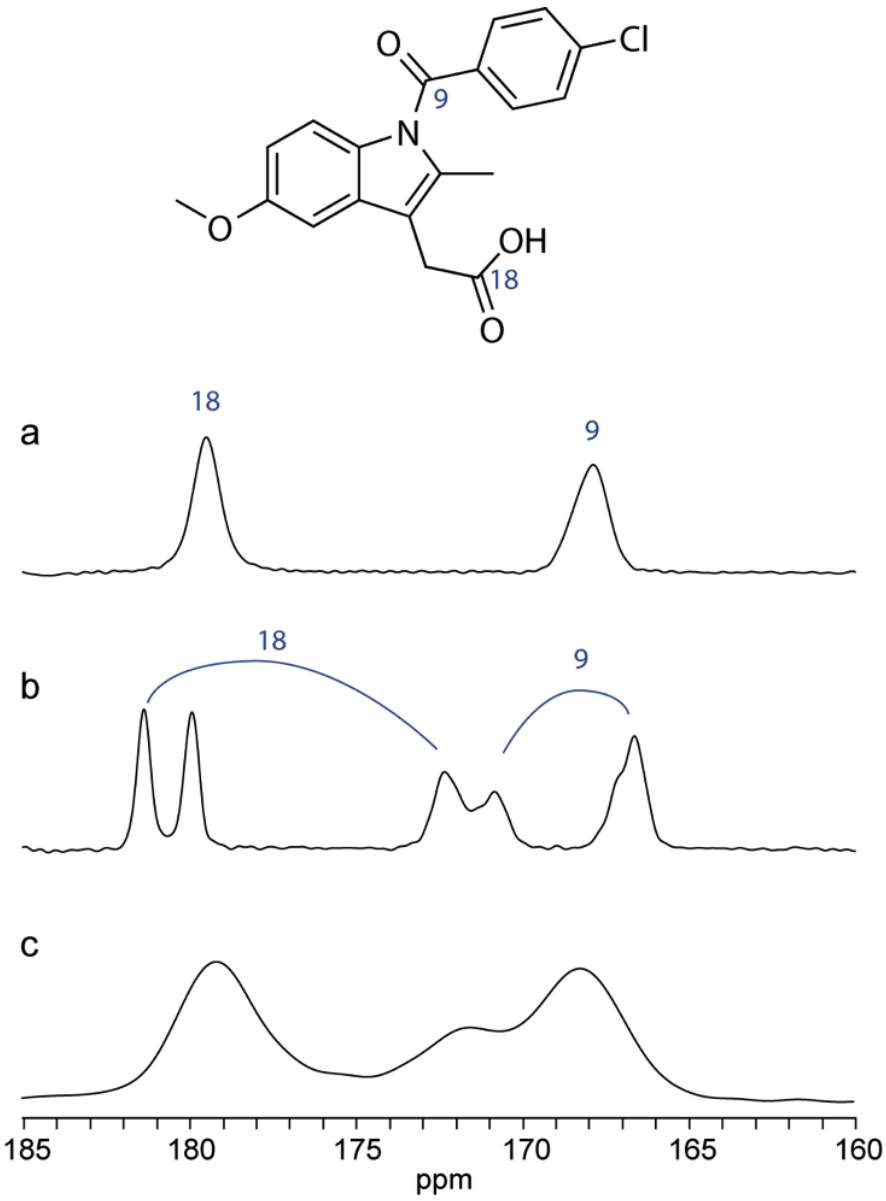

Figure 4.3. Carbonyl region of ^{13}C SSNMR spectra of (a) γ crystalline indomethacin, (b) α crystalline indomethacin, and (c) amorphous indomethacin.

4.3.2 Hydrogen Bonding Interactions of Amorphous Indomethacin

Indomethacin ^{13}C isotopically labeled at the carboxyl carbon was used at a 5% level to study the hydrogen bonding interactions of amorphous indomethacin. The method was used by Munson and co-workers to study stereo-defects in polylactide.[97] Figure 4.4 illustrates this process. Figure 4.4a shows the spectrum of ^{13}C labeled amorphous indomethacin. Because the labeling is at only one specific carbon, the carboxyl carbon, the signal of that carbon was significantly enhanced while the signals of all other carbons were essentially unaltered. The greater intensity between 180 and 170 ppm is the result of the isotopic labeling. Figure 4.4b shows the spectrum of the natural abundance (i.e. unlabeled) amorphous indomethacin. The unlabeled spectrum was subtracted from the labeled spectrum while maintaining the same signal intensity for the aromatic and aliphatic carbon regions of the two spectra (160-0 ppm region). The end result is a spectrum that only contains the carboxylic acid carbon, as shown in Figure 4.4c.

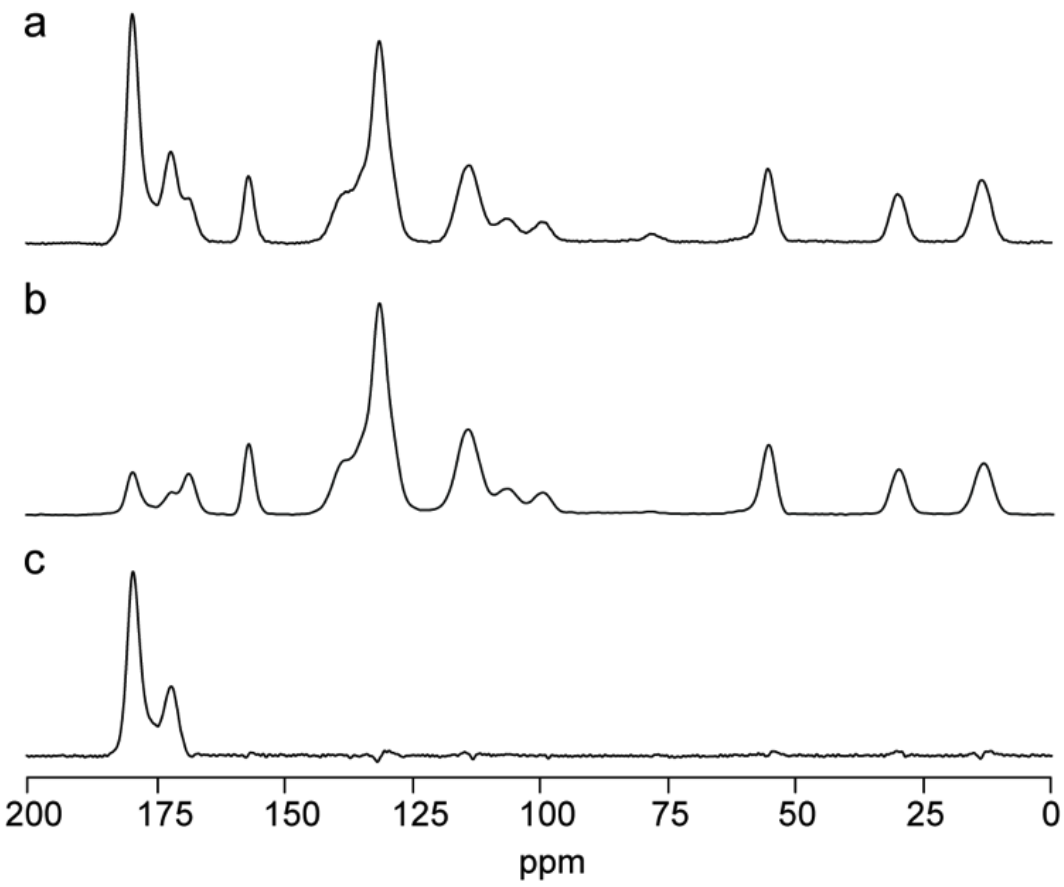

Figure 4.4. ^{13}C SSNMR spectra of (a) ^{13}C labeled amorphous indomethacin, (b) natural abundance amorphous indomethacin, and (c) carboxyl carbon of amorphous indomethacin.

The spectrum of the carboxyl carbon after the subtraction contains two clear peaks, with a potential third peak in the middle, as shown in Figure 4.5. The downfield (high ppm) peak with the highest intensity was assigned to the cyclic dimer, due to its similar chemical shift compared to the same type of hydrogen bond that exists in the crystalline forms. The upfield (low ppm) peak was assigned to the carboxylic acid carbon hydrogen bonded to the amide carbonyl, due to its relatively similar chemical shift compared to the same type of hydrogen bond that exists in the α form. However, it is more difficult to assign the peak with the lowest intensity in the middle. The literature seems to be divided on the assignment of this peak. Miyoshi et al. observed three peaks for the carboxylic acid carbon in the PAA/PEO polymer complex and assigned the peak in the center to the free carboxyl group that formed no particular hydrogen bonds.[85, 86] Recently, however, Fortier-McGill et al. studied PMAA complexes with a series of polymers and attributed the resonance in the middle to disordered carboxylic acid chains through ^{1}H double-quantum MAS NMR.[98, 99]

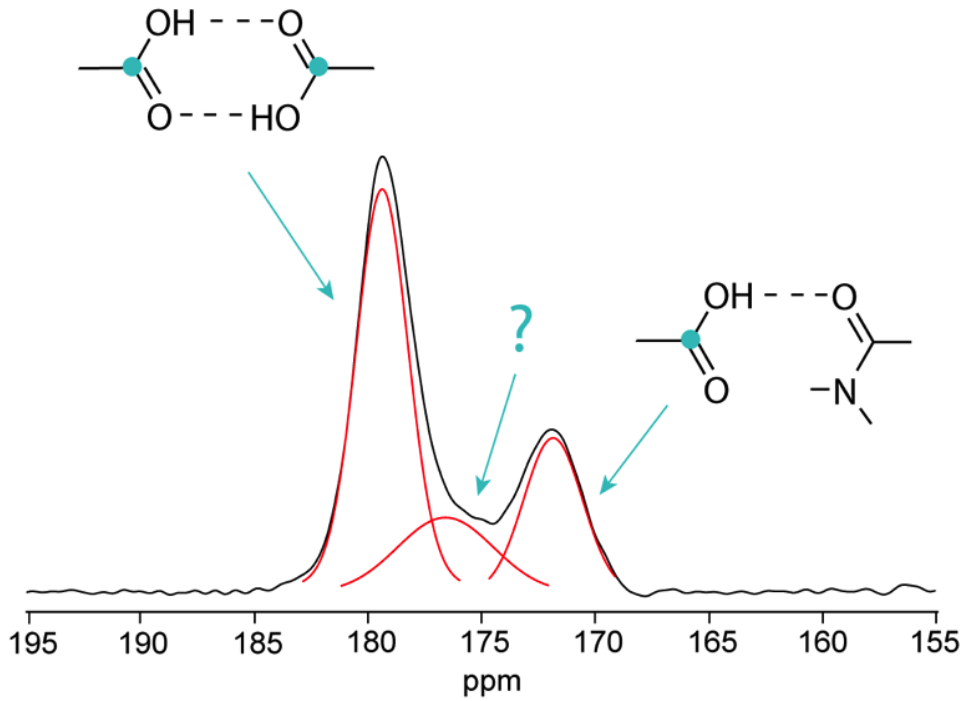

Figure 4.5. CPMAS ^{13}C spectrum of the carboxylic acid of amorphous indomethacin. Simulated peaks are shown in red to illustrate the potential species. The carbons highlighted in teal correspond to the carbons in carboxyl groups that are involved in hydrogen bonds.

Several experiments were conducted using polystyrene to assist in assigning the peak in the center. Polystyrene is a suitable polymer for this purpose because it can form an amorphous solid dispersion with indomethacin, yet it has little capability to form a substantial hydrogen bond with the drug. At sufficiently low concentrations of indomethacin, some percentage of the indomethacin is likely to be hydrogen-bond free. Figure 4.6 shows the carboxylic acid region of the ^{13}C CPMAS spectrum of 1% indomethacin in an amorphous solid dispersion with polystyrene prepared via solvent evaporation. Since the indomethacin is labeled at the carboxylic acid carbon, the signals from other indomethacin carbons are non-observable due to the low concentration of indomethacin. There are two peaks present in the spectrum in Figure 4.6, one at 179.4 ppm and the other at 170.3 ppm. The peak at 179.4 ppm agrees well with the chemical shift of the dimer shown in Figure 4.5. The other peak, however, has a chemical shift of 170.3 ppm, significantly different from the upfield resonance in Figure 5 (171.8 ppm). This suggests that this peak at 170.3 ppm could be a different species and may be the free carboxylic acid of indomethacin. The broad center resonance in Figure 4.5 could represent disordered hydrogen bonded chains that are absent when indomethacin concentration is very low (Figure 4.6). Herein we define disordered chains as carboxylic acid chains having various lengths. Chain ends may be included, as suggested by Fortier-McGill et al.[98, 99] and possibly rings larger than dimers could be formed between carboxylic acids. After cryogrinding, the dispersion showed a decreased intensity of the peak at 179.4 ppm compared to the peak at 170.3 ppm (spectrum shown in red). This observation also agrees with the assignment of the 170.3 ppm peak as the free carboxylic acid as cryogrinding is known to break down molecular interactions and introduce

disorder into the system.[51, 100] Consequently, the fraction of free IMC is expected to increase compared to the dimeric form.

To further confirm our assignments, amorphous solid dispersions with 5%, 2% and 0.2% indomethacin in polystyrene were investigated. The spectra are shown in Figure 4.7. It is immediately obvious that the ratio between the two resonances at 179.4 and 170.3 ppm decreased as IMC concentration decreased. This observation supports the idea that the resonance at 170.3 ppm is associated with the free carboxylic acid of indomethacin because more free indomethacin molecules are expected on dilution.

Variable-temperature solid-state NMR was also used to investigate the temperature-dependent behavior of the dispersion. The 1 % indomethacin and polystyrene amorphous solid dispersion was heated from 20 to 160 °C, and a spectrum was recorded at each temperature as shown in Figure 4.8. It is anticipated that the ratio between the carboxylic acid dimer and the free carboxylic acid should decrease as the temperature increases because of the negative enthalpy for hydrogen bond formation, at least at temperatures close to and above the glass transition temperature, such that equilibrium can be achieved. Indeed, this is what is seen in Figure 4.9, which shows the ratio between the carboxylic acid dimer and the free carboxylic acid as a function of temperature. As illustrated by the figure, the ratio between the two species decreases as the temperature increases, further confirming our assignment of the peak at 170.3 ppm as the free carboxylic acid of IMC.

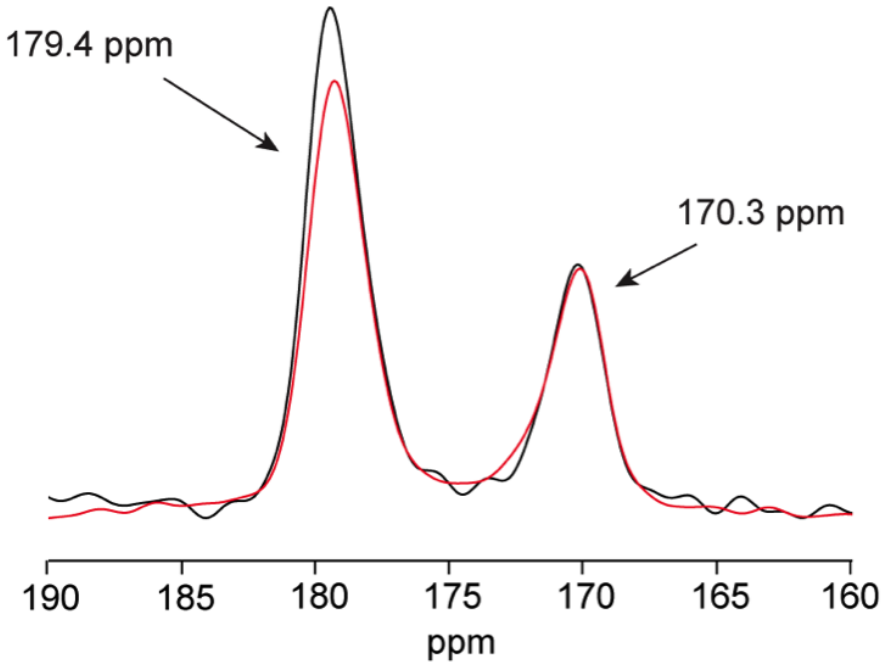

Figure 4.6. ^{13}C CPMAS spectrum of the carboxylic acid region of 1% indomethacin in polystyrene. The spectrum in red is obtained from the sample after cryogrinding.

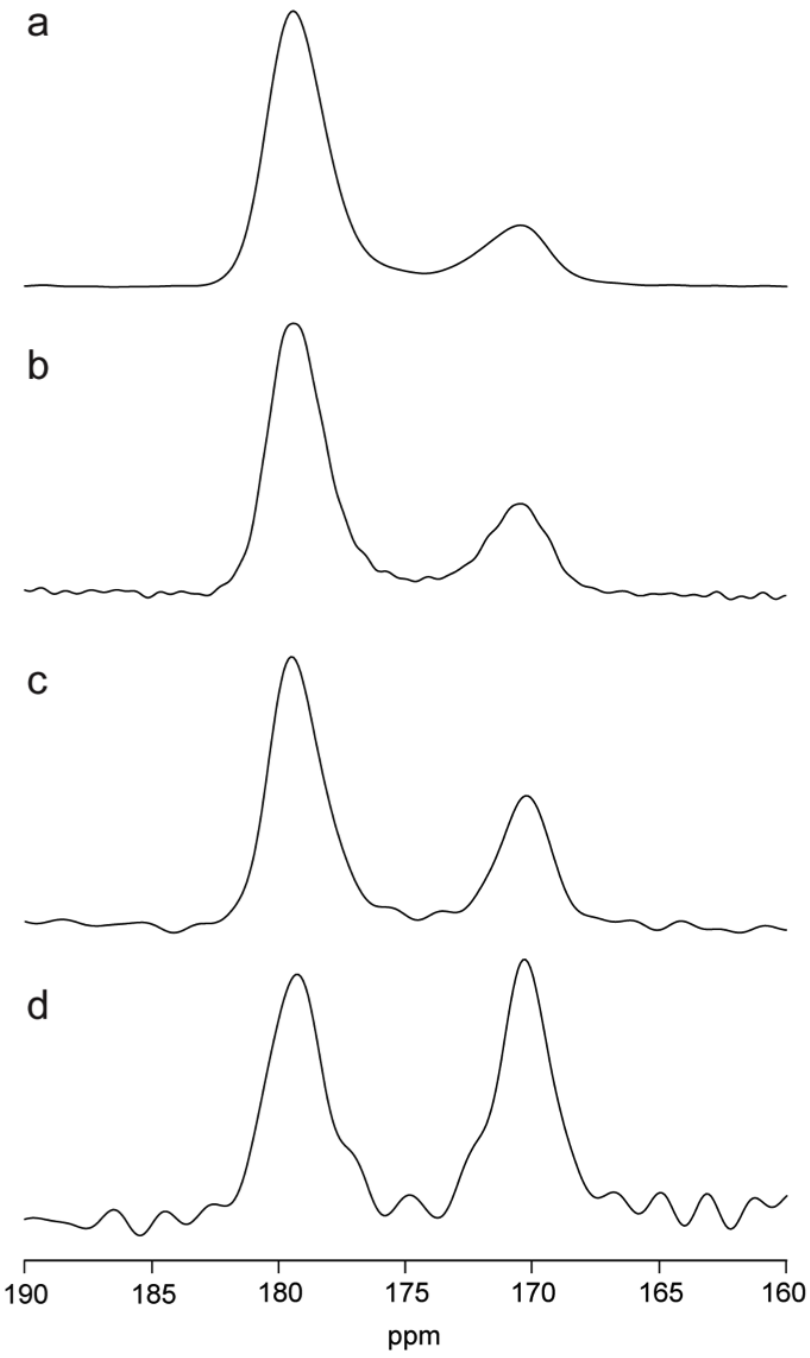

Figure 4.7. ^{13}C CPMAS spectra of the carboxylic acid region of (a) 5% indomethacin, (b) 2% indomethacin, (c) 1% indomethacin, and (d) 0.2% indomethacin in amorphous solid dispersions with polystyrene.

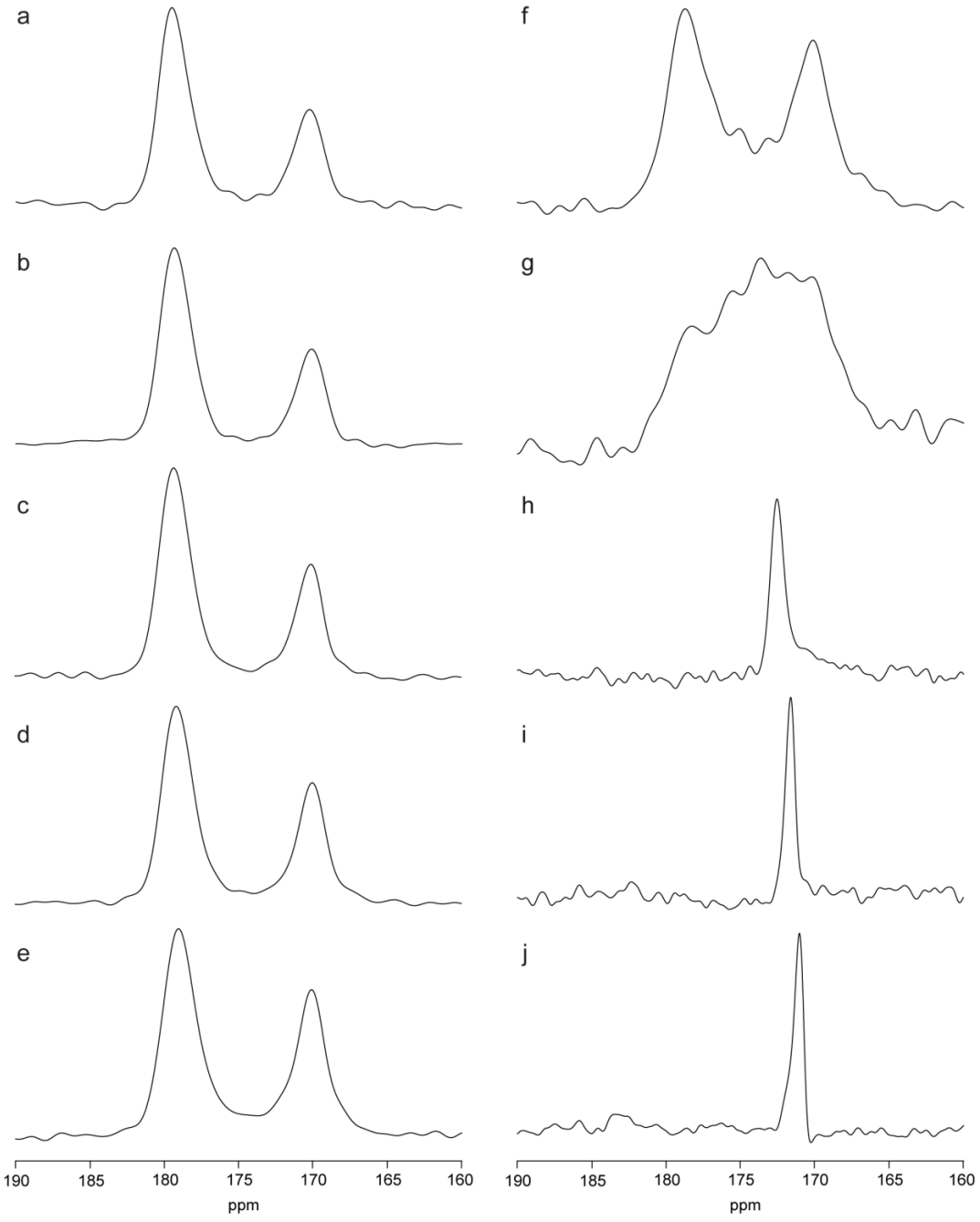

Figure 4.8. ^{13}C spectra of the carboxylic acid carbon of 1% amorphous indomethacin in polystyrene at (a) 20 °C, (b) 30 °C, (c) 40 °C, (d) 50 °C, (e) 60 °C, (f) 70 °C, (g) 80 °C, (h) 110 °C, (i) 140 °C, and (j) 160 °C. Spectra a-g were collected by cross polarization. Spectra h-j were collected by direct polarization.

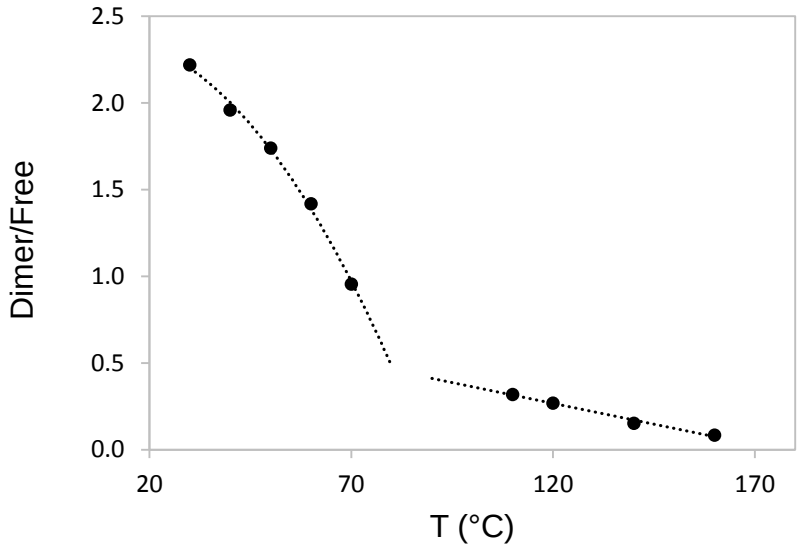

Figure 4.9. Peak area ratio between the carboxylic acid dimer and the free carboxylic acid as a function of temperature. Lines were drawn as a guide to the eye.

Based on this information, four species may contribute to the spectrum in Figure 4.5, namely the carboxylic acid cyclic dimer, disordered carboxylic acid chains, the carboxylic acid-amide hydrogen bonded complex, and the free carboxylic acid. To increase the confidence in spectral deconvolution, the IMC spectrum was fitted together with the spectra of IMC-polymer amorphous solid dispersions. The details will be discussed in the next section. The fitted spectrum and the fitting parameters are shown in Figure 4.10 and Table 4.1, respectively. From the deconvolution we can see that the majority of the IMC molecules appear to be hydrogen bonded through either carboxylic acid cyclic dimers (59%) or carboxylic acid chains (15%). In addition, 19% of molecules are hydrogen-bonded through carboxylic acid-amide interactions. The remaining 7% of molecules are not hydrogen bonded.

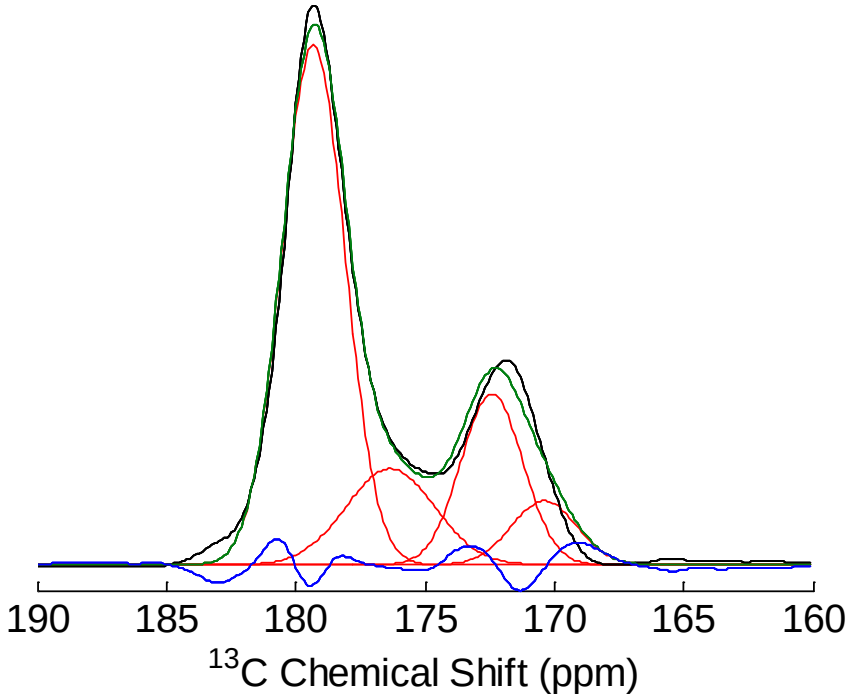

Figure 4.10. Deconvolution of the CPMAS ^{13}C spectrum of the carboxylic acid carbon of amorphous indomethacin. The experimental spectrum is shown in black; the fitting of the individual species are shown in red; the sum of the species contributions is shown in green; the residual difference between the experimental and fitted peaks is shown in blue.

Table 4.1. The fitting parameters for the deconvolution of ^{13}C SSNMR spectrum of amorphous indomethacin. [a]

Chemical Shift (ppm)	Species	Peak Area (%)	Linewidth (Hz)
179.3 ± 0.006	cyclic dimer	58.5 ± 0.5	216 ± 0.8
176.3 ± 0.02	carboxylic acid chain	15.2 ± 0.4	303 ± 5
172.4 ± 0.004	carboxylic acid-amide	18.9 ± 0.4	212 ± 0.6
170.4 ± 0.05	free carboxylic acid	7.5 ± 0.3	225 ± 5

[a] ± indicates the standard error.

4.3.3 Hydrogen Bonding Interactions in Indomethacin Amorphous Solid Dispersions with PVP and PVP/VA

Amorphous solid dispersions with 10 to 50% PVP or PVP/VA were studied to quantitatively understand how the addition of polymers may change the HB interactions in the systems. The spectra of dispersions containing natural abundance IMC were subtracted from those containing ^{13}C labeled IMC, as detailed in the previous section. After subtraction, only the signal from the carboxylic acid carbon of IMC in the amorphous solid dispersions remains in the spectra. While neat amorphous indomethacin was previously shown to have four major carboxylic acid species, there are potentially five or six carboxylic acid species in the amorphous solid dispersions, with the new species being the carboxylic acid hydrogen bonded to the PVP carbonyl and with the vinyl acetate carbonyl of PVP/VA. Since indomethacin and PVP each contain an amide group, it is difficult to differentiate between the carboxylic acid groups that hydrogen bond with the IMC amide and those that hydrogen bond with the PVP amide. Besides, we observed that the chemical shift of the IMC carboxylic acid hydrogen bonded to polyvinyl acetate has a similar chemical shift to that hydrogen bonded to PVP (data not shown). As a result, the IMC carboxylic acid species that hydrogen bond with either IMC amide, PVP or PVP/VA were treated as one peak in the deconvolution.

The spectra of amorphous IMC, IMC-PVP and IMC-PVP/VA amorphous solid dispersions were simultaneously fitted by a combination of four Gaussian functions using MATLAB (MathWorks, Natick, MA). Each Gaussain function represents a carboxylic acid species, with varying intensities for each spectrum representing the change of the species concentration with the composition. The chemical shift and linewidth for each

Gaussian function were shared parameters and fixed across all eleven spectra to reduce bias in the fitting process. The fitted spectra of IMC-PVP and IMC-PVP/VA amorphous solid dispersions are shown in Figure 4.11. The fitting parameters are shown in Table 4.2.

It is clear from Figure 4.11a that the carboxylic acid dimers are gradually disrupted with increasing PVP content. As the polymer concentration increases, the IMC carboxylic acid chains also decrease. On the other hand, the carboxylic acid-amide complex increases and gradually dominates the spectra as the polymer concentration increases. The percentage of free carboxylic acid did not seem to be affected as much as the other species as the polymer concentration increased. Similar to the IMC-PVP amorphous dispersion, the carboxylic acid dimer interaction is greatly reduced in the presence of PVP/VA. The disordered chains also decrease with the increase of PVP/VA content. On the other hand, the carboxylic acid-polymer complex increases and dominates the spectrum with high PVP/VA content.

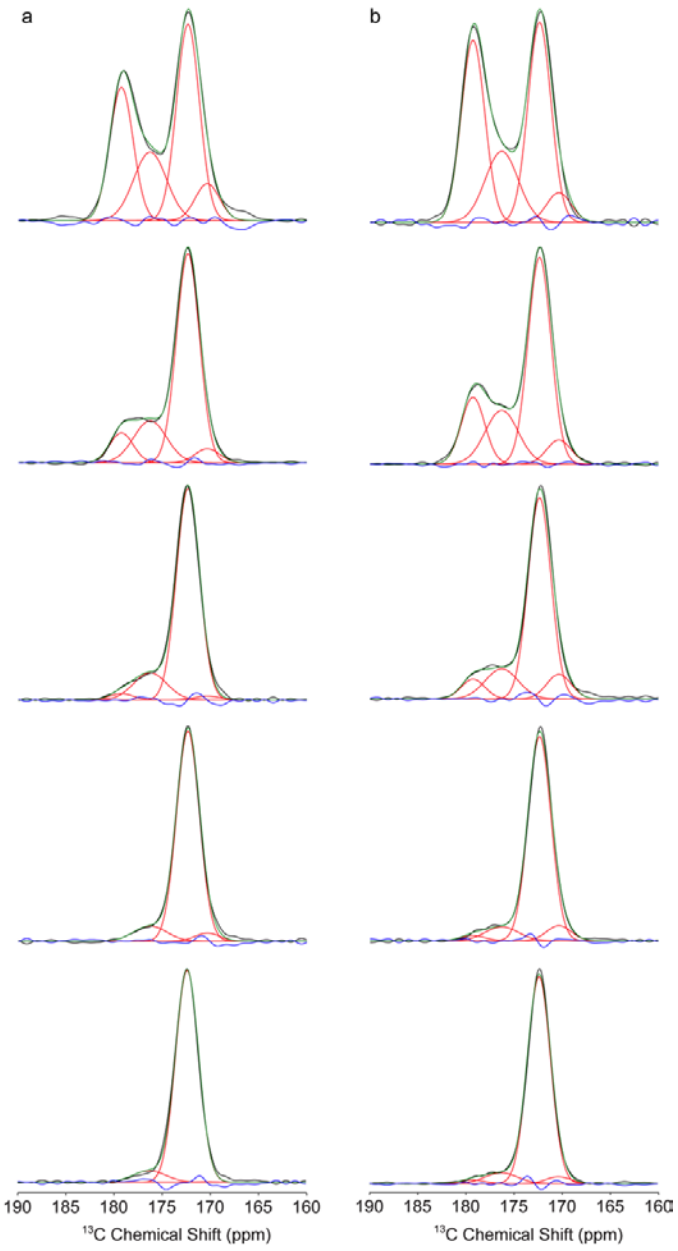

Figure 4.11. CPMAS ^{13}C spectrum of IMC carboxylic acid carbon in (a) IMC-PVP and (b) IMC-PVP/VA amorphous solid dispersions. From top to bottom: 90% IMC, 80% IMC, 70% IMC, 60% IMC and 50% IMC (wt %). The experimental spectrum is shown in black; the fitted peaks representing each species are shown in red; the sum of the fit is shown in green; the residual difference between the experimental and fitted peaks is shown in blue.

Table 4.2. The fitting parameters of CPMAS ^{13}C spectra of IMC carboxylic acid carbon in IMC-PVP and IMC-PVP/VA amorphous solid dispersions.[a,b]

		parameters	carboxylic acid dimer	carboxylic acid chain	carboxylic acid complex	free
		δ (ppm)	179.3 ± 0.006	176.3 ± 0.02	172.4 ± 0.004	170.4 ± 0.05
		Width (Hz)	216 ± 0.8	303 ± 5	212 ± 0.6	225 ± 5
IMC-PVP Ratio (wt)	90-10	Area (%)	28.9 ± 0.4	20.1 ± 0.4	41.9 ± 0.5	8.3 ± 0.3
	80-20	Area (%)	9.7 ± 0.3	19.1 ± 0.4	66.5 ± 0.6	4.7 ± 0.3
	70-30	Area (%)	2.5 ± 0.3	14.5 ± 0.4	81.0 ± 0.7	1.6 ± 0.4
	60-40	Area (%)	0 ± 0.3	9.0 ± 0.4	87.4 ± 0.7	3.6 ± 0.4
	50-50	Area (%)	0 ± 0.3	7.2 ± 0.3	92.6 ± 0.8	0.2 ± 0.4
IMC-PVP/VA Ratio (wt)	90-10	Area (%)	35.8 ± 0.4	19.5 ± 0.4	38.6 ± 0.4	6.0 ± 0.3
	80-20	Area (%)	18.0 ± 0.3	20.4 ± 0.4	54.8 ± 0.5	6.8 ± 0.3
	70-30	Area (%)	6.9 ± 0.3	14.8 ± 0.4	69.4 ± 0.7	8.9 ± 0.4
	60-40	Area (%)	2.1 ± 0.3	8.1 ± 0.3	83.3 ± 0.8	6.5 ± 0.4
	50-50	Area (%)	1.7 ± 0.3	6.6 ± 0.3	88.6 ± 0.7	3.1 ± 0.4

[a] ± indicates the standard error.

[b] The chemical shift of free carboxylic acid hits the upper boundary at 170.4 ppm, which was set based on the chemical shift observed for the free species in polystyrene. When the boundary is lifted, the fitted chemical shift of this peak moves up to 171.5, which loses any physical meaning. All other parameters remained within the boundaries set during the fitting procedure.

There are a few aspects to be noted from the fitting results. First, the spectrum of amorphous IMC could not be fitted as well as the spectra of the drug-polymer dispersions. One possible explanation is that the addition of polymer in the amorphous solid dispersions alters the disordered chain structures resulting in a different distribution in the types of the disordered species. Thus, the peak shape and position for disordered chains could be different with and without the polymer. Second, all hydrogen-bonded carboxylic acid complexes were treated as a single peak in the fitting process, due to the inability of the present data to differentiate between the different species in the spectra. This treatment could have led to an underestimation of the errors of the fitted parameters as fewer parameters were allowed than likely existed. That being said, the most reliable results obtained are those parameters reflecting the dimer species due to its large separation from the carboxylic acid complexes. The concentration of the free carboxylic acid species may be the least certain due to the fact that its chemical shift was restricted to 170.4. As a result, the true error estimates in the results should be expected to be more than what is computed.

Figure 4.12 compares the percentages of HB species of IMC plotted as a function of PVP and PVP/VA percentages. As the plots suggest, the trend for IMC to hydrogen bond with both polymers is the same. The difference lies in the hydrogen bond accepting capability of the two polymers. There are fewer carboxylic acid complex forms in the dispersions of PVP/VA than in the dispersions of PVP. Concomitantly, the fractions of dimer and disordered carboxylic acid chains in the PVP/VA dispersions are higher than those in the PVP dispersions at the same polymer weight percentage. This suggests that PVP/VA is a weaker hydrogen bond acceptor than PVP, probably due to the vinyl acetate

groups in the polymer. This was confirmed by analyzing an IMC-polyvinyl acetate (PVAc) amorphous solid dispersion with 50% (wt) of IMC, in which approximately 20% of the IMC carboxylic acids were still existing in cyclic dimers (data not shown). Matsumoto and Zografi have also studied the hydrogen bonding interactions of indomethacin with PVP and PVP/VA in amorphous solid dispersions.[31] They observed a distinct loss of the indomethacin dimer peak over the range of 5-30% polymer using IR spectroscopy. This is in good agreement with our results that the dimer is reduced to a very small amount with 30% of polymer. The current study, however, is able to detect the existence of more hydrogen bonding species and also quantify those species.

One unexpected trend observed in Figure 4.12 is that the disordered chain species seems to be less disrupted than the dimer species, and remains present when the dimer species completely disappears from the sample. Considering the similar equilibrium of the formations of dimers and chains, one would assume that the chains disappear at a similar rate as the dimers. Current data can not explain this phenomenon. One might speculate that the disordered chain species could contain some species not yet identified.

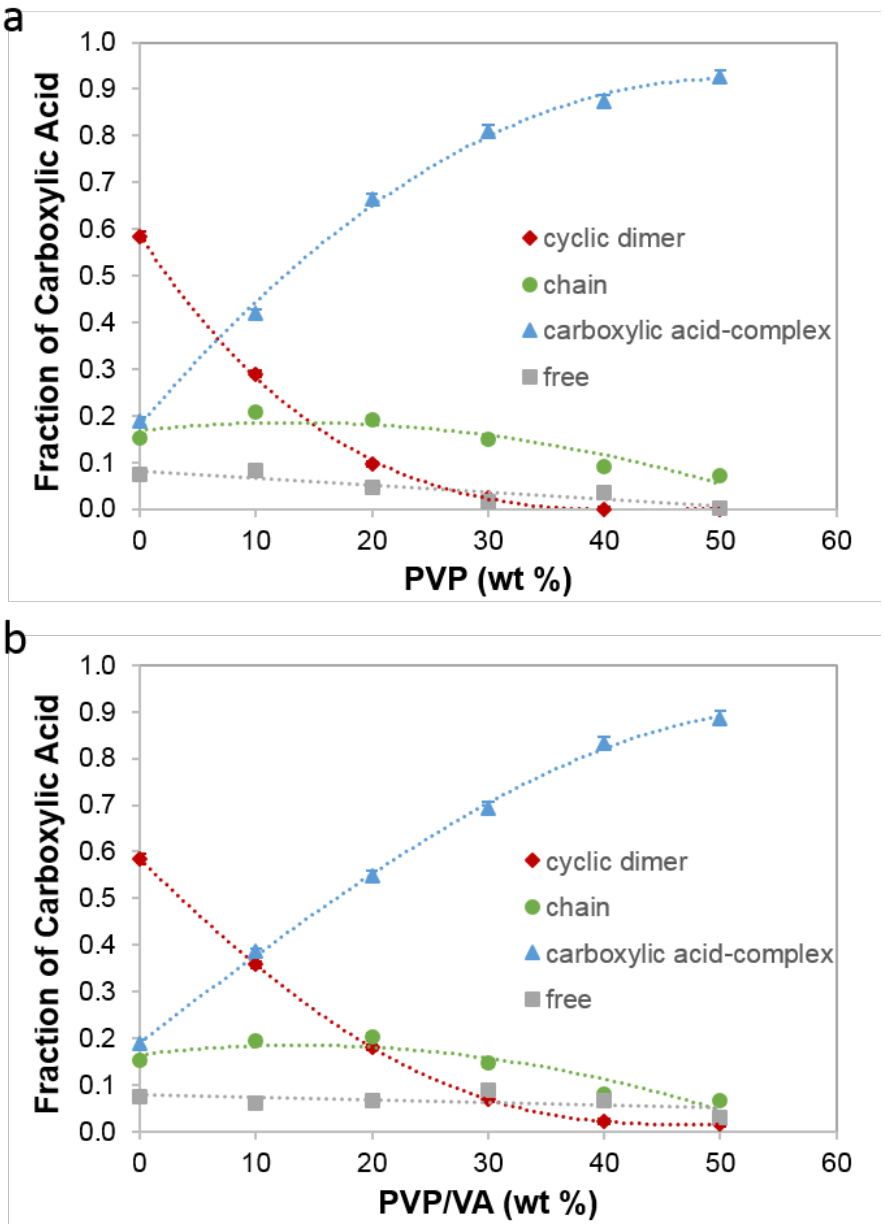

Figure 4.12. Fraction of IMC carboxylic acid participating in various hydrogen-bonding interactions in the amorphous solid dispersion with (a) PVP and (b) PVP/VA as a function of polymer concentration. The error bars indicate the 95% confidence intervals. Curves are drawn as a guide to the eye.

4.3.4 Investigating Hydrogen Bonds in Amorphous Indomethacin

Chemical shift anisotropy (CSA) tensor was studied in neat amorphous indomethacin and an amorphous solid dispersion of 1% indomethacin in polystyrene to gain further understanding of the nature of these different types of hydrogen bonds in amorphous indomethacin. Generally, the isotropic chemical shift provides an "averaged" value of the chemical shift, while the CSA tensor provides three-dimensional information about the local electronic environment at the site of interest. CSA tensor has been used to study hydrogen bonding in the solid state and has been shown to be very sensitive to the protonation state and the hydrogen bonding environment of carboxylic acid groups in amino acids.[101-104]

Table 4.3 lists the principal components of the CSA tensor of the amorphous IMC carboxylic acid carbon that participated in various hydrogen bonding states. As seen from the table, δ_{11} and δ_{22} differ by a large degree and shift in opposite directions in the three carboxyl group species, while δ_{33} is essentially invariant. This trend is consistent with literature reports on chemical shift tensor analysis of amino acid carboxylic acid groups.[102, 103] Gu and McDermott surveyed 35 amino acids and correlated the asymmetries of the carboxylic acid groups to their chemical shift tensors.[102] It was found that the protonation state of the carboxylic acid can be characterized by the asymmetry function $A=\delta_{11}+ \delta_{33}- \delta_{22}$. Deprotonated species are characterized by $A<185$ and protonated species are characterized by $A>195$. In the present study, the peak at $\delta_{iso}=179.3$ ppm clearly falls into the category of deprotonated species ($A=164$), which suggests that protons are delocalized in these carboxyl groups, resulting in a high degree of symmetry. This confirms the assignment of this peak to the cyclic dimer form. The

peak at δ_{iso}=172.4 ppm falls into the category of protonated species (A=215), which suggests a low degree of symmetry in this hydrogen bond. This result is consistent with the assignment of this peak to the carboxylic acid-amide complex. The peak at δ_{iso}=176.3 ppm falls in between the deprotonated and protonated categories, with an asymmetry function of 185. The protons in these carboxyl groups are neither deprotonated nor protonated, and are at an "in-between" state. This suggests that these carboxyl groups may be in carboxylic acid chains including chain ends, where protons are partially delocalized. The broad nature of this resonance could be partially explained by the variations in the types and lengths of chains. Rings larger than dimer may also exist.

Table 4.4 lists the principal components of the CSA tensor of the IMC carboxylic acid carbon in the amorphous dispersion with polystyrene (1% IMC). As expected, the tensor elements of the cyclic dimer are very similar to those in neat amorphous indomethacin (Table 4.3). Free indomethacin, on the other hand, showed different principal components compared to either carboxylic acid chains or carboxylic acid-amide complexes in neat amorphous indomethacin. This is consistent with the assignment of the free indomethacin in IMC-PS amorphous solid dispersion as a different species, despite having an isotropic chemical shift close to that of the carboxylic acid-amide hydrogen bond. Again, the asymmetric function A equals 207 for the free carboxylic acid, falling into the category of protonated species with a low degree of symmetry, which is what would be expected for a free carboxylic acid.

Table 4.3. Principal components of the CSA tensors of the amorphous IMC carboxylic acid carbon that participates in various hydrogen bonding states.[a] Free carboxylic acid was omitted in the analysis due to the small amount present.

	cyclic dimer	carboxylic acid chain	carboxylic acid-amide
δ_{iso}	179.3	176.3	172.4
δ_{11}	233 ± 0.8	238 ± 2.0	248 ± 2.4
δ_{22}	187 ± 0.5	173 ± 1.3	151 ± 1.5
δ_{33}	118 ± 0.6	120 ± 1.5	118 ± 1.8
A	164	185	215

[a] ± indicates the standard error.

Table 4.4. Principal components of the CSA tensor of the IMC carboxylic acid carbon in a 1% IMC amorphous solid dispersion with polystyrene.[a]

	cyclic dimer	free
δ_{iso}	179.3	170.3
δ_{11}	231 ± 0.6	231 ± 1.0
δ_{22}	187 ± 0.3	152 ± 0.6
δ_{33}	120 ± 0.5	128 ± 0.8
A	164	207

[a] ± indicates the standard error.

4.3.5 Investigating the Carboxylic Acid-Amide Hydrogen Bond

As discussed previously, there are two types of carboxylic acid-amide hydrogen bonds encountered in the present study. Depending on the system, this peak likely consists of carboxylic acid hydrogen bonded to the IMC amide and that hydrogen bonded to PVP amides. The chemical shift anisotropy (CSA) tensors of the carboxylic acid carbons involved in these hydrogen bonds were explored because the CSA tensor is very sensitive to the local chemical environment as discussed in previous sections. Neat amorphous indomethacin and the 50-50 IMC-PVP amorphous solid dispersion were examined because the former represents the carboxylic acid hydrogen bonding with the IMC amide and the latter predominantly represents hydrogen bonding with PVP amides.

The principal components of the tensors of the carboxylic acid carbon in neat amorphous IMC and in the 50-50 IMC-PVP amorphous solid dispersion are very similar (Table 4.5). This similarity suggests that the two types of carboxylic acid-amide hydrogen bonds are comparable in their strengths and experience very similar electronic environments. This result indicates that some other mechanisms besides the strength of the hydrogen bond must exist to favor the PVP amide group as the preferred hydrogen bond acceptor in the amorphous solid dispersions. One of the contributing factors is the concentration effect. The molar concentration of PVP monomer is approximately three times of that of indomethacin for equal weights of the compounds. Thus, every 10% (wt) increase of PVP is accompanied by a 10% decrease in carboxylic acids available to form dimers or chains, and a 20% increase in the concentration of amides available to form the carboxylic acid-amide hydrogen bonds. With 50% PVP, the molar concentration of amides has doubled, while the molar concentration of carboxylic acids has decreased by

half. The increasing concentration of amides could in part explain the higher percentages of the IMC carboxylic acid-amide hydrogen bonds when PVP is added.

4.3.6 Thermodynamics of Amorphous Indomethacin Dimerization in a Dilute System

The indomethacin carboxylic acid dimer and the free carboxylic acid can be assumed to be in equilibrium in the amorphous state at temperatures above T_g. This equilibrium can be described by the following equations,

$$free + free \overset{K_{eq}}{\leftrightarrow} dimer \tag{4.1}$$

$$K_{eq} = \frac{[dimer]}{[free]^2} \tag{4.2}$$

where *free* denotes the IMC monomer having free carboxylic acid groups, *dimer* denotes the carboxylic acid dimer of IMC, and K_{eq} is the equilibrium constant between the free carboxylic acid and the dimer. The temperature dependence of K_{eq} can be described by the Van't Hoff equation,

$$ln\, K_{eq} = -\frac{\Delta H^\circ}{RT} + \frac{\Delta S^\circ}{R} \tag{4.3}$$

where ΔH° is the standard enthalpy of dimerization, ΔS° is the standard entropy of dimerization, T is the temperature and R is the gas constant. In the amorphous solid dispersion of 1% IMC with polystyrene, the IMC molecules could be treated as the solute in a solid solution where polystyrene is the "solvent". The standard state is defined as the hypothetical state with unit activity coefficient and 1 molar concentration of IMC in

polystyrene at 25 ℃ and 1 atmosphere. The reference state is defined as the state with infinite dilute molar concentration of IMC in polystyrene (unit activity coefficient) at 25 ℃ and 1 atmosphere.

The weight fractions of the cyclic dimer and free carboxylic acid below the coalescence temperature can be deconvoluted from the CPMAS spectra as shown in Figures 4.8 d-f. The weight fractions of these two species above the coalescence temperature can be calculated from the chemical shift of the observed coalesced peak (Figures 4.8 h-j) by the following,

$$\delta_{obs} = w_d \cdot \delta_d + w_f \cdot \delta_f \tag{4.4}$$

where δ_{obs} is the observed chemical shift of the coalesced peak, δ_d and δ_f are the chemical shifts of the dimer and the free species before coalescence, respectively, and w_d and w_f are the weight fractions of two respective species. Since the dimer species contains two indomethacin molecules and thus double signal intensity for each mole of the species, the dimer weight fraction was divided in two to convert to the mole fraction. The mole fractions of the two species were then converted into molar concentrations by the following,

$$[dimer] = \frac{x_d/mw_{IMC}}{0.01/\rho_{IMC}+0.99/\rho_{PS}} \tag{4.5}$$

$$[free] = \frac{x_f/mw_{IMC}}{0.01/\rho_{IMC}+0.99/\rho_{PS}} \tag{4.6}$$

where x_d and x_f are the molar fractions of the dimer and the free species, respectively, mw_{IMC} is the molecular weight of indomethacin, and ρ_{IMC} and ρ_{PS} are the densities of amorphous indomethacin and polystyrene, respectively.

From equations 4.2-4.6, the standard enthalpy and entropy of dimerization were calculated. The standard dimerization enthalpy ($\Delta H°$) was calculated to be -38 kJ/mol and the standard dimerization entropy ($\Delta S°$) was calculated to be -83 J/(mol·K). The Van't Hoff plot is shown in Figure 4.13.

As seen from Figure 4.13, the Van't Hoff plot begins to deviate from linearity below 50 °C. The deviation of the plot from linearity represents the free energy difference between the real glass and a hypothetical equilibrium state of a fully relaxed amorphous glass. This free energy difference was calculated to be approximately 2.3 kJ/mol at 25 °C.

The standard dimerization enthalpy of acetic acid has been reported to be between -31 and -44 kJ/mol in organic solvents such as benzene, CCl_4, and n-heptane.[105, 106] The standard dimerization enthalpy of glacial acetic acid was estimated to be -44 kJ/mol.[107] Overall, the amorphous IMC carboxylic acid dimerization enthalpy is in very good agreement with the literature values for acetic acids. The standard dimerization entropy of acetic acid has been reported to be between -52 and -94 J/(mol·K) in organic solvents such as benzene, CCl_4, and n-hexane.[108] The calculated amorphous IMC carboxylic acid dimerization entropy is also reasonable based on the range of literature reported values.

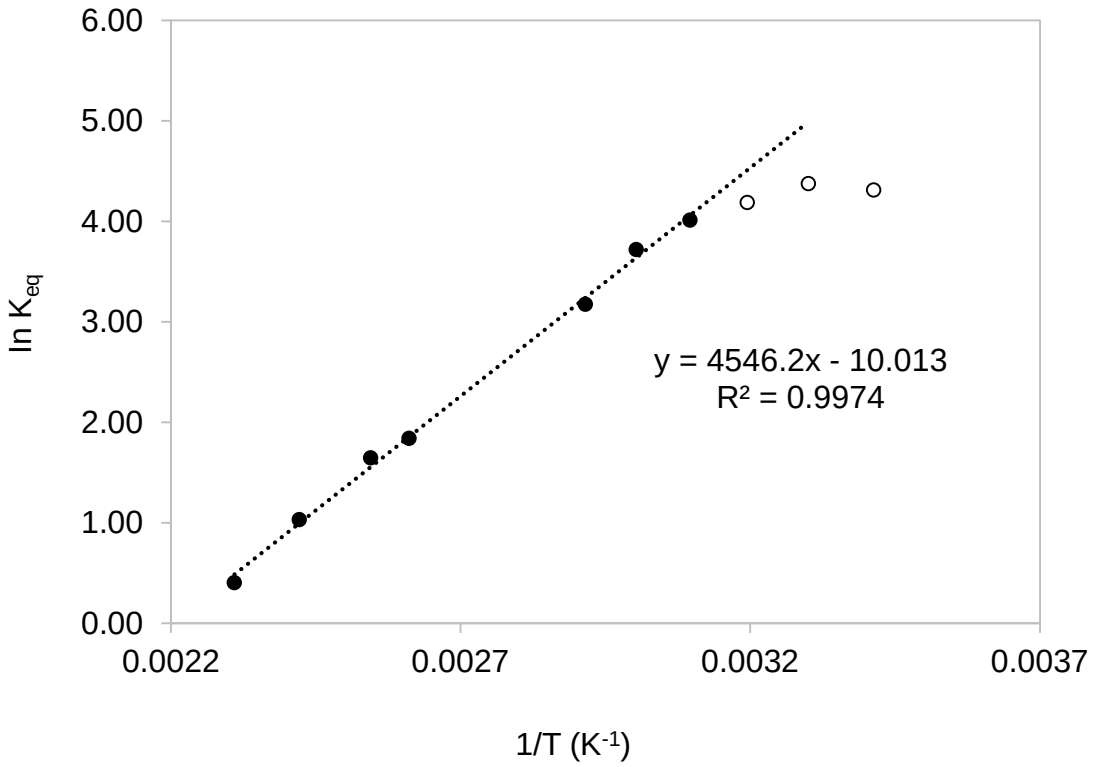

Figure 4.13. Van't Hoff plot of Keq for indomethacin carboxylic acid dimerization in a 1% solid dispersion in polystyrene.

4.3.7 Hydrogen Bonding Effects on Miscibility and Physical Stability of Amorphous Solid Dispersions

The miscibilities of IMC-PVP and IMC-PVP/VA amorphous solid dispersions were studied by SSNMR ^{1}H T_1 and $T_{1\rho}$ relaxation times using methods described previously.[47] A common relaxation time for both ^{1}H T_1 and $T_{1\rho}$ was found for all solid dispersions, indicating phase homogeneity. The miscible domain size was calculated to be less than 5 nm, based on the length scale of ^{1}H spin diffusion

$$\langle L \rangle = \sqrt{6Dt} \qquad (4.7)$$

where D, the ^{1}H spin diffusion coefficient, is typically assumed to 10^{-12} cm^2/s for organic solids,[46, 66] and t is the relaxation time. Typical ^{1}H $T_{1\rho}$ relaxation times obtained from these samples are on the order of 50 ms.

Modulated DSC studies also showed a single glass transition event and no crystallization or melting peak for all of the amorphous solid dispersions, agreeing with SSNMR relaxation measurements that they are phase homogeneous. The existence of strong hydrogen bonds between the drug and the polymer will decrease the enthalpy of mixing and lower the overall free energy of mixing. This will promote miscibility between the drug and polymer even when the polymer concentration is relatively low.

Carboxylic acid dimers exist in both known indomethacin polymorphs, indicating that dimer formation is an important component in the crystallization process. If the dimer formation is eliminated in the amorphous state, then the drug is less likely to crystallize. The current study shows that with 40% (wt) PVP, the indomethacin cyclic dimers are completely disrupted. At this PVP concentration, the majority of the drug is

hydrogen bonded to PVP. Thus, it is reasonable to hypothesize that 40% (wt) of PVP can effectively inhibit the crystallization of amorphous indomethacin at 20°C for years or even decades. We are currently testing the stability of several amorphous solid dispersions to see if this approach can potentially serve as a predictive tool for the long-term physical stability of amorphous solid dispersions.

Table 4.5. Principal components of the chemical shift tensor of the IMC carboxyl carbon that participates in the carboxyl-amide hydrogen bond. [a]

	amorphous IMC	50-50 IMC-PVP
δ_{11}	248 ± 2.4	250 ± 1.3
δ_{22}	151 ± 1.5	151 ± 0.8
δ_{33}	118 ± 1.8	117 ± 1.1

[a] ± indicates the standard error.

4.3.8 Comparison of Experimental Data with MD Simulation Results in the Literature

Xiang and Anderson performed molecular dynamics (MD) simulations on amorphous IMC and reported that 79% (± 3%) of IMC molecules were hydrogen bonded with at least one hydrogen bond and 21% (± 3%) of IMC molecules were not involved in any hydrogen bonds.[87] The experiments from the current study found approximately 7% free IMC in neat amorphous IMC. The MD simulations predicted that of the hydrogen bonds being formed, 73% were between IMC carboxylic acids. The current experiments estimated that number to be 79%.

The same authors also reported MD simulations of IMC-PVP amorphous systems.[88] It was found that as PVP concentration increased, IMC self-interactions were gradually displaced by IMC-PVP interactions.[88] The experimental data herein showed the same trend that the IMC self-interactions were displaced with IMC-PVP interactions. The MD simulations also identified an almost constant amount of free IMC in all compositions, although the percentage of free IMC determined in the MD simulations was greater.

The greater percentage of free IMC found in MD simulations may have been resulted from the difference in cooling rate for an experimental glass in comparison to that employed in MD simulations. The cooling rate reported in the MD simulation was 30 K/ns, which is more than 10 orders of magnitude faster than the experimental cooling rate. At such a rapid cooling rate, the simulated melt of indomethacin fell out of equilibrium at a considerably higher temperature, resulting in a reported glass transition temperature of 111 °C, which is 65 °C higher than the glass transition temperature determined

experimentally in this study. The discrepancy in the glass transition temperature can lead to the differences in the amount of free IMC molecules observed by these two methods. This can be rationalized through the temperature dependence of the equilibrium constant for IMC dimer formation. Above the glass transition temperature, the amorphous indomethacin is a supercooled liquid and is expected to follow the solution state equilibrium. At the temperature of 46 °C, where the experimental amorphous system is about to solidify into a glass, the equilibrium constant for dimer formation is calculated to be 70 M^{-1}, whereas at the temperature of 111 °C, where the MD simulated amorphous system is about to solidify, the equilibrium constant for dimer formation is calculated to be only 6.3 M^{-1}. Consequently, the percentage of free indomethacin is estimated to be approximately three times greater in the MD simulated indomethacin glass than in the experimental samples.

4.4 Conclusions

Amorphous IMC was found to consist mainly of three types of carboxylic acids from solid-state NMR experiments, representing the carboxylic acid cyclic dimer, disordered carboxylic acid chains, and the carboxylic acid hydrogen bonded to the amide carbonyl. Deconvolution revealed that approximately 59% of the IMC molecules form cyclic dimers, 15% form chains, 19% form carboxylic acid-amide hydrogen bonds, and 7% remain hydrogen bond free. The standard dimerization enthalpy ($\Delta H°$) and entropy ($\Delta S°$) of indomethacin were calculated to be -38 kJ/mol and -83 J/(mol·K), respectively, in amorphous solid dispersions with polystyrene. Adding PVP to IMC created an amorphous solid dispersion and disrupted the IMC self-interactions. With 40% (w/w)

PVP present, no carboxylic dimers could be detected. The extent of hydrogen bond formation between IMC and PVP increased as PVP concentration increased. IMC also formed hydrogen bonds with PVP/VA in a similar fashion as PVP, but less effectively, due to the weaker hydrogen bonding capability of vinyl acetate groups of the polymer.

The experimental results were compared with previous MD simulations reported in the literature. The two approaches agreed in their general trends, with the major difference lying in the greater percentage of free IMC molecules in the MD simulated glass. This was rationalized by the fast cooling rate employed in the simulations which resulted in a higher energy state of the simulated amorphous solid. The results from the current study have practical values in both understanding and designing stable amorphous solid dispersions as well as providing useful experimental results for improving MD simulations.

Chapter 5. Molecular Mobility of Amorphous Solid Dispersions near the Glass Transition Temperature

5.1 Introduction

In the past two chapters, we have discussed the role of phase homogeneity and drug-polymer interaction on the physical stability of amorphous solid dispersions. In addition to these two factors, a number of studies have shown the link between physical stability and molecular mobility in the amorphous state.[58, 109-111] In general, molecular mobility encompasses both global and local motions. Global mobility reflects cooperative motions and is the governing motion at temperatures greater than the glass transition temperature. Historically, global mobility is often described as the α-relaxation. On the other hand, local mobility reflects noncooperative motions stemming from portions of the molecule, such as motions of polymer side chains. Local mobility is often termed β-relaxation.

Several techniques have been used to gain information on the molecular mobility of amorphous pharmaceutical systems, such as DSC,[112-114] isothermal microcalorimetry,[115] viscosity measurements,[116] dielectric spectroscopy [117, 118] and solid-state NMR.[71, 77, 119] Both DSC and isothermal microcalorimetry have been used to study enthalpy relaxation of amorphous systems during an "aging" process. These two methods typically do not directly measure the relaxation time, and the relaxation time parameter extracted from these studies reflects the structural relaxation of the system. Dielectric spectroscopy has also been used to study molecular mobilities in amorphous systems, where the relaxation time can be directly measured and reflects the reorientation of

dipoles under an applied electric field. Typically, the α and/or β relaxation time is identified by dielectric spectroscopy as a function of temperature. The disadvantage of this approach is that the relaxation time reflects the average mobility of the entire system, and is not component specific.

Solid-state NMR spectroscopy can provide information about molecular mobility through either the direct measurement of relaxation times or through exchange processes. It is very useful for detecting motions occurring over a very broad frequency range, depending on the nuclei being studied and the types of motions being probed. One example is information provided by ^{1}H T_1 and $T_{1\rho}$ relaxation times. It is important to note that ^{1}H relaxation times provide somewhat "global" information on molecular motions, due to the strong ^{1}H homonuclear dipolar interactions which usually result in all of the protons in the spin system having a single common relaxation time.[39] Because of the fast proton spin diffusion that averages out ^{1}H relaxation time, the interpretation of mobility from ^{1}H relaxation time is not very straightforward. On the contrary, relaxation times of ^{13}C nuclei may often better reflect the motions of the functional groups of interest, because ^{13}C nuclei are sparse and are thus relatively unaffected by homonuclear dipolar interactions. Thus, the motional processes of different regions of the molecules could be better preserved. The spin-lattice relaxation T_1 is known to be sensitive in the MHz region and usually detects faster motions such as methyl group rotations.[42] The rotating frame spin-lattice relaxation time $T_{1\rho}$ is sensitive in the kHz region and detects slower motions such as polymer side group motions. ^{13}C $T_{1\rho}$ relaxation times have been shown to be valuable probes of polymer chain dynamics in the 10-50 kHz region.[120]

In addition to relaxation time measurements, exchange NMR spectroscopy is well suited for studying molecular dynamics of amorphous materials. An extensive body of literature exists in the study of molecular dynamics of amorphous polymers using two-dimensional (2D) exchange NMR.[86, 121-123] In a 2D exchange experiment, the change in the chemical environment of the atoms in a molecule during a specific time period, known as the mixing time, is translated into a change in frequency afterwards. Off diagonal peaks correlate the two different frequencies observed before and after the mixing time and represent the chemical exchange occurring during the mixing time. Correlation times extracted from 2D exchange experiments have been correlated with dielectric relaxation times.[124] Specific motional processes have also been elucidated in poly(methyl methacrylate) for the β-relaxation observed with both dielectric and dynamic mechanical spectroscopy.[122]

In this chapter, the dynamics of three types of amorphous systems were studied, namely a pure amorphous API, API-polymer amorphous solid dispersions, and an amorphous API in very dilute environment with a polymer. Indomethacin was used as the model hydrophobic API, poly(vinylpyrrolidone) was used as a polymer to form amorphous solid dispersions with indomethacin, and polystyrene was used to form a dilute solid solution of indomethacin. This work aims to understand how polymer affects the motional processes of the API in each of these situations.

5.2 Materials and Methods

5.2.1 Materials

Indomethacin (IMC, γ form, minimum purity 99%) was purchased from Sigma-Aldrich (St Louis, MO). ^{13}C isotopically labeled indomethacin (99% ^{13}C at the carboxylic acid carbon) was custom synthesized by Chemtos (Austin, TX). Polystyrene (PS, average M_w=35 kg/mole) was purchased from Sigma-Aldrich (St Louis, MO). Poly(vinylpyrrolidone), (PVP, Kollidon 25, M_w=28-34 kg/mole) was obtained from BASF (Edison, NJ). PVP was vacuum dried at 70 °C over night and stored over Drierite™ at all times. The chemical structures of indomethacin, PVP, and polystyrene are shown in Figure 5.1.

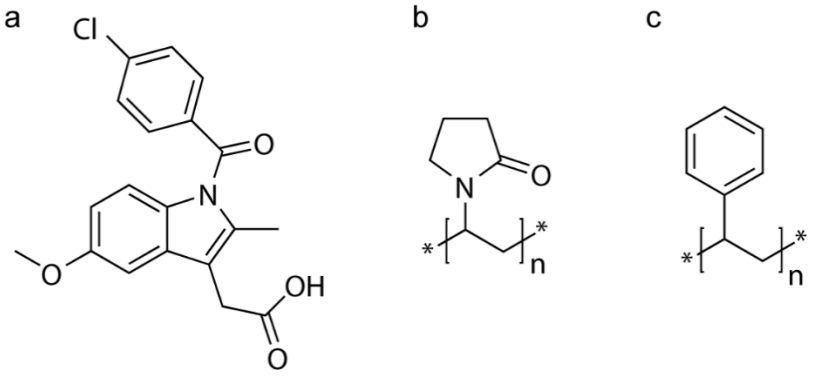

Figure 5.1. Chemical structures of (a) nifedipine, (b) indomethacin, (c) PVP, and (d) polystyrene.

5.2.2 Preparation of Amorphous Solid Dispersions

Amorphous solid dispersions of indomethacin and PVP were prepared by cryomilling followed by *in situ* melt quenching in NMR rotors while spinning. ^{13}C isotopically enriched indomethacin (3% wt ^{13}C-labeled and 97% wt unlabeled at the carboxylic acid carbon) was used. 1 g samples of drug and polymer in weight ratios of 9:1, 8:2 and 7:3 drug:polymer were cryomilled at 10 Hz (SPEX SamplePrep 6770 Freezer/Mill, SPEX SamplePrep LLC., Metuchen, NJ) for five cycles. Each cycle consisted of 2 minutes of milling and 2 minutes of cool down. Liquid nitrogen was used as a coolant. The cryomilling procedure was used to ensure optimum mixing between the drug and polymer prior to melting. The mixtures were then transferred into 7.5 mm zirconia NMR rotors with Teflon or Kel-F end caps (Revolution NMR, LLC, Fort Collins, CO). The top end cap had a small hole to allow moisture to evaporate during heating. The rotors were heated in the NMR probe at 170 °C for approximately 10 minutes while spinning at 4 kHz and then rapidly cooled to room temperature, resulting in the amorphous solid dispersions.

Amorphous solid dispersions of indomethacin and polystyrene were prepared by solvent evaporation using a Büchi Rotavapor R-215 (Büchi, Switzerland). A low level of indomethacin (1%) that was ^{13}C labeled at the carboxylic acid carbon were used. The drug and polymer were dissolved in methylene chloride and the solvent was rotary evaporated at 35 °C. The obtained solids were subsequently vacuum dried at room temperature overnight to remove residual solvent.

5.2.3 Modulated DSC

The glass transition temperatures of the amorphous solid dispersions were determined by modulated DSC (MDSC) using a Q2000 differential scanning calorimeter equipped with an RCS90 refrigerated cooling system (TA Instruments, Newcastle, DE). Nitrogen gas was used as the purge gas at a flow rate of 50 mL/min. Temperature and enthalpy were calibrated using indium. Samples (2-5 mg) prepared by melt quenching as described above were placed in TZero™aluminum pans and sealed with TZero™aluminum hermetic lids with one pinhole (TA Instruments, New Castle, DE). Samples were equilibrated at 0 °C, and then heated at 1 °C/min to 200 °C with an amplitude of ±0.5 °C and a modulation period of 60 s. The glass transition was separated into the reversing heat flow signal and was determined by half height at midpoint using the Universal Analysis software (TA Instruments, Newcastle, DE).

5.2.4 Solid-State NMR Experiments

All solid-state NMR spectra were acquired using a Tecmag Redstone HF3 2RX spectrometer (Tecmag, Inc., Houston, TX), operating at 75.48 MHz for ^{13}C. Samples were packed into 7.5 mm zirconia rotors and sealed with Teflon or Kel-F end caps (Revolution NMR, LLC, Fort Collins, CO). Experiments were performed using a 7.5 mm double-resonance MAS probe (Varian, Palo Alto, CA). All ^{13}C spectra were acquired under magic angle spinning (MAS) [43] at 4 kHz if not specified otherwise, using ramped-amplitude CP,[45] total sideband suppression (TOSS)[44] and SPINAL64 decoupling[73] with a ^{1}H decoupling field of about 62 kHz. A 2 ms contact time was used in all experiments. 3-

Methylglutaric acid was used to optimize spectrometer settings and as an external standard, with the methyl peak referenced to 18.84 ppm.[74]

The spectra of IMC-PS amorphous solid dispersions were acquired using MAS of 5.2 kHz to avoid residual spinning sideband overlap. The spectra of IMC-PS amorphous solid dispersions were collected as a function of temperature using a variable-temperature accessory stack (Varian, Palo Alto, CA). Samples were equilibrated at each temperature for at least 15 min before data acquisition. At temperatures above 100 °C, direct polarization was used to acquire the spectra because cross-polarization efficiency was greatly reduced in the highly mobile environment.

^{1}H $T_{1\rho}$ relaxation times of amorphous solid dispersions were determined as a function of temperature using a variable-temperature accessory stack (Varian, Palo Alto, CA). Lead nitrate was used to calibrate the temperature prior to the experiment.[90] A linear slope of 0.75 was obtained for the temperature range between 20 and 180 °C, agreeing very well with the literature reported value.[90] Samples were equilibrated at each temperature for at least 15 min before data acquisition. ^{1}H $T_{1\rho}$ values were determined between 20 and 120 °C for both nifedipine and PVP in the amorphous solid dispersions, by varying the spin-lock duration time following a 90° pulse. A recycle delay of about 1.5 – 2 times the measured T_1 was used to maximize the signal-to-noise ratio. A frequency field of about 65 KHz was used for the spin-lock field. The peak of interest was integrated and plotted against the spin-lock duration times and the values were fitted to the following equation using GraphPad Prism (GraphPad Software, Inc., La Jolla, CA)

$$M = M_0 \cdot e^{-\frac{\tau}{T_{1\rho}}} \qquad (5.1)$$

where M is the integrated signal intensity and τ is the spin-lock duration time. M_0 is an amplitude parameter obtained from the fit and $T_{1\rho}$ is the obtained spin-lattice relaxation time in the rotating frame.

2D exchange ^{13}C NMR spectra were collected with MAS using a hypercomplex data set.[125] Two sets of spectra were collected at each time increment to generate both real and imaginary components of the spectra. A mixing time of 2 s and a spectral width of 2000 Hz were used. 40 data points were collected in the direct dimension and 80 were collected in the indirect dimension. Sine bell apodization was applied to both dimensions during processing. Symmetrization was performed on the spectra of 70-30 IMC-PVP to reduce t_1 noise.

5.3 Results and Discussion

5.3.1 Molecular Mobility of Amorphous Indomethacin

In this section, studies of the molecular mobility of a pure amorphous compound, indomethacin, by 2D exchange NMR experiments below and above its glass transition temperature are reported. Figure 5.1 shows the 2D exchange ^{13}C NMR spectra of the carbonyl region of amorphous indomethacin at 20 °C, 40 °C and 50 °C using a 2 s mixing time. No visible cross peaks were found in the spectrum of amorphous IMC carboxylic acid carbon at 20 °C and 40 °C (Figure 5.1a and b). The absence of cross peaks suggests that below the glass transition temperature, which is 46 °C for amorphous indomethacin, the molecules do not possess a high degree of translational mobility, which is required for exchange processes to occur. Two clear cross peaks between the dimer and the carboxylic acid-amide complex can be seen from Figure 5.1c for the spectrum collected at 50 °C.

The off diagonal peaks suggest that above the glass transition temperature, the dimers are breaking and forming carboxylic acid-amide complexes, and vice versa. This means the amorphous IMC is a very dynamic system at 50 °C as the molecules not only have to break the one type of hydrogen bond but also have to possess enough translational mobility to form another type of hydrogen bond.

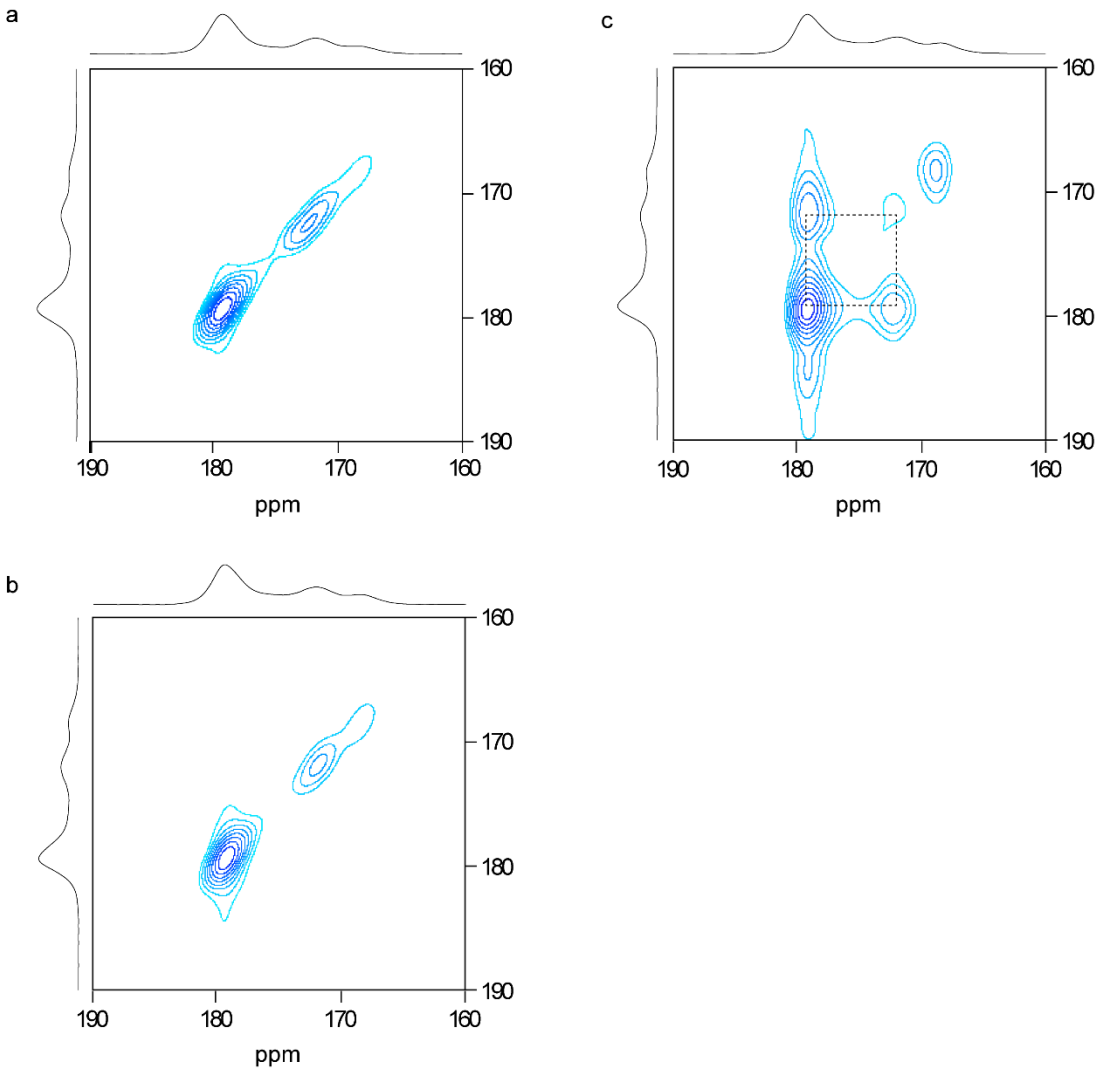

Figure 5.1. 2D exchange ^{13}C MAS NMR spectra of the carbonyl region of amorphous indomethacin at (a) 20 °C, (b) 40 °C, and (c) 50 °C. The sample contained 5% ^{13}C labeled indomethacin (carboxyl carbon) and 95% natural abundant indomethacin. A mixing time of 2 s was used.

5.3.2 Molecular Mobility of Amorphous Indomethacin in Amorphous Solid Dispersions with PVP

This section describes the dynamics of indomethacin-PVP amorphous solid dispersions studied via 2D exchange NMR experiments and how the presence of a polymer affects the dynamics of the drug. Amorphous solid dispersions with 70-90% drug loadings were used, representing the higher end of drug/polymer ratios found in amorphous solid dispersions. Figure 5.2 shows the 2D exchange ^{13}C NMR spectra of the carbonyl carbon region of a 90-10 IMC-PVP amorphous solid dispersion at 40, 50 and 60 °C. The glass transition temperature of the 90-10 IMC-PVP amorphous solid dispersion is 53 °C at the midpoint and 48 °C at the onset. No cross peaks were found in the spectrum collected at 40 °C, indicating limited translational mobility and dynamics below the glass transition temperature. The spectrum collected at 50 °C shows two cross peaks between the carboxylic acid dimers and the carboxylic acid-amide complexes. This suggests that the IMC molecules gained sufficient mobility near the glass transition temperature so that the carboxylic acid dimers interconverted with the carboxylic acids that hydrogen bond with the amides. The spectrum collected at 60 °C shows the two cross peaks with greater intensity, indicating the exchange was faster at temperatures slightly higher than T_g, where the system was in the rubbery state. The disordered carboxylic acid species was not found to exchange with either the dimer or the carboxylic acid-amide complex. Like discussed in the previous chapter, one possible explanation is that this peak may not repsent entirely the chain species and may contain some unknown species that do not participate in the exchange. The exact reason is not clear at this point.

Figure 5.3 shows the 2D exchange ^{13}C NMR spectra of the carbonyl carbon region in an 80-20 IMC-PVP amorphous solid dispersion at 50, 60 and 70 °C. Similar to the 90-10 IMC-PVP, no cross peaks were detected below the glass transition temperature (Figure 5.3a). The midpoint glass transition temperature for 80-20 IMC-PVP is 64 °C and the onset glass transition temperature is 60 °C. At close to the glass transition temperature (60 °C), cross peaks between the carboxylic acid dimers and the carboxylic acid-amide complexes were seen. Above the glass transition temperature at a temperature of 70 °C, the intensity of the cross peaks increased. Once again, disordered chains were not found to exchange with any other species.

Figure 5.4 shows the 2D exchange ^{13}C NMR spectra of the carbonyl carbon region in a 70-30 IMC-PVP amorphous solid dispersion at 70 and 80 °C. While the midpoint glass transition temperature for this system is 73 °C, no cross peaks could be detected at either 70 or 80 °C. As described in chapter 4, there were essentially no dimers present in this drug/polymer ratio. The result suggested that the carboxylic acid chains (176 ppm) did not participate in the exchange with the carboxylic acid-amide complexes (172 ppm). Similarly, the carboxylic acid chains were not found to participate in exchange in any other systems investigated, which include the neat amorphous indomethacin, and indomethacin amorphous solid dispersions with 90% and 80% drug loadings.

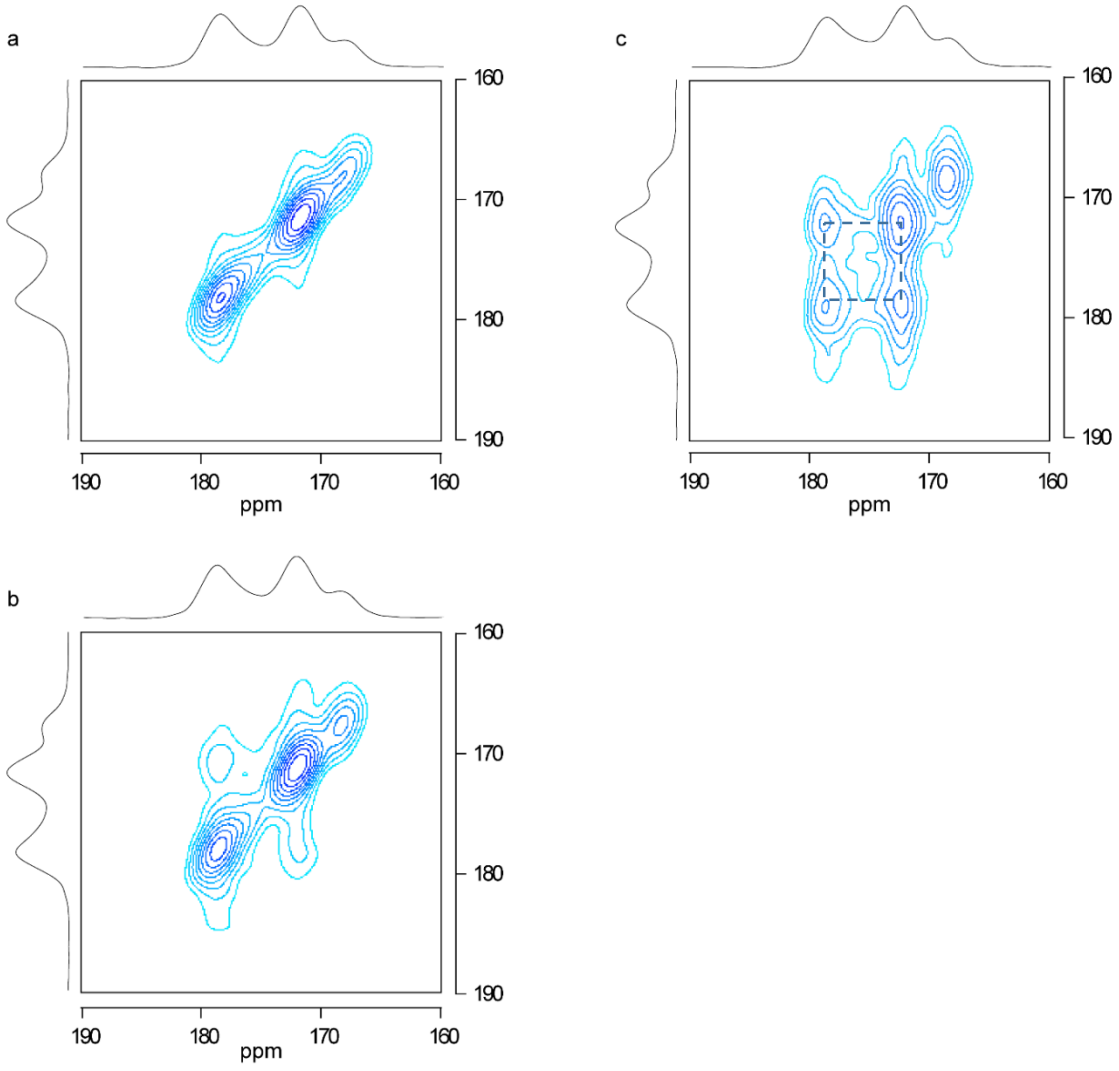

Figure 5.2. 2D exchange ^{13}C MAS NMR spectra of the carbonyl region of 90-10 IMC-PVP amorphous solid dispersions at (a) 40 °C, (b) 50 °C and (c) 60 °C. The sample contained 3% ^{13}C labeled indomethacin (carboxyl carbon) and 97% natural abundant indomethacin. A mixing time of 2s was used.

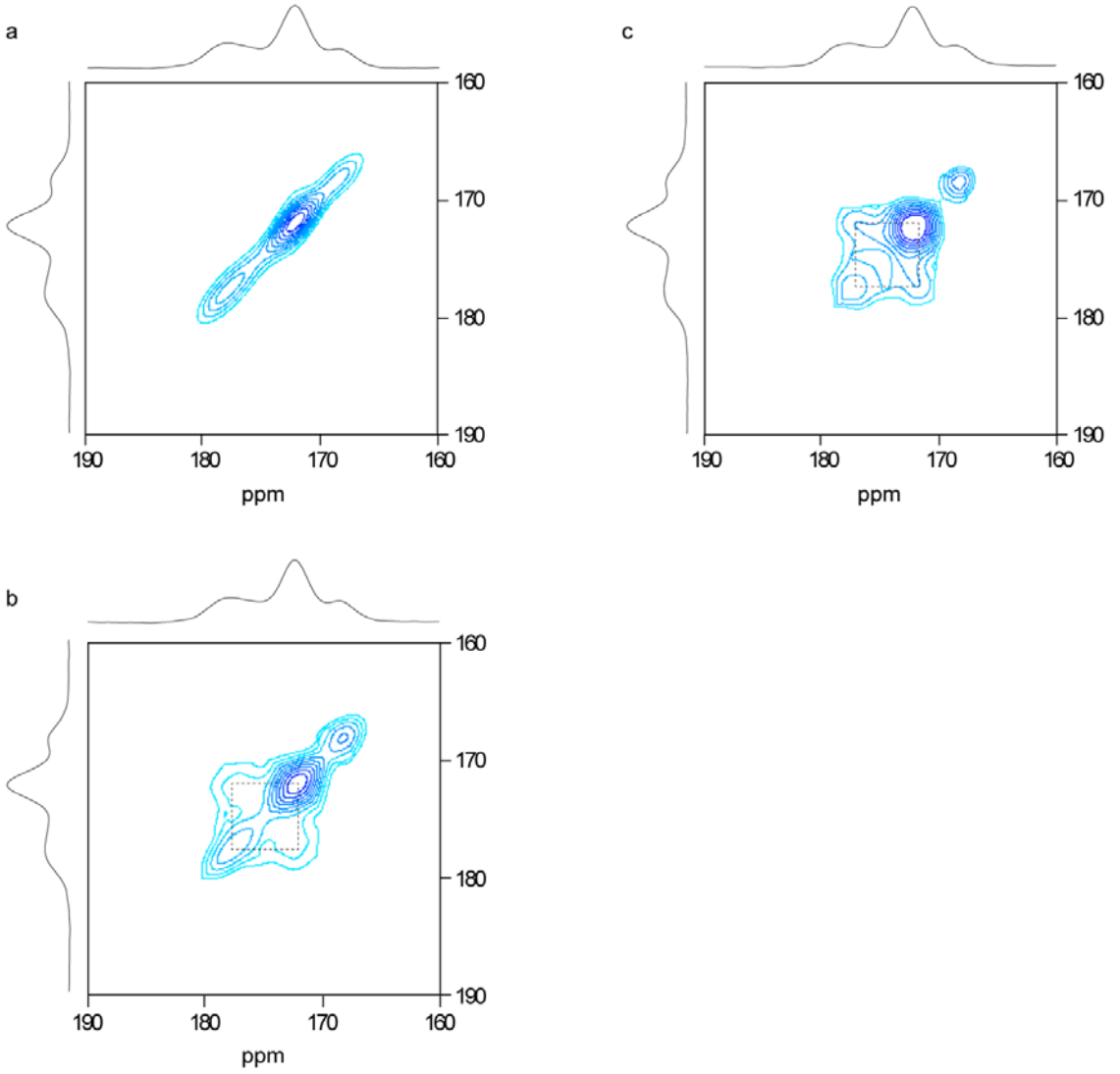

Figure 5.3. 2D exchange ^{13}C MAS NMR spectra of the carbonyl region of 80-20 IMC-PVP amorphous solid dispersions at (a) 50 °C, (b) 60 °C and (c) 70 °C. The sample contained 3% ^{13}C labeled indomethacin (carboxyl carbon) and 97% natural abundant indomethacin. A mixing time of 2s was used. The spectra were symmetrized.

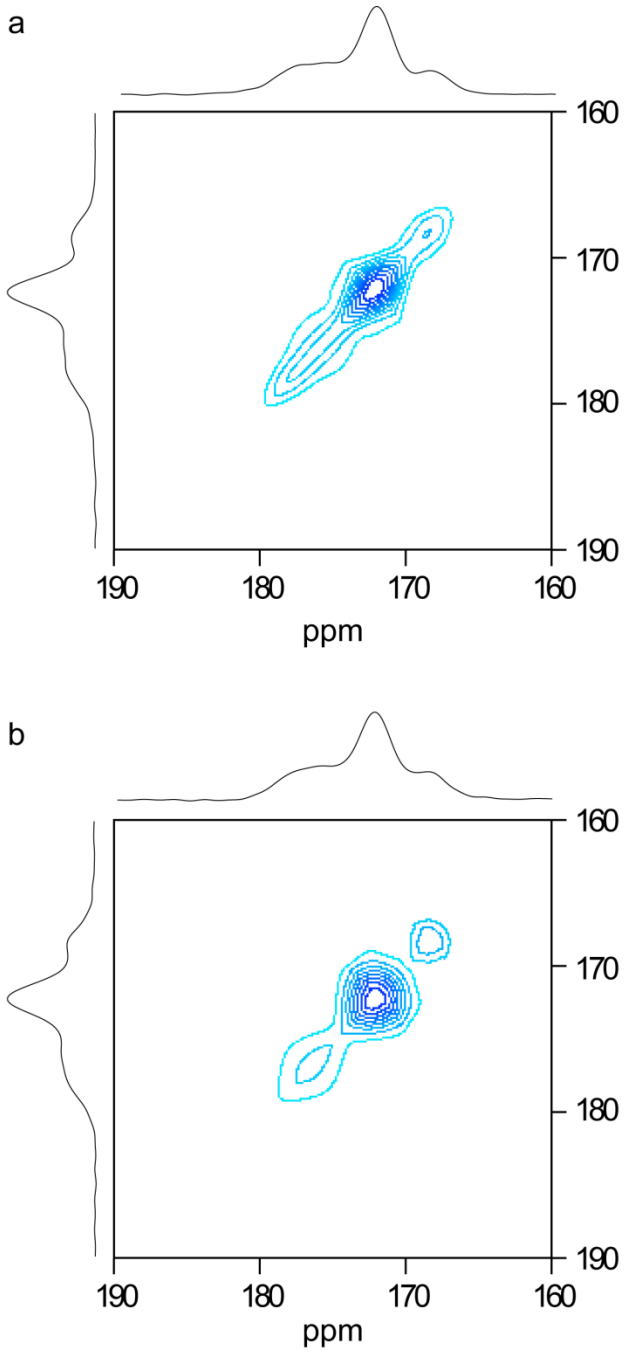

Figure 5.4. 2D exchange ^{13}C MAS NMR spectra of the carbonyl region of 70-30 IMC-PVP amorphous solid dispersions at (a) 70 °C, and (b) 80 °C. The sample contained 3% ^{13}C labeled indomethacin (carboxyl carbon) and 97% natural abundant indomethacin. A mixing time of 2s was used. The spectra were symmetrized.

5.3.3 Molecular Mobility of Amorphous Indomethacin in a Dilute System

An indomethacin-polystyrene amorphous solid dispersion with 1% drug loading was investigated as a model system to study the mobility of the drug in a very dilute environment. Figure 5.5 shows the 2D exchange ^{13}C NMR spectra of the carbonyl region of the sample at 40 and 50 °C. No cross peaks were detected at 40 °C, but cross peaks were observed at 50 °C. The onset glass transition temperature of the system is 49 °C and the midpoint value is 59 °C. The cross peaks suggested interconversion between the indomethacin cyclic dimers and the free carboxylic acids even in a very dilute environment in the rubbery state. Since the onset T_g value of the sample is 49 °C, IMC at 50 °C is a glass that is not at the equilibrium. This is exactly what is shown from the 2D exchange NMR spectra in Figure 5.5. One can recall Figure 4.13 of Chapter 4 where the Van't Hoff plot also deviates from linearity at temperatures below 50 °C. These two studies are in excellent agreement with each other

Besides exchange experiments, mobility can also be studied by spectral line shape. Figure 5.6 shows the carbonyl region of the ^{13}C spectra of 1% IMC in polystyrene at ten different temperatures. At low temperatures, the spectra consist of two resolved peaks, representing the carboxylic acid dimer and the free carboxylic acid. Above the glass transition temperature, the peaks gradually became broadened. At 80 °C, the two peaks became so broad that they were indistinguishable. Beyond this temperature, the two peaks coalesced into a single peak which became narrower again as temperature increased. The broadening of the peaks and the eventual coalescence are a result of the overlap between the NMR spectral time scale and the time scale of the interconversion between the dimer and the free carboxylic acid. The chemical shift of the collapsed single

peak is given by the mean of the two chemical shifts, weighted by the equilibrium concentrations of the two species. Thus, a gradual upfield shift towards the free carboxylic acid species is seen as temperature increases.

Because of the coalensce, it is difficult to measure the extent of spectral broadening of indomethacin. For this reason, the non-protonated phenyl carbon in polystyrene was instead investigatead to determine the temperature dependence of the linewidth. Figure 5.7 shows the linewidth of this carbon as a function of temperature. The linewidth is invariant below T_g, and starts to increase above T_g. The spectra achieves maximum broadening at around 353 K, which is approximately 30 K higher than T_g. The maximum line broadening corresponds to a motional frequency of the molecule that is equivalent to the line narrowing technique, which is the proton decoupling field or the magic angle spinning (MAS) rate. To differentiate between the two mechanisims, experiments were carried out where the sample was spun at 1.5 kHz and 20 °C. Little difference in linewidth was observed between the two spectra obtained with MAS of 4 kHz and 1.5 kHz, indicating MAS was not the mechanism interfering with the molecular motions in the systems, but the dipolar decoupling was. Taking the proton decoupling field of 62.5 kHz, the average correlation time at 353 K can be estimated by

$$\langle \tau \rangle = \frac{1}{\omega_H} = \frac{1}{2\pi\nu} \qquad (5.2)$$

where ν equals 62.5 kHz. The average correlation time $\langle \tau \rangle$ is estimated to be 2.5 μs at 353 K. Temperature dependent linewidth broadening has been observed in PEO[126] and in a small molecule amorphous blend[127], where the average correlation times were estimated

to be 2.3 μs at 328 K and 1.9 μs at 325 K using this method. The value obtained in this study is quite reasonable compared to these results.

It is interesting to see from Figures 5.6 and 5.7 that both indomethacin and polystyrene achieve the maximum spectral linewidth at the same temperature. This is an indication that these two components are miscible and undergo the same motional processes. To investigate the phase homogeneity of the system, ^{1}H $T_{1\rho}$ relaxation times of the two components were measured at selected temperatures and the results are shown in Table 5.1. As is seen from the table, indomethacin and polystyrene are intimately mixed on the nanometer scale at all temperatures investigated, as indicated by the similar ^{1}H $T_{1\rho}$ relaxation times of the two components. The relaxation times of indomethacin carboxylic acid protons seem to be closer in value to the polystyrene phenyl ring protons than the backbone alkyl protons, even though the differences are not very significant. This observation could indicate that the indomethacin molecules are primarily associated with the phenyl ring of polystyrene through hydrophobic interactions.

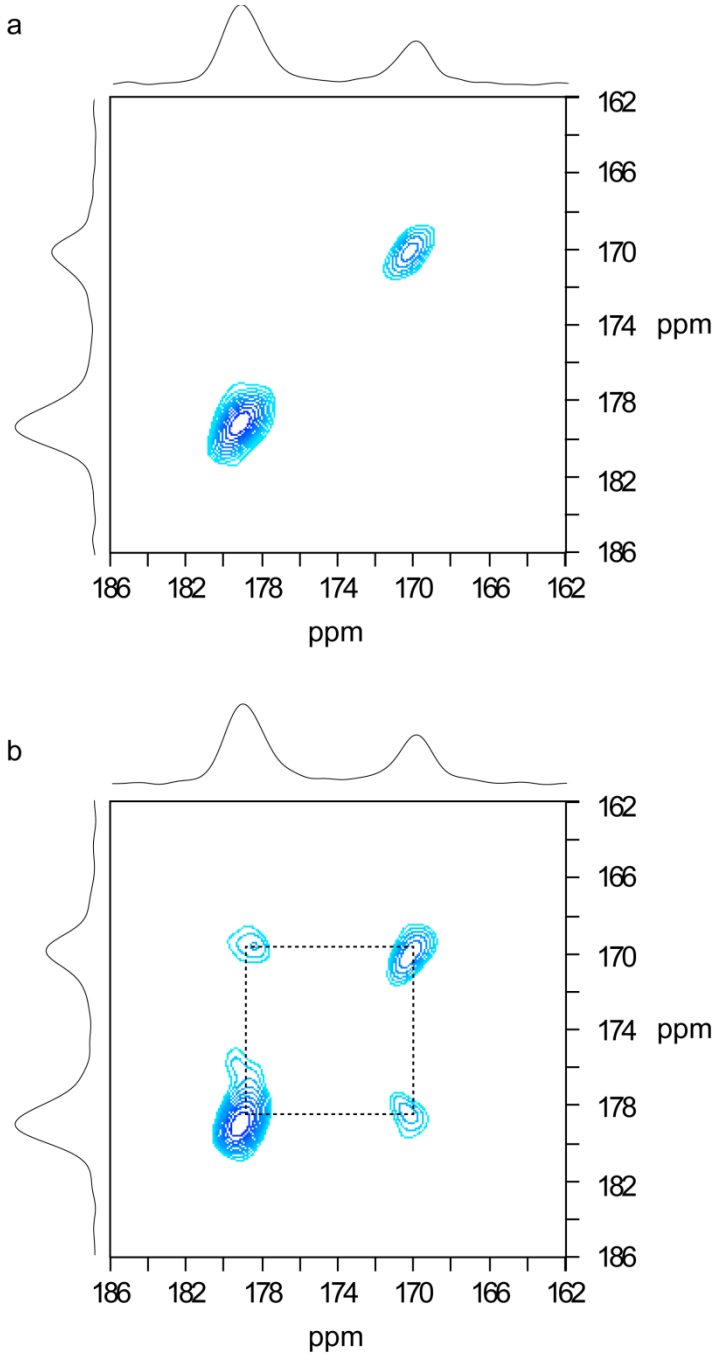

Figure 5.5. 2D exchange ^{13}C MAS NMR spectra of the carbonyl region of 1% IMC in polystyrene at (a) 40 °C, and (b) 50 °C. IMC was ^{13}C labeled at the carboxylic acid carbon. A mixing time of 2s was used.

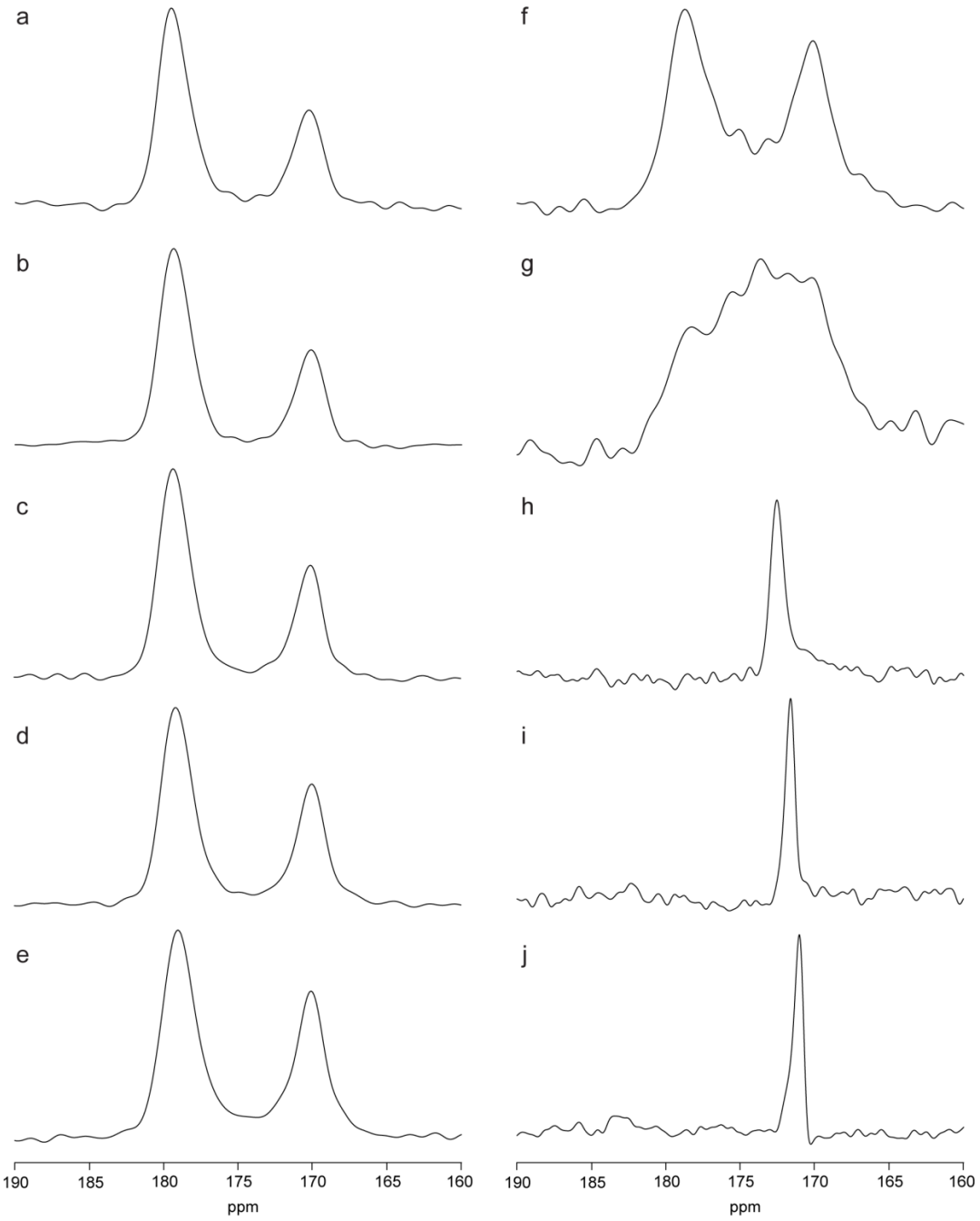

Figure 5.6. ^{13}C spectra of the carboxylic acid carbon of 1% amorphous indomethacin in polystyrene at (a) 20 °C, (b) 30 °C, (c) 40 °C, (d) 50 °C, (e) 60 °C, (f) 70 °C, (g) 80 °C, (h) 110 °C, (i) 140 °C, and (j) 160 °C. Spectra a-g were collected by cross polarization. Spectra h-j were collected by direct polarization.

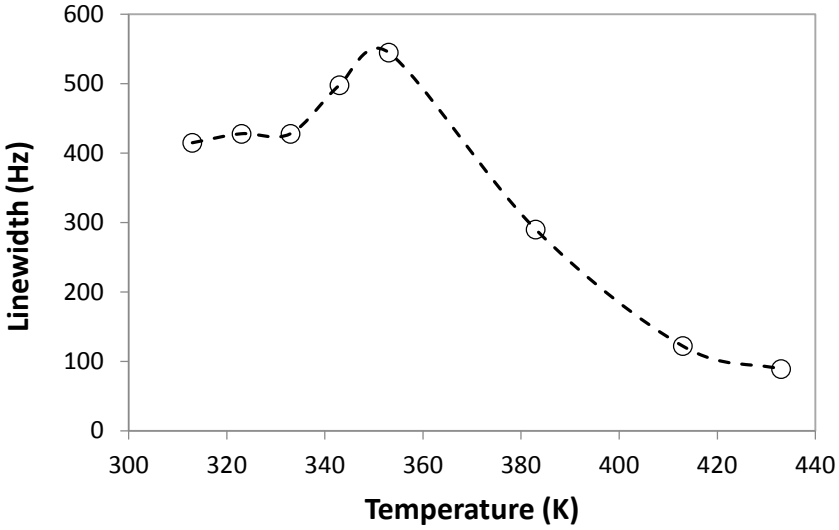

Figure 5.7. Temperature dependence of ^{13}C SSNMR linewidth of the non-protonated phenyl carbon of polystyrene in the IMC-polystyrene amorphous solid dispersion.

Table 5.1. ^{1}H $T_{1\rho}$ relaxation times of different species in the IMC-PS amorphous solid dispersion with 1% IMC.

		IMC (179 ppm)	IMC (170 ppm)	PS (147 ppm)	PS (128 ppm)	PS (41 ppm)
20 °C	^{1}H $T_{1\rho}$	7.3	6.8	7.0	6.6	6.6
	SE	0.3	0.6	0.2	0.1	0.1
	95% CI	6.684 to 7.974	5.412 to 8.220	6.590 to 7.436	6.331 to 6.938	6.438 to 6.851
40 °C	^{1}H $T_{1\rho}$	6.2	5.7	5.9	6.1	6.0
	SE	0.3	0.5	0.1	0.1	0.1
	95% CI	5.557 to 6.806	4.480 to 6.961	5.726 to 6.173	5.925 to 6.357	5.782 to 6.293
50 °C	^{1}H $T_{1\rho}$	4.5	5.3	4.4	4.2	3.8
	SE	0.2	0.4	0.2	0.1	0.1
	95% CI	4.034 to 5.062	4.418 to 6.264	4.014 to 4.852	3.881 to 4.530	3.618 to 4.033

5.1 Conclusions

In this chapter, molecular mobilities and dynamics of three types of amorphous systems were studied using solid-state NMR relaxation times, 2D exchange experiments and linewidth analyses. The systems under study were neat amorphous indomethacin, high drug loadings of indomethacin amorphous solid dispersions with PVP, and dilute dispersions of amorphous indomethacin in polystyrene. Cross peaks between the carboxylic acid dimers and carboxylic acid-amide complexes were observed near the glass transition temperature for all systems that exhibited these two species. Cross peaks between the carboxylic acid dimers and the free carboxylic acid were observed near the glass transition temperature for the dilute indomethacin system. The cross peaks indicated exchange processes between dimers and the carboxylic acid-amide complexes or between dimers and the free carboxylic acids. Disordered chains were not found to exchange with the other species in all systems. The exact reason for this is unclear.

For the dilute amorphous indomethacin system, spectral line shapes were analyzed as a function of temperature. The analysis revealed that the motional processes of indomethacin and polystyrene were coupled above the glass transition temperature. This is confirmed by the analysis of ^{1}H $T_{1\rho}$ relaxation times of the two components as a function of temperature. The result also suggested that the system was at equilibrium above the glass transition temperature.

Chapter 6. Impact of Miscibility, Hydrogen Bonding, and Mobility on Physical Stability of Amorphous Solid Dispersions

6.1 Introduction

Amorphous solid dispersions represent a major enabling technique to increase the bioavailability of poorly water soluble compounds. This type of amorphous solid dispersion is an amorphous system where the active pharmaceutical ingredients (APIs) in the amorphous state are homogeneously dispersed in matrices of polymer or other excipients. One of the biggest issues concerning this approach is achieving the physical stability needed for maintaining shelf life. Crystallization during storage often leads to reduced dissolution rate and bioavailability. Thus, the ability to assess the risk and predict the physical stability is critical in developing amorphous solid dosage forms.

Crystallization process of an API from an amorphous solid dispersion is very complicated, as several factors impact the crystallization behavior of an API. These include: the intrinsic crystallization tendency of the amorphous API,[26, 72, 128, 129] miscibility between the API and polymer,[62] molecular-level interactions between the API and polymer,[32, 56] and mobility of the amorphous system.[57, 111, 130-132] In addition, the absorption of water has been shown to promote crystallization from amorphous APIs and amorphous solid dispersions due to the plasticizing effect of water.[34, 133, 134]

In Chapters 3, a method was established to determine the miscibility of the API and polymer in an amorphous solid dispersion on the nanometer length scale using solid-state NMR ^{1}H relaxation times. In Chapter 4, it was demonstrated that with a 70% drug

loading, indomethacin carboxylic acid dimers were almost fully disrupted in amorphous solid dispersions with PVP, and most of hydrogen bonds were between the drug and the polymer. In Chapter 5, molecular mobility in indomethacin amorphous systems was studied using solid-state NMR relaxation times and exchange processes. While understanding these fundamental interactions is critical to evaluate the molecular environment in amorphous solid dispersions, it is important to understand how these interactions impact crystallization of amorphous drugs. In this chapter, the physical stabilities of three miscible amorphous solid dispersions, each having different degrees of hydrogen bonding between the API and the polymer under different storage conditions were studied.

Indomethacin, nifedipine and indomethacin methyl ester were selected as the three APIs to represent three cases with varying degrees of hydrogen bonding capabilities with poly(vinylpyrrolidone) (PVP). Among the three different molecules, indomethacin having a carboxylic acid group will form the strongest hydrogen bond with PVP. Nifedipine can form an intermediate-strength hydrogen bond with PVP through a secondary amine. Indomethacin methyl ester, having no carboxylic acid functional group, cannot form hydrogen bonds with PVP. A drug/polymer weight ratio of 7:3 was selected for all three systems because this is the ratio corresponding to a near total disruption of indomethacin dimers. The ratio was kept the same for the other two systems for the purpose of comparison. Powder X-ray diffraction (PXRD), Raman spectroscopy, and polarized light microscopy were performed to detect crystallization. Modulated DSC (MDSC) was performed to detect miscibility. TGA was performed to obtain the water

content. Solid-state NMR spectroscopy was used to determine miscibility, mobility and crystallinity of the amorphous solid dispersions.

6.2 Materials and Methods

6.2.1 Materials

Indomethacin (IMC, γ form, minimum purity 99%) was purchased from Sigma-Aldrich (St Louis, MO). Nifedipine (NIF, minimum purity 98.0 %) was purchased from TCI America (Portland, OR) and was protected from light whenever possible. Indomethacin methyl ester was synthesized from indomethacin and methanol. The details are described in the next section. PVP K25 (Kollidon 25, M_w=28-34 kg/mole) was obtained from BASF (Edison, NJ). PVP was vacuum dried at 70 °C overnight and stored over Drierite™ at all times. Sodium bromide (NaBr) and sodium chloride (NaCl) were purchased from EMD Chemicals (Gibbstown, NJ). The chemical structures of indomethacin, nifedipine, indomethacin methyl ester and PVP are shown in Figure 6.1.

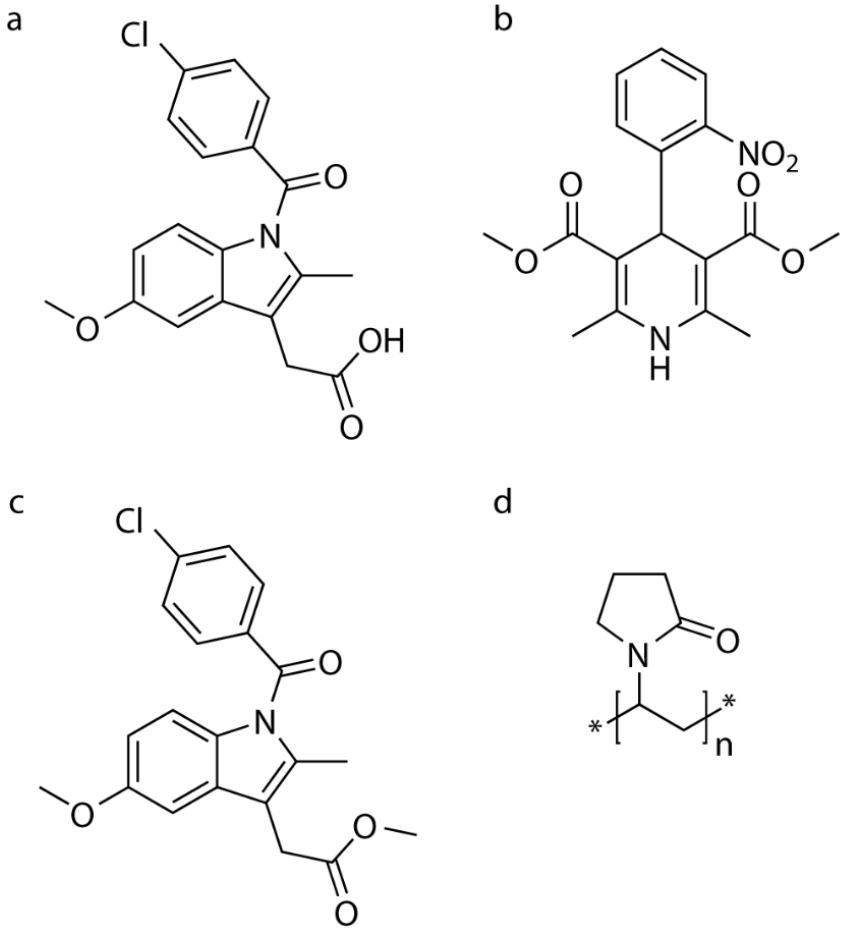

Figure 6.1. Chemical structures of (a) indomethacin, (b) nifedipine, (c) indomethacin methyl ester, and (d) PVP.

6.2.2 Synthesis of Indomethacin Methyl Ester

Indomethacin methyl ester was synthesized by refluxing indomethacin and methanol in the presence of sulphuric acid. 10 grams of γ-indomethacin, 200 ml of methanol, 0.5 ml of sulphuric acid, and approximately 1 gram of molecular sieves (3Å, 4x8 mesh size) were added into a round-bottom flusk. The molecular sieves acted as a "water trap" to remove water (water is a product of the reaction) and favor the reversible reaction towards esterification. The solution was refluxed overnight at 70 °C in an oil bath with a stirring rate of 100 rpm. When the reaction was stopped, molecular sieves were filtered out and crystallization occurred immediately as the temperature dropped. The obtained crystals were washed with methanol and then with MilliQ water several times before being vacuum dried at room temperature overnight. The obtained product was pure as determined by thin layer chromatography (TLC). The compound was characterized by solution ^{1}H NMR, PXRD, ^{13}C solid-state NMR, DSC and TGA.

6.2.3 Preparation of Amorphous Solid Dispersions

Amorphous solid dispersions of IMC-PVP, NIF-PVP and IMC methyl ester-PVP were prepared via melt quenching. One gram samples of drug and polymer in weight ratio of 7:3 drug:polymer were cryomilled at 10 Hz (SPEX SamplePrep 6770 Freezer/Mill, SPEX SamplePrep LLC., Metuchen, NJ) for five cycles. Each cycle consisted of 2 minutes of milling and 2 minutes of cool down. Liquid nitrogen was used as a coolant. The cryomilling procedure was used to ensure the optimum mixing between the drug and polymer prior to melting. The cryomilled mixtures were then transferred

into a Teflon beaker and heated in an oil bath for several minutes until melted. The mixtures were slightly stirred using a spatula to ensure mixing. The IMC amorphous solid dispersion was heated at 170 °C, the NIF dispersion was heated at 180 °C, and the IMC methyl ester dispersion was heat at 160 °C. The mixtures typically melted within 10 minutes of heating. The melted mixtures were then solidified by quench-cooling with liquid nitrogen. The solid dispersions were vacuum dried at room temperature overnight to minimize residual moisture. The IMC and NIF amorphous solid dispersions were ground with a mortar and pestle and sieved using a sieve shaker (Gilson Performer III SS-3, Gilson Company, Lewis Center, OH). Particles of size between 45-300 μm were retained. The IMC methyl ester amorphous solid dispersion was not ground or sieved due to its low glass transition temperature and stickiness at room temperature.

6.2.4 Stability Studies

The IMC-PVP and NIF-PVP amorphous solid dispersions were stored at three different conditions: 50 °C/0% RH, 40 °C/57% RH, and 40 °C/75% RH. Drierite™ desiccants ($CaSO_4$) were used to create the near zero relative humidity. Saturated salt solutions of sodium bromide and sodium chloride were used to control the relative humidity levels of 57% and 75% RH, respectively. The IMC methyl ester-PVP amorphous solid dispersion was stored at 4 °C/0% RH. The reason for choosing 50 °C as a dry condition for the IMC and NIF dispersions was that these amorphous solid dispersions had a glass transition temperature of about 70 °C. A temperature of 50 °C is about 20 °C below their glass transition temperature. Similarly, the IMC methyl ester

dispersion had a glass transition temperature of about 20 °C and the storage temperature was about 16 °C below its glass transition temperature. These conditions were chosen to minimize the effect of glass transition temperature on these different amorphous systems. Samples were analyzed at time 0, and after storage of 1 week, 2 weeks, 1 month, 2 months, and 6 months by PXRD, MDSC, TGA, Raman spectroscopy, polarized light microscopy and solid-state NMR spectroscopy. Dissolution tests were conducted at time 0 and after 6 months of storage.

6.2.5 Powder X-ray Diffraction

Crystallization of amorphous solid dispersions was monitored using a powder X-ray diffractometer (MiniFlex 600, Rigaku Corporation, Japan) with Cu Kα radiation operating at 40 kV and 15 mA. Samples were scanned from 2θ of 2-42° at the rate of 2°/min and a step size of 0.02°.

6.2.6 Microscopic and Spectroscopic Characterization

Crystallization of the samples was monitored at various time points using a optical microscope (Olympus BX 51, Olympus America Inc., Center Valley, PA) equipped with a polarizer (Instec, Boulder, CO) and a first order red compensator (U-TP530, Olympus America Inc., Center Valley, PA). Images were captured using a SPOT Insight digital camera (Diagnostic Instruments, Inc., Sterling Heights, MI).

Crystallization and polymorphic forms of the samples were also studied using Raman spectroscopy (DXR Raman Microscope, Thermo Scientific, Madison, WI) with a

780 nm laser source. Spectra were collected with 20 s exposure time and 20 scans, through a 50x objective and using a 25 μm pinhole aperture. Laser power was typically set between 1 – 2 mW. Fluorescence was removed from the spectra using baseline corrections.

6.2.7 Thermal Characterization

The glass transition temperatures of amorphous solid dispersions at various time points were determined by modulated DSC (MDSC) using a Q2000 differential scanning calorimeter equipped with an RCS90 refrigerated cooling system (TA Instruments, Newcastle, DE). Nitrogen gas was used as the purge gas at a flow rate of 50 mL/min. Temperature and enthalpy were calibrated using indium. Samples (2-5 mg) prepared by melt quenching as described above were placed in TZero™aluminum pans and sealed with TZero™aluminum hermetic lids with one pinhole (TA Instruments, New Castle, DE). Samples were equilibrated at 0 °C, and then heated at 1 °C/min to 200 °C with an amplitude of ±0.5 °C and a modulation period of 60 s. The glass transition was separated into the reversing heat flow signal and was determined by half-height at midpoint using the Universal Analysis software (TA Instruments, Newcastle, DE).

The water contents of amorphous solid dispersions at various time points were measured using thermogravimetric analysis (TGA Q20, TA Instruments, Newcastle, DE). Nitrogen gas was used as the purge gas at a flow rate of 40 mL/min for the balance and 60 mL/min for the sample. Temperature was calibrated using a nickel standard and a magnetic bar for the Curie Point Temperature. Weight was calibrated using standard weights (200 mg and 1 g). During the experiments, approximately 10 mg of sample was

placed on a platinum pan and heated at 10 °C/min from room temperature to 200 °C. The weight loss from room temperature to 120 °C was analyzed for the water content.

6.2.8 Solid-State NMR Spectroscopy

All solid-state NMR spectra were acquired using a Tecmag Redstone HF3 2RX spectrometer (Tecmag, Inc., Houston, TX), operating at 75.48 MHz for ^{13}C. Samples were packed into 7.5 mm zirconia rotors and sealed with Teflon or Kel-F end caps (Revolution NMR, LLC, Fort Collins, CO). Experiments were performed using a 7.5 mm double-resonance MAS probe (Varian, Palo Alto, CA). All ^{13}C spectra were acquired under magic angle spinning (MAS)[43] at 4 kHz, using ramped-amplitude CP,[45] total sideband suppression (TOSS)[44] and SPINAL64 decoupling[73] with a ^{1}H decoupling field of about 62 kHz. A spectral width of 15 kHz, a ^{1}H 90° pulse width of about 4.5 μs, a contact time of 2 ms and a pulse delay of 1.5 – 2 times the measured T_1 were used in all experiments. 3-Methylglutaric acid was used to optimize spectrometer settings and was used as an external standard, with the methyl peak referenced to 18.84 ppm.[74] All experiments were conducted at -30 °C to avoid crystallization during the experiments. For samples that did not show crystallization from PXRD and microscope observation, a total of 512 points were acquired and the FIDs were zero-filled to 4096 points. For samples that showed crystallization from PXRD and microscope observation, a total of 2048 points were acquired and the FIDs were zero-filled to 16384 points. No line-broadening was used to transform the spectra.

^{1}H T_1 relaxation values were measured using the saturation-recovery experiment through ^{13}C observation. For samples that did not show crystallization, a total of 512

points were acquired and the FIDs were zero-filled to 4096 points with 80 Hz of Gaussian line-broadening. For samples that showed crystallization, a total of 1024 points were acquired and the FIDs were zero-filled to 16384 points with 20 Hz of Gaussian line-broadening. In the Fourier-transformed spectrum, the peak of interest was integrated and plotted against recovery delay times and the values were fitted to the following equation using GraphPad Prism (GraphPad Software, Inc., La Jolla, CA)

$$M = M_0 \cdot (1 - e^{-\frac{\tau}{T_1}}) \quad (6.1)$$

where M is the integrated signal intensity and τ is the recovery delay time. M_0 is an amplitude parameter obtained from the fit and T_1 is the obtained spin-lattice relaxation time.

^{1}H $T_{1\rho}$ relaxation times were measured by varying the spin-lock duration time following a 90° pulse. A frequency of about 55-60 kHz was used for the spin-lock field. The acquisition points and Fourier transform conditions are the same as those used in the ^{1}H T_1 experiment. The peak of interest was integrated and plotted against the spin-lock duration times and the values were fitted to the following equation using GraphPad Prism (GraphPad Software, Inc., La Jolla, CA)

$$M = M_0 \cdot e^{-\frac{\tau}{T_{1\rho}}} \quad (6.2)$$

where M is the integrated signal intensity and τ is the spin-lock duration time. M_0 is an amplitude parameter obtained from the fit and $T_{1\rho}$ is the obtained spin-lattice relaxation time in the rotating frame.

In order to quantify the crystallinity of the NIF sample stored at 40 °C/75% RH, the 163-173 ppm regions in the spectra of these samples were fitted by a linear combination of three reference spectra (i.e. amorphous, the α form, and the β form) that

represent the possible components in the sample using least square procedures with MATLAB (MathWorks, Natick, MA).

6.2.9 Dissolution Studies

Dissolution experiments were carried out using a Pion μDiss Profiler with a fiber optic detection system (Pion Inc., Billerica, MA). The dissolution medium used was 20 mL of pH 2 HCl buffer for IMC amorphous solid dispersions and 20 mL of 50 mM pH 6.8 phosphate buffer for NIF amorphous solid dispersions. The dissolution media were chosen to minimize the pH effect of ionizable drugs. Tween 80 (15 μg/mL, below CMC) was added to the dissolution media to help wet the particles. Calibration stock solutions for both drugs were prepared in methanol. The stock solution was added into the respective dissolution medium to construct the calibration curve. Concentration of indomethacin was measured at 296 nm from the second-derivative spectrum; concentration of nifedipine was measure at 256 nm from the second derivative spectrum. The use of the second-derivative spectrum mitigates the particle scattering effect.[135, 136] Calibration and dissolution were conducted at 37 °C. Samples weighing 2 mg were used in the dissolution experiments, equivalent to 70 μg/mL of total drug concentration if fully dissolved. Sink conditions were not maintained because the dissolution study was designed to assess supersaturation levels. The dissolution process was monitored over a period of 4 hours, with data collection every 15 seconds for the first hour and every 2 minutes for the rest.

6.3 Results

6.3.1 Characterization of Indomethacin Methyl Ester

As a derivative of indomethacin, the indomethacin methyl ester was synthesized to compare its hydrogen bonding capabilities and the implications on physical stability with the parent compound, indomethacin. The synthesized molecule was fully characterized using solution ^{1}H NMR, PXRD, ^{13}C solid-state NMR, DSC and TGA.

The ^{1}H NMR spectrum of indomethacin methyl ester in $CDCl_3$ is shown in Figure 6.2. The chemical shifts are: 2.37 (s, $-CH_3$), 3.65 (s, $-CH_2$), 3.68 (s, $-OCH_3$), 3.82 (s,-$COOCH_3$), 6.6 (dd, H-6), 6.83/6.85 (d, H-7), 6.93/6.94 (d, H-4), 7.44/7.45 (d, A_2/B_2), 7.64/7.65 (d, A_2/B_2). The chemical shifts are in very good agreement with values reported in the literature.[137]

Indomethacin methyl ester crystal has a pale-yellow color and a long needle shape under the polarized microscope, as shown in Figure 6.3. The crystal was also characterized by DSC, TGA, PXRD and ^{13}C solid-state NMR. The compound has a melting temperature of 91.7 °C as seen in the DSC thermogram (Figure 6.4). The obtained crystal has a minimal amount of residual solvent as shown from the TGA in Figure 6.5. Degradation starts to occur at approximately 195 °C. Figure 6.6 shows the powder X-ray diffractogram, which matches very well with the solved single crystal structure.[138] Figure 6.7 shows the ^{13}C solid-state NMR spectrum. The methyl ester carbonyl carbon has a chemical shift of approximately 174 ppm, an upfield shift of 5 ppm compared to the carboxylic acid carbon in indomethacin (179 ppm). The formation of a methyl ester is also indicated by the new peak emerging around 54 ppm.

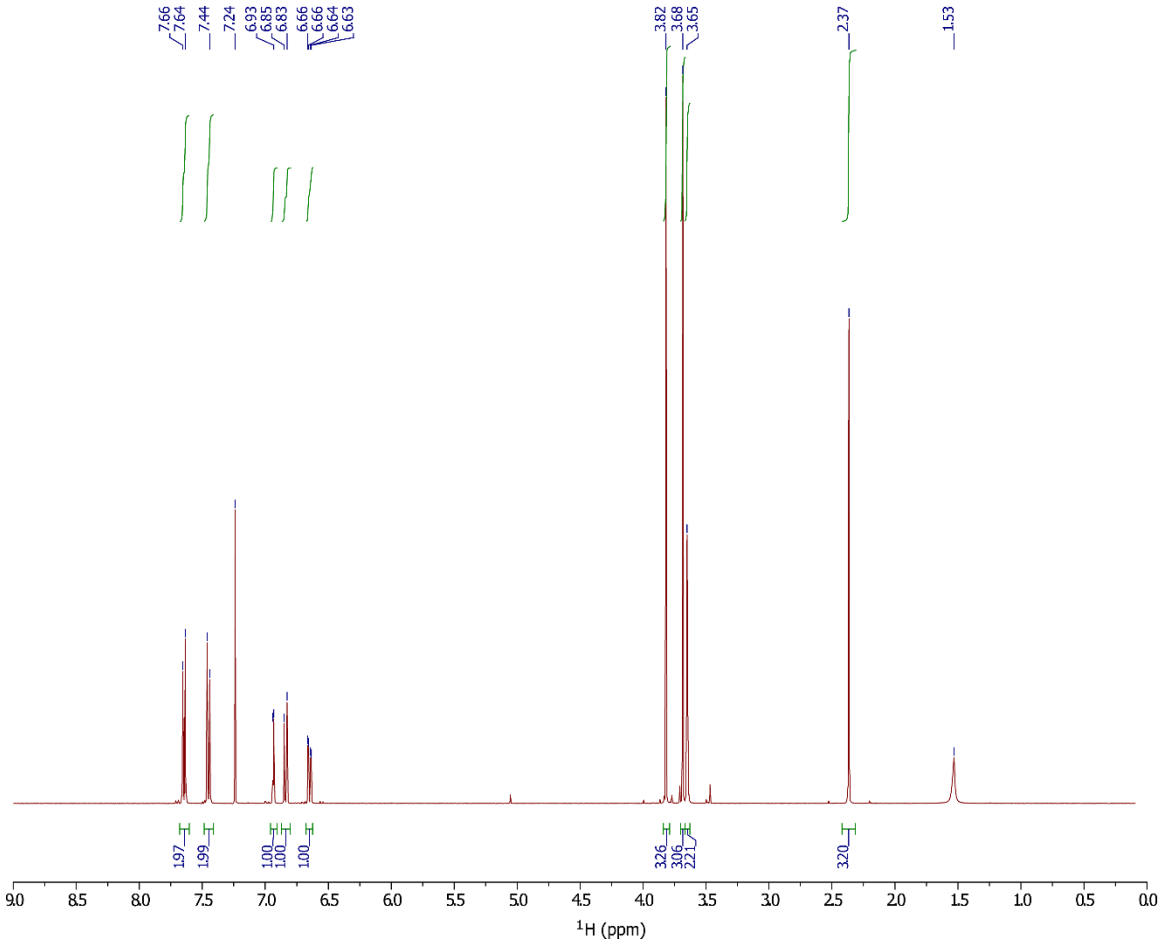

Figure 6.2. ^{1}H NMR spectrum of indomethacin methyl ester in $CDCl_3$.

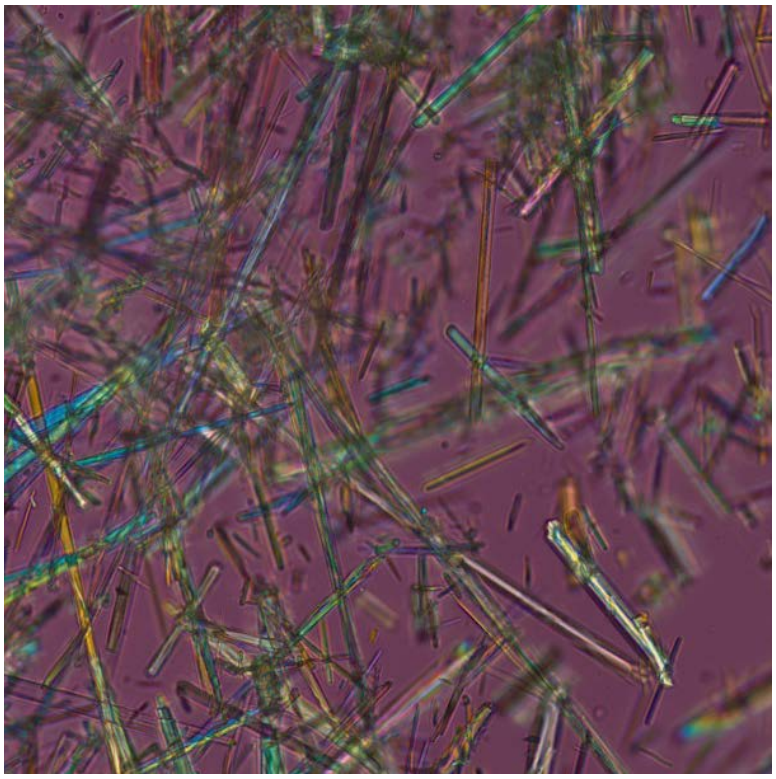

Figure 6.3. Polarized light microscopy image of indomethacin methyl ester.

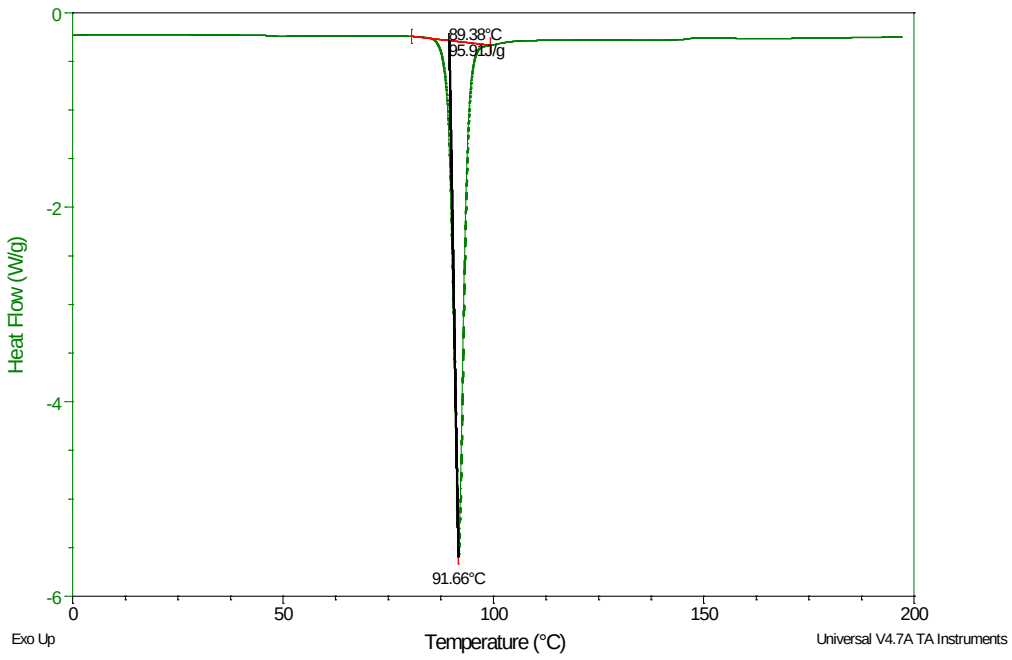

Figure 6.4. DSC thermogram of indomethacin methyl ester.

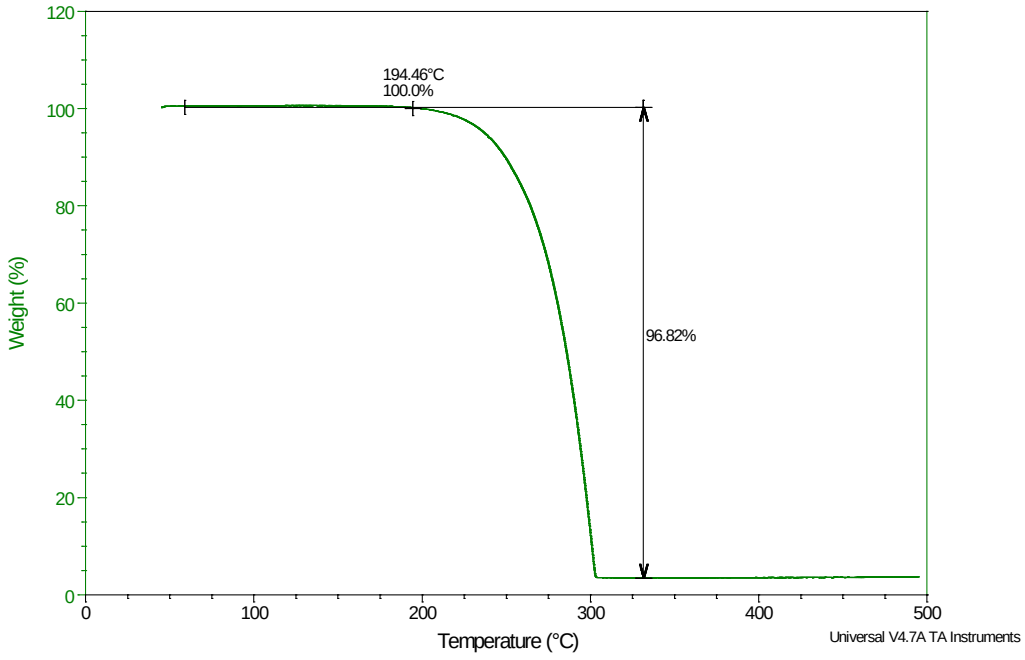

Figure 6.5. TGA of indomethacin methyl ester.

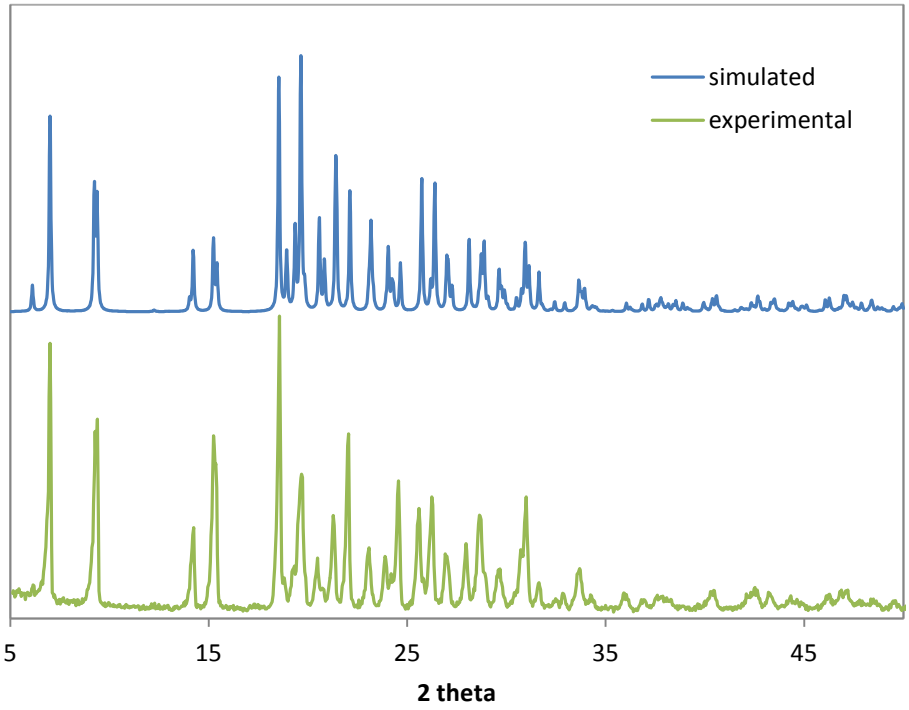

Figure 6.6. Powder X-ray diffractogram of indomethacin methyl ester compared with simulated pattern from solved structure.[138]

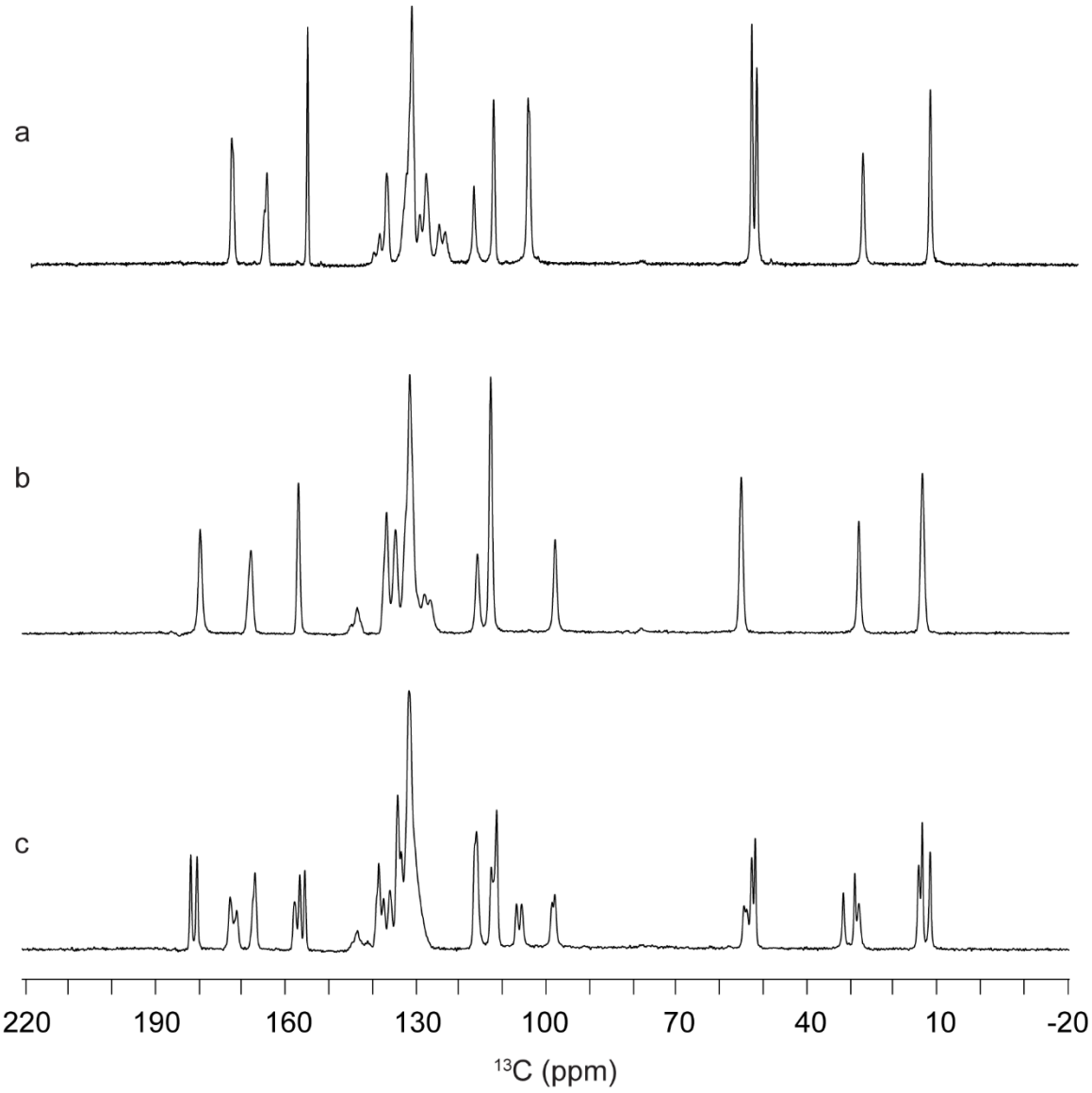

Figure 6.7. ^{13}C CPMAS spectra of (a) indomethacin methyl ester, (b) γ-indomethacin, and (c) α-indomethacin.

6.3.2 Analysis of Stability Samples by Various Techniques

Seven samples that underwent the stability studies were analyzed by PXRD, Raman spectroscopy, polarized light microscopy, MDSC, TGA and solid-state NMR spectroscopy at each time point. This section is organized by techniques and the results obtained through each of these techniques will be discussed. Results obtained from solid-state NMR experiments will be discussed in the end in a separate section.

6.3.2.1 Powder X-ray Diffraction

Figures 6.8 - 6.14 show the powder X-ray diffractograms of 70-30 IMC methyl ester-PVP, 70-30 IMC-PVP and 70-30 NIF-PVP amorphous solid dispersions under different storage conditions. No crystallization was observed from the PXRD patterns for the IMC methyl ester-PVP amorphous solid dispersions stored at 4 °C/0% RH for up to 6 months (Figure 6.8). No crystallization was observed in the IMC-PVP amorphous solid dispersion stored at 50 °C/ 0% RH and that stored at 40 °C/57%RH (Figure 6.9 and 6.10). The IMC-PVP sample stored at 40 °C/75%RH exhibited minor crystalline peaks after 1 month of storage (Figure 6.11). These peaks grew in intensity at the 2 month and 6 month time points. The crystalline peaks correspond to the IMC γ polymorph. Similarly, the NIF-PVP amorphous solid dispersion stored at 50 °C/0% RH and that stored at 40 °C/57%RH exhibited no crystallization for up to 6 months (Figure 6.12 and 6.13). However, the NIF-PVP sample stored at 40 °C/75%RH exhibited crystallinity after just 1 week of storage (Figure 6.14). The crystalline peaks correspond to the β polymorph.

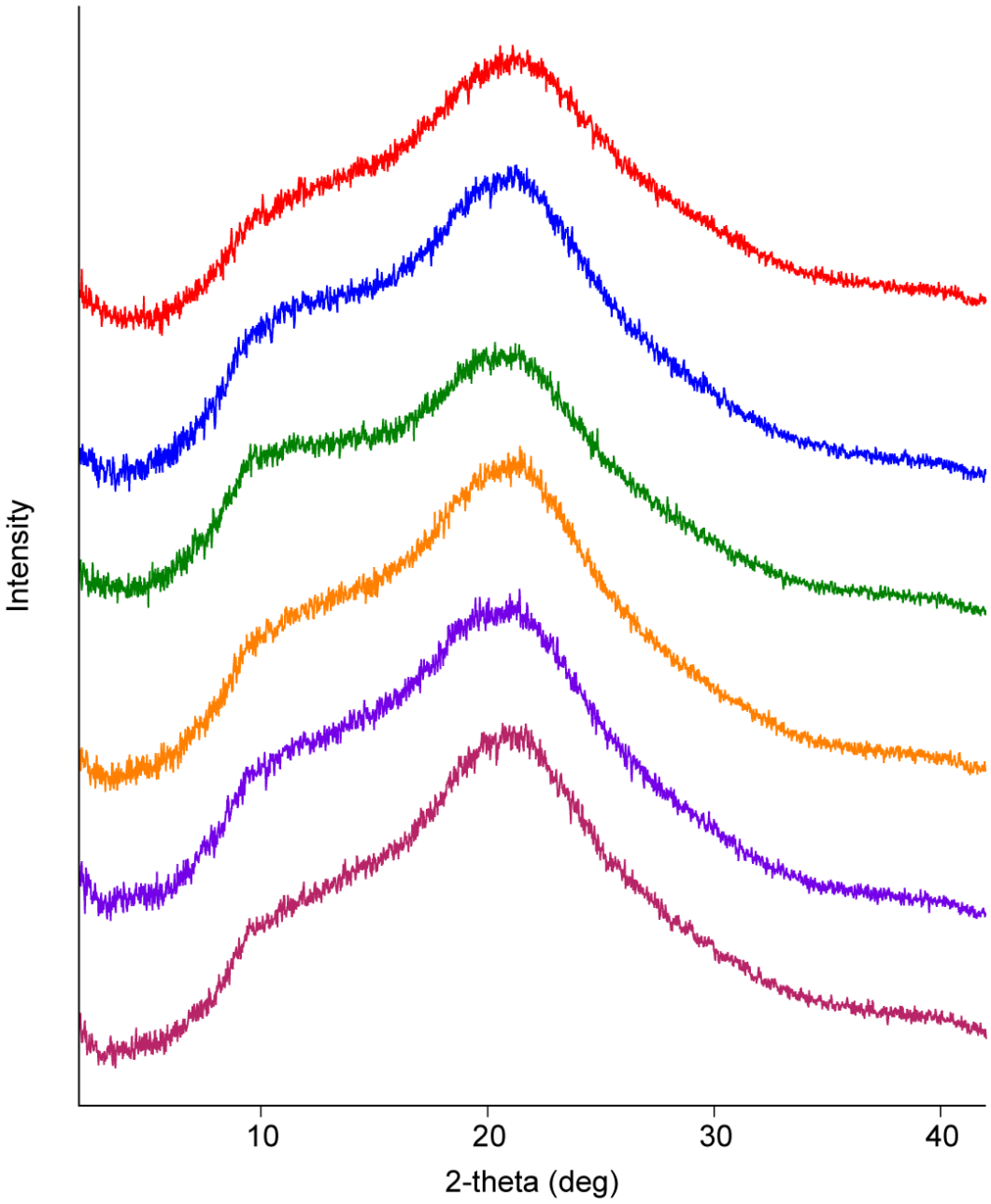

Figure 6.8. PXRD patterns of 70-30 IMC methyl ester-PVP amorphous solid dispersions stored at 4 °C/0% RH. The diffractograms from top to bottom were collected at time 0, 1 week, 2 weeks, 1 month, 2 months and 6 months.

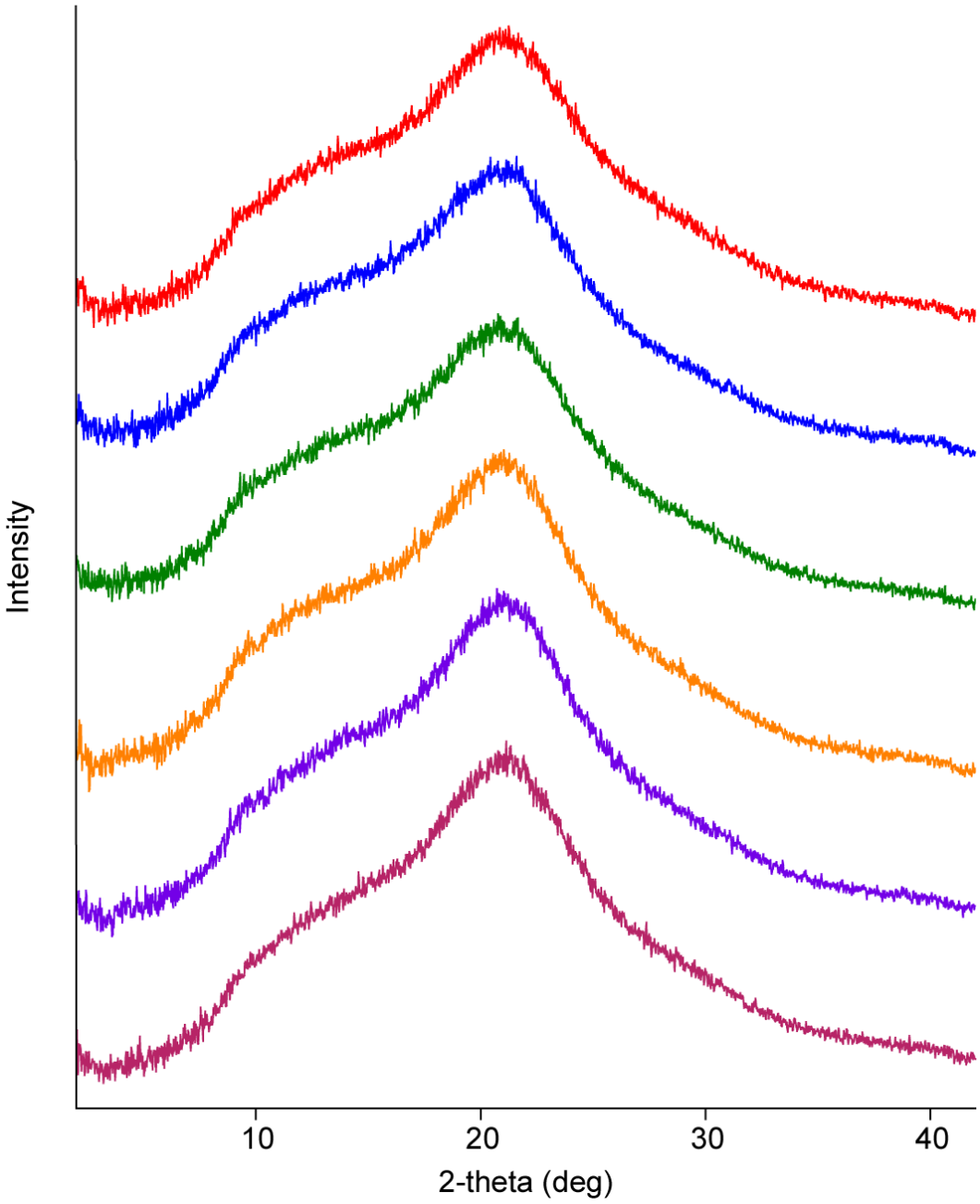

Figure 6.9. PXRD patterns of 70-30 IMC-PVP amorphous solid dispersions stored at 50 °C/0% RH. The diffractograms from top to bottom were collected at time 0, 1 week, 2 weeks, 1 month, 2 months and 6 months.

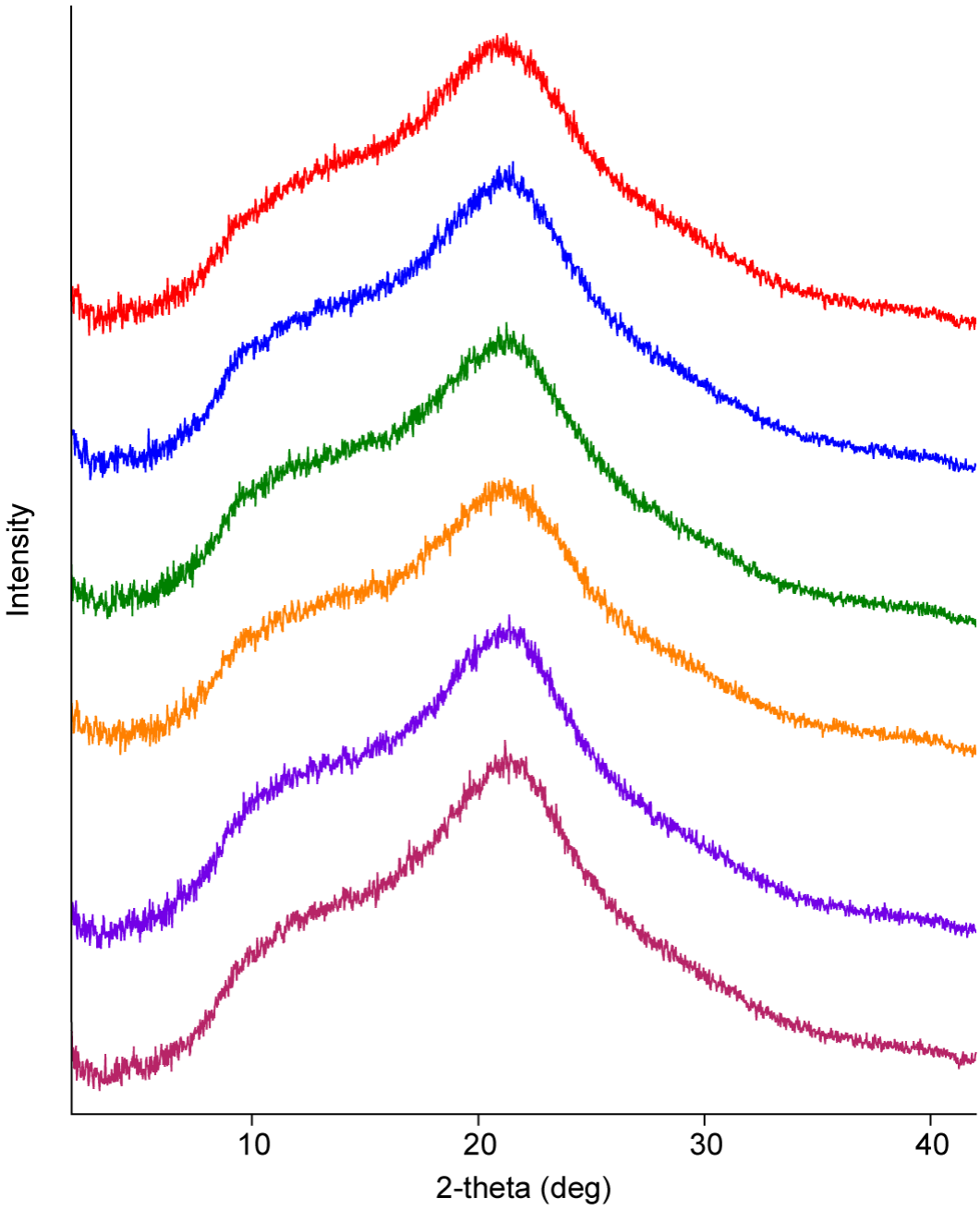

Figure 6.10. PXRD patterns of 70-30 IMC-PVP amorphous solid dispersions stored at 40 °C/57%RH. The diffractograms from top to bottom were collected at time 0, 1 week, 2 weeks, 1 month, 2 months and 6 months.

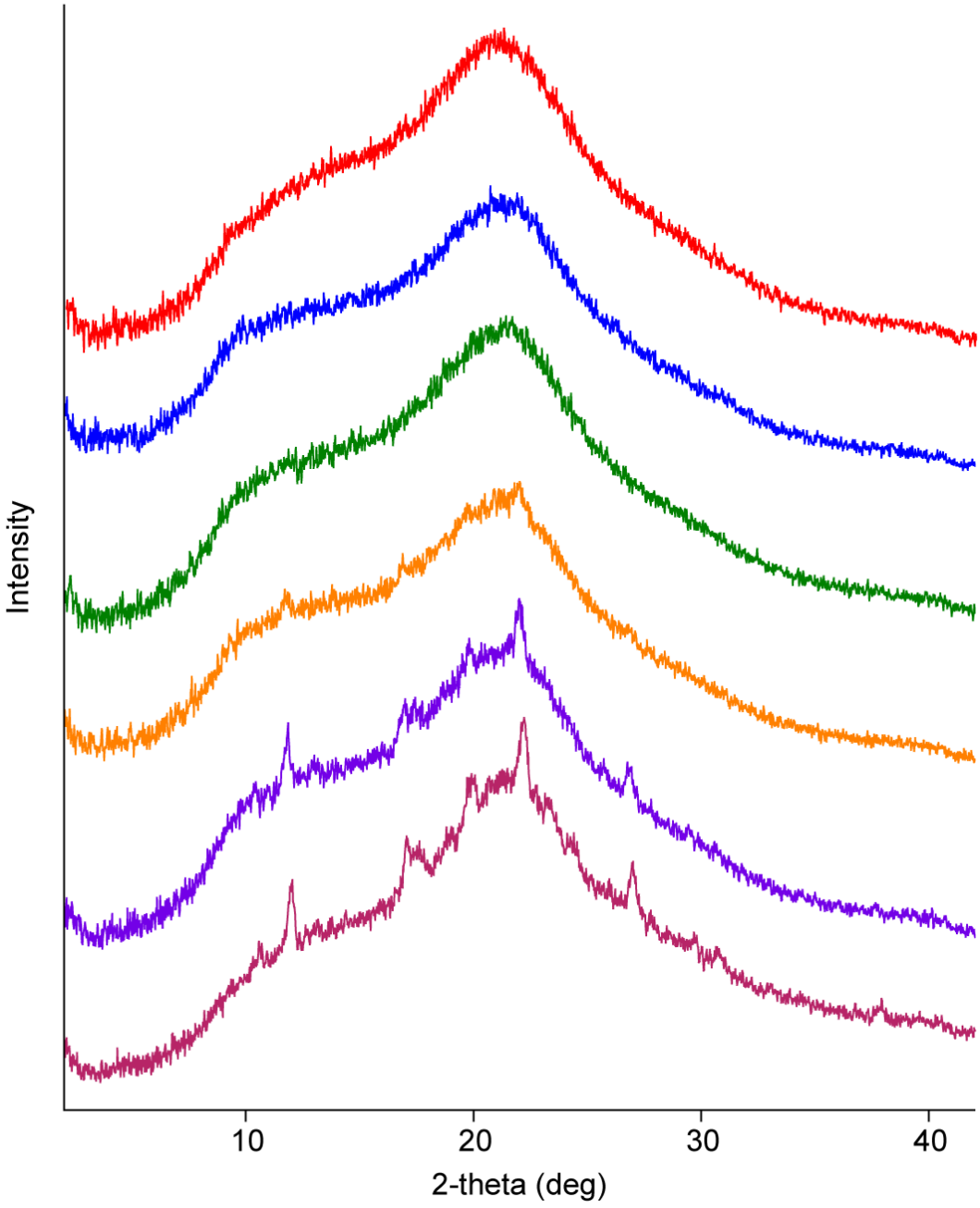

Figure 6.11. PXRD patterns of 70-30 IMC-PVP amorphous solid dispersions stored at 40 °C/75%RH. The diffractograms from top to bottom were collected at time 0, 1 week, 2 weeks, 1 month, 2 months and 6 months.

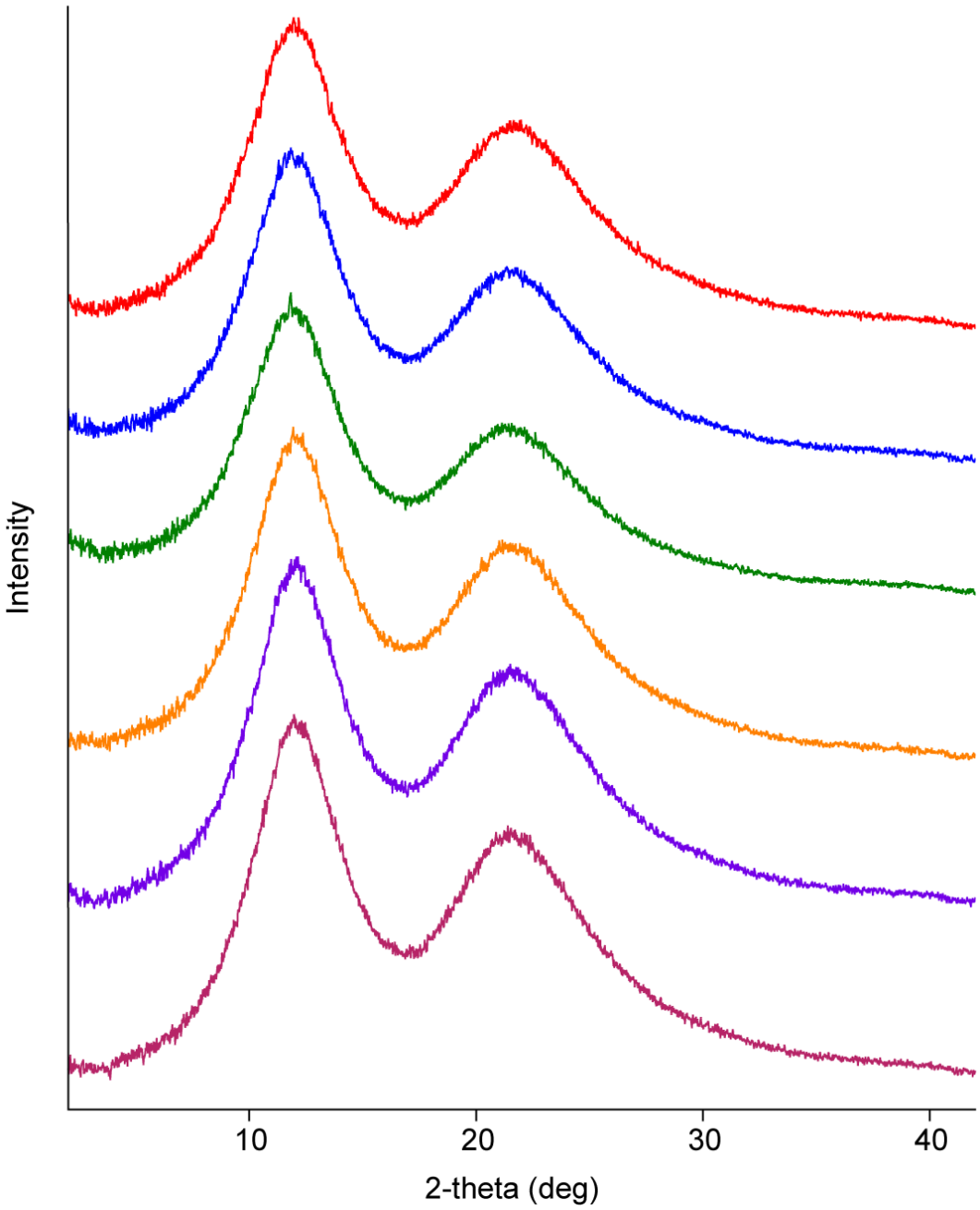

Figure 6.12. PXRD patterns of 70-30 NIF-PVP amorphous solid dispersions stored at 50 °C/0% RH. The diffractograms from top to bottom were collected at time 0, 1 week, 2 weeks, 1 month, 2 months and 6 months.

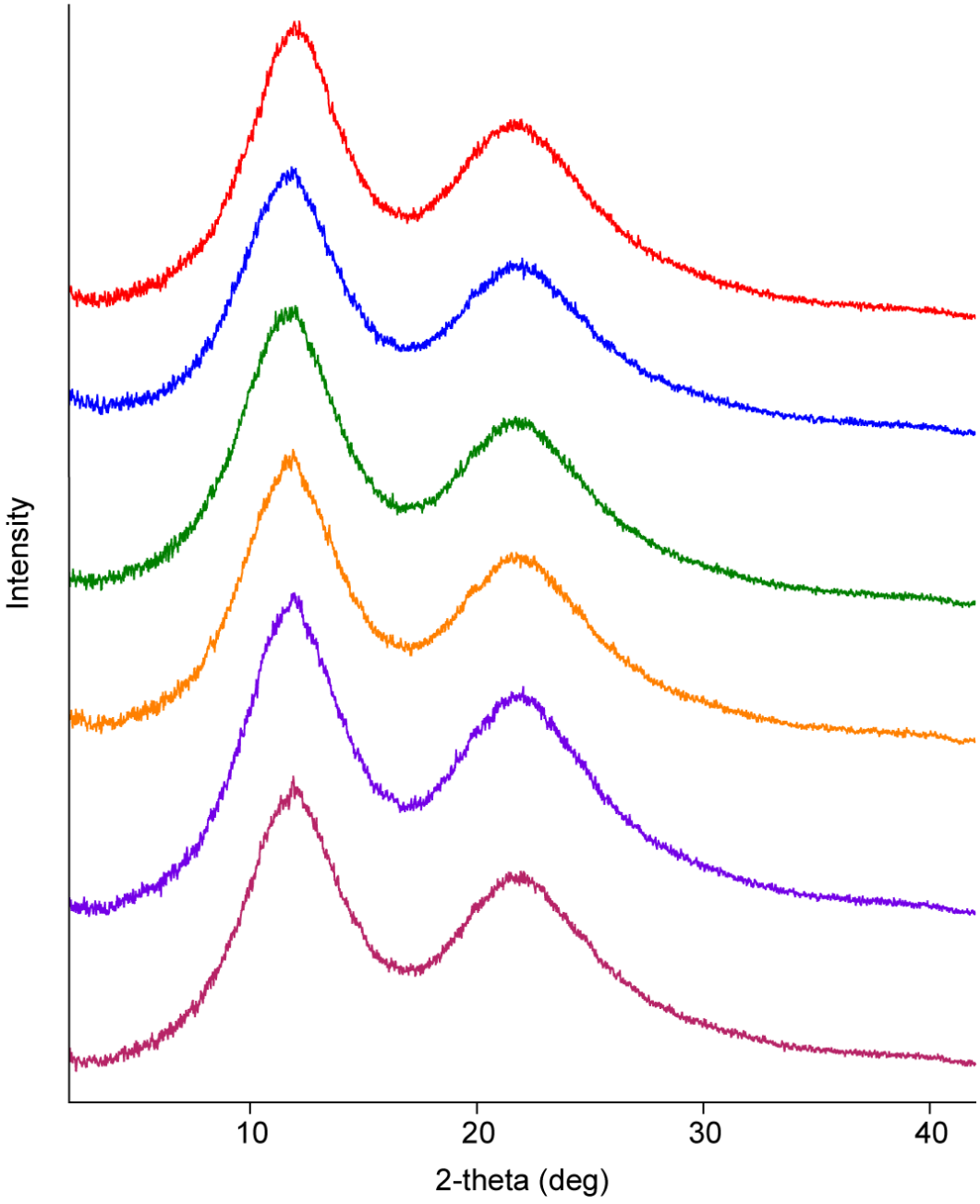

Figure 6.13. PXRD patterns of 70-30 NIF-PVP amorphous solid dispersions stored at 40 °C/57%RH. The diffractograms from top to bottom were collected at time 0, 1 week, 2 weeks, 1 month, 2 months and 6 months.

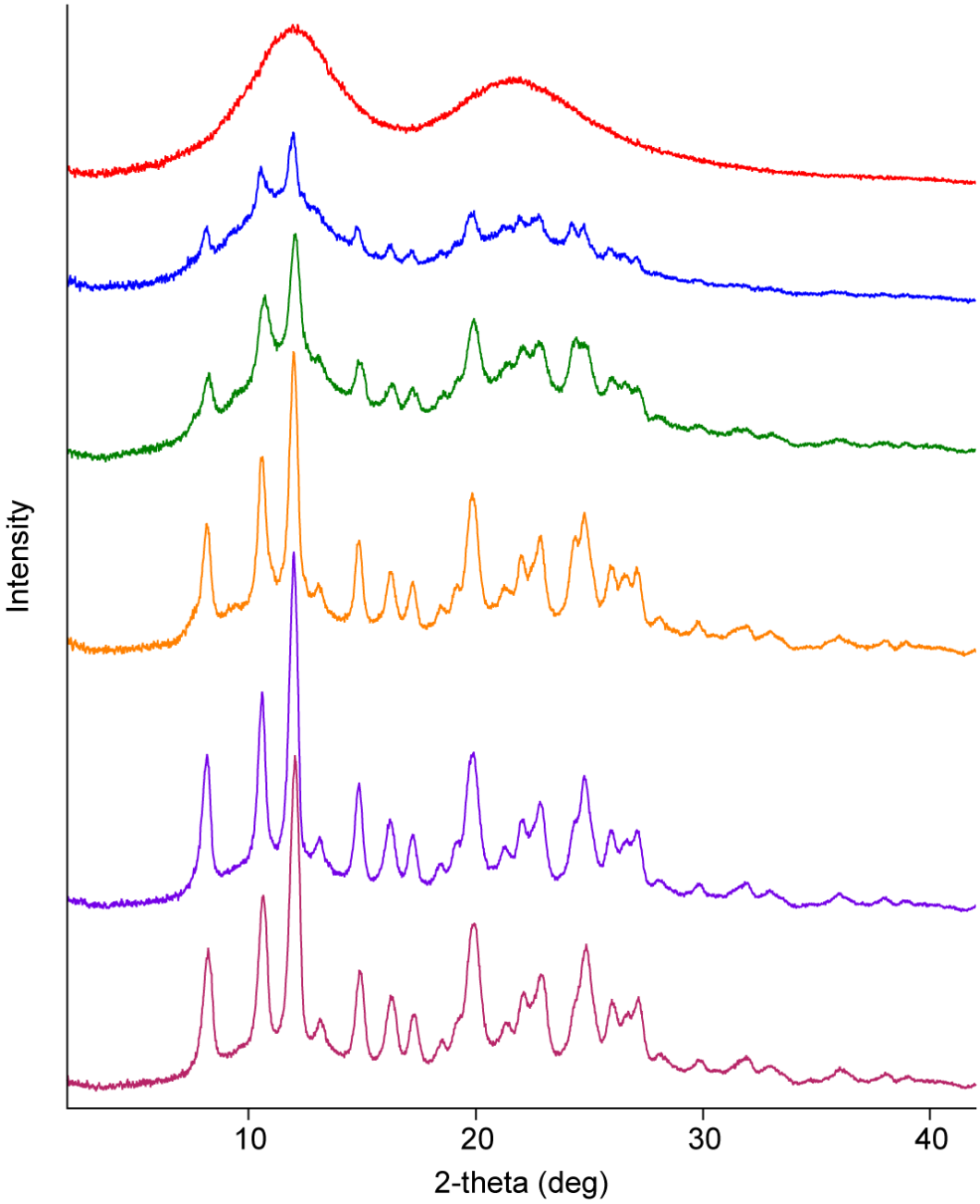

Figure 6.14. PXRD patterns of 70-30 NIF-PVP amorphous solid dispersions stored at 40 °C/75%RH. The diffractograms from top to bottom were collected at time 0, 1 week, 2 weeks, 1 month, 2 months and 6 months.

6.3.2.2 Raman Spectroscopy

Figures 6.15-6.21 show the Raman spectra of the 70-30 IMC methyl ester-PVP, 70-30 IMC-PVP and 70-30 NIF-PVP amorphous solid dispersions under different storage conditions. Similar to the results obtained by PXRD, no crystallization was observed from the Raman spectra for the IMC methyl ester-PVP amorphous solid dispersions (Figure 6.15), the IMC-PVP amorphous solid dispersion stored at 50 °C/0% RH (Figure 6.16) and that stored at 40 °C/57%RH (Figure 6.17), or the NIF-PVP amorphous solid dispersion stored at 50 °C/0% RH (Figure 6.18) and that stored at 40 °C/57%RH (Figure 6.19) for up to 6 months. Crystallization was seen in the spectrum of the IMC-PVP amorphous solid dispersion stored at 40 °C/75%RH after 2 months of storage, which is 1 month later than the detection of crystallization by PXRD. This is presumably due to either sub sampling or a higher detection limit, and could potentially be improved by sampling more particles and areas of each sample. The peak at 1700 cm^{-1} corresponds to the γ polymorph. Similar to what was found using PXRD, crystallization was seen in the spectrum of the NIF-PVP amorphous solid dispersion stored at 40 °C/75%RH after just 1 week of storage. The peak at 1680 cm^{-1} is characteristic of the NIF β form. The spectrum recorded after 2 weeks of storage seemed to show a less extent of crystallization than the spectrum recorded after 1 week of storage. This is also presumably due to sub sampling of the dispersion, which is one of the drawbacks of Raman spectroscopy. In general, the results obtained from the Raman spectra agreed very well with those obtained from PXRD diffractograms.

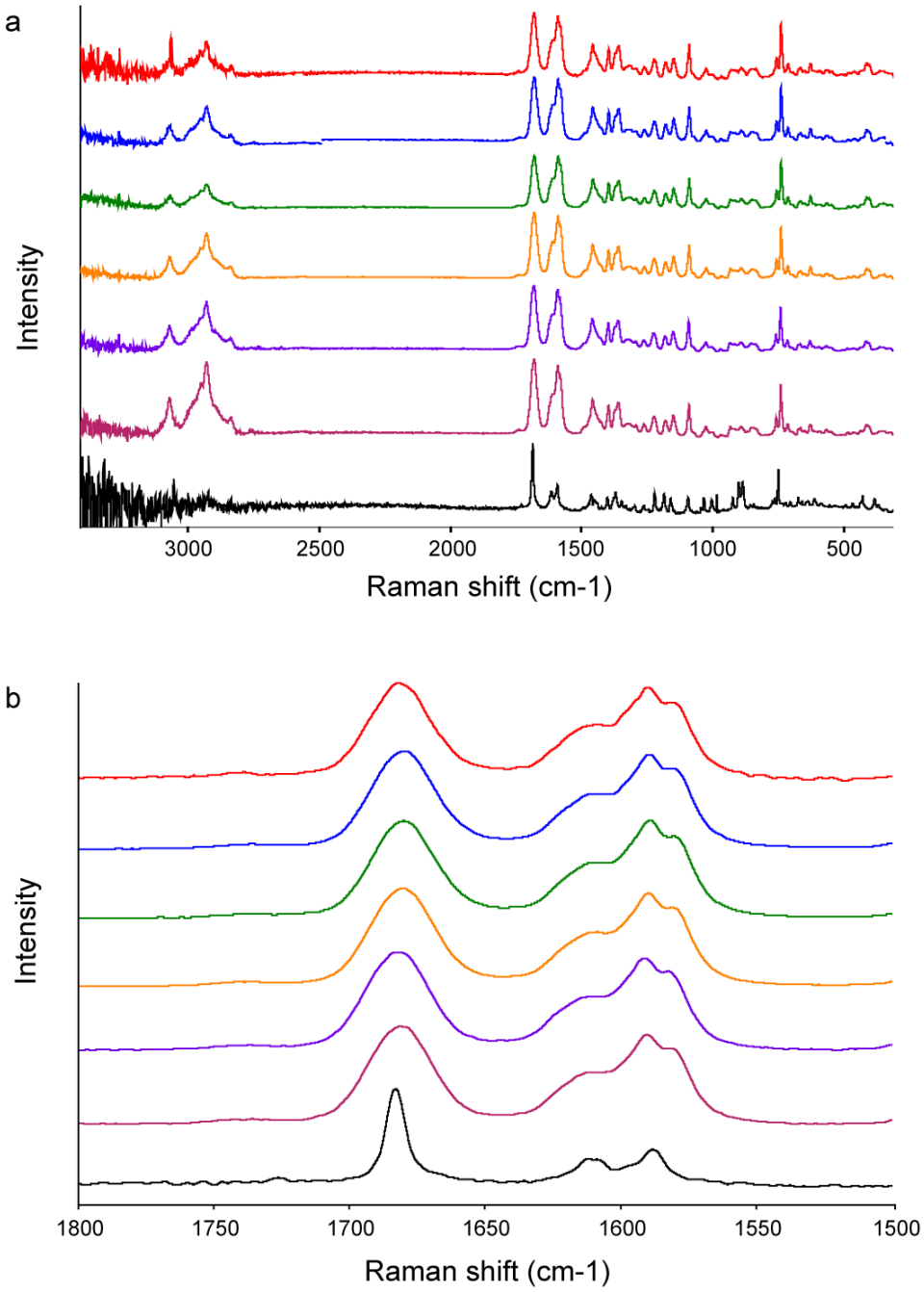

Figure 6.15. (a) Raman spectra and (b) the carbonyl region of the Raman spectra of 70-30 IMC methyl ester-PVP amorphous solid dispersion stored at 4 °C/0% RH. From top to bottom are spectra collected at time 0, 1 week, 2 weeks, 1 month, 2 months, 6 months, and crystalline IMC methyl ester. No crystallization was observed in any of these samples.

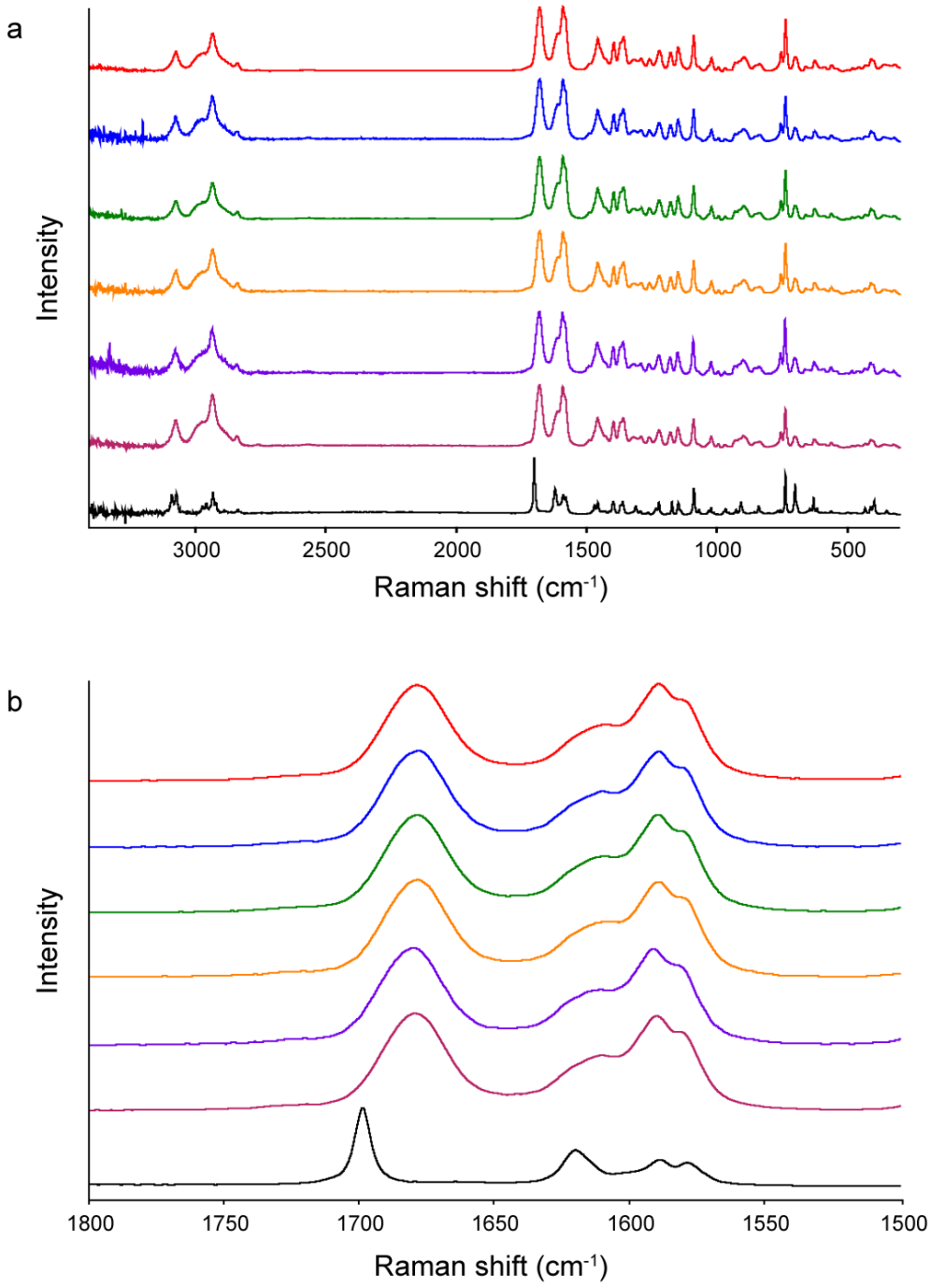

Figure 6.16. (a) Raman spectra and (b) the carbonyl region of the Raman spectra of 70-30 IMC-PVP amorphous solid dispersion stored at 50 °C/0% RH. From top to bottom are spectra collected at time 0, 1 week, 2 weeks, 1 month, 2 months, 6 months, and γ-IMC. No crystallization was observed in any of these samples.

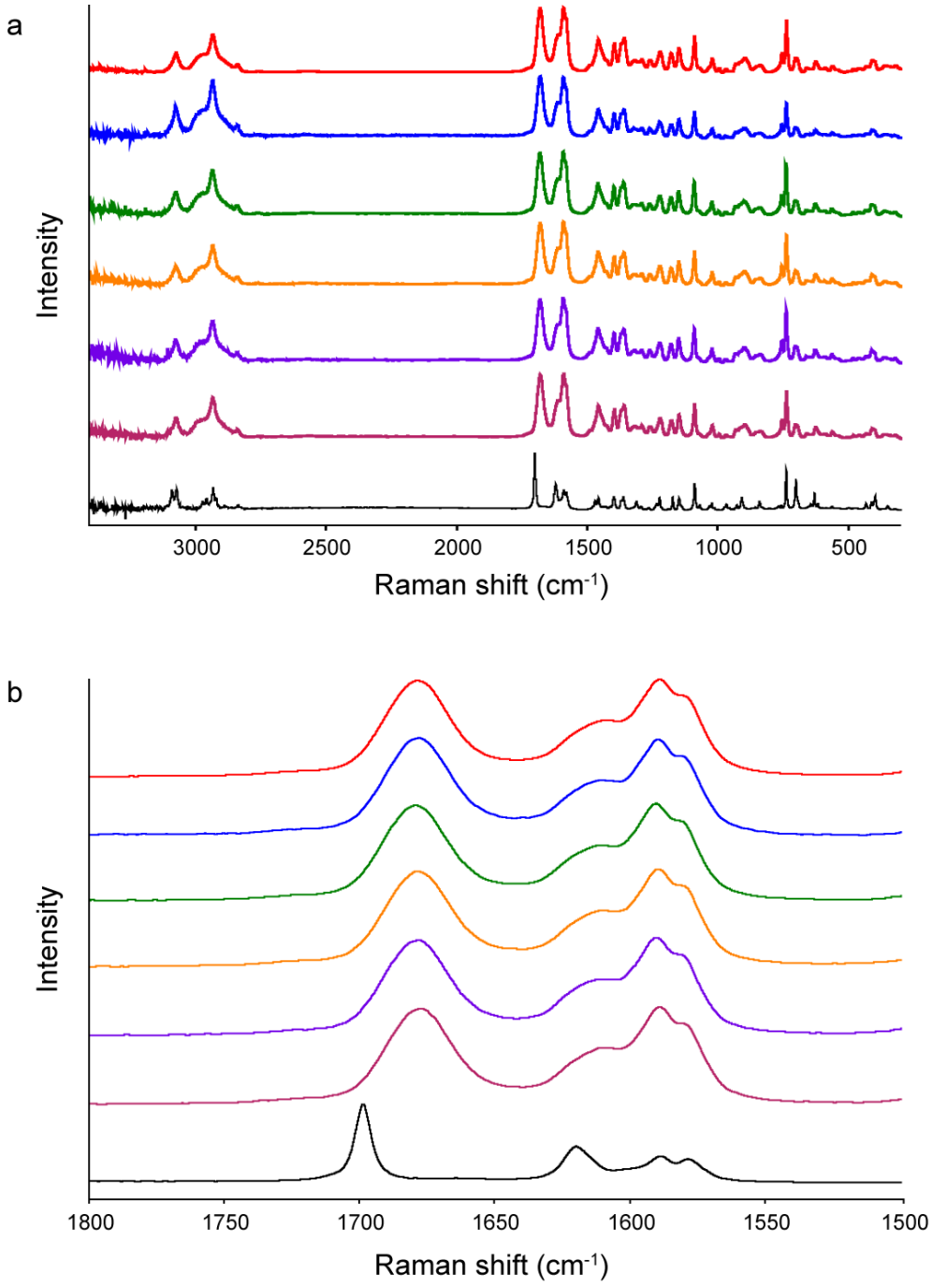

Figure 6.17. (a) Raman spectra and (b) the carbonyl region of the Raman spectra of 70-30 IMC-PVP amorphous solid dispersion stored at 40 °C/57% RH. From top to bottom are spectra collected at time 0, 1 week, 2 weeks, 1 month, 2 months, 6 months, and γ-IMC. No crystallization was observed in any of these samples.

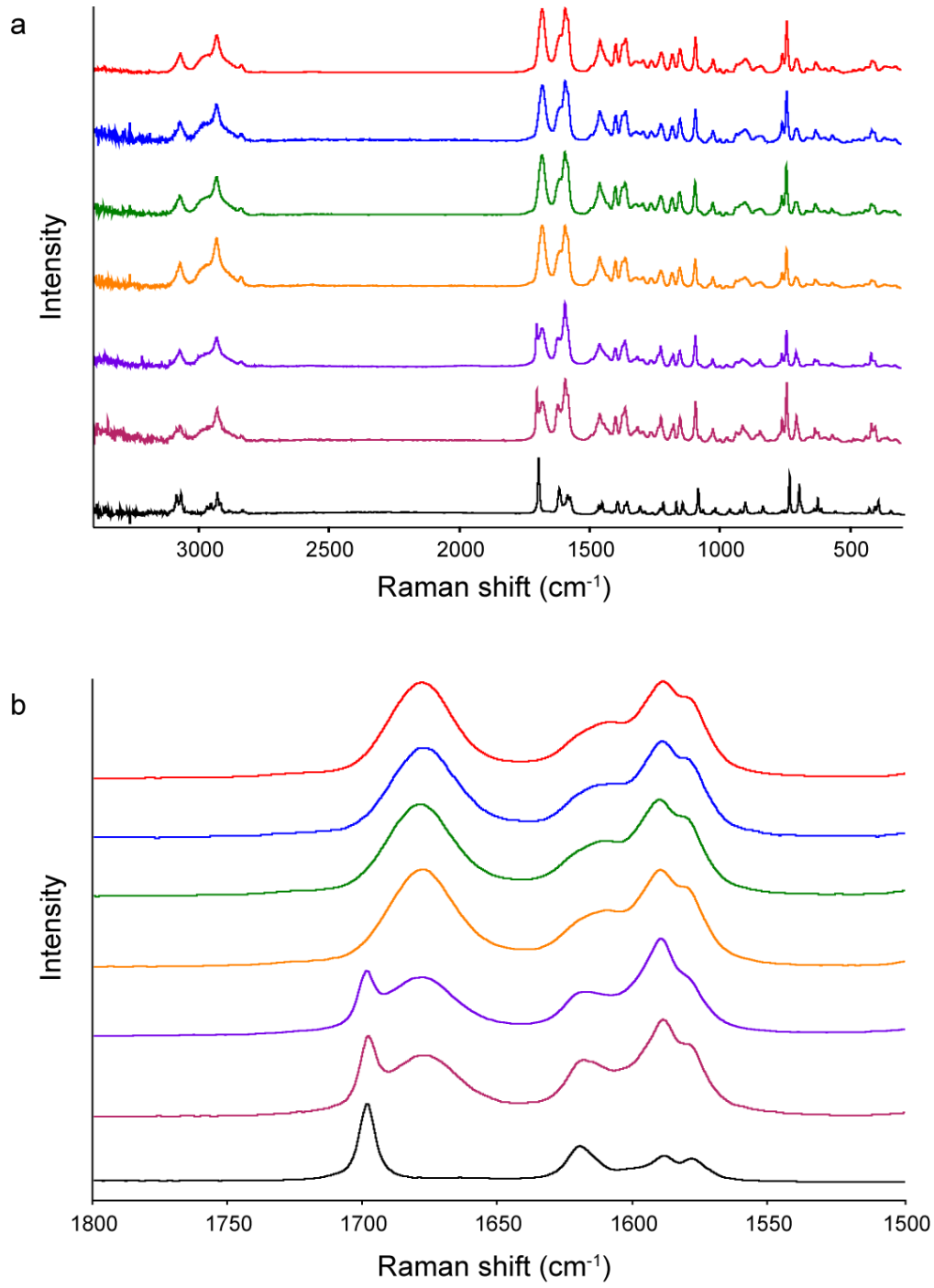

Figure 6.18. (a) Raman spectra and (b) the carbonyl region of the Raman spectra of 70-30 IMC-PVP amorphous solid dispersion stored at 40 °C/75% RH. From top to bottom are spectra collected at time 0, 1 week, 2 weeks, 1 month, 2 months, 6 months, and γ-IMC. Crystallization was observed in the sample after 2 months of storage.

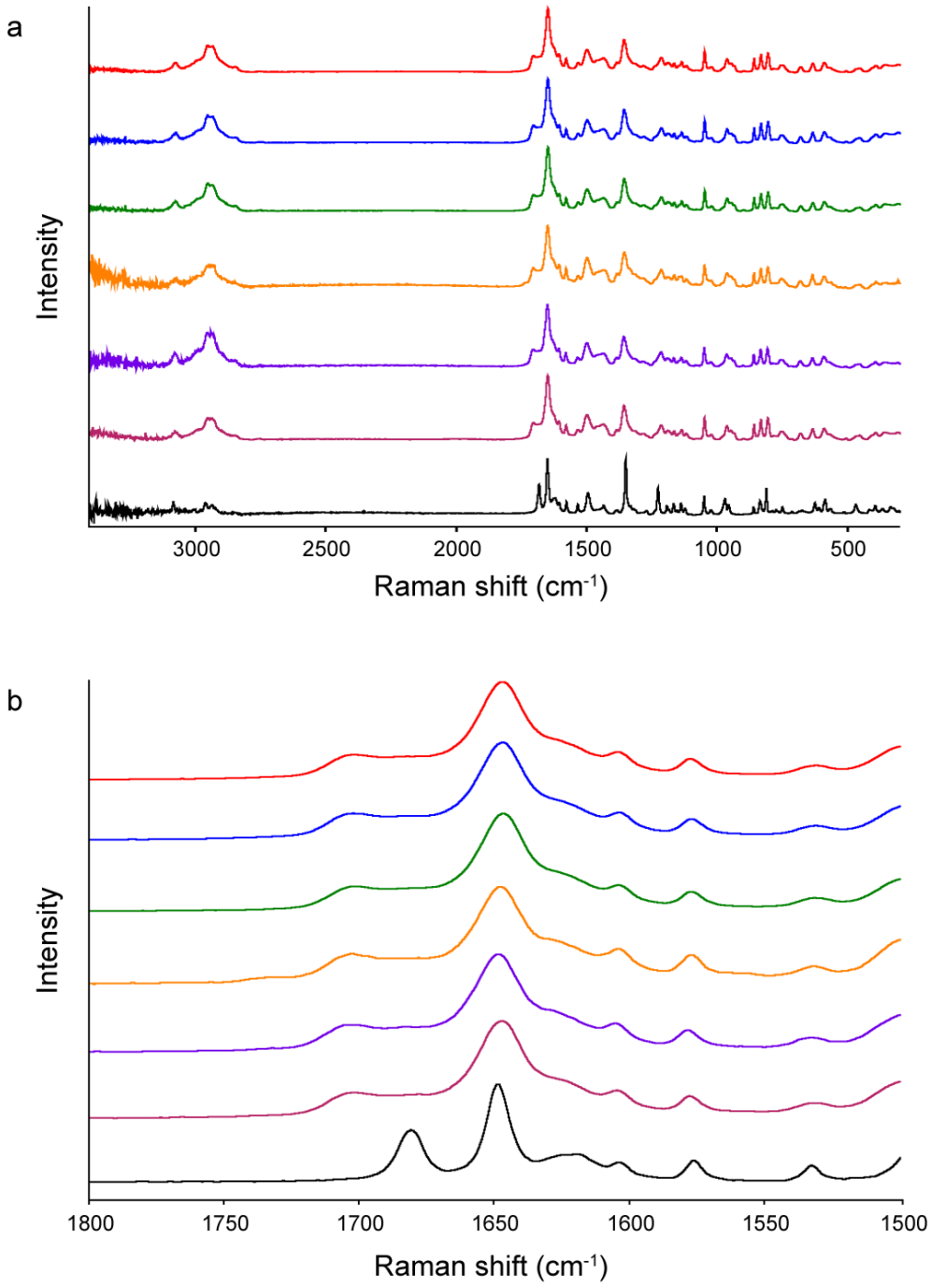

Figure 6.19. (a) Raman spectra and (b) the carbonyl region of the Raman spectra of 70-30 NIF-PVP amorphous solid dispersion stored at 50 °C/0% RH. From top to bottom are spectra collected at time 0, 1 week, 2 weeks, 1 month, 2 months, 6 months, and α-NIF. No crystallization was observed in any of these samples.

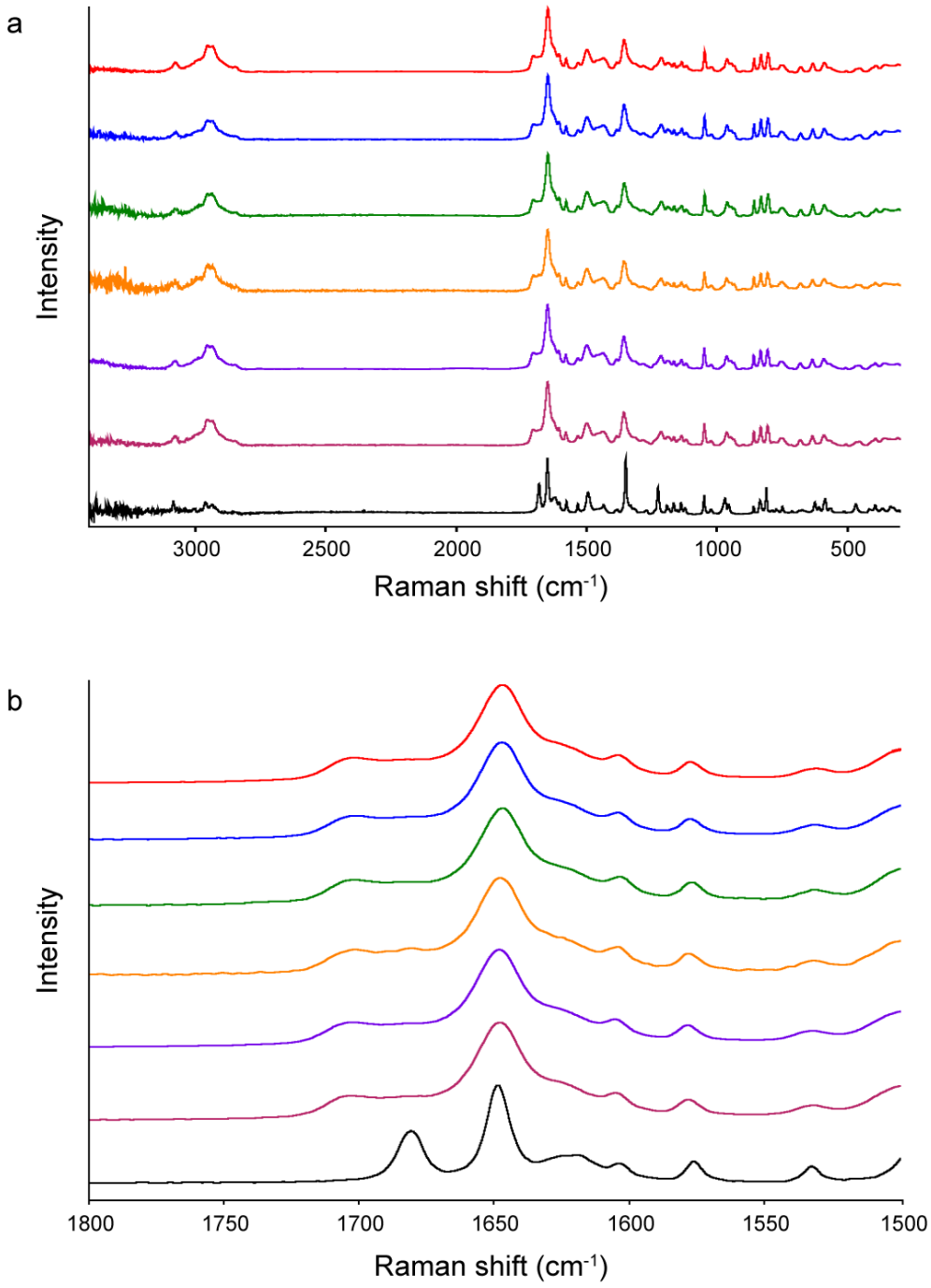

Figure 6.20. (a) Raman spectra and (b) the carbonyl region of the Raman spectra of 70-30 NIF-PVP amorphous solid dispersion stored at 40 °C/57% RH. From top to bottom are spectra collected at time 0, 1 week, 2 weeks, 1 month, 2 months, 6 months, and α-NIF. No crystallization was observed in any of these samples.

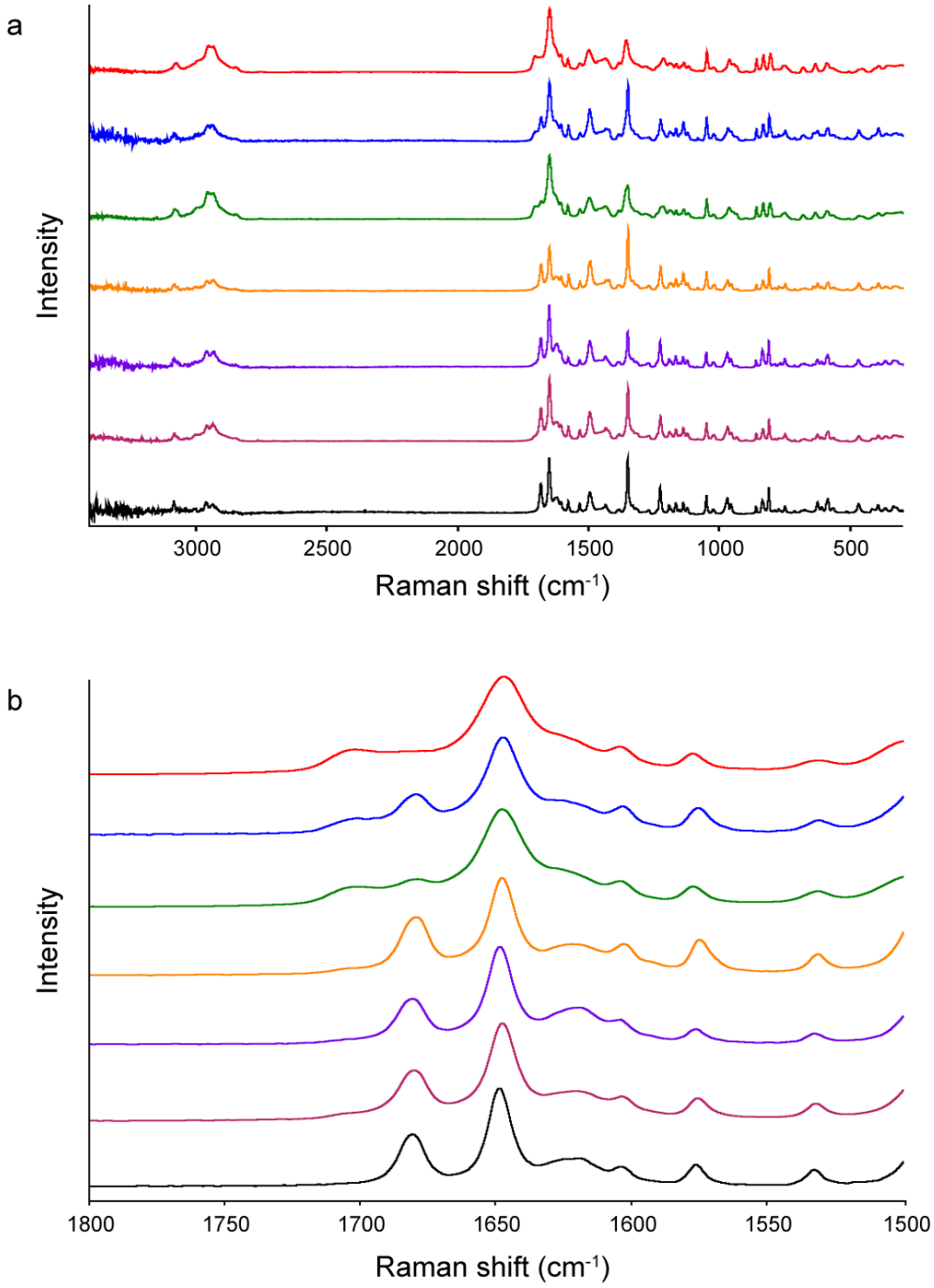

Figure 6.21. (a) Raman spectra and (b) the carbonyl region of the Raman spectra of 70-30 NIF-PVP amorphous solid dispersion stored at 40 °C/75% RH. From top to bottom are spectra collected at time 0, 1 week, 2 weeks, 1 month, 2 months, 6 months, and α-NIF. Crystallization was observed in the sample after only 1 week of storage.

6.3.2.3 Polarized Light Microscopy

Figures 6.22 - 6.28 show the polarized light microscopy images of the 70-30 IMC methyl ester-PVP, 70-30 IMC-PVP and the 70-30 NIF-PVP amorphous solid dispersion stored at various conditions. No crystallization was seen in the IMC methyl ester-PVP sample being stored up to 6 months. Also, no crystallization was seen for the IMC-PVP sample stored at 50 °C/0% RH. For the IMC-PVP sample stored at 40 °C/57% RH, some small crystallites were seen on the surface after 6 months of storage. This small amount of crystallization was not detected by PXRD or Raman spectroscopy. Small crystallites were noticed for IMC-PVP sample stored at 40 °C/75% RH after 2 weeks of storage, which is earlier than the detection of crystallization by PXRD or Raman spectroscopy. Gradually more crystals were seen after 1 month, 2 months and 6 months of storage. For the NIF-PVP amorphous solid dispersion, no crystallization was seen in the sample stored at 50 °C/0% RH for up to 6 months. Very limited amount of small crystallites were spotted on the surface for the sample stored at 40 °C/57% RH for 6 months, which again was not detected by PXRD or Raman. Extensive crystallization was seen for the NIF-PVP sample stored at 40 °C and 75% RH, consistent with the results obtained from PXRD and Raman spectroscopy.

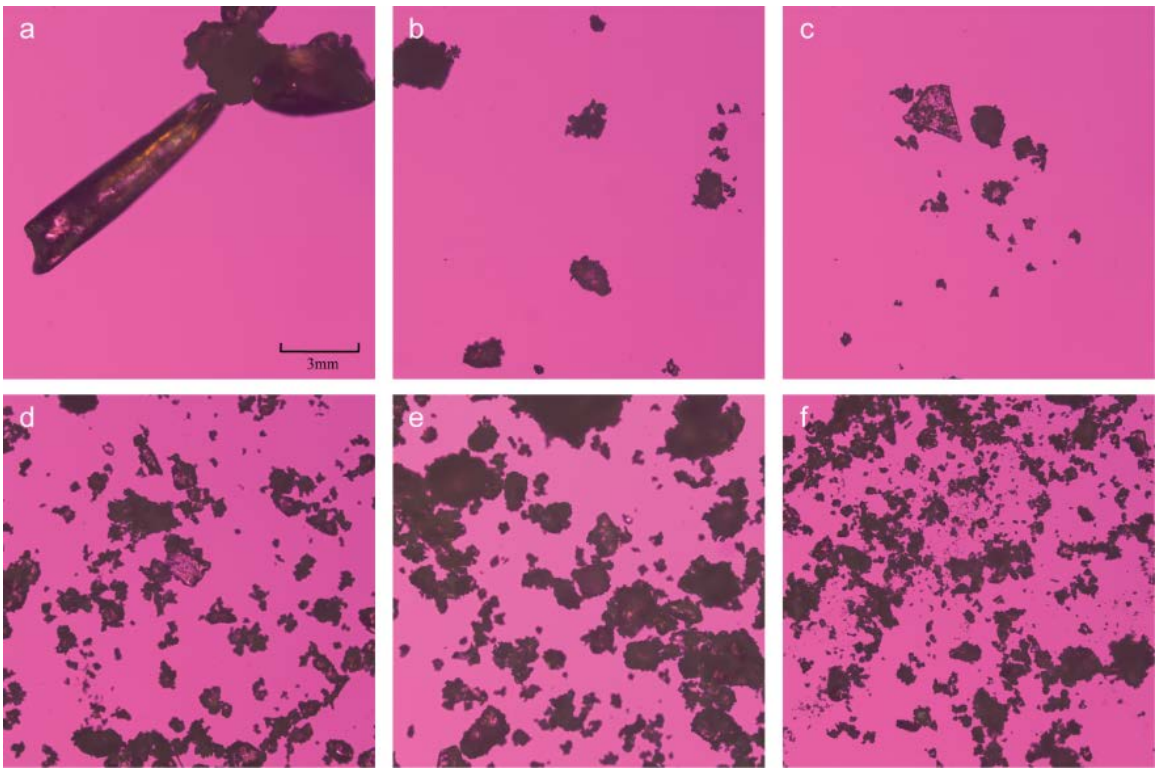

Figure 6.22. Polarized light microscopy image of 70-30 IMC methyl ester-PVP amorphous solid dispersion stored at 4 °C/0% RH at (a) time 0, (b) 1 week, (c) 2 weeks, (d) 1 month, (e) 2 months, and (f) 6 months of storage.

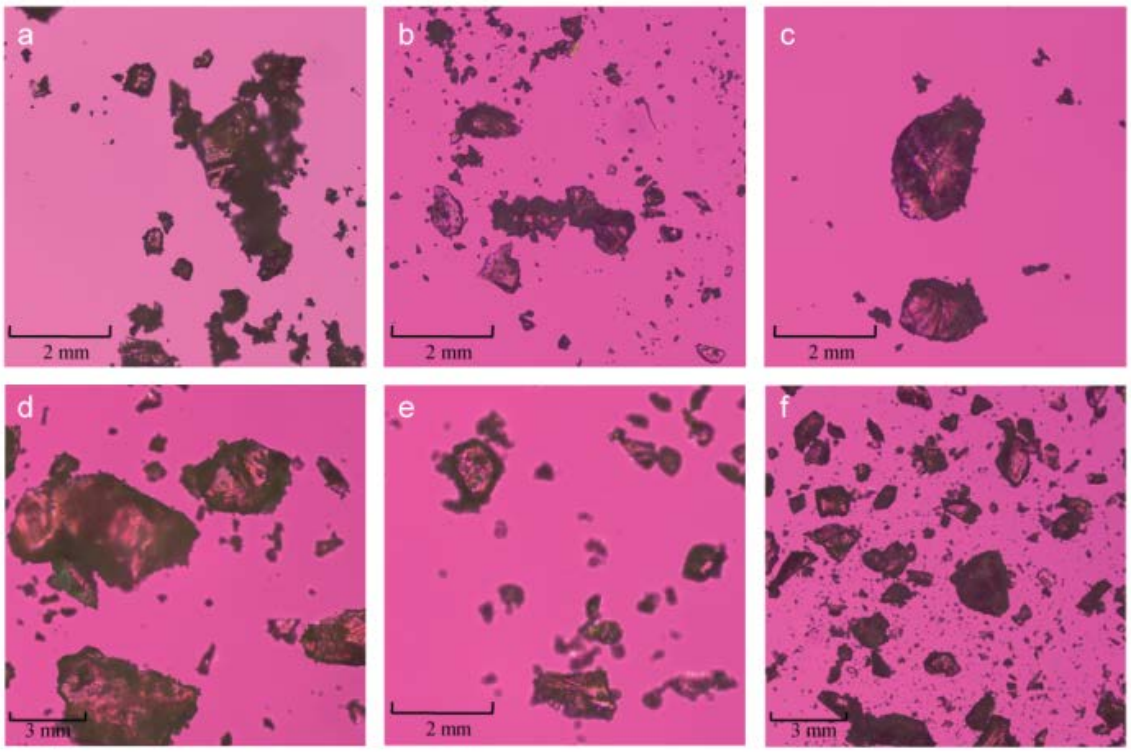

Figure 6.23. Polarized light microscopy image of 70-30 IMC-PVP amorphous solid dispersion stored at 50 °C/0% RH at (a) time 0, (b) 1 week, (c) 2 weeks, (d) 1 month, (e) 2 months, and (f) 6 months of storage.

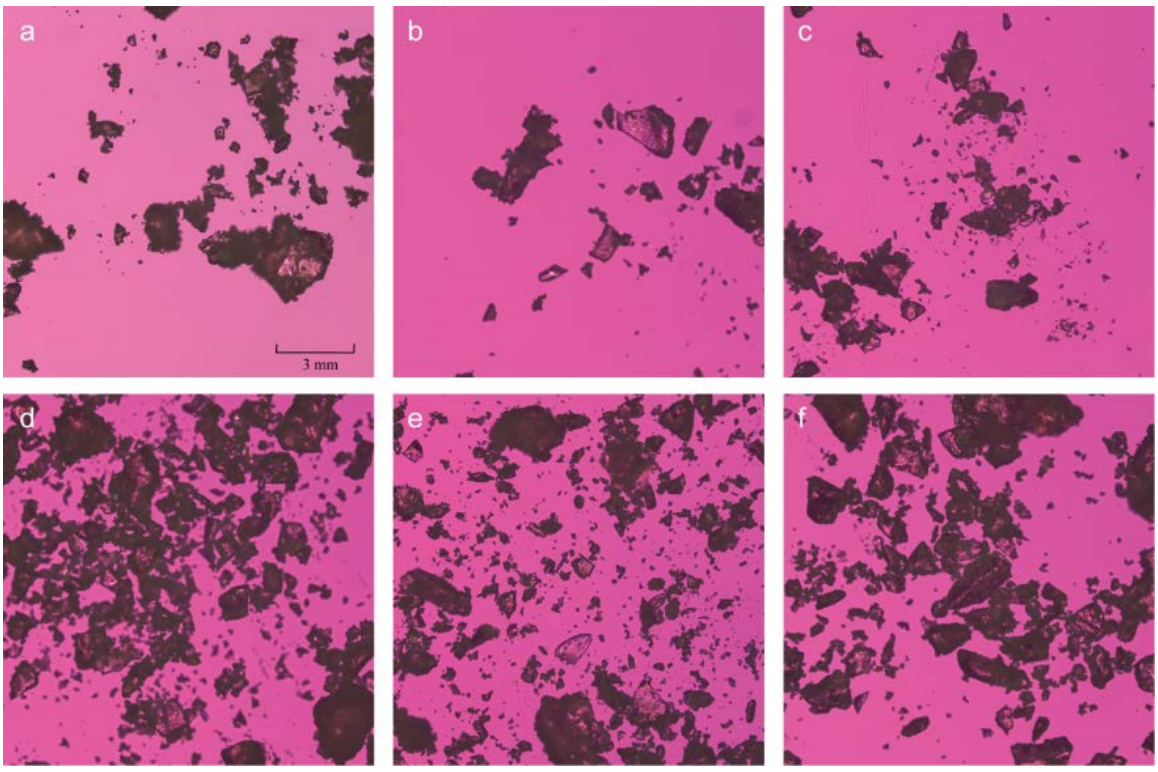

Figure 6.24. Polarized light microscopy image of 70-30 IMC-PVP amorphous solid dispersion stored at 40 °C/57% RH at (a) time 0, (b) 1 week, (c) 2 weeks, (d) 1 month, (e) 2 months, and (f) 6 months of storage.

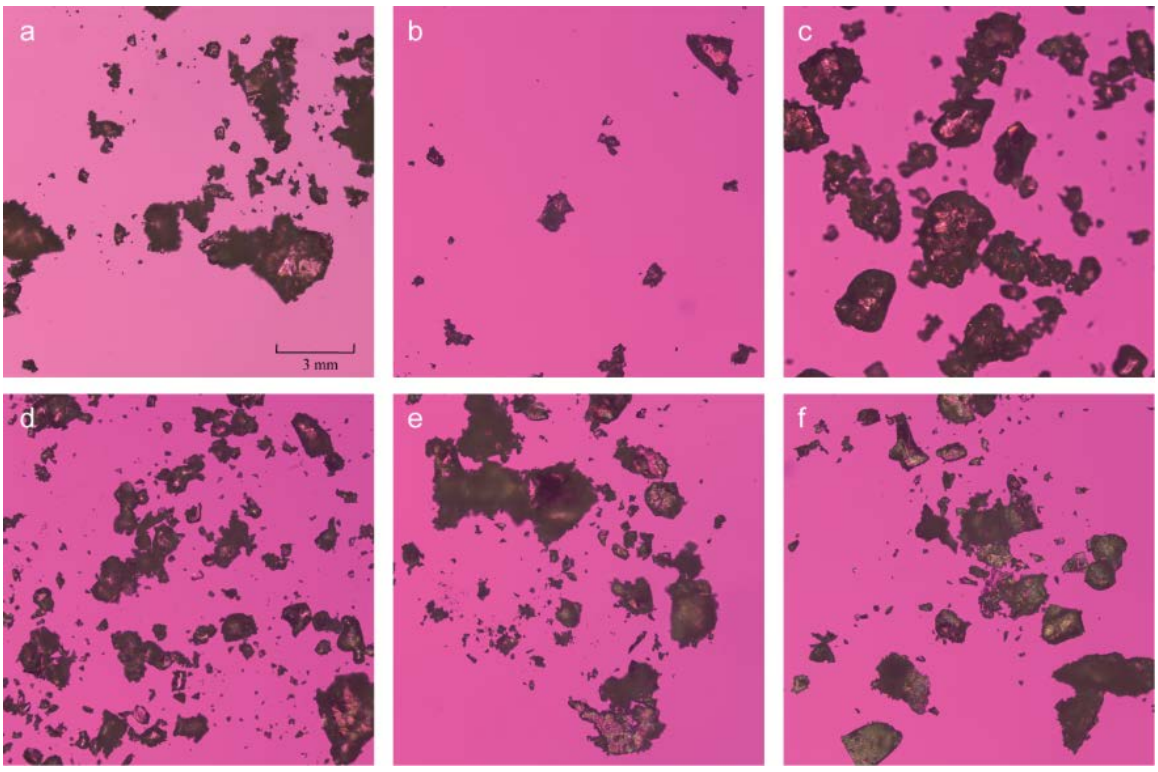

Figure 6.25. Polarized light microscopy image of 70-30 IMC-PVP amorphous solid dispersion stored at 40 °C/75% RH at (a) time 0, (b) 1 week, (c) 2 weeks, (d) 1 month, (e) 2 months, and (f) 6 months of storage.

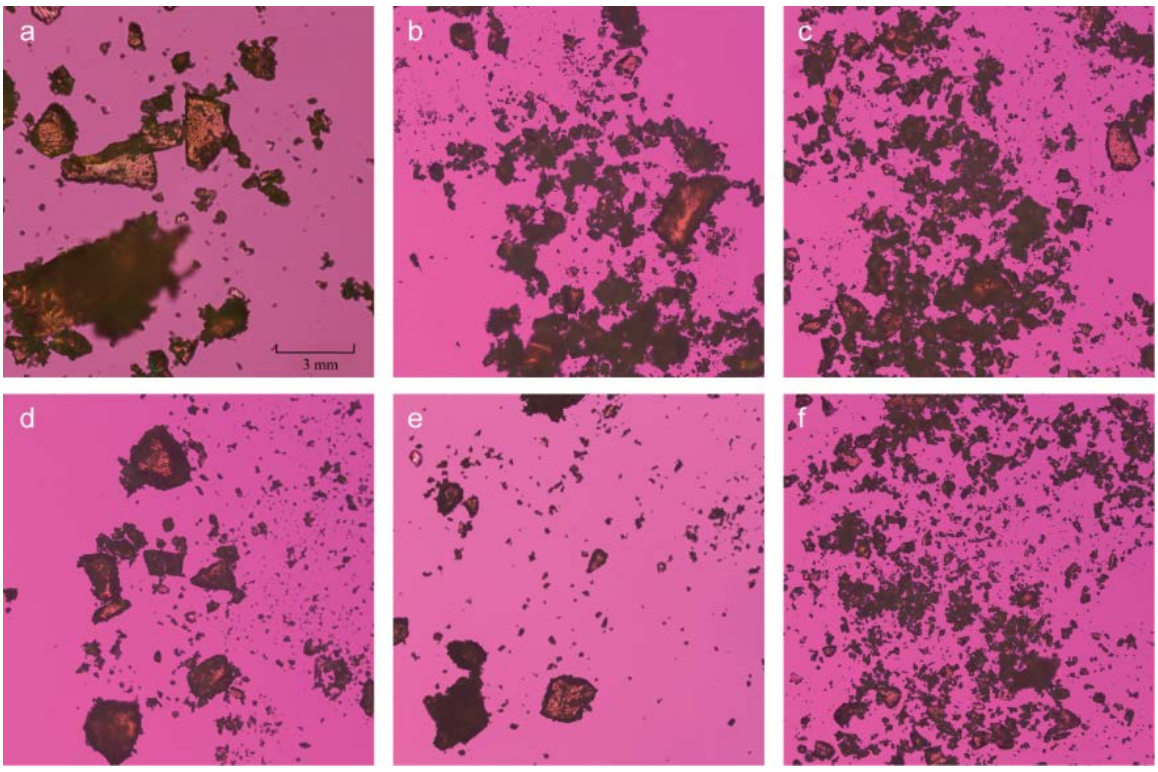

Figure 6.26. Polarized light microscopy image of 70-30 NIF-PVP amorphous solid dispersion stored at 50 °C/0% RH at (a) time 0, (b) 1 week, (c) 2 weeks, (d) 1 month, (e) 2 months, and (f) 6 months of storage.

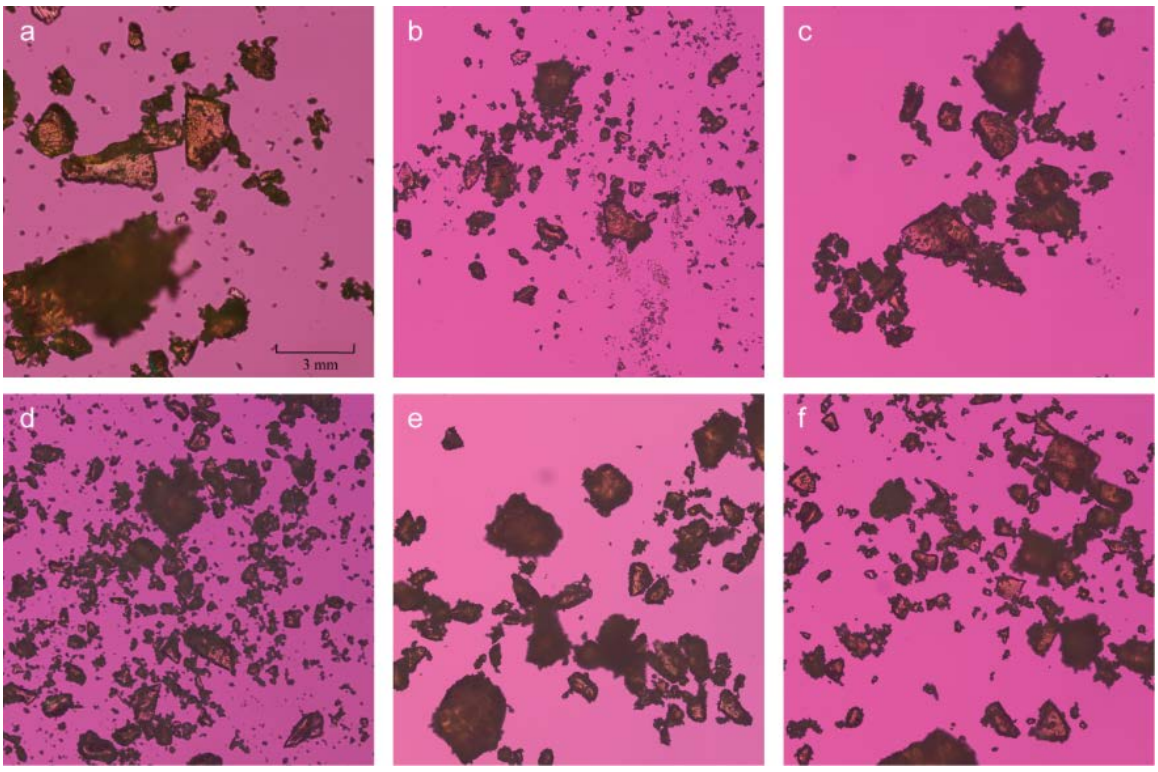

Figure 6.27. Polarized light microscopy image of 70-30 NIF-PVP amorphous solid dispersion stored at 40 °C/57% RH at (a) time 0, (b) 1 week, (c) 2 weeks, (d) 1 month, (e) 2 months, and (f) 6 months of storage.

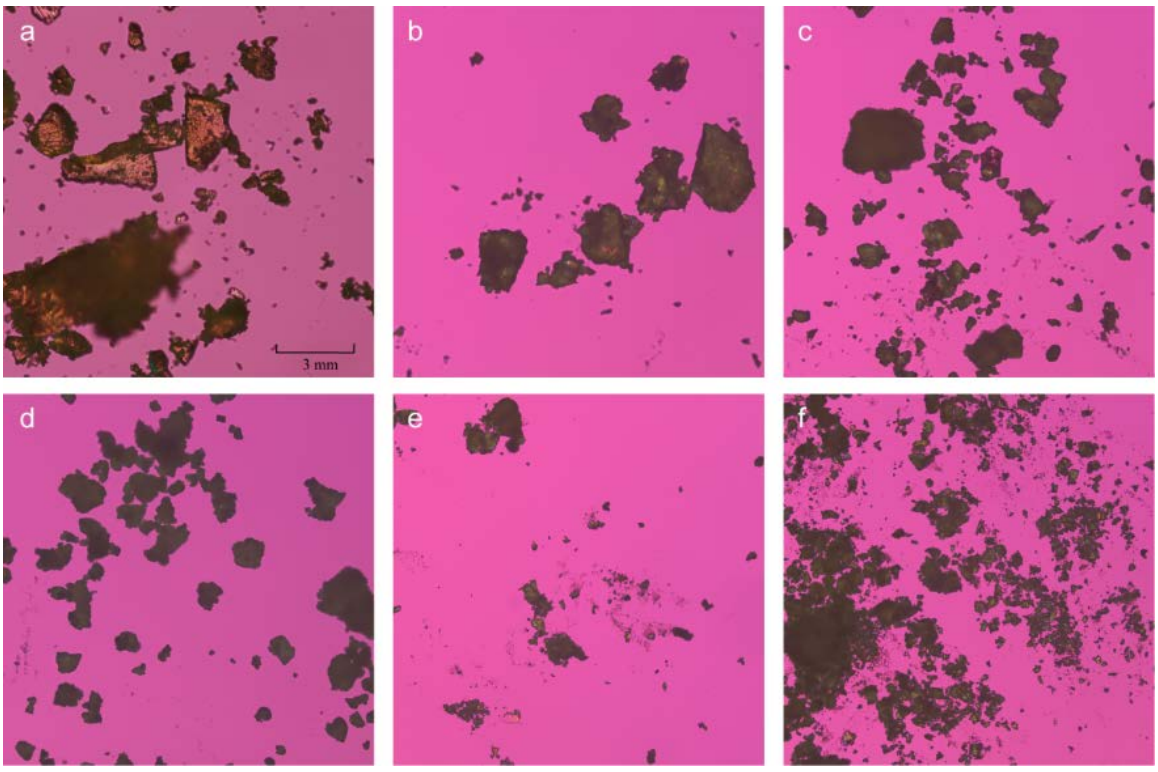

Figure 6.28. Polarized light microscopy image of 70-30 NIF-PVP amorphous solid dispersion stored at 40 °C/75% RH at (a) time 0, (b) 1 week, (c) 2 weeks, (d) 1 month, (e) 2 months, and (f) 6 months of storage.

6.3.2.4 Modulated DSC

Figures 6.29 - 6.35 show the MDSC thermograms of 70-30 IMC methyl ester-PVP, 70-30 IMC-PVP and 70-30 NIF-PVP amorphous solid dispersions under different storage conditions. Thermograms shown herein were obtained with a pinhole lid; thermograms obtained with the hermetic lid are not shown for the sake of conserving space. However, glass transition temperatures are listed in Tables 6.1 - 6.3 for experiments obtained with both the pinhole and the hermetic lid.

For the sake of brevity, only samples analyzed with hermetic lids/pans are discussed here, because samples that are hermetically sealed better represent the true chemical environment of the samples. A gradual increase of the glass transition temperature of the IMC methyl ester-PVP sample over time can be seen in Table 6.1. This is presumably due to drying of the sample over desiccant. A small melting peak at ~90 °C was observed for the sample at all time points.

The IMC-PVP sample stored at 50 °C/0% RH also showed a gradual increase in the glass transition temperature over time. The IMC-PVP sample stored at 40 °C/57% RH showed a decrease in glass transition temperature after 1 week of storage. There was no further decrease in the glass transition temperature of this sample upon further storage, which suggests that the water content was almost fully equilibrated after 1 week. Similarly, the IMC-PVP sample stored at 40 °C/75% RH showed a decrease in glass transition temperature after 1 week of storage with no further decrease in temperature detected. No melting peaks were observed for any of the IMC-PVP samples stored at these three conditions.

Similar to the IMC-PVP amorphous solid dispersion, the NIF-PVP sample stored at 50 °C/0% RH also showed a gradual increase in the glass transition temperature over time. The NIF-PVP sample stored at 40 °C/57% RH showed a decrease in glass transition temperature after 1 week of storage. The glass transition temperature seemed to slightly increase after 1 month of storage, presumably due to a decrease in water content. However, the reason for this is unclear because crystallization was not observed for this sample. Compared with the IMC-PVP sample stored at the same condition, the glass transition temperature of the NIF-PVP sample was lower at the same time point, which is presumably due to the hygroscopicity of PVP. When PVP is hydrogen bonded with the drug, it will not have as much capability to hydrogen bond to water as neat PVP. Considering that the hydrogen bond between NIF and PVP is not as strong as the hydrogen bond between IMC and PVP, PVP in the NIF-PVP sample would have more capability to hydrogen bond to water, which leads to lower glass transition temperatures in the NIF-PVP sample. The NIF-PVP sample stored at 40 °C/75% RH showed an even larger decrease in glass transition temperature after 1 week of storage. The glass transition temperature was not observable after 1 month of storage, probably due to the large extent of crystallization at that time. A melting peak can be observed for all NIF-PVP samples stored at three conditions.

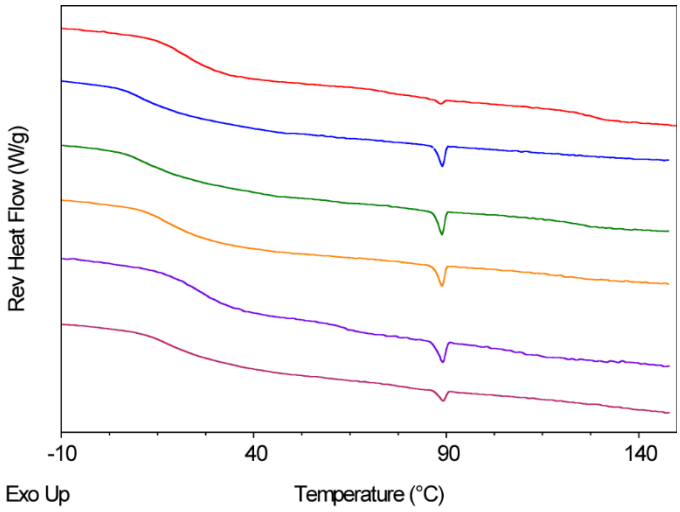

Figure 6.29. MDSC of 70-30 IMC methyl ester-PVP amorphous solid dispersions stored at 4 °C/0% RH. The thermograms from top to bottom were collected at time 0, 1 week, 2 weeks, 1 month, 2 months and 6 months (pinhole).

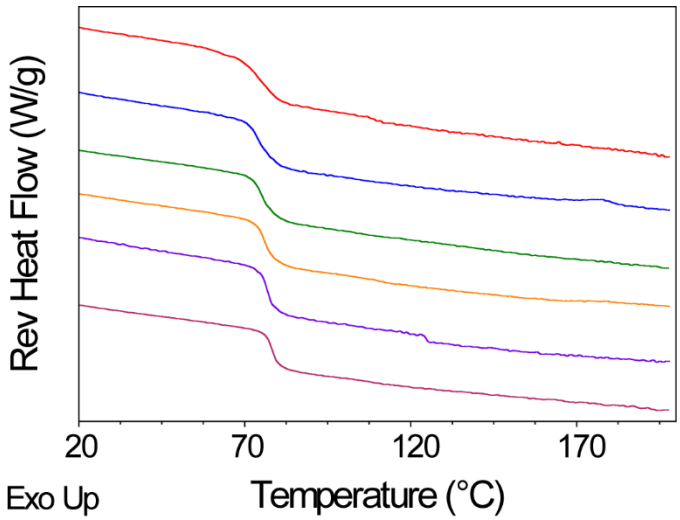

Figure 6.30. MDSC of 70-30 IMC-PVP amorphous solid dispersions stored at 50 °C/0% RH. The thermograms from top to bottom were collected at time 0, 1 week, 2 weeks, 1 month, 2 months and 6 months (pinhole).

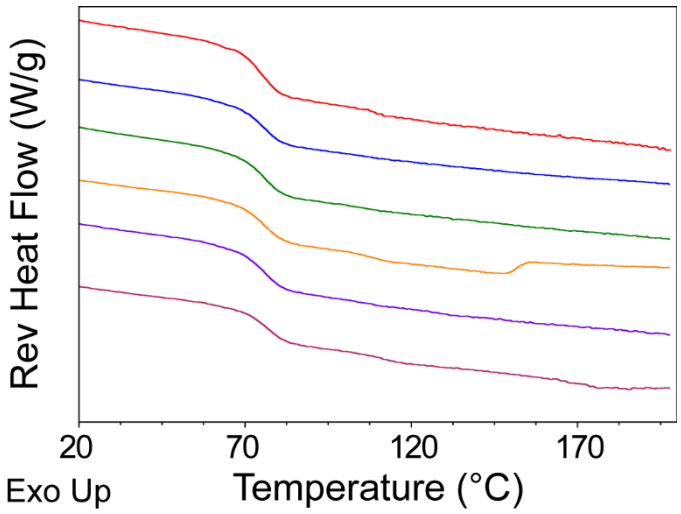

Figure 6.31. MDSC of 70-30 IMC-PVP amorphous solid dispersions stored at 40 °C/57%RH. The thermograms from top to bottom were collected at time 0, 1 week, 2 weeks, 1 month, 2 months and 6 months (pinhole).

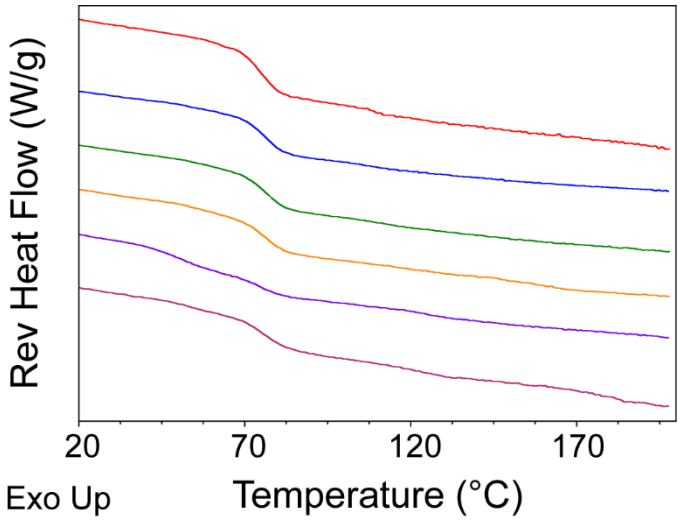

Figure 6.32. MDSC of 70-30 IMC-PVP amorphous solid dispersions stored at 40 °C/75%RH. The thermograms from top to bottom were collected at time 0, 1 week, 2 weeks, 1 month, 2 months and 6 months (pinhole).

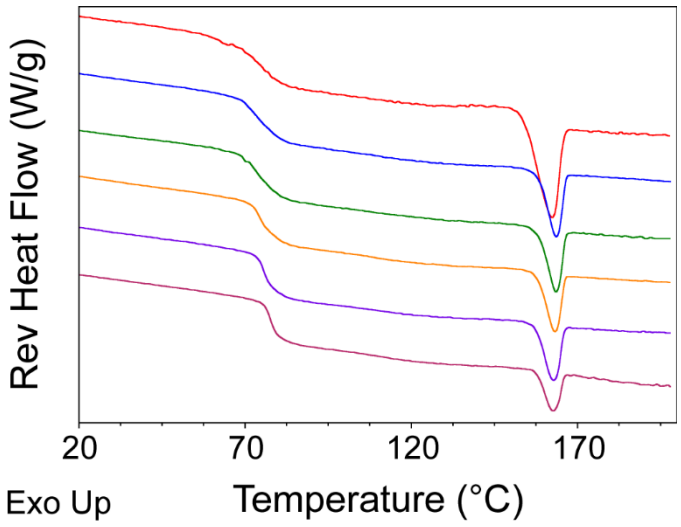

Figure 6.33. MDSC of 70-30 NIF-PVP amorphous solid dispersions stored at 50 °C/0% RH. The thermograms from top to bottom were collected at time 0, 1 week, 2 weeks, 1 month, 2 months and 6 months (pinhole).

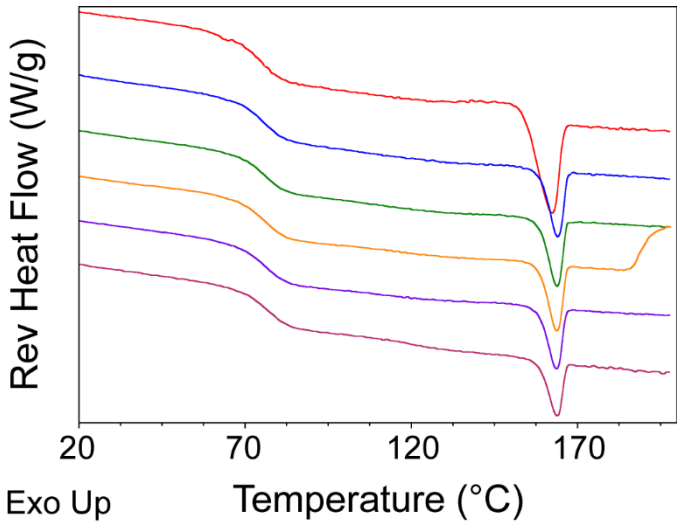

Figure 6.34. MDSC of 70-30 NIF-PVP amorphous solid dispersions stored at 40 °C/57%RH. The thermograms from top to bottom were collected at time 0, 1 week, 2 weeks, 1 month, 2 months and 6 months (pinhole).

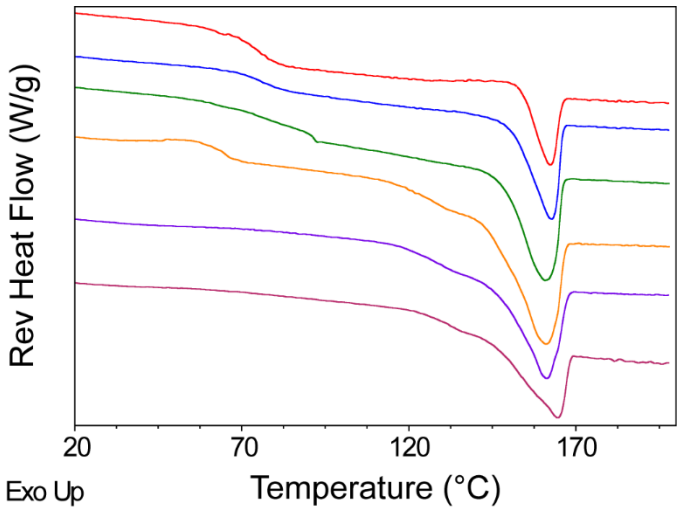

Figure 6.35. MDSC of 70-30 NIF-PVP amorphous solid dispersions stored at 40 °C/75%RH. The thermograms from top to bottom were collected at time 0, 1 week, 2 weeks, 1 month, 2 months and 6 months (pinhole).

Table 6.1. Glass transition temperatures of 70-30 IMC methyl ester-PVP amorphous solid dispersions stored at 4 °C/0% RH at different time points.

	Hermetic (°C)	Pinhole (°C)	Crystallization
Time 0	19.4	22.9	No
1 week	19.2	16.0	No
2 weeks	21.1	16.9	No
1 month	22.5	20.5	No
2 months	24.1	25.4	No
6 months	24.1	21.3	No

Table 6.2. Glass transition temperatures of 70-30 IMC-PVP amorphous solid dispersions stored at various conditions at different time points.

	50 °C/0% RH			40 °C 57%RH			40 °C 75%RH		
	Hermetic (°C)	Pinhole (°C)	Crystal lization	Hermetic (°C)	Pinhole (°C)	Crystal lization	Hermetic (°C)	Pinhole (°C)	Crystal lization
Time 0	62.4	74.0	No	62.4	74.0	No	62.4	74.0	No
1 week	71.7	74.7	No	52.7	74.1	No	41.4	74.9	No
2 weeks	71.4	75.3	No	52.8	74.4	No	41.1	75.2	No
1 month	70.7	75.9	No	51.8	74.6	No	41.3	74.3	Yes
2 months	73.0	76.8	No	50.4	74.4	No	39.9	76.6	Yes
6 months	74.3	78.3	No	52.0	75.0	No	43.7	74.7	Yes

Table 6.3. Glass transition temperatures of 70-30 NIF-PVP amorphous solid dispersions stored at various conditions at different time points.

	50 °C/0% RH			40 °C 57%RH			40 °C 75%RH		
	Hermetic (°C)	Pinhole (°C)	Crystallization	Hermetic (°C)	Pinhole (°C)	Crystallization	Hermetic (°C)	Pinhole (°C)	Crystallization
Time 0	63.9	73.4	No	63.9	73.4	No	63.9	73.4	No
1 week	67.2	73.9	No	44.3	74.4	No	35.3	75.4	Yes
2 weeks	69.0	74.0	No	44.3	74.5	No	35.2	-	Yes
1 month	70.0	74.8	No	46.1	74.4	No	-	63.59/ 121.46	Yes
2 months	71.7	76.0	No	46.4	74.9	No	-	124.1	Yes
6 months	72.1	77.6	No	48.3	76.0	No	-	129.3	Yes

6.3.2.5 Water Content Determined by TGA

Tables 6.4 - 6.6 list the water contents of the 70-30 IMC methyl ester-PVP, 70-30 IMC-PVP and 70-30 NIF-PVP amorphous solid dispersions under different storage conditions at different time points. The water content of the IMC methyl ester-PVP amorphous solid dispersion decreased slightly over time, presumably due to the storage over desiccants. The same trends were observed for IMC-PVP and NIF-PVP amorphous solid dispersions stored over desiccants. These results are consistent with the observations of slightly increased glass transition temperatures over storage time for these samples. The IMC-PVP and NIF-PVP amorphous solid dispersions stored in humidity chambers showed various degrees of water absorption; the amount of water absorption is consistent with the humidity levels in each chamber. As discussed in the previous section, the NIF-PVP amorphous solid dispersions absorbed more water than the IMC-PVP amorphous solid dispersions at each time point under the same storage condition, indicating lesser degree of hydrogen-bonding interactions in NIF-PVP amorphous solid dispersions compared with IMC-PVP amorphous solid dispersions.

Table 6.4. Water content of 70-30 IMC methyl ester-PVP amorphous solid dispersion at various time points.

	Weight Loss (%)
Time 0	1.5
1 week	1.6
2 weeks	0.9
1 month	0.8
2 months	0.4
6 months	0.4

Table 6.5. Water contents of 70-30 IMC-PVP amorphous solid dispersions stored at different conditions at various time points.

	50 °C dry	40 °C 57%RH	40 °C 75%RH
Time 0	0.8	0.8	0.8
1 week	0.2	2.0	3.2
2 weeks	0.3	1.8	3.2
1 month	0.0	1.8	3.4
2 months	0.1	1.9	3.5
6 months	0.2	1.9	3.0

Table 6.6. Water contents of 70-30 NIF-PVP amorphous solid dispersions stored at different conditions at various time points.

	50 °C dry	40 °C 57%RH	40 °C 75%RH
Time 0	0.8	0.8	0.8
1 week	0.4	3.2	4.6
2 weeks	0.5	3.1	5.2
1 month	0.4	2.9	5.8
2 months	0.3	2.7	4.5
6 months	0.3	2.6	5.4

6.3.3 Analysis of Stability Samples by Solid-State NMR Spectroscopy

Figures 6.36 - 6.42 show the CPMAS NMR spectra of the 70-30 IMC methyl ester-PVP, 70-30 IMC-PVP and the 70-30 NIF-PVP amorphous solid dispersions stored at various conditions. Similar to the results obtained from PXRD, no crystallization peaks were seen in the spectra of IMC methyl ester-PVP amorphous solid dispersions, the IMC-PVP amorphous solid dispersion stored at 50 °C/0% RH and that stored at 40 °C/57%RH for up to 6 months. However, polarized light microscopy suggested that there might be a limited amount of crystallites on the surface of the particles for the sample stored at 40 °C/57%RH for 6 months. For this reason, a CPMAS spectrum was collected with a ^{1}H $T_{1\rho}$ filter of 40 ms to selectively detect more crystalline signals. This spectrum is shown in Figure 6.43. There are no obvious crystalline peaks in the spectrum (Figure 6.43b), suggesting the crystallinity is too low for the detection of solid-state NMR, or that the crystallites had a shorter ^{1}H $T_{1\rho}$ value that was similar to the amorphous form.

Crystallization peaks were seen as shoulders at 179.7 ppm, 136.5 ppm, 113 ppm and 98 ppm in the IMC amorphous solid dispersion after storage at 40 °C/75%RH for 2 and 6 months. Crystallization was observed after 1 month of storage from the PXRD diffractogram. This might suggest that PXRD is a better technique in detecting crystallization, however, a CPMAS spectrum collected with a ^{1}H $T_{1\rho}$ filter of 40 ms revealed crystallization in the sample after storage of 1 month (Figure 6.44). Figure 6.44b shows crystalline peaks in the dispersion that corresponds to those in γ-indomethacin. Peaks at 43 ppm and 32 ppm are residual signals from PVP.

No crystallization peaks were seen in the CPMAS NMR spectra of the NIF amorphous solid dispersions stored at 50 °C/0% RH and at 40 °C/57%RH for up to 6

months, agreeing with the PXRD data. Since polarized light microscopy suggested that there might be a limited amount of crystallites on the surface of the particles for the sample stored at 40 °C/57%RH for 6 months, a CPMAS spectrum was collected with a ^{1}H $T_{1\rho}$ filter of 40 ms to selectively detect more crystalline signals. This spectrum is shown in Figure 6.45. The narrow peaks at 170.5 ppm, 168.6 ppm, 103.4 ppm, 101.8 ppm and 19.7 ppm indicated crystallinity in the sample. As is seen from Figure 6.45e, two small crystalline peaks at 170.5 ppm and 168.6 ppm in the carbonyl region corresponded to the α polymorph. This was not detected by PXRD or the regular CPMAS NMR spectrum.

Crystallization peaks were seen in the spectrum of the NIF amorphous solid dispersion stored at 40 °C/75%RH for just 1 week. The carbonyl region of the spectrum showed that the crystalline peaks were a mixture of the α and β polymorphs (Figure 6.46). The spectra between 163 and 173 ppm of all time points were fitted by a linear combination of reference spectra of the amorphous, the α and the β forms using least square procedures with MATLAB (MathWorks, Natick, MA). The obtained relative amount of each species was plotted as a function of the time points and is shown in Figure 6.47. The figure reveals that both the α and the β forms emerged in the beginning. The α form steadily increased as the storage time increased, whereas the meta-stable β form peaked at about 2 weeks of storage time and then converted to the α form. The overall crystallinity seems to reach a plateau of approximately 90% after 2 months of storage. A small amount (~ 7%) of the β form was still observed at the end of the 6 months stability study.

The ^{1}H relaxation times of the three amorphous solid dispersions stored at various conditions were determined and the differences between the APIs and the polymers were calculated and normalized with respect to the relaxation times of the APIs. The normalized differences for each sample are shown in Figures 6.48-6.54.

As suggested by both ^{1}H T_1 and $T_{1\rho}$ relaxation time differentials in Figure 6.48, IMC methyl ester and PVP were intimately mixed when stored up to six months at 4 °C/0% RH. The ^{1}H $T_{1\rho}$ relaxation times showed differences after 2 months and 6 months that were close to the 95% confidence intervals, which may suggest the system was experiencing some degree of immiscibility. The ^{1}H T_1 and $T_{1\rho}$ relaxation time differentials of the IMC dispersion stored at 50 °C/0% RH were small and within the 95% confidence intervals, indicating miscibility up to six months of storage (Figure 6.49).

Figure 6.50 shows the normalized relaxation time differentials of the IMC dispersion stored at 40 °C/57% RH, where the sample seemed to be miscible the entire storage time as indicated by ^{1}H T_1 and $T_{1\rho}$ relaxation times. However, sorbed water can increase the molecular mobility of amorphous systems and has been shown to possess a high degree of translational mobility in glassy matrices.[77] Thus, sorbed water can act as a plasticizer and a relaxation sink, resulting in a decrease in ^{1}H relaxation times. Indeed, this is what is observed for the ^{1}H $T_{1\rho}$ relaxation times in the IMC-PVP amorphous solid dispersions plotted as a function of water content, as shown in Figure 6.55a. The ^{1}H T_1 relaxation time differentials did not change significantly in the range of water content studied (Figure 6.55b). In the ternary system consisting of IMC, PVP and water, the ^{1}H $T_{1\rho}$ relaxation of either IMC or PVP is reduced by water, which exists in the vicinity of both IMC and PVP as loosely bound molecules that have a considerably high degree of

mobility. The relaxation times of the drug and the polymer essentially reflect the relaxation times of the drug-water and polymer-water micro domains.

Taylor and coworkers have shown that a 75-25 IMC-PVP amorphous solid dispersion did not phase separate upon exposure to 94% RH for 84 days at 25 °C.[36] However, the conclusion was based on the detection of hydrogen bonding between IMC and PVP after the moisture was removed from the sample. The result does not necessarily reflect miscibility with water present. It is known that hydrogen bond formations generally change as a function of water content in the system, so the hydrogen bonding interactions between IMC and PVP could be different with and without water. Nonetheless, the present data show one glass transition temperature and nearly constant water content for the entire time of storage, indicating a good chance of miscibility in the system, as phase separation is known to lead to higher water vapor sorption in some amorphous dispersion systems including the IMC-PVP system.[139]

Figure 6.51 shows the normalized ^{1}H relaxation time differentials of the IMC dispersion stored at 40 °C/75% RH. Crystallization of this system was detected after 1 month of storage, which means there had to be some degree of phase separation at that point. However, the ^{1}H T_1 relaxation time seems to suggest miscibility for the entire storage period, while the ^{1}H $T_{1\rho}$ relaxation times suggest possible immiscibility in the sample after 1 and 2 months of storage, and definite immiscibility after 6 months of storage. The detection of immiscibility is most likely due to the fact that crystalline indomethacin has a much longer relaxation time.

Figure 6.52 shows the normalized ^{1}H relaxation time differentials of the NIF amorphous solid dispersions stored at 50 °C/0% RH. Similar to the relaxation behaviors

of the IMC amorphous solid dispersion stored in the same condition, both ^{1}H T_1 and $T_{1\rho}$ relaxation time differentials indicate miscibility for this NIF system. For the NIF system stored at 40 °C/57% RH, the ^{1}H T_1 relaxation time differentials indicated miscibility and the $T_{1\rho}$ relaxation time differentials indicated borderline miscibility for the entire storage period (Figure 6.53). Since the NIF amorphous solid dispersion stored at 40 °C/75% RH showed substantial crystallization after just one week of storage, both ^{1}H T_1 and $T_{1\rho}$ relaxation time differentials for this sample were quite large indicating phase separation as expected (Figure 6.54).

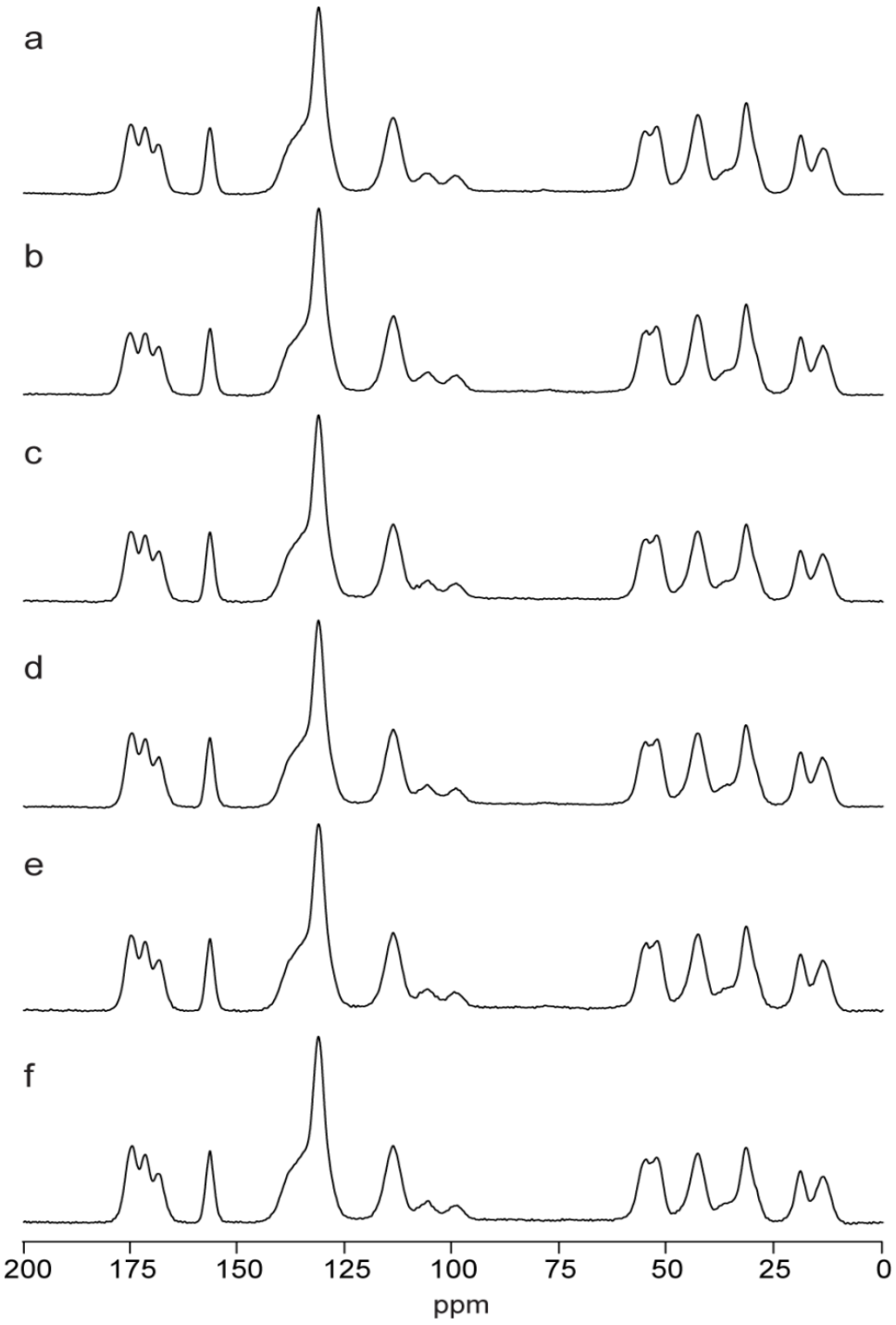

Figure 6.36. ^{13}C CPMAS spectra of 70-30 IMC methyl ester-PVP amorphous solid dispersion stored at 4 °C/0% RH at (a) time 0, (b) 1 week, (c) 2 weeks, (d) 1 month, (e) 2 months, and (f) 6 months of storage. No crystallization is observed in any spectra.

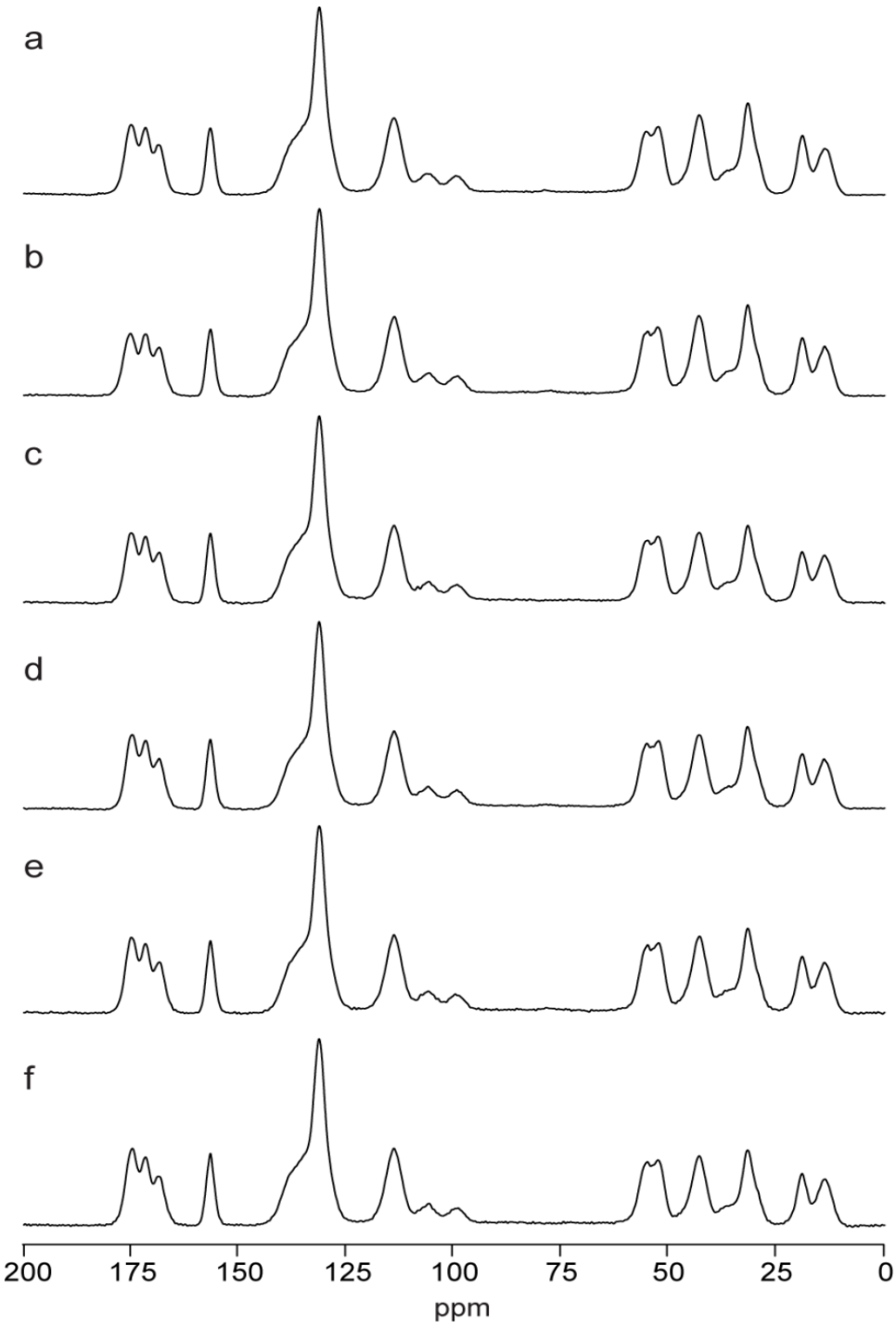

Figure 6.37. ^{13}C CPMAS spectra of 70-30 IMC-PVP amorphous solid dispersion stored at 50 °C/0% RH at (a) time 0, (b) 1 week, (c) 2 weeks, (d) 1 month, (e) 2 months, and (f) 6 months of storage. No crystallization is observed in any spectra.

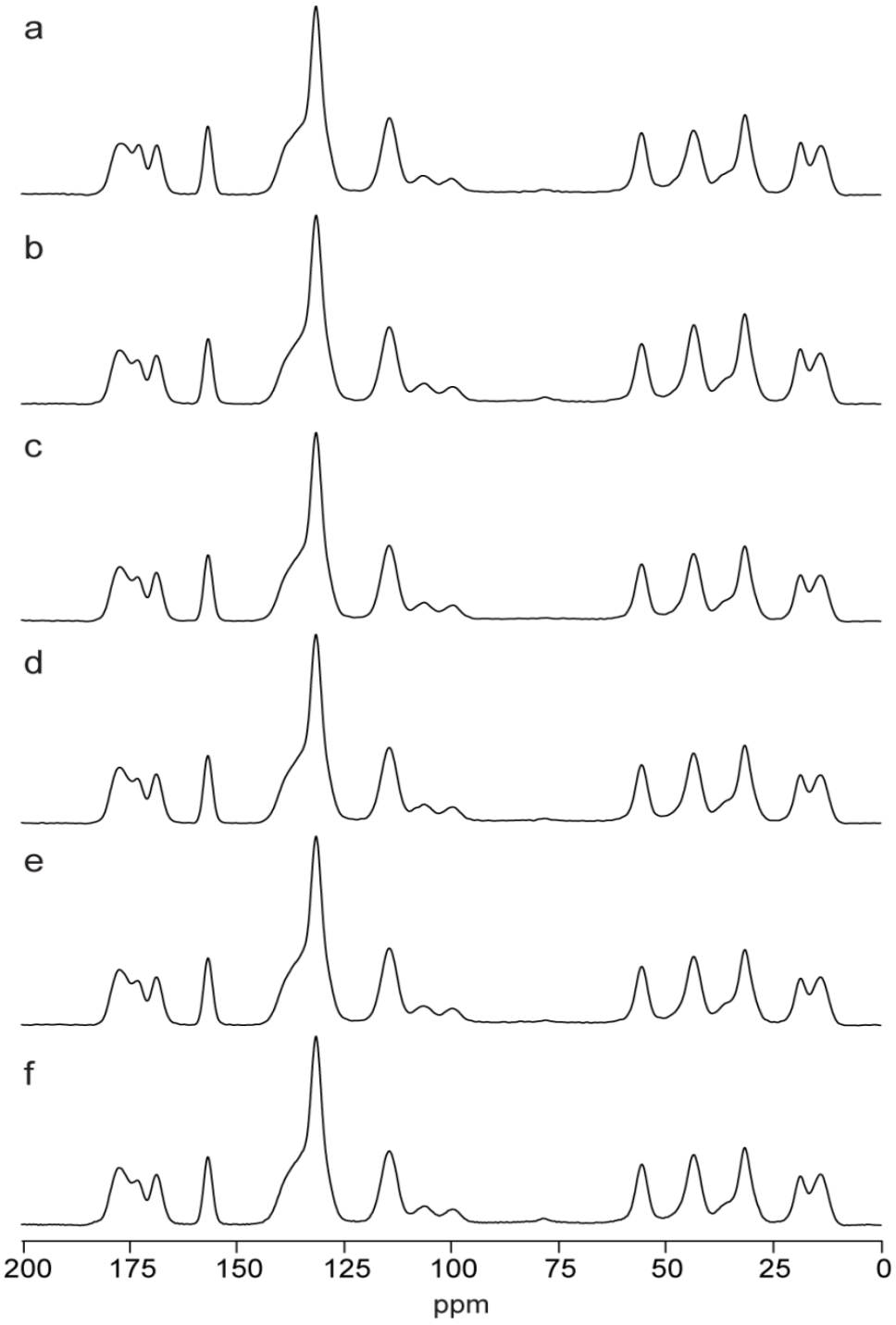

Figure 6.38. ^{13}C CPMAS spectra of 70-30 IMC-PVP amorphous solid dispersion stored at 40 °C/57% RH at (a) time 0, (b) 1 week, (c) 2 weeks, (d) 1 month, (e) 2 months, and (f) 6 months of storage. No crystallization is observed in any spectra.

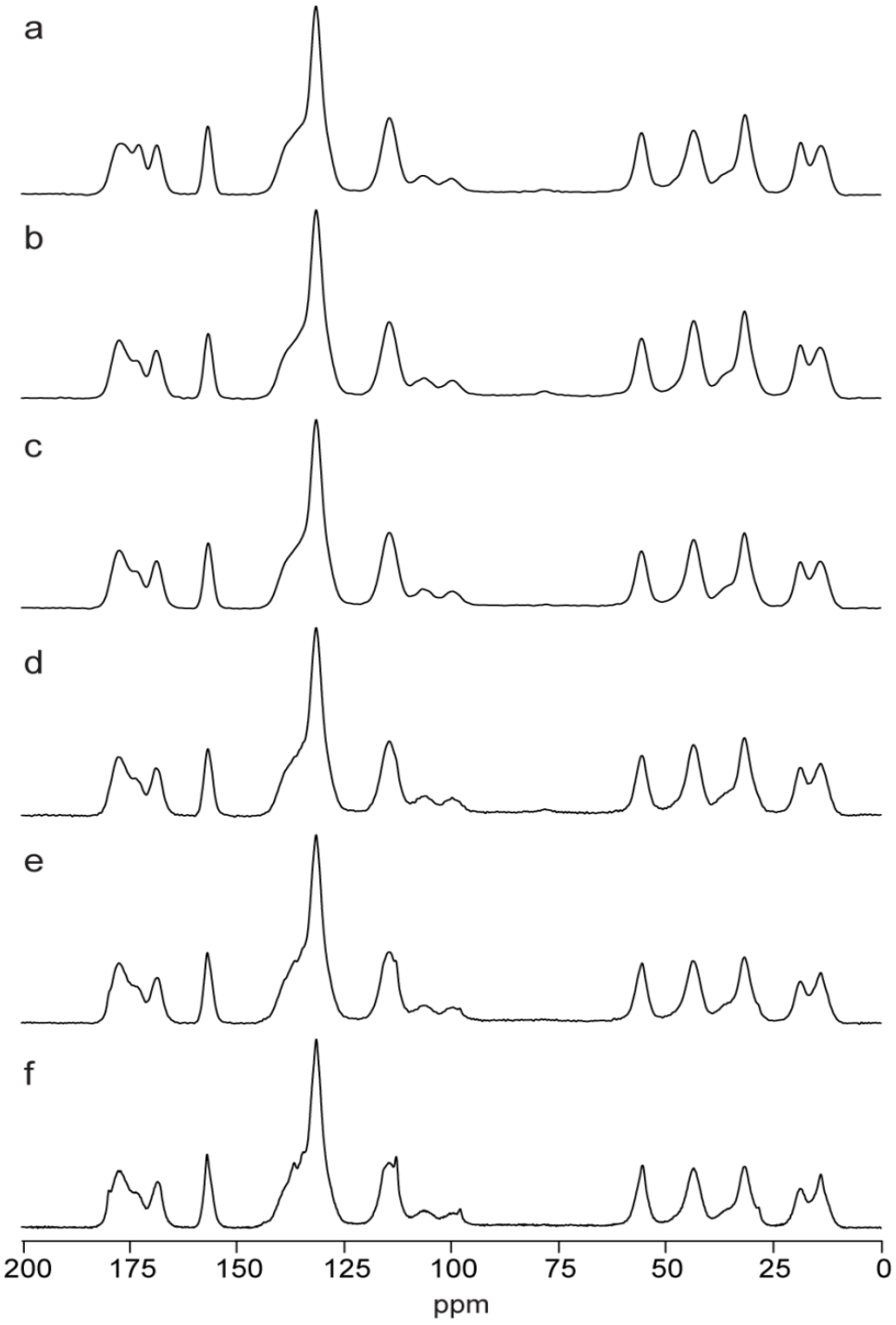

Figure 6.39. ^{13}C CPMAS spectra of 70-30 IMC-PVP amorphous solid dispersion stored at 40 °C/75% RH at (a) time 0, (b) 1 week, (c) 2 weeks, (d) 1 month, (e) 2 months, and (f) 6 months of storage. Crystallization is observed in (e) and (f).

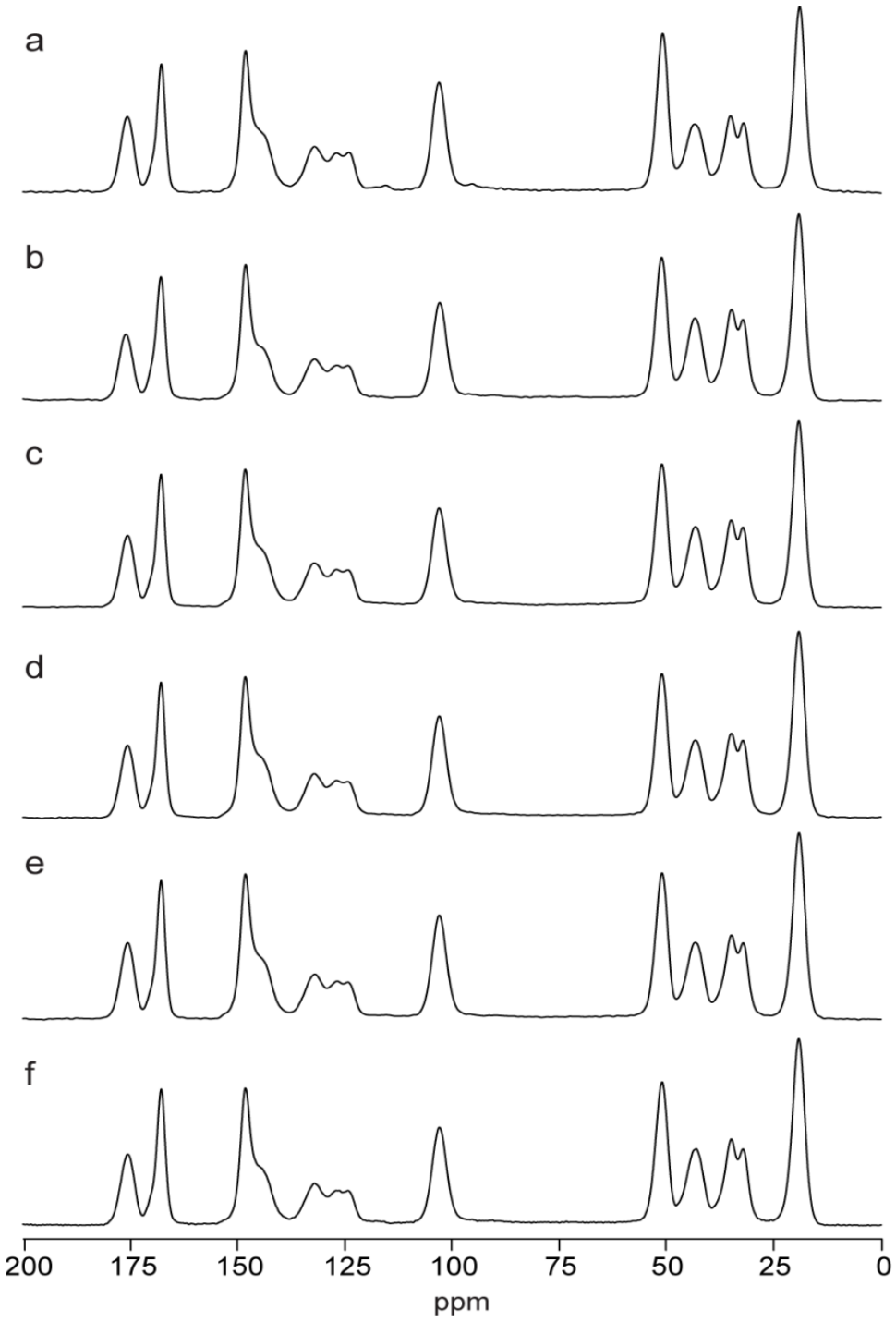

Figure 6.40. ^{13}C CPMAS spectra of 70-30 NIF-PVP amorphous solid dispersion stored at 50 °C/0% RH at (a) time 0, (b) 1 week, (c) 2 weeks, (d) 1 month, (e) 2 months, and (f) 6 months of storage. No crystallization is observed in any spectra.

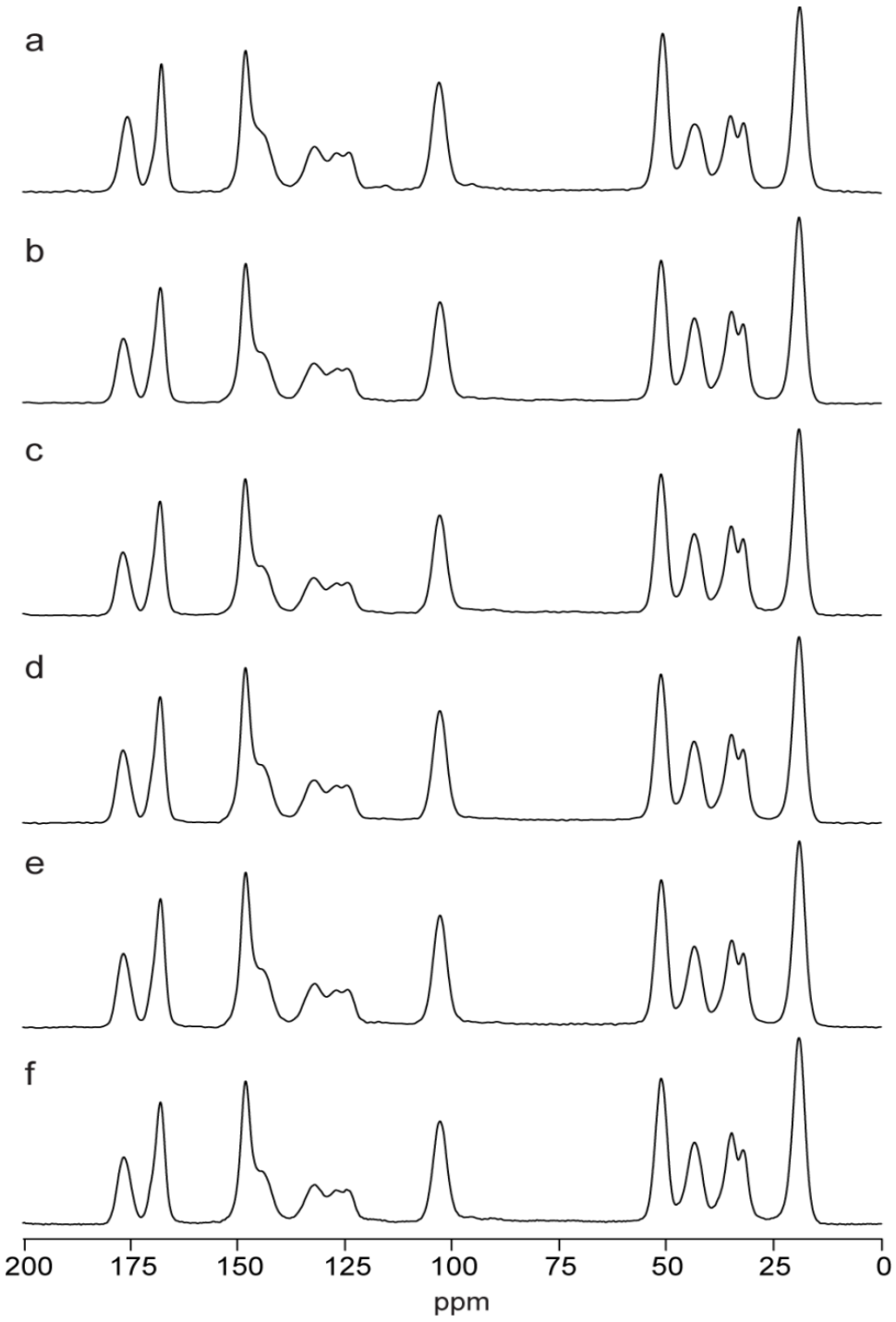

Figure 6.41. ^{13}C CPMAS spectra of 70-30 NIF-PVP amorphous solid dispersion stored at 40 °C/57% RH at (a) time 0, (b) 1 week, (c) 2 weeks, (d) 1 month, (e) 2 months, and (f) 6 months of storage. No crystallization is observed in any spectra.

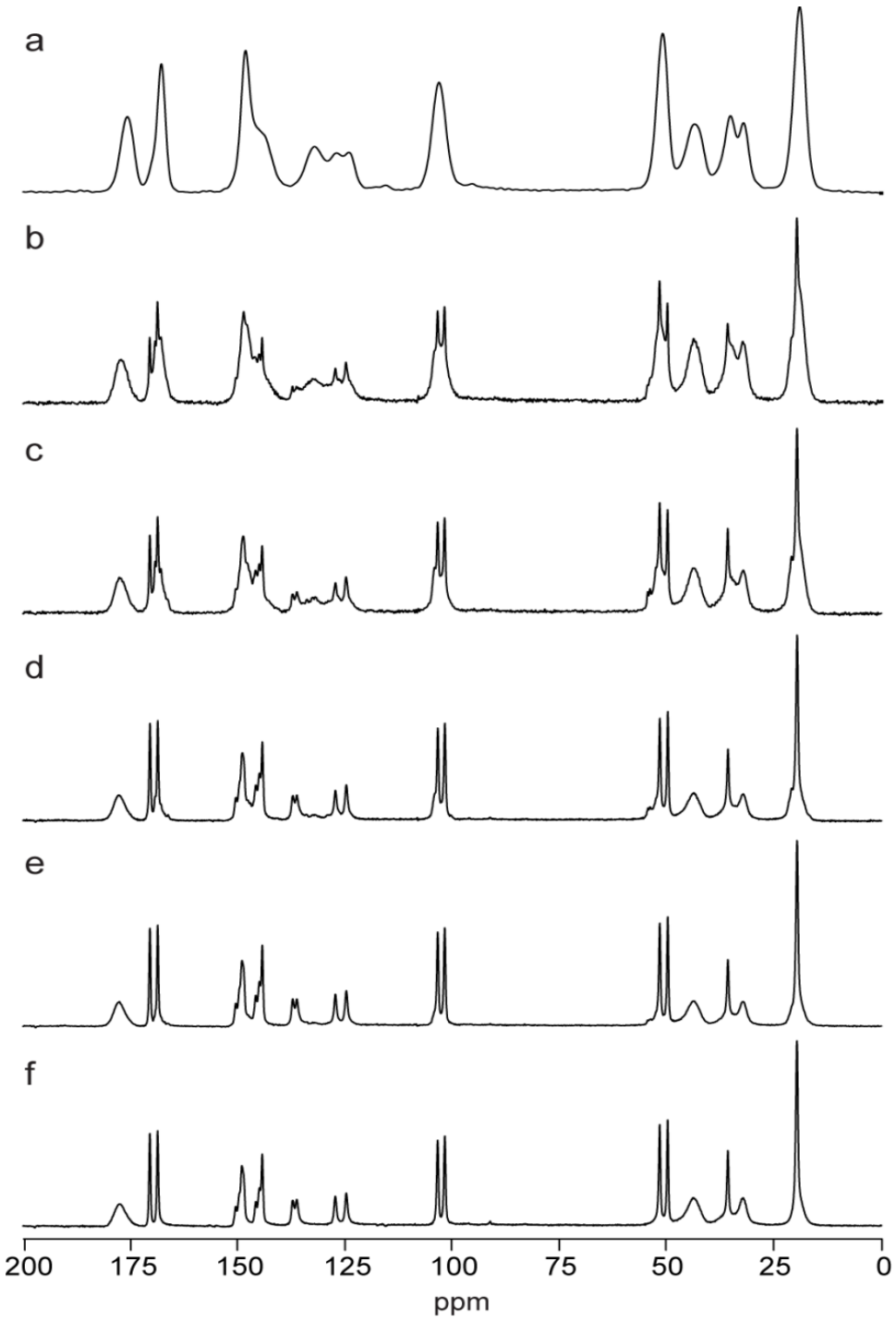

Figure 6.42. ^{13}C CPMAS spectra of 70-30 NIF-PVP amorphous solid dispersion stored at 40 °C/75% RH at (a) time 0, (b) 1 week, (c) 2 weeks, (d) 1 month, (e) 2 months, and (f) 6 months of storage. Crystallization is observed in (b), (c), (d), (e) and (f).

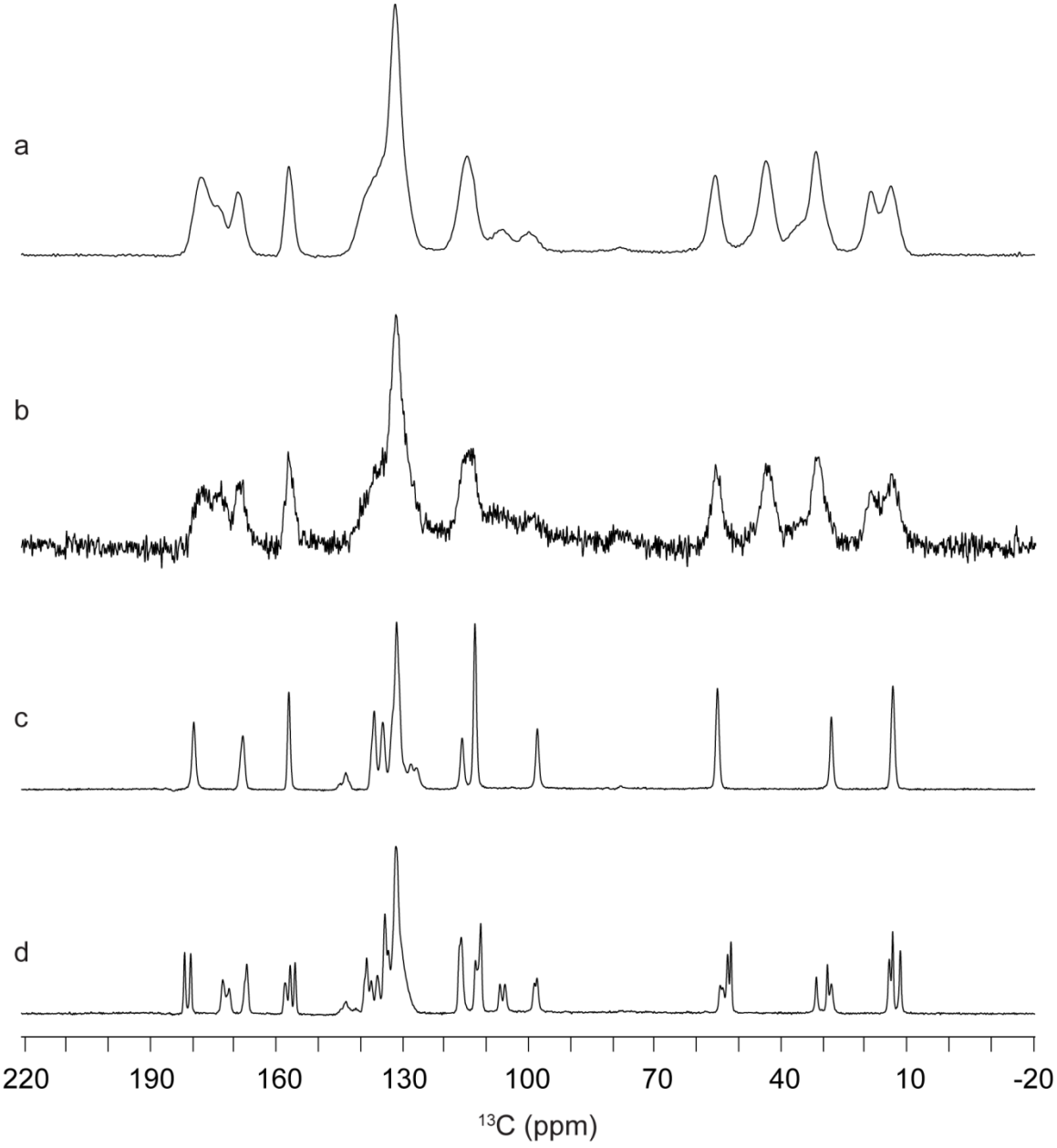

Figure 6.43. ^{13}C CPMAS spectra of (a) 70-30 IMC-PVP amorphous solid dispersion stored at 40 °C/57% RH for 6 months, (b)) 70-30 IMC-PVP amorphous solid dispersion stored at 40 °C/57% RH for 6 months collected with a 40 ms ^{1}H $T_{1\rho}$ filter, (c) γ-indomethacin, and (d) α-indomethacin.

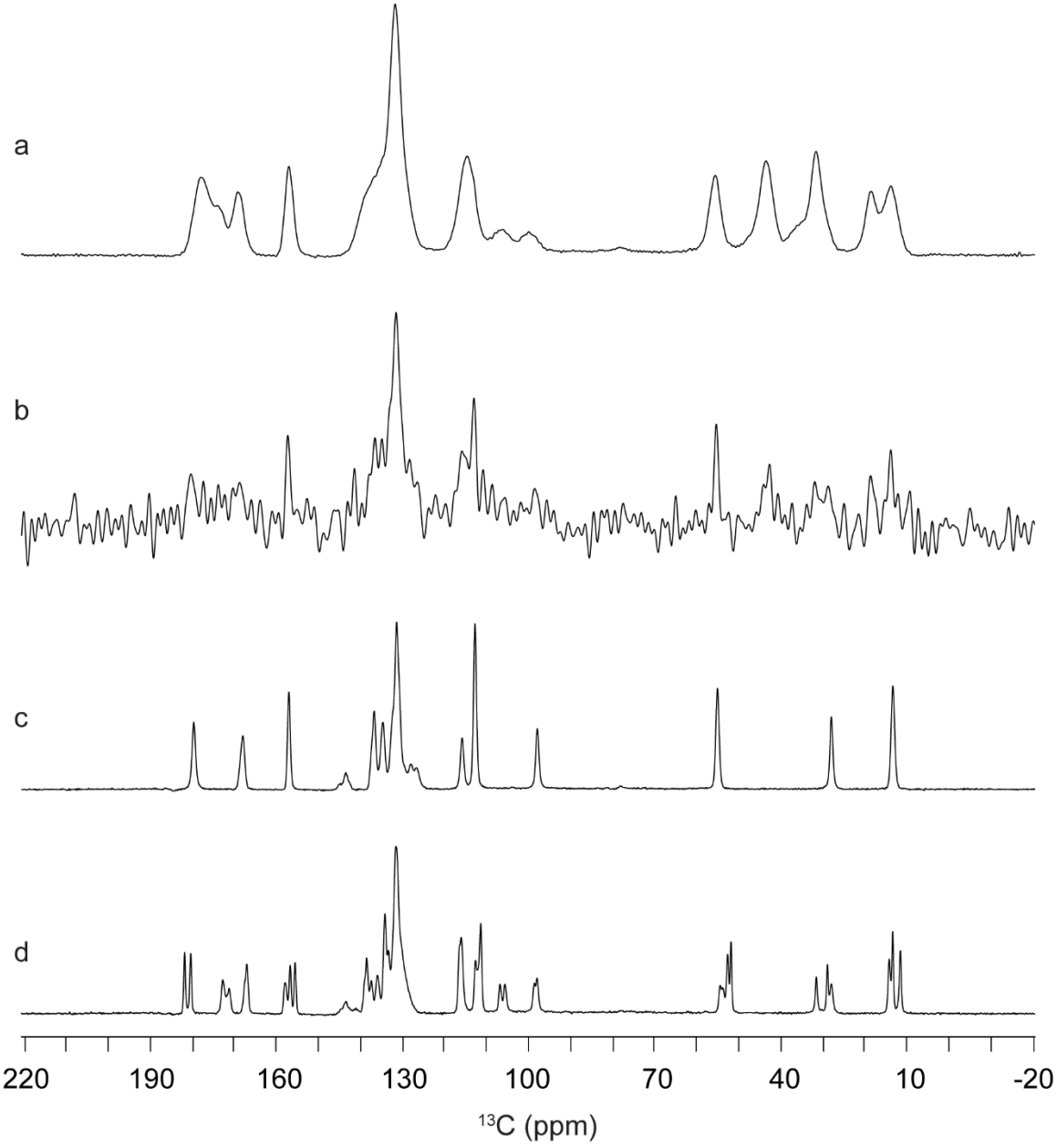

Figure 6.44. ^{13}C CPMAS spectra of (a) 70-30 IMC-PVP amorphous solid dispersion stored at 40 °C/75% RH for 1 month, (b)) 70-30 IMC-PVP amorphous solid dispersion stored at 40 °C/75% RH for 1 month collected with a 40 ms ^{1}H $T_{1\rho}$ filter, (c) γ-indomethacin, and (d) α-indomethacin.

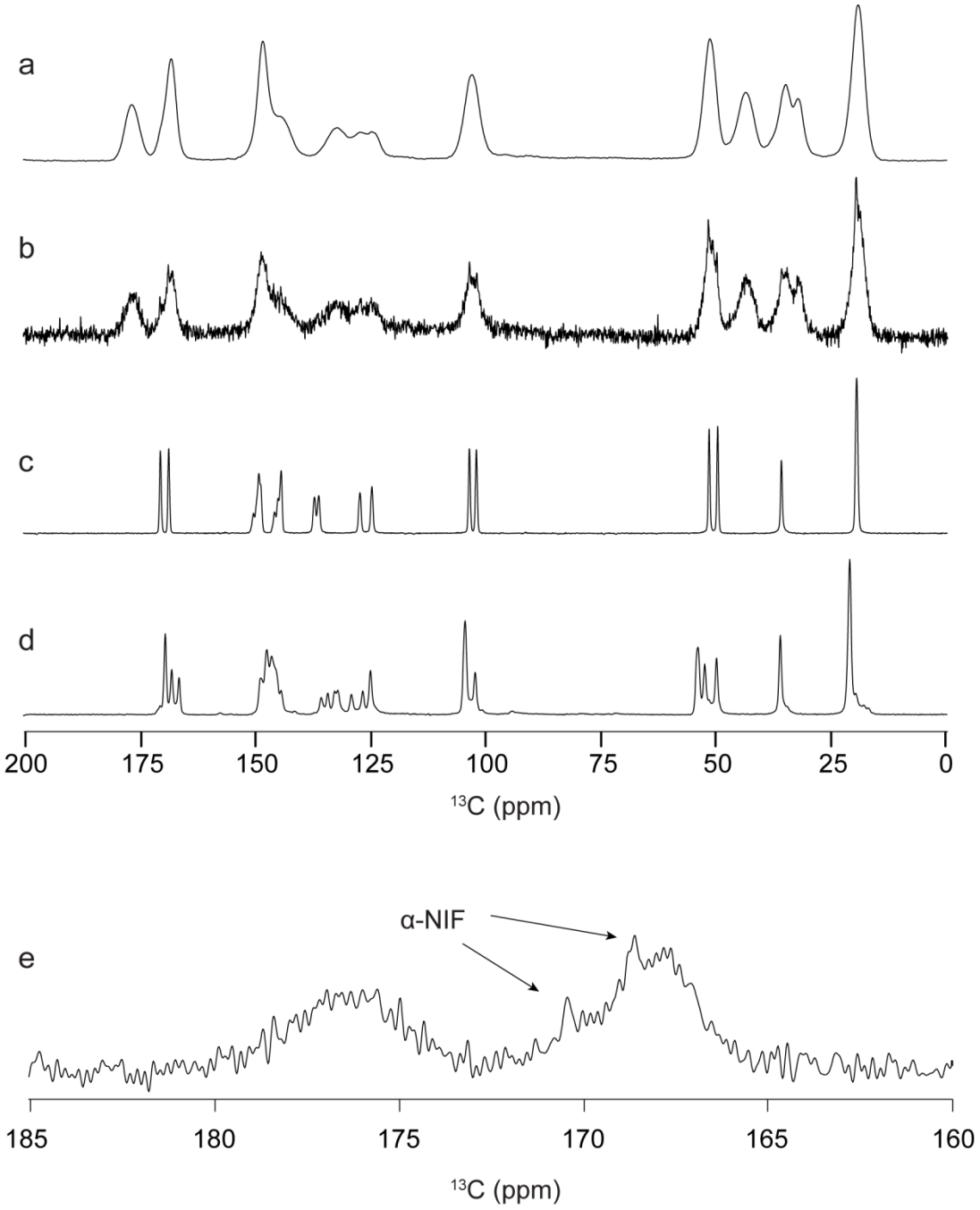

Figure 6.45. ^{13}C CPMAS spectra of (a) 70-30 NIF-PVP amorphous solid dispersion stored at 40 °C/75% RH for 1 month, (b)) 70-30 NIF-PVP amorphous solid dispersion stored at 40 °C/75% RH for 1 month collected with a 40 ms ^{1}H $T_{1\rho}$ filter, (c) α-nifedipine, (d) β-nifedipine, and (e) carbonyl region of (b).

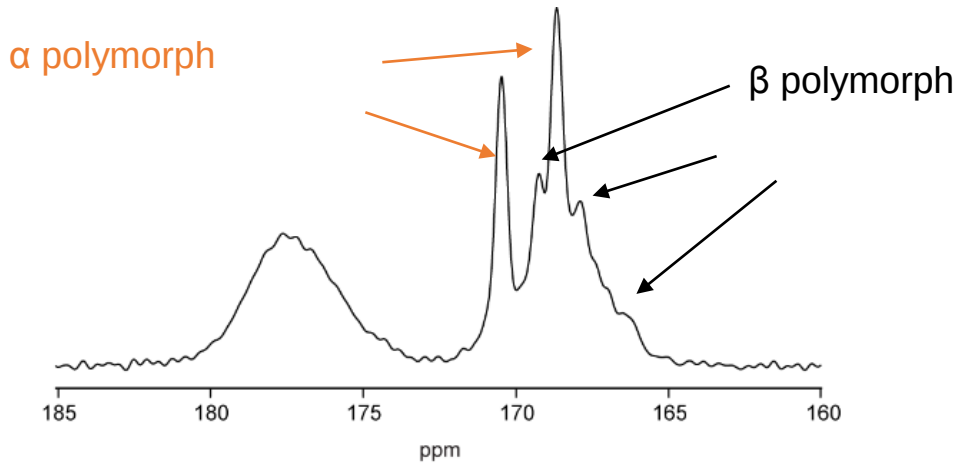

Figure 6.46. ^{13}C CPMAS spectrum of the carbonyl region of 70-30 NIF-PVP amorphous solid dispersion stored at 40 °C/75% RH after 1 week.

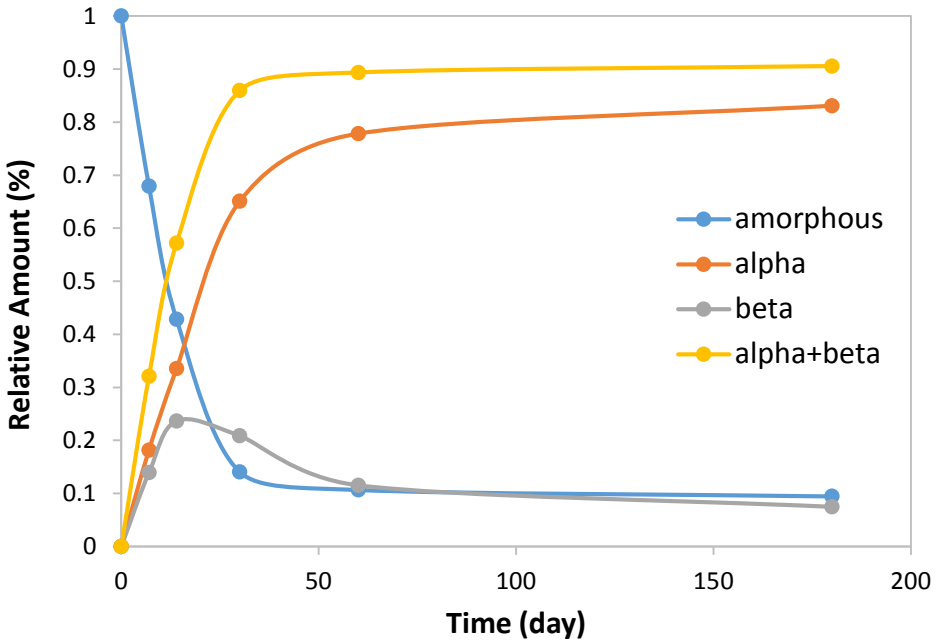

Figure 6.47. Crystallization of amorphous NIF in the 70-30 NIF-PVP amorphous solid dispersion stored at 40 °C/75% RH as a function of time. The circle represents amorphous NIF; triangle represents the α polymorph; square represents the β polymorph; and cross represents the total crystallinity (sum of α and β polymorphs).

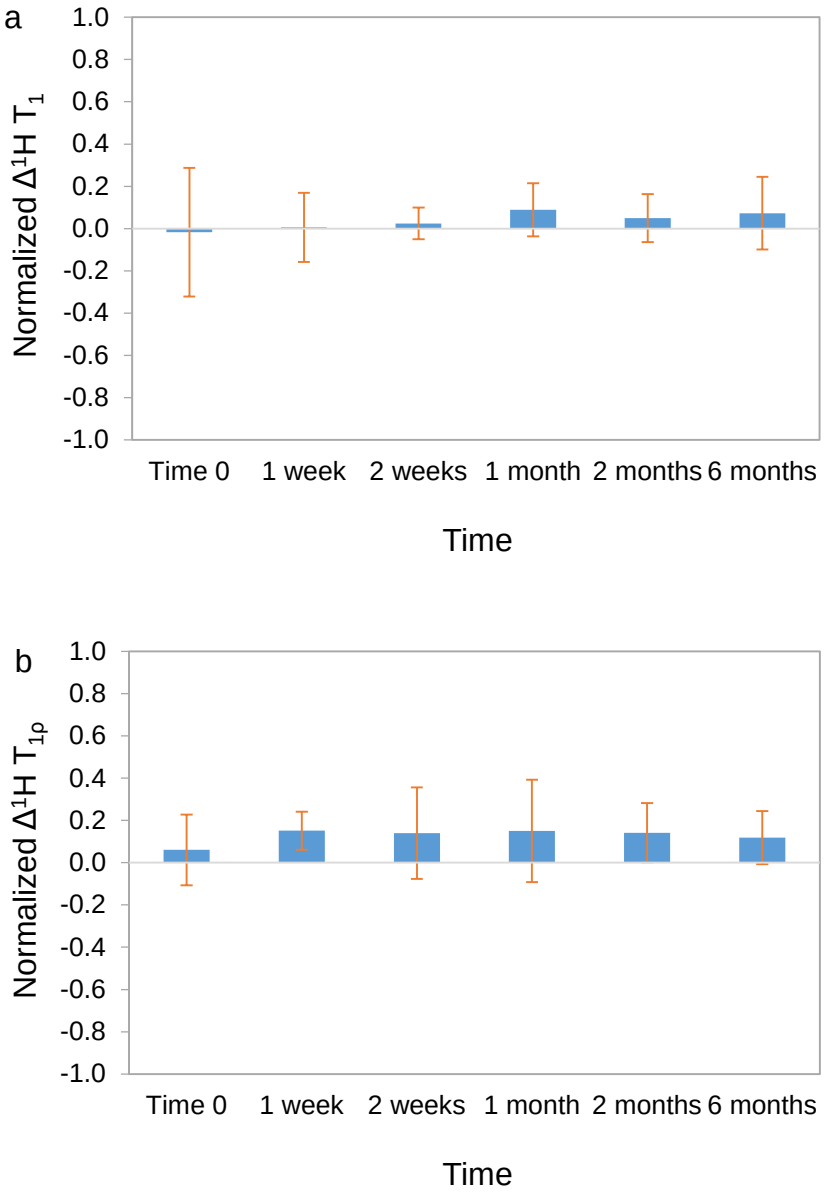

Figure 6.48. Normalized differences of (a) ^{1}H T_1 and (b) ^{1}H $T_{1\rho}$ relaxation times between IMC methyl ester and PVP in the 70-30 IMC methyl ester-PVP amorphous solid dispersion a function of storage time at 4 °C/0% RH.

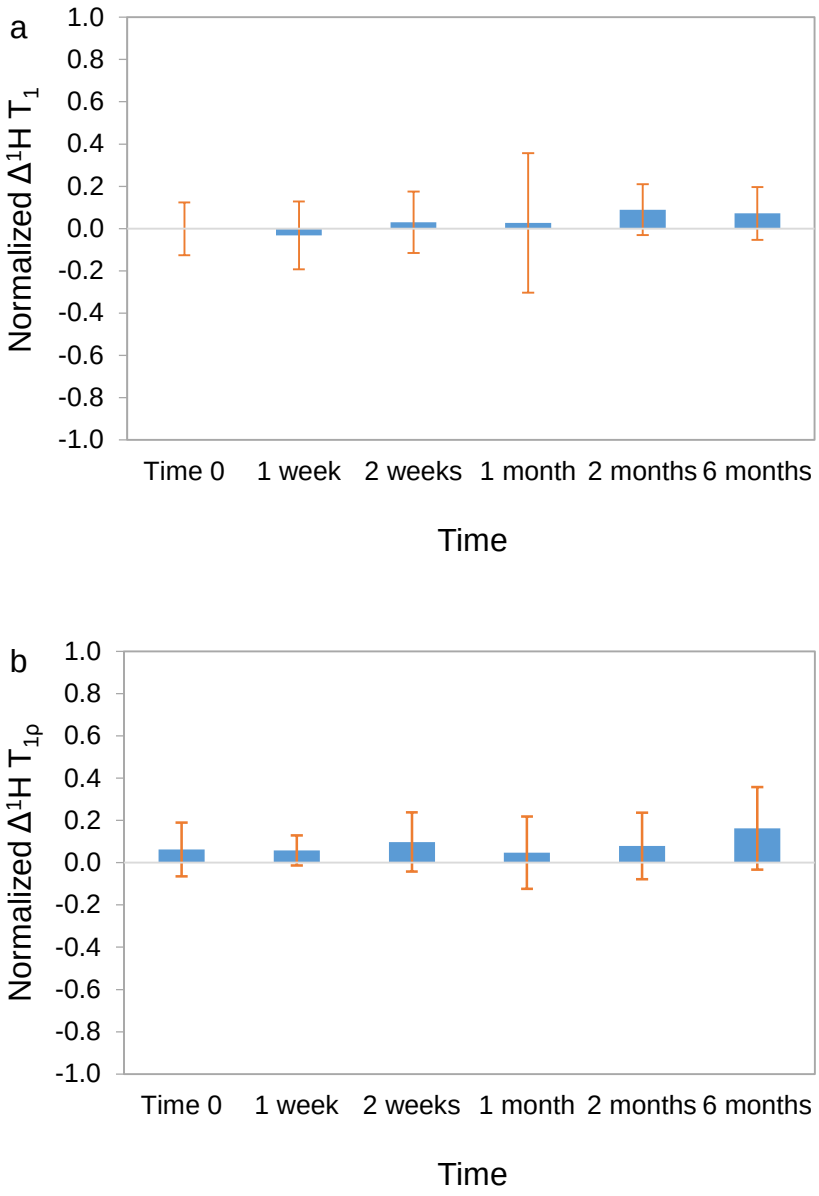

Figure 6.49. Normalized differences of (a) ^{1}H T_1 and (b) ^{1}H $T_{1\rho}$ relaxation times between IMC and PVP in the 70-30 IMC-PVP amorphous solid dispersion a function of storage time at 50 °C/0% RH.

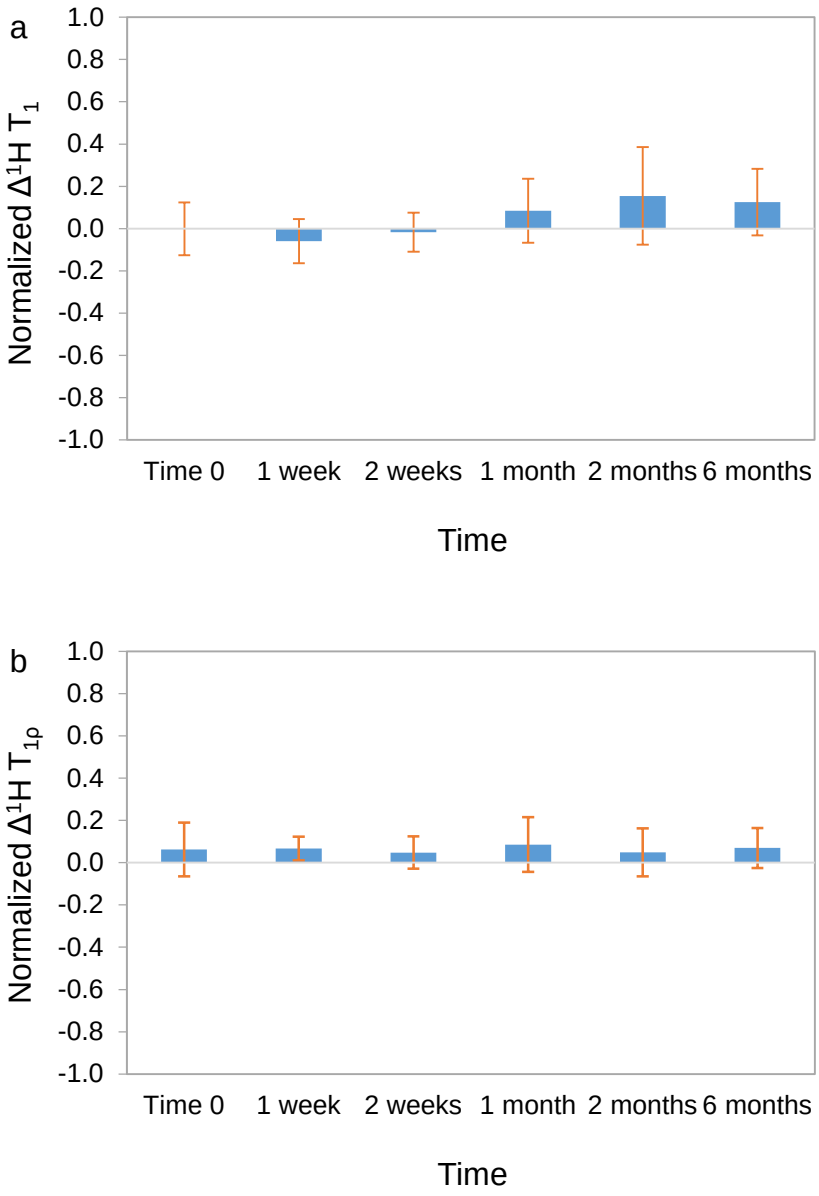

Figure 6.50. Normalized differences of (a) ^{1}H T_1 and (b) ^{1}H $T_{1\rho}$ relaxation times between IMC and PVP in the 70-30 IMC-PVP amorphous solid dispersion a function of storage time at 40 °C/57% RH.

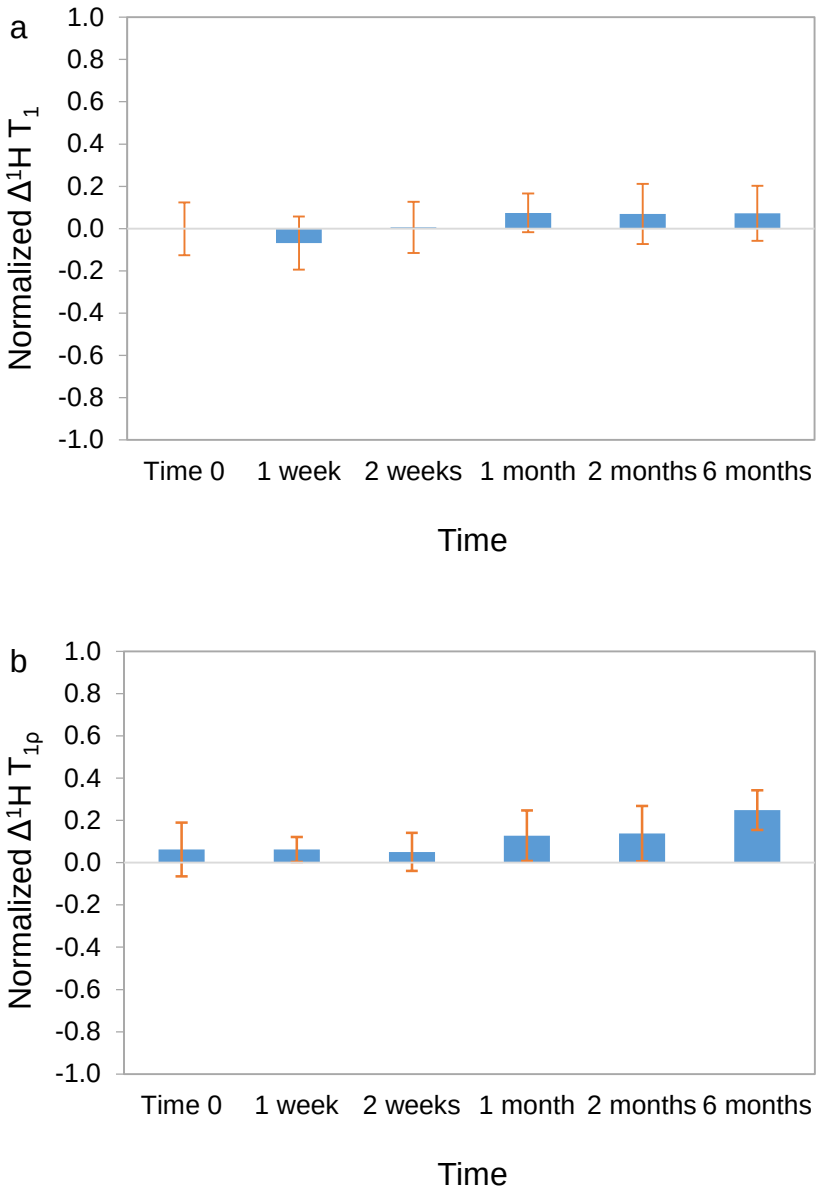

Figure 6.51. Normalized differences of (a) ^{1}H T_1 and (b) ^{1}H $T_{1\rho}$ relaxation times between IMC and PVP in the 70-30 IMC-PVP amorphous solid dispersion a function of storage time at 40 °C/75% RH.

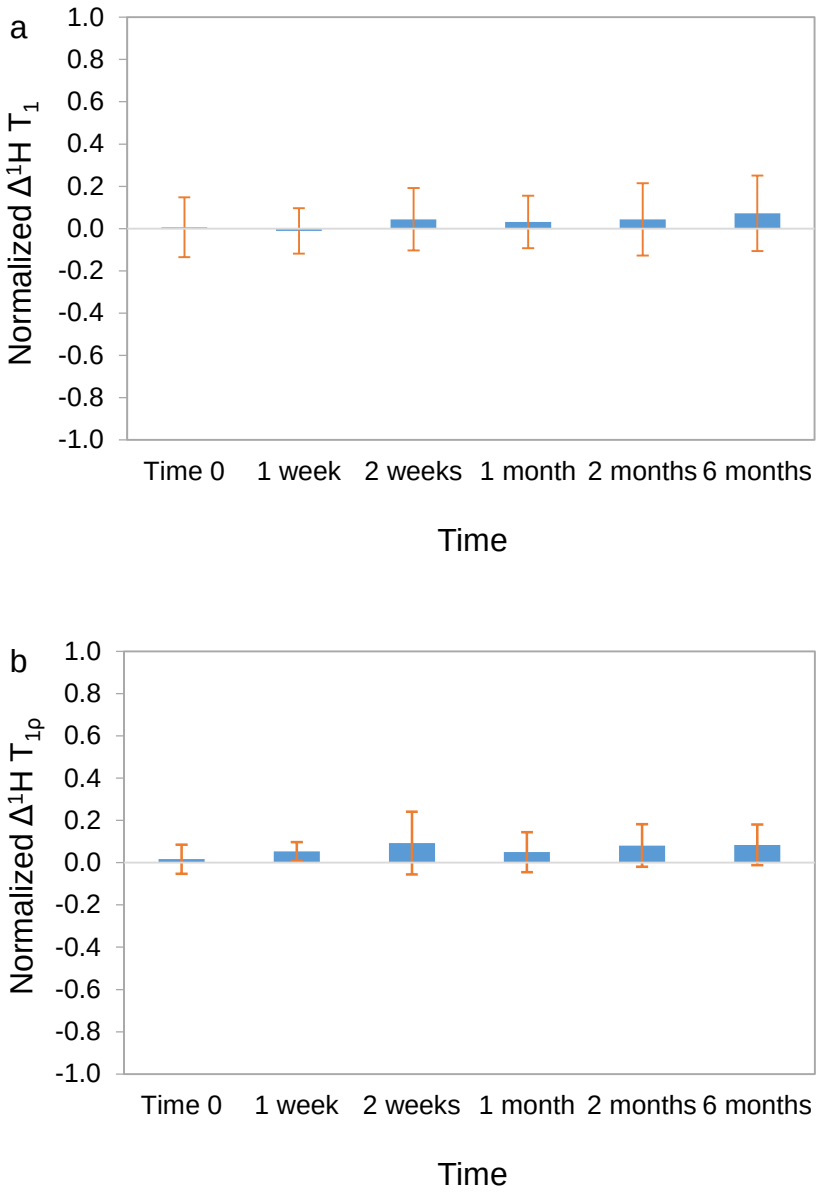

Figure 6.52. Normalized differences of (a) ^{1}H T_1 and (b) ^{1}H $T_{1\rho}$ relaxation times between NIF and PVP in the 70-30 NIF-PVP amorphous solid dispersion a function of storage time at 50 °C/0% RH.

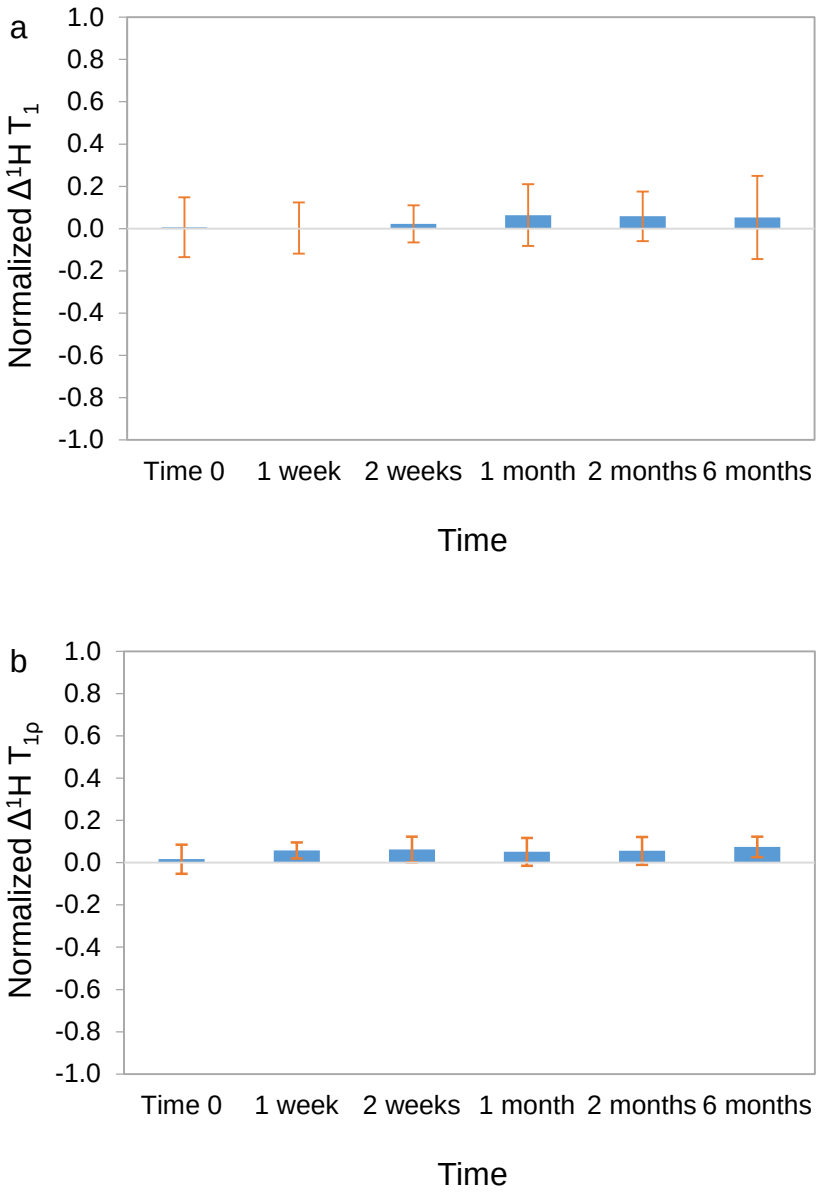

Figure 6.53. Differences of (a) ^{1}H T_1 and (b) ^{1}H $T_{1\rho}$ relaxation times between NIF and PVP in the 70-30 NIF-PVP amorphous solid dispersion a function of storage time at 40 °C/57% RH.

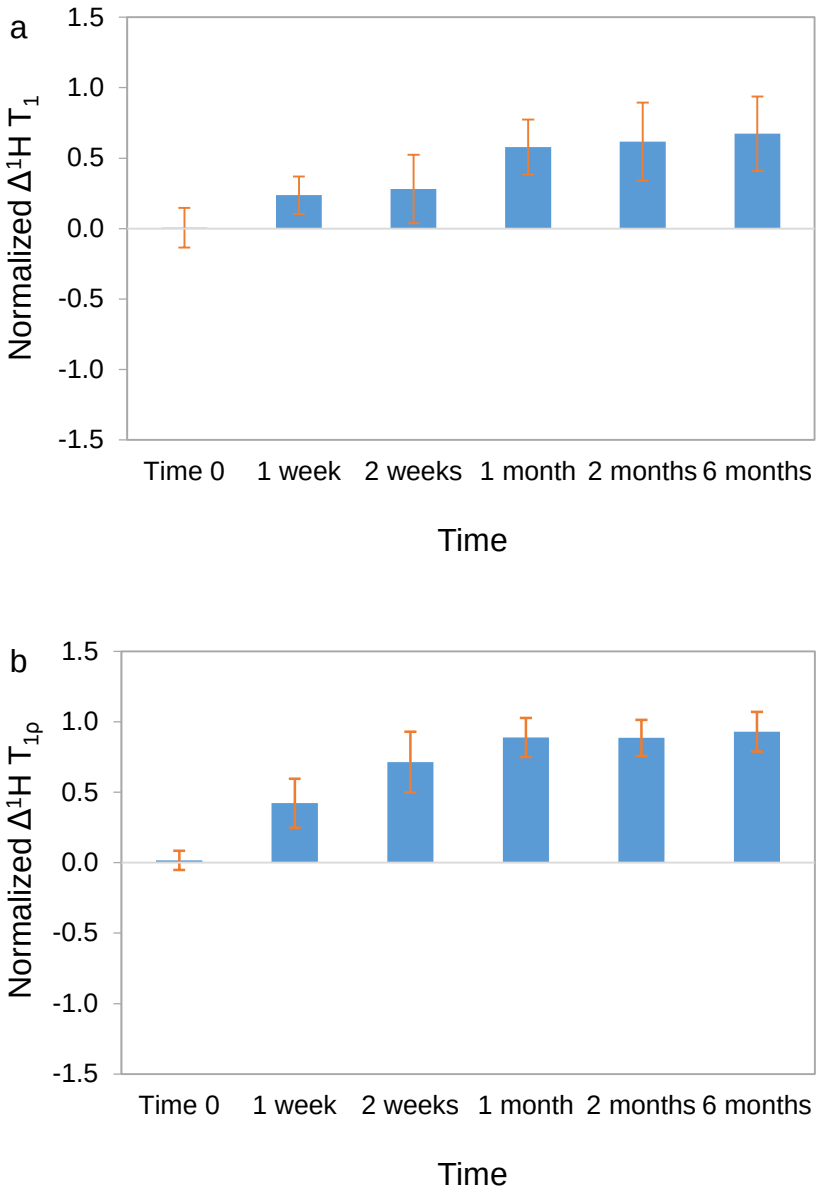

Figure 6.54. Differences of (a) ^{1}H T_1 and (b) ^{1}H $T_{1\rho}$ relaxation times between NIF and PVP in the 70-30 NIF-PVP amorphous solid dispersion a function of storage time at 40 °C/75% RH.

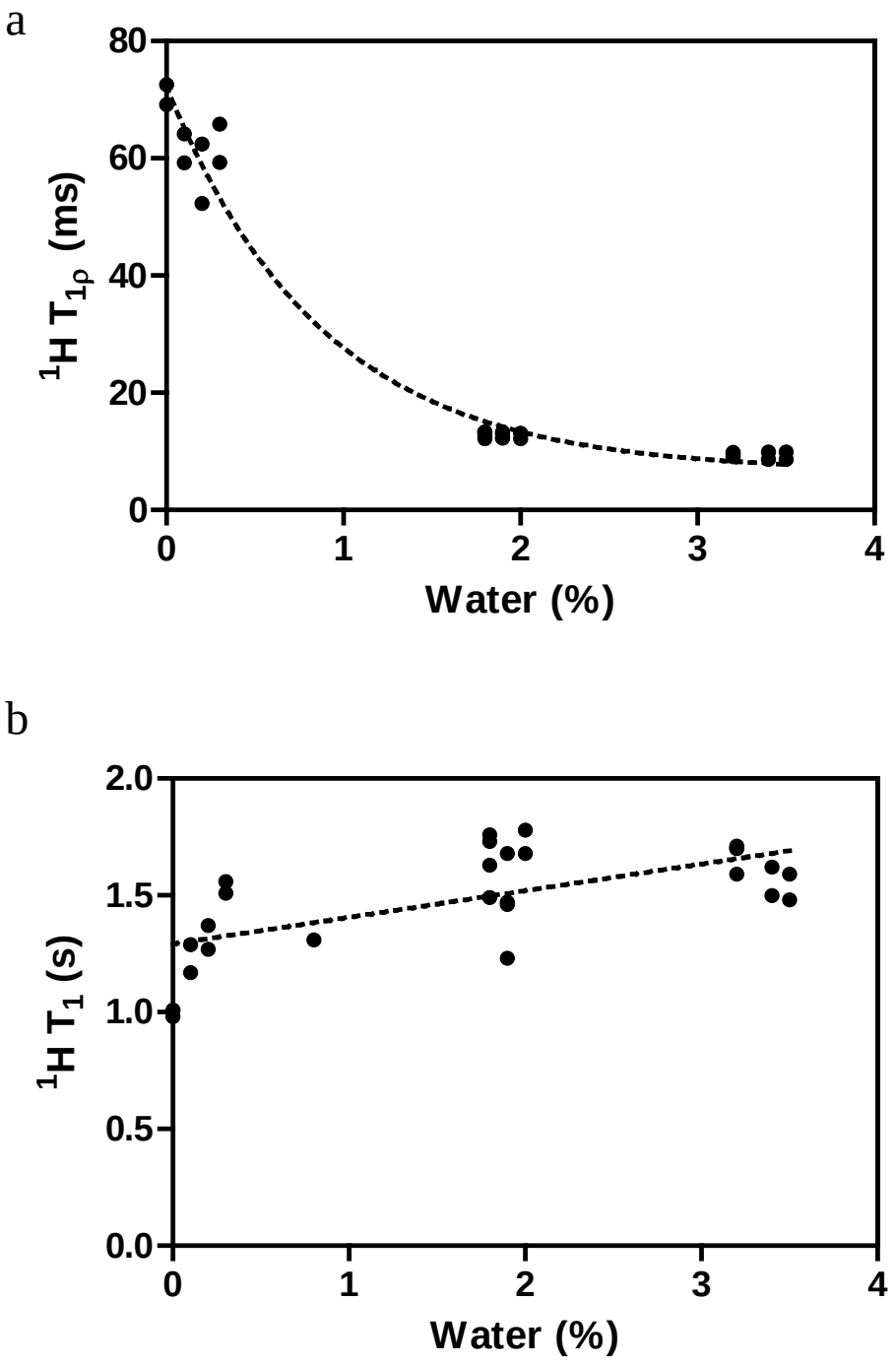

Figure 6.55. Dependence of (a) ^{1}H $T_{1\rho}$ relaxation time, and (b) ^{1}H T_1 relaxation time on water content for the 70-30 IMC-PVP amorphous solid dispersion.

6.3.4 Dissolution Studies

Dissolution profiles of the IMC-PVP and NIF-PVP amorphous solid dispersions at time 0 and after 6 months of storage are shown in Figures 6.56 and 6.57. As shown in Figure 4.56, the fresh IMC amorphous solid dispersion exhibited a very quick supersaturation and achieved a concentration of approximately 8 μg/mL before precipitation occurred. The final concentration after 4 hours was 4.5 μg/mL. The dispersion after 6 months of storage at 50 °C/dry achieved a lower supersaturation value of about 6 μg/mL before declining to about 3.4 μg/mL. The dispersion after 6 months of storage at 40 °C/57% RH achieved a much lower supersaturation value of 3.4 μg/mL before precipitation and had a final concentration of 2.4 μg/mL. The dispersion after 6 months of storage at 40 °C/75% RH did not exhibit prominent supersaturation but the final concentration was 3.1 μg/mL.

Comparing Figure 6.57 with 6.58, we can see that the NIF amorphous solid dispersions did not exhibit any super saturation expected from the dissolution of an amorphous solid dispersion. This could be due to the slow wetting of the particles. It is observed that the particles floated on top of the dissolution medium for a longer period of time compared with the IMC amorphous solid dispersions. The amorphous solid dispersions of NIF achieved a final drug concentration equivalent to that of dissolution of the crystalline α form. This suggests that the rate limiting step in this dissolution process was probably wetting of the particles, which also explains why the there was no difference in the dissolution profiles among all the samples including the sample that was mostly crystalline (sample stored at 40 °C/75% RH for six months).

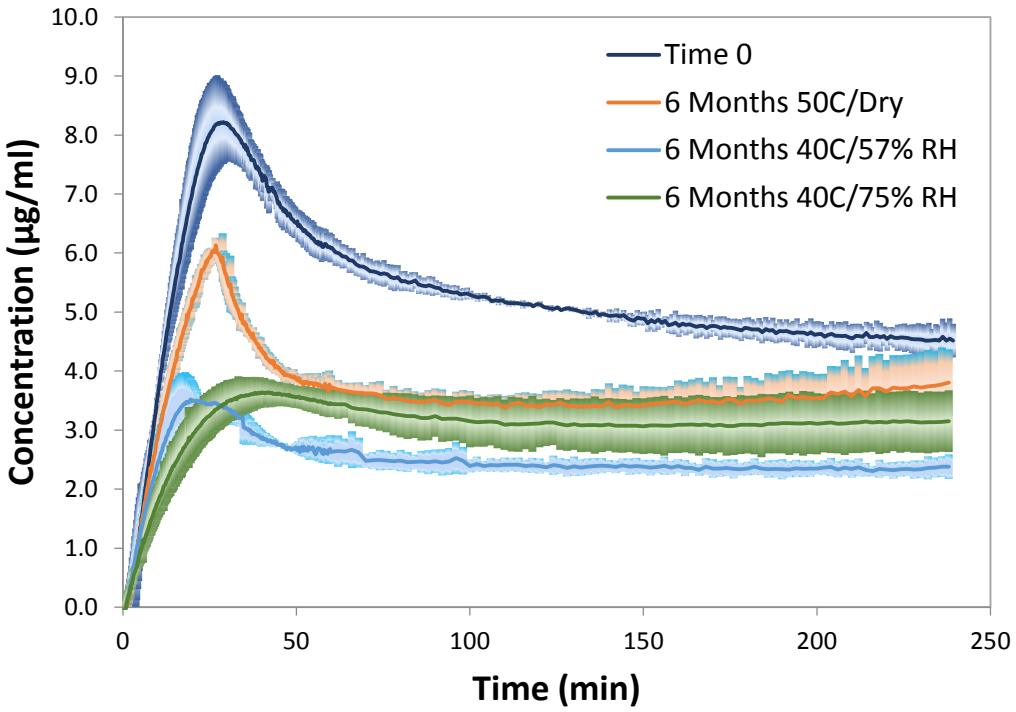

Figure 4.56. Dissolution profiles of 70-30 IMC-PVP amorphous solid dispersion at time 0 and after storage for 6 months. The shaded area represents the standard deviation (n=3).

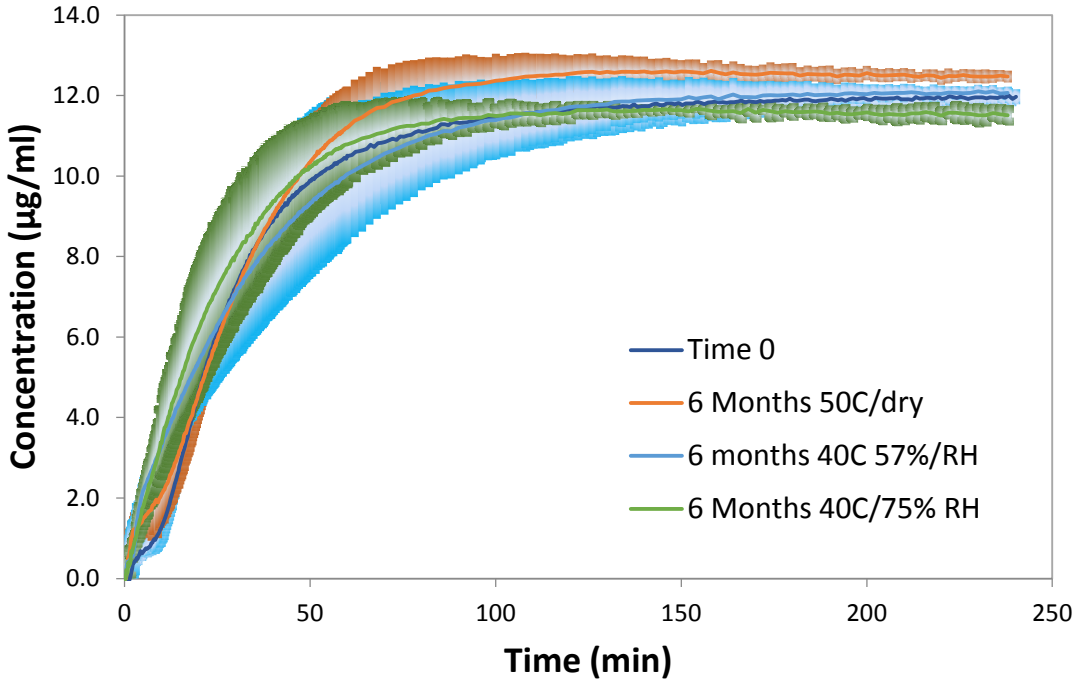

Figure 6.57. Dissolution profiles of 70-30NIF-PVP amorphous solid dispersion at time 0 and after storage for 6 months. The shaded area represents the standard deviation (n=3).

6.3.5 Implications of Miscibility, Hydrogen Bonding and Mobility on Physical Stability

Out of the three different amorphous systems and seven total conditions under study, all three systems stored in the dry condition remained completely amorphous after 6 months. The storage temperatures corresponded to, on average, 18 °C, 22 °C, and 20 °C below their respective midpoint glass transition temperatures. Also, all three systems were miscible by MDSC and solid-state NMR ^{1}H relaxation time measurements. The IMC and NIF systems stored at 40 °C/57% RH also remained amorphous after 6 months as detected by PXRD and regular CPMAS NMR spectra. However, the NIF system stored at 40 °C/57% RH for 6 months did show a very small amount of crystallization as detected by a CPMAS spectrum with a ^{1}H $T_{1\rho}$ filter. These storage temperatures corresponded to 12 °C and 6 °C below the respective midpoint glass transition temperatures. The IMC and NIF systems stored at 40 °C/75% RH are the only two samples that showed significant crystallization at some points during storage. Their storage temperatures before substantial crystallization occurred corresponded to 1 °C below and 5 °C above the respective midpoint glass transition temperatures. The IMC system was first observed to crystallize after 1 month of storage, while the NIF system was first observed to crystallize after only 1 week of storage and it also exhibited higher degree of crystallinity.

From the above observations, a few conclusions can be drawn. First, miscible systems with limited mobility are relatively stable for long periods of time. This is demonstrated by all three systems stored in the dry conditions, despite their differences in

forming hydrogen bonds between the API and the polymer. A number of studies have demonstrated the correlation between the crystallization rates or onsets of amorphous pharmaceuticals and their molecular mobilities.[111, 132, 140] Kothari et al. showed a correlation between the crystallization rates of three model systems and their α-relaxation times measured by dielectric spectroscopy.[140] The present data also suggest good physical stability in amorphous systems with limited translational mobilities.

Second, molecular mobility gained by the absorption of water vapor negatively influences the physical stability of amorphous solid dispersions. The IMC and NIF systems that were stored close to or above their respective glass transition temperatures (40 °C/75% RH) crystallized within 1 month of storage. Sorbed water has shown to markedly increase the molecular mobility of amorphous excipients such as PVP.[77] Combined with the plasticizing effect, sorbed water increased the molecular mobilities of the samples stored at 40 °C/75% RH in the current study and resulted in crystallization of these samples.

Third, the physical stabilities of systems that are initially miscible but gain considerable mobility via water sorption during storage are influenced by the specific interactions between the API and the polymer. This is demonstrated by the IMC and NIF systems stored at 40 °C/75% RH, where a stronger hydrogen bonding interaction exists between IMC and PVP than that between NIF and PVP, and the NIF system crystallized at a much faster rate. Drug-polymer interaction has been found to enhance the inhibition of crystallization of amorphous drugs.[141, 142] Mistry et al. correlated the delay of crystallization onset temperature of ketoconazole solid dispersions with reduced molecular mobilities and stronger drug-polymer interactions.[142] In the present study, the

stronger interaction between IMC and PVP is also reflected in the differences in water vapor sorption behaviors of the two systems, where the IMC system adsorbed less water and showed higher glass transition temperatures compared to the NIF system. A stronger API-polymer interaction is expected to result in a reduced water vapor sorption for a hydrophobic API, due to a decrease in the availability of the percentage of the polymer that can uptake water. Physical mixtures have been shown to adsorb considerably higher amounts of water compared to their amorphous solid dispersions for this reason.[139]

6.4 Conclusions

In this study, miscible amorphous solid dispersions of 70-30 IMC-PVP, 70-30 NIF-PVP and 70-30 IMC methyl ester-PVP were studied under three different storage conditions by a combination of techniques. All three amorphous systems that were stored dry and about 20 °C below their respective glass transition temperatures remained miscible and completely amorphous after 6 months. The IMC system stored at 40 °C/57% RH remained miscible and did not crystallize after 6 months, but the system stored at 40 °C/75% RH crystallized after 1 month of storage. The NIF system stored at 40 °C/57% RH seemed to be borderline miscible for the entire storage period, and showed a very small amount of crystallinity after 6 months of storage. The crystallization was not detected by PXRD but was detected by a CPMAS NMR spectrum acquired with a ^{1}H $T_{1\rho}$ filter. The NIF system stored at 40 °C/75% RH crystallized after only 1 week. The study showed that both molecular mobility and hydrogen bonding interactions played a role in the physical stability of miscible amorphous solid dispersions. While storage below the

glass transition temperature is very important, strong hydrogen bonding interactions can delay the onset of crystallization.

Chapter 7. Conclusions and Future Directions

Amorphous solid dispersions have emerged as one of the leading enabling strategies to increase the oral bioavailability of poorly water-soluble compounds in pharmaceutical development. However, one reservation about the use of amorphous solid dispersions is their long-term physical stability. Crystallization of the amorphous API can occur during storage if not properly stabilized, resulting in lowering of bioavailability. For the amorphous API to be properly stabilized, it has to form a miscible, single phase amorphous system with a suitable excipient. Specific interactions between the API and the excipient will contribute to the miscibility of the two components and the overall physical stability of the system against phase separation and crystallization.

Phase homogeneity is a prerequisite in forming stable amorphous solid dispersions. Conventional methods such as DSC often fail to adequately determine the miscibility and phase homogeneity. In this research, a method that can detect miscibility on the nanometer scale using solid-state NMR ^{1}H relaxation times was tested on nifedipine and PVP amorphous systems (Chapter 3). This method successfully differentiated miscible, partially miscible and immiscible systems, where DSC was unable to determine any differences between them.

Specific interactions such as hydrogen bonding interactions of amorphous pharmaceuticals have been proposed as a way of stabilizing amorphous solid dispersions. Previous studies using IR spectroscopy have detected interactions between drugs and polymers, but not at a quantitative level. Quantitative understanding of molecular-level

interactions in amorphous solid dispersions is of great interest both intellectually and practically, because when such interactions exist between the API and the excipient, better miscibility between the two may result. In Chapter 4, a novel method was developed to identify and quantify various hydrogen bonding interactions in a model amorphous API indomethacin and its amorphous solid dispersions using ^{13}C solid-state NMR spectroscopy. The method employed single-site ^{13}C isotopic labeling, spectral subtraction and simultaneous spectral fitting. The study of amorphous indomethacin unraveled new information regarding the molecular interactions of this well-studied molecule, identifying the existence of carboxylic acid cyclic dimers, disordered carboxylic acid chains and carboxylic acid-amide complexes. The relative percentages of these species were determined to be 59%, 15% and 19%, respectively. The remaining 7% was ascribed to free indomethacin molecules not involving in any hydrogen bonds. Indomethacin monomer and dimer were found to be at equilibrium above 50 °C in a 1% (wt) dispersion with polystyrene. Thermodynamic parameters of indomethacin dimerization through the carboxylic acids were calculated. The study also quantitatively tracked the percentage of each species when different concentrations of polymer PVP or PVP/VA were present in the amorphous solid dispersions. At between 30% and 40% (wt) PVP, no carboxylic acid dimers and very few carboxylic acid chains could be detected. The result provides evidence of the predictive power of this approach, since cyclic dimers are present in both crystalline forms and the elimination of this species in the amorphous state would effectively inhibit nucleation and crystallization if molecular mobility is being limited.

Besides miscibility and specific interactions, molecular mobility adds another dimension important for physical stability of amorphous solid dispersions. Mobility plays a crucial role in nucleation and crystal growth from the amorphous state. For this reason, a supercooled liquid above T_g typically sees a much higher crystallization rate than a glass. In Chapter 5, molecular motions of amorphous indomethacin and indomethacin amorphous solid dispersions were studied via 2D exchange NMR experiments. Indomethacin carboxylic acid cyclic dimers were found to exchange with carboxylic acid-amide complexes or free carboxylic acids in these systems. Disordered carboxylic acid chains were not found to exchange with the other species. Despite an increase in molecular mobility above the glass transition temperature, the API and the polymer were found to undergo similar motional processes in a 1% (wt) indomethacin-polystyrene amorphous solid dispersion.

Using the analytical tools and knowledge developed from Chapters 3, 4 and 5, the physical stabilities of three miscible amorphous solid dispersions with different degrees of hydrogen bonding capabilities between the API and the polymer were tested at various storage conditions that reflect different molecular mobilities. All three amorphous systems, when stored in a condition that limited their molecular mobilities, remained completely amorphous after 6 months despite the varying hydrogen bonding capabilities among them. The two amorphous systems stored at 40 °C/75% RH, which allowed a higher degree of molecular motions within the system, both crystallized but at different times. The nifedipine-PVP system crystallized after only 1 week of storage, while the indomethacin-PVP system crystallized after 1 month of storage. Besides their different intrinsic crystallization tendencies, the ability to form stronger hydrogen bonds between

indomethacin and PVP is likely the reason for the delayed onset of crystallization observed.

Due to the complexity and the vast scope of amorphous pharmaceutical systems, many avenues of possible research were left unexplored in this dissertation. In particular, how do solid-state NMR relaxation times relate to the other techniques that can measure relaxation processes, such as dielectric spectroscopy or dynamic mechanical analysis? Granted that each of these techniques measures different relaxation processes, the ultimate goal is to infer a physical meaning from these relaxation parameters. In this dissertation, the solid-state NMR relaxation times being studied were ^{1}H T_1 and $T_{1\rho}$ relaxation times, which are suitable for detecting phase homogeneities but less useful in measuring molecular mobilities, due to the fast ^{1}H spin diffusion that averages out all motional processes. ^{13}C $T_{1\rho}$, on the other hand, is less affected by motional averages and is likely to provide more information on the local motions of an amorphous system. It would be very interesting to compare ^{13}C $T_{1\rho}$ relaxation times with other techniques, and use it to study the mobility of amorphous pharmaceutical systems in the glassy state, which is most relevant to the physical stability of practical concern because most amorphous formulations will be stored as glasses.

Another important question relating to amorphous pharmaceutical systems is how water affects the physicochemical properties of the system, including the API and the excipients. The ubiquitous nature of water makes it a very important factor to consider when dealing with amorphous systems. The preliminary studies included in the appendices showed that different types of API-water interactions were likely to exist in an amorphous solid dispersion. ^{1}H T_2 relaxation time is thought to be very sensitive to

water and has been used to elucidate the dynamics of water in food materials. It would be a very valuable tool if applied to pharmaceutical amorphous dispersion systems to help understand the interactions with water, and eventually the physical stability with water present.

Appendix A. Investigate the Effects of Water on Hydrogen Bonding Interactions of Indomethacin-Poly(Vinylpyrrolidone) Amorphous Solid Dispersions

A.1 Introduction

The ubiquitous nature of water makes it an important factor to consider in pharmaceutical development, especially in amorphous solid dosage forms. It is well known that water absorbed by amorphous solids can act as a plasticizer and lower the glass transition temperature of the system.[33] Consequently, sorbed water has been shown to increase the crystallization rates of neat amorphous drugs and amorphous drugs in solid dispersions with polymers.[34, 35, 134] Taylor and co-workers studied the drug-polymer interactions of several drug-polymer systems in the presence of moisture using IR spectroscopy and found that sorbed water disrupted the drug-polymer interactions in some systems but not others.[36] Thus it was hypothesized that crystallization of amorphous drugs in solid dispersions in the presence of moisture can occur from either a one-phase miscible system or a moisture-induced, phase-separated system.

Previously in Chapter 4, a method was developed to quantify various hydrogen bonding interactions between a model compound indomethacin and PVP using solid-state NMR spectroscopy. Thus, it is of interest of this chapter to quantitatively investigate the effect of sorbed water on the hydrogen bonding interactions between indomethacin and PVP in amorphous solid dispersions.

A.2 Materials and Methods

A.2.1 Materials

Indomethacin (minimum purity 99%) was purchased from Sigma-Aldrich (St Louis, MO). ^{13}C isotopically labeled indomethacin (99% ^{13}C at carboxyl carbon) was custom synthesized by Chemtos (Austin, TX). PVP (Kollidon® 25, M_w=28-34 kg/mole) was obtained from BASF (Edison, NJ). The polymers was vacuum dried at 70 °C overnight and stored over Drierite™ at all times. Potassium carbonate (K_2CO_3) was purchased from Alfa Aesar (Wardhill, MA). Sodium bromide (NaBr) and sodium chloride (NaCl) were purchased from EMD Chemicals (Gibbstown, NJ). The chemical structures of indomethacin and PVP are shown in Figure A.1.

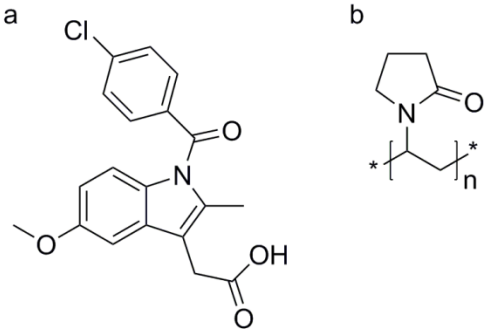

Figure A.1. Chemical structures of (a) indomethacin and (b) PVP.

A.2.2 Preparation of Amorphous Samples with Different Water Contents

Amorphous solid dispersions of indomethacin and PVP were prepared by cryomilling followed by melt quenching with liquid nitrogen. Samples of both natural abundance and ^{13}C isotopically enriched (3% wt) were prepared. 1 g of drug and polymer

in the weight ratio of 8:2 and 7:3, respectively, was cryomilled at 10 Hz (SPEX SamplePrep 6770 Freezer/Mill, SPEX SamplePrep LLC., Metuchen, NJ) for five cycles. Each cycle contained 2 minutes of milling and 2 minutes of cool down. Liquid nitrogen was used as coolant. The cryomilling procedure was used to ensure the optimum mixing between drug and polymer prior to melting. The amorphous solid dispersions were prepared by melting the aforementioned cryomilled mixtures of indomethacin and PVP in an oil bath at 170 °C for approximately five minutes until melt. The sample was stirred during heating with a spatula to ensure mixing. The sample was then quench cooled using liquid nitrogen. The solidified glass was ground with mortar and pestle. It was then sieved and particles with a size range of 45-300 μm were retained.

The prepared amorphous samples were stored over various saturated salt solutions to achieve various water contents. Saturated salt solutions of potassium carbonate (43% RH), sodium bromide (60% RH) and sodium chloride (75% RH) were used to control the relative humidity. The amorphous solid dispersion sample was stored over the saturated salt solutions for a period of 5-16 days at 4 °C. The water content was determined using TGA (Q50, TA Instruments, New Castle, DE). Solid-state NMR experiments of these samples were conducted at -20 °C.

A.2.3 Solid-State NMR Experiments

All solid-state NMR spectra were acquired using a Tecmag Redstone HF3 2RX spectrometer (Tecmag, Inc., Houston, TX), operating at 75.48 MHz for ^{13}C. Experiments were performed using a 7.5 mm double-resonance MAS probe (Varian, Palo Alto, CA). All ^{13}C spectra were acquired under magic angle spinning (MAS)[43] at 4 kHz, using

ramped-amplitude CP,[45] total sideband suppression (TOSS)[44] and SPINAL64 decoupling[73] with a ^{1}H decoupling field of about 62 kHz. A 2 ms contact time was used in all experiments. 3-Methylglutaric acid was used to optimize spectrometer settings and was used as an external standard, with the methyl peak referenced to 18.84 ppm.[74] A pulse delay of 5 s was used. All experiments were conducted at -20 °C. The data were zero-filled to 4096 points with no line-broadening.

Spectral subtraction was performed between the labeled and natural abundant samples as detailed in Chapter 4. After the subtraction, spectra of each dispersion system (80-20 IMC-PVP and 70-30 IMC-PVP) in the region of 160-190 ppm were fitted simultaneously by appropriate number of Gaussian functions, each representing a carboxylic acid species using MATLAB (MathWorks, Natick, MA). The details of the fitting procedure are explained in the results section.

A.3 Results and Discussion

In Chapter 4, the 80-20 IMC-PVP amorphous solid dispersion were fitted with four peaks, namely the dimer, chain, the carboxylic acid-amide complex and the free carboxylic acid. Besides those species, the 80-20 IMC-PVP amorphous solid dispersion with sorbed water should in theory has at least one more peak representing the carboxylic acid-water interaction. Since the free carboxylic acid only accounted for a very small percentage, it was neglected in the analysis. Thus, the spectra were fitted by four peaks, each representing the dimer, chain, the carboxylic acid-amide complex and the carboxylic acid-water complex. The chemical shifts and linewidths of the dimer, chain and the carboxylic acid-amide complex were fixed to the values obtained in Chapter 4. A new

peak was allowed to be determined from the simultaneous fitting to represent the carboxylic acid-water interactions. This peak was fitted with a chemical shift of 173.8 ± 0.04 ppm and a linewidth of 211 ± 5 Hz. The fitted spectra are shown in Figure A.2.

Since the 70-30 IMC-PVP amorphous solid dispersion was determined to be consisted mostly of carboxylic acid chains and the carboxylic acid-amide complexes (Chapter 4), the 70-30 IMC-PVP amorphous solid dispersions with sorbed water were fitted with these two species and a new species representing the carboxylic acid-water interaction. However, three peaks were not adequate to described all of features of the spectra. As a result, two peaks had to be used to adequately fit the spectra. The chemical shifts and the linewidths of the carboxylic acid chain and the carboxylic acid-amide complex were fixed to the values obtained in Chapter 4. The chemical shifts and the linewidths of the two new fitted peaks are 173.1 ± 0.09 ppm and 208 ± 7 Hz, and 174.3 ± 0.09 ppm and 443 ± 4 Hz, respectively. The peak at 173.1 ppm is ascribed to the carboxylic acid hydrogen bonded to both an amide and a water molecule, while the peak at 174.3 is ascribed to the carboxylic acid hydrogen bonded to water. The former type of interaction is named Type I interaction and the latter Type II interaction. Some of the possible arrangements for these two types of carboxylic acid-water interactions are illustrated in Figure A.4.

Figure A.5 shows the percentages of the indomethacin hydrogen bonding species in 80-20 and 70-30 IMC-PVP amorphous solid dispersions as a function of water content. The general trend observed is that the carboxylic acid-amide complex decreases as the water content increases. The dimer and chain are not influenced as much as the carboxylic acid-amide complex. At the same time the carboxylic acid-water interaction

increases. For the 70-30 IMC-PVP amorphous solid dispersions, the Type I carboxylic acid-water interaction seems to reach a plateau at approximately 1.6 (wt) % of water, while the Type II carboxylic acid-water interaction continues to increase as water content increases.

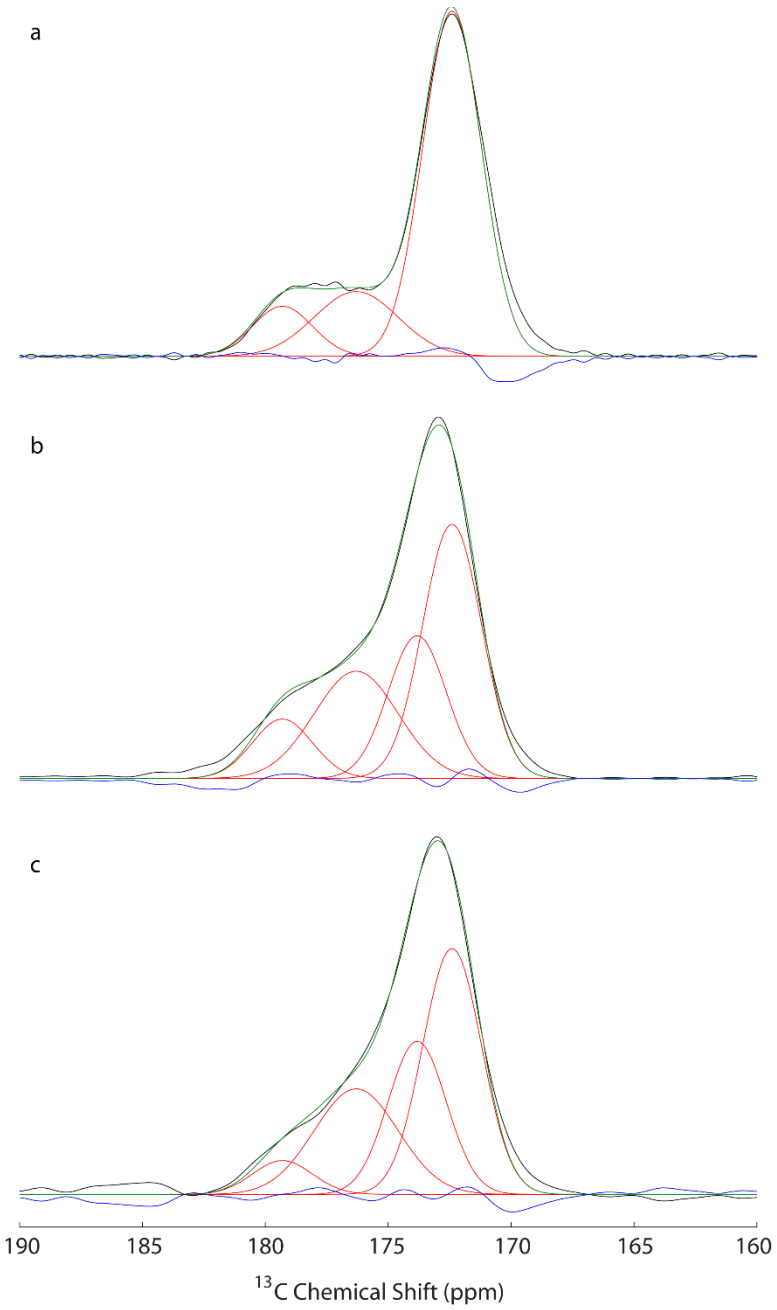

Figure A.2. CPMASS ^{13}C spectrum of IMC carboxylic acid carbon in a 80-20 IMC-PVP amorphous solid dispersion with (a) 0.2 % water, (b) 1.2 % water and (c) 1.6% water (wt %). The experimental spectrum is shown in black; the fitted peaks representing each species are shown in red; the sum of the fit is shown in green; the residual difference between the experimental and fitted peaks is shown in blue.

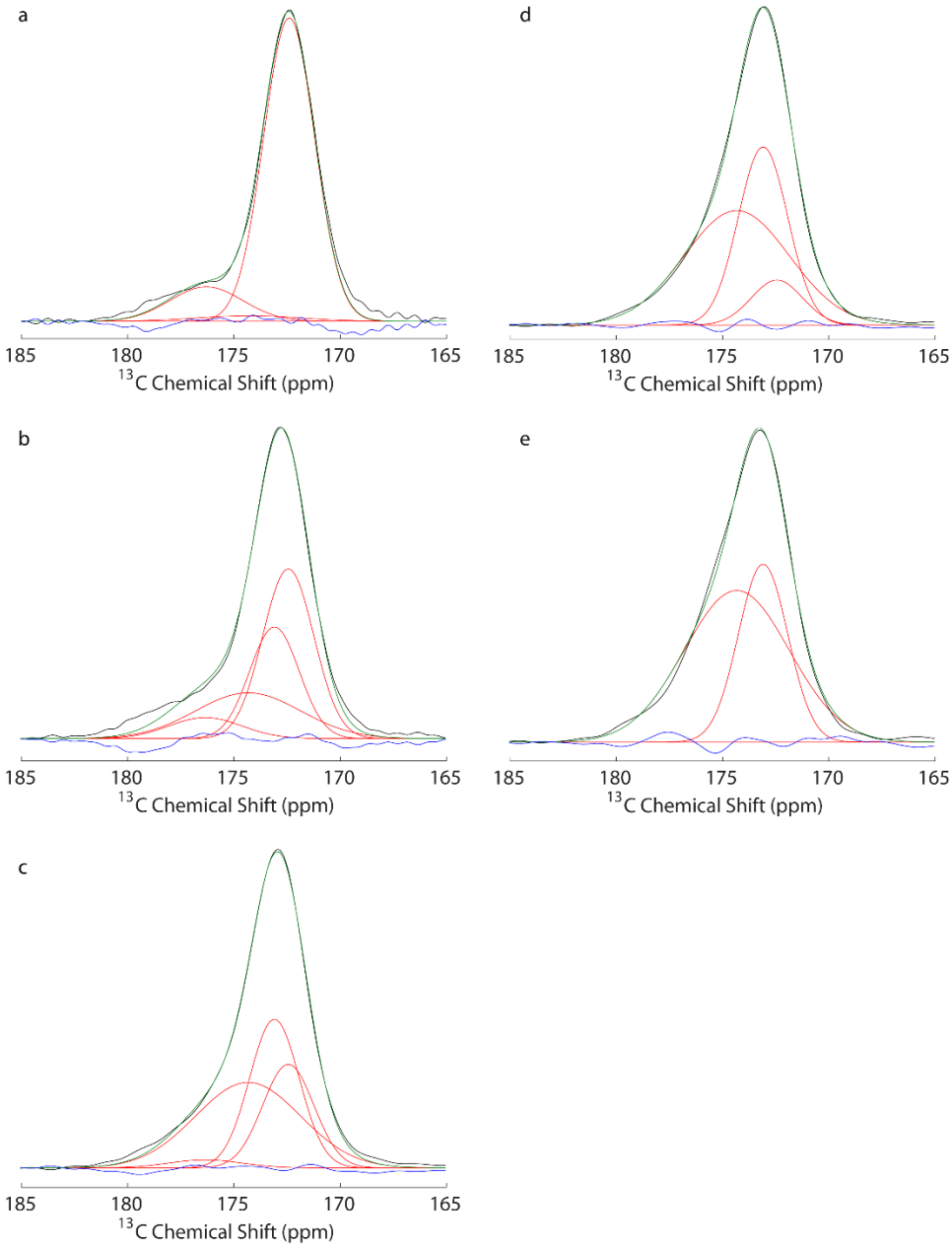

Figure A.3. CPMASS ^{13}C spectrum of IMC carboxylic acid carbon in a 70-30 IMC-PVP amorphous solid dispersion with (a) ~0% water, (b) 0.7% water, (c) 1.7% water, (d) 2.5% water and (e) 3.6% water (wt %). The experimental spectrum is shown in black; the fitted peaks representing each species are shown in red; the sum of the fit is shown in green; the residual difference between the experimental and fitted peaks is shown in blue.

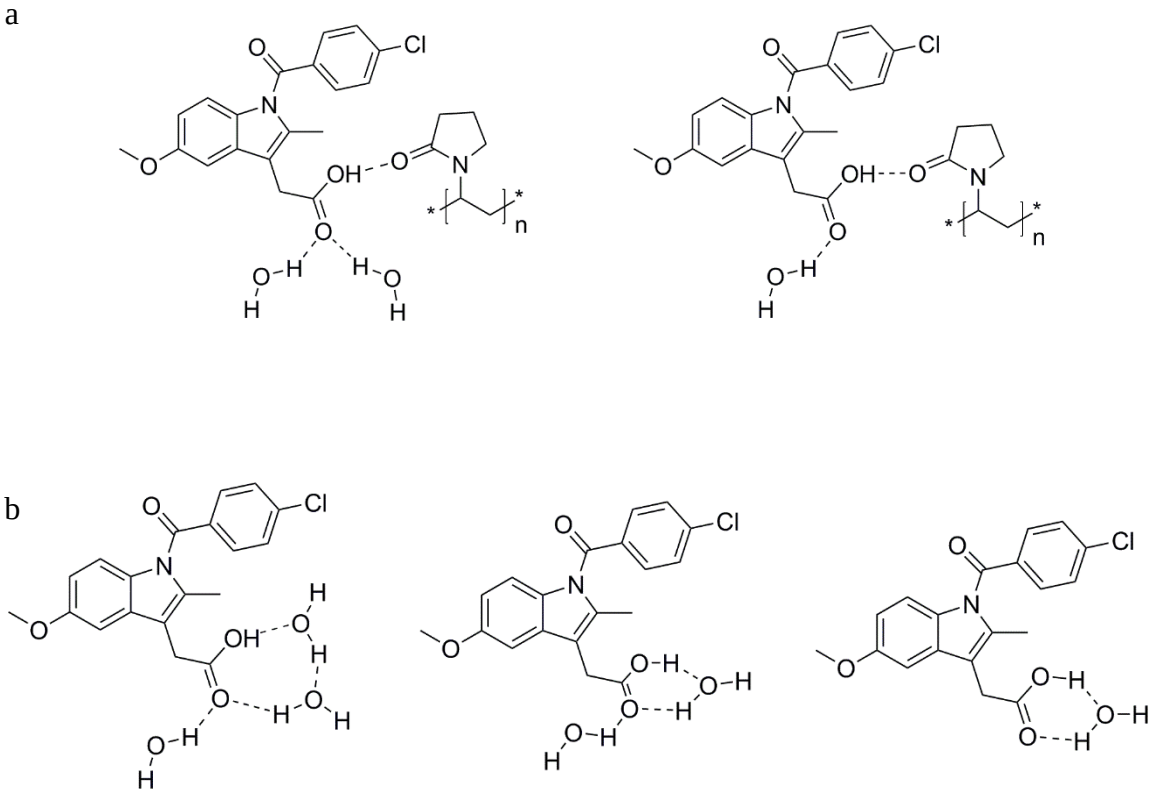

Figure A.4. Illustrations of (a) carboxylic acid-amide-water (Type I) and (b) carboxylic acid-water (Type II) interactions.

a

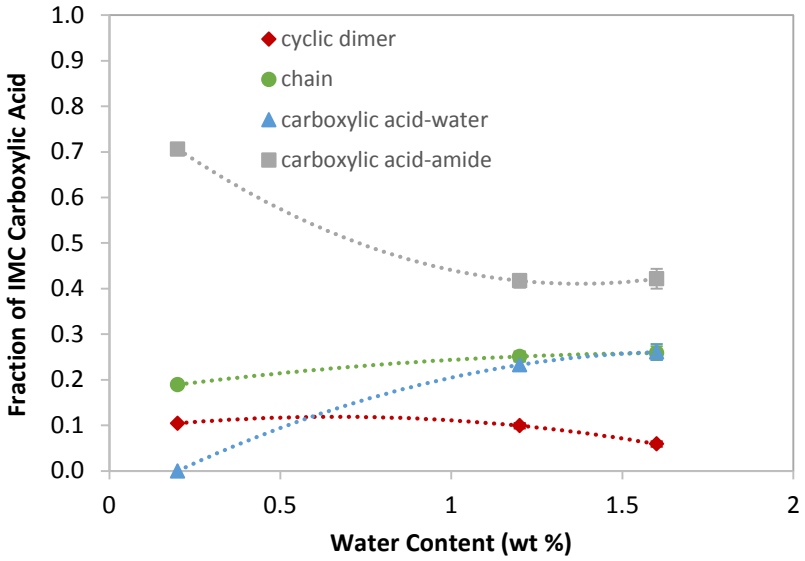

b

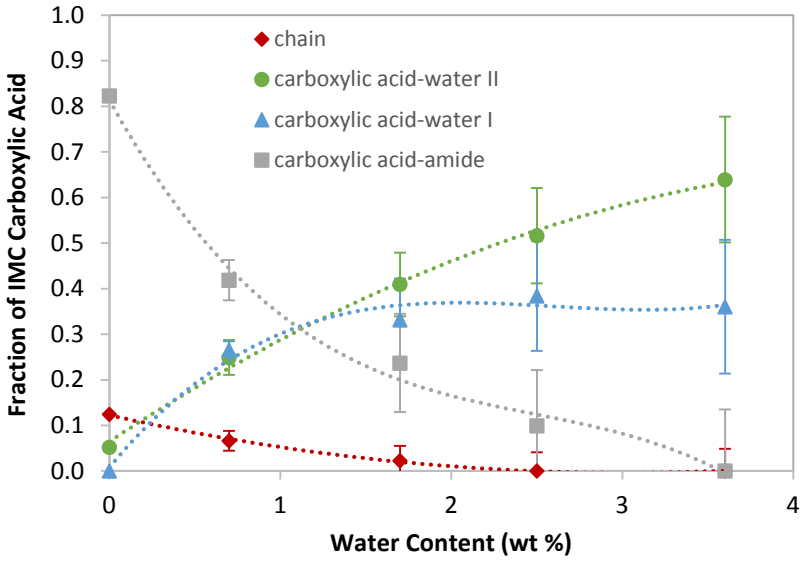

Figure A.5. Fraction of IMC carboxylic acid participating in various hydrogen-bonding interactions in the (a) 80-20 IMC-PVP and (b) 70-30 IMC-PVP amorphous solid dispersion as a function of water content. The error bars indicate the 95% confidence intervals. Curves are drawn as a guide to the eye.

A.4 Conclusions

Indomethacin was found to interact with sorbed water in the amorphous solid dispersions with PVP. The carboxylic acid-amide complex was found to be displaced by the carboxylic acid-water complex as the water content increased in the 80-20 IMC-PVP amorphous solid dispersions. In the 70-30 IMC-PVP amorphous solid dispersions, two possible types of carboxylic acid-water interactions were identified. One type involved indomethacin interacting with both an amide and the water molecule(s). The other type only involved the indomethacin and water. Similar to the 80-20 IMC-PVP system, it was found that the carboxylic acid-amide complex was gradually displaced by the two types of carboxylic acid-water interactions as the water content increased in the 70-30 IMC-PVP system.

References

1. Byrn, S. R.; Pfeiffer, R. R.; Stowell, J. G., *Solid-State Chemistry of Drugs*. 2 ed.; SSCI, Inc.: West Lafayette, IN, 1999.

2. McCrone, W. C., Polymorphism. In *Physics and Chemistry of the Organic Solid State*, Fox, D.; Labes, M. M.; Weissberger, A., Eds. Interscience Publishers: New York, 1965; Vol. 2, pp 725-767.

3. Chemburkar, S. R.; Bauer, J.; Deming, K.; Spiwek, H.; Patel, K.; Morris, J.; Henry, R.; Spanton, S.; Dziki, W.; Porter, W.; Quick, J.; Bauer, P.; Donaubauer, J.; Narayanan, B. A.; Soldani, M.; Riley, D.; McFarland, K. Dealing with the impact of ritonavir polymorphs on the late stages of bulk drug process development. *Org. Process Res. Dev.* 2000, *4*, (5), 413-417.

4. Stahly, G. P. Diversity in single- and multiple-component crystals. The search for and prevalence of polymorphs and cocrystals. *Cryst. Growth Des.* 2007, *7*, (6), 1007-1026.

5. Burger, A.; Ramberger, R. On the polymorphism of pharmaceuticals and other molecular crystals. I. *Mikrochim Acta* 1979, *72*, (3-4), 259-271.

6. Cheng, Y.-T.; Johnson, W. L. Disordered materials: a survey of amorphous solids. *Science* 1987, *235*, (4792), 997-1002.

7. Kawabata, Y.; Wada, K.; Nakatani, M.; Yamada, S.; Onoue, S. Formulation design for poorly water-soluble drugs based on biopharmaceutics classification system: Basic approaches and practical applications. *Int. J. Pharm.* 2011, *420*, (1), 1-10.

8. Hancock, B. C.; Zografi, G. Characteristics and significance of the amorphous state in pharmaceutical systems. *J. Pharm. Sci.* 1997, *86*, (1), 1-12.

9. Mullin, J. W., *Crystallization*. Butterworth-Heinemann: Oxford, 2001.

10. Gutzow, I.; Avramov, I.; Kästner, K. Glass formation and crystallization. *J. Non-Cryst. Solids* 1990, *123*, (1–3), 97-113.

11. Descamps, M.; Dudognon, E. Crystallization from the amorphous state: nucleation–growth decoupling, polymorphism interplay, and the role of interfaces. *J. Pharm. Sci.* 2014, *103*, (9), 2615-2628.

12. Ragone, D. V., *Thermodynamics of Materials*. John Wiley & Sons: 1994.

13. Turnbull, D.; Cohen, M. H., Crystallization kinetics and glass formation. In *Modern Aspects of the Vitreous State*, Mackenzie, J. D., Ed. Butterworths: London, 1960; Vol. 1, pp 38-62.

14. Greet, R. J.; Turnbull, D. Glass transition in o-terphenyl. *J. Chem. Phys.* 1967, *46*, (4), 1243-1251.

15. Hikima, T.; Adachi, Y.; Hanaya, M.; Oguni, M. Determination of potentially homogeneous-nucleation-based crystallization in O-terphenyl and an interpretation of the nucleation-enhancement mechanism. *Phys. Rev. B* 1995, *52*, (6), 3900-3908.

16. Hatase, M.; Hanaya, M.; Oguni, M. Studies of homogeneous-nucleation-based crystal growth: Significant role of phenyl ring in the structure formation. *J. Non-Cryst. Solids* 2004, *333*, (2), 129-136.

17. Sun, Y.; Xi, H.; Ediger, M. D.; Yu, L. Diffusionless Crystal Growth from Glass Has Precursor in Equilibrium Liquid. *J. Phys. Chem. B* 2007, *112*, (3), 661-664.

18. Sun, Y.; Xi, H.; Chen, S.; Ediger, M. D.; Yu, L. Crystallization near glass transition: Transition from diffusion-controlled to diffusionless crystal growth studied with seven polymorphs. *J. Phys. Chem. B* 2008, *112*, (18), 5594-5601.

19. Sun, Y.; Xi, H.; Ediger, M. D.; Richert, R.; Yu, L. Diffusion-controlled and ``diffusionless'' crystal growth near the glass transition temperature: Relation between liquid dynamics and growth kinetics of seven ROY polymorphs. *J. Chem. Phys.* 2009, *131*, (7), 074506-9.

20. Hasebe, M.; Musumeci, D.; Powell, C. T.; Cai, T.; Gunn, E.; Zhu, L.; Yu, L. Fast surface crystal growth on molecular glasses and its termination by the onset of fluidity. *J. Phys. Chem. B* 2014, *118*, (27), 7638-7646.

21. Sun, Y.; Zhu, L.; Wu, T.; Cai, T.; Gunn, E.; Yu, L. Stability of Amorphous Pharmaceutical Solids: Crystal Growth Mechanisms and Effect of Polymer Additives. *The AAPS Journal* 2012, *14*, (3), 380-388.

22. Wu, T.; Yu, L. Surface crystallization of indomethacin below T_g. *Pharm. Res.* 2006, *23*, (10), 2350-2355.

23. Zhu, L.; Wong, L.; Yu, L. Surface-enhanced crystallization of amorphous nifedipine. *Mol. Pharmaceutics* 2008, *5*, (6), 921-926.

24. Sun, Y.; Zhu, L.; Kearns, K. L.; Ediger, M. D.; Yu, L. Glasses crystallize rapidly at free surfaces by growing crystals upward. *Proc. Natl. Acad. Sci. U.S.A.* 2011, *108*, (15), 5990-5995.

25. Zhu, L.; Brian, C. W.; Swallen, S. F.; Straus, P. T.; Ediger, M. D.; Yu, L. Surface self-diffusion of an organic glass. *Phys. Rev. Lett.* 2011, *106*, (25), 256103.

26. Zhou, D.; Zhang, G. G. Z.; Law, D.; Grant, D. J. W.; Schmitt, E. A. Physical stability of amorphous pharmaceuticals: Importance of configurational thermodynamic quantities and molecular mobility. *J. Pharm. Sci.* 2002, *91*, (8), 1863-1872.

27. Gordon, M.; Taylor, J. S. Ideal copolymers and the second-order transitions of synthetic rubbers. I. Non-crystalline copolymers. *J. Appl. Chem.* 1952, *2*, (9), 493-500.

28. Newman, A.; Engers, D.; Bates, S.; Ivanisevic, I.; Kelly, R. C.; Zografi, G. Characterization of amorphous API:Polymer mixtures using X-ray powder diffraction. *J. Pharm. Sci.* 2008, *97*, (11), 4840-4856.

29. Qian, F.; Huang, J.; Zhu, Q.; Haddadin, R.; Gawel, J.; Garmise, R.; Hussain, M. Is a distinctive single T_g a reliable indicator for the homogeneity of amorphous solid dispersion? *Int. J. Pharm.* 2010, *395*, (1–2), 232-235.

30. Yoshioka, M.; Hancock, B. C.; Zografi, G. Inhibition of indomethacin crystallization in poly(vinylpyrrolidone) coprecipitates. *J. Pharm. Sci.* 1995, *84*, (8), 983-986.

31. Matsumoto, T.; Zografi, G. Physical properties of solid molecular dispersions of indomethacin with poly(vinylpyrrolidone) and poly(vinylpyrrolidone-co-vinyl-acetate) in relation to indomethacin crystallization. *Pharm. Res.* 1999, *16*, (11), 1722-1728.

32. Khougaz, K.; Clas, S.-D. Crystallization inhibition in solid dispersions of MK-0591 and poly(vinylpyrrolidone) polymers. *J. Pharm. Sci.* 2000, *89*, (10), 1325-1334.

33. Levine, H.; Slade, L., Water as a plasticizer: Physico-chemical aspects of low-moisture polymer systems. In *Water Science Reviews 3: Water Dynamics*, Franks, F., Ed. Cambridge University Press: Cambridge, UK, 1988; pp 79-185.

34. Andronis, V.; Yoshioka, M.; Zografi, G. Effects of sorbed water on the crystallization of indomethacin from the amorphous state. *J. Pharm. Sci.* 1997, *86*, (3), 346-351.

35. Marsac, P.; Konno, H.; Rumondor, A. F.; Taylor, L. Recrystallization of nifedipine and felodipine from amorphous molecular level solid dispersions containing poly(vinylpyrrolidone) and sorbed water. *Pharm. Res.* 2008, *25*, (3), 647-656.

36. Rumondor, A. C. F.; Marsac, P. J.; Stanford, L. A.; Taylor, L. S. Phase behavior of poly(vinylpyrrolidone) containing amorphous solid dispersions in the presence of moisture. *Mol. Pharmaceutics* 2009, *6*, 1492-1505.

37. Purcell, E.; Torrey, H.; Pound, R. Resonance absorption by nuclear magnetic moments in a solid. *Phys. Rev.* 1946, *69*, (1-2), 37-38.

38. Bloch, F.; Hansen, W.; Packard, M. Nuclear induction. *Phys. Rev.* 1946, *69*, (3-4), 127-127.

39. Fyfe, C. A., *Solid State NMR for Chemists*. 1 ed.; C. F. C. Press: Guelph, Ontario, Canada, 1983.

40. Apperley, D. C.; Harris, R. K.; Hodgkinson, P., *Solid-state NMR: Basic Principles & Practices*. Momentum Press, LLC: New York, 2012.

41. Geppi, M.; Mollica, G.; Borsacchi, S.; Veracini, C. A. Solid-state NMR studies of pharmaceutical systems. *Appl. Spectrosc. Rev.* 2008, *43*, (3), 202-302.

42. Harris, R. K., *Nuclear Magnetic Resonance Spectroscopy: A Physicochemical View*. John Wiley & Sons, Inc.: New York, 1986.

43. Andrew, E. R.; Bradbury, A.; Eades, R. G. Removal of dipolar broadening of nuclear magnetic resonance spectra of solids by specimen rotation. *Nature* 1959, *183*, (4678), 1802-1803.

44. Dixon, W. T.; Schaefer, J.; Sefcik, M. D.; Stejskal, E. O.; McKay, R. A. Total suppression of sidebands in CPMAS C-13 NMR. *J. Magn. Reson.* 1982, *49*, (2), 341-345.

45. Pines, A.; Gibby, M. G.; Waugh, J. S. Proton-enhanced NMR of dilute spins in solids. *J. Chem. Phys.* 1973, *59*, (2), 569-590.

46. Bovey, F. A.; Mirau, P. A., *NMR of Polymers*. 1 ed.; Academic Press: San Diego, CA, 1996.

47. Yuan, X.; Sperger, D.; Munson, E. J. Investigating miscibility and molecular mobility of nifedipine-PVP amorphous solid dispersions using solid-state NMR spectroscopy. *Mol. Pharmaceutics* 2014, *11*, (1), 329-337.

48. Kaplan, D. S. Structure–property relationships in copolymers to composites: Molecular interpretation of the glass transition phenomenon. *J. Appl. Polym. Sci.* 1976, *20*, (10), 2615-2629.

49. Ando, I.; Asakura, T., *Solid Sate NMR of Polymers*. 1 ed.; Elsevier Science: Amsterdam, 1998.

50. Krause, S.; Iskandar, M. Phase separation in styrene-α-methyl styrene block copolymers. *Polym. Sci. Technol.* 1977, *10*, 231-43.

51. Lubach, J. W.; Xu, D.; Segmuller, B. E.; Munson, E. J. Investigation of the effects of pharmaceutical processing upon solid-state NMR relaxation times and implications to solid-state formulation stability. *J. Pharm. Sci.* 2007, *96*, (4), 777-787.

52. Duer, M. J., *Solid-State NMR Spectroscopy: Principles and Applications*. Blackwell Science: Walden, MA, 2002.

53. Gao, P. Determination of the composition of delavirdine mesylate polymorph and pseudopolymorph mixtures using ^{13}C CP/MAS NMR. *Pharm. Res.* 1996, *13*, (7), 1095-1104.

54. Offerdahl, T. J.; Salsbury, J. S.; Dong, Z.; Grant, D. J. W.; Schroeder, S. A.; Prakash, I.; Gorman, E. M.; Barich, D. H.; Munson, E. J. Quantitation of crystalline and amorphous forms of anhydrous neotame using ^{13}C CPMAS NMR spectroscopy. *J. Pharm. Sci.* 2005, *94*, (12), 2591-2605.

55. Chiou, W. L.; Riegelman, S. Pharmaceutical applications of solid dispersion systems. *J. Pharm. Sci.* 1971, *60*, (9), 1281-1302.

56. Miyazaki, T.; Yoshioka, S.; Aso, Y.; Kojima, S. Ability of polyvinylpyrrolidone and polyacrylic acid to inhibit the crystallization of amorphous acetaminophen. *J. Pharm. Sci.* 2004, *93*, 2710-2717.

57. Van den Mooter, G.; Wuyts, M.; Blaton, N.; Busson, R.; Grobet, P.; Augustijns, P.; Kinget, R. Physical stabilization of amorphous ketoconazole in solid dispersions with polyvinylpyrrolidone K25. *Eur. J. Pharm. Sci.* 2001, *12*, 261-269.

58. Bhugra, C.; Pikal, M. J. Role of thermodynamic, molecular, and kinetic factors in crystallization from the amorphous state. *J. Pharm. Sci.* 2008, *97*, (4), 1329-1349.

59. Marsac, P. J.; Shamblin, S. L.; Taylor, L. S. Theoretical and practical approaches for prediction of drug-polymer miscibility and solubility. *Pharm. Res.* 2006, *23*, 2417-2426.

60. Rumondor, A.; Ivanisevic, I.; Bates, S.; Alonzo, D.; Taylor, L. Evaluation of drug-polymer miscibility in amorphous solid dispersion systems. *Pharm. Res.* 2009, *26*, (11), 2523-2534.

61. Rumondor, A. F.; Stanford, L.; Taylor, L. Effects of polymer type and storage relative humidity on the kinetics of felodipine crystallization from amorphous solid dispersions. *Pharm. Res.* 2009, *26*, (12), 2599-2606.

62. Ivanisevic, I. Physical stability studies of miscible amorphous solid dispersions. *J. Pharm. Sci.* 2010, *99*, (9), 4005-4012.

63. Lodge, T. P.; Wood, E. R.; Haley, J. C. Two calorimetric glass transitions do not necessarily indicate immiscibility: The case of PEO/PMMA. *J. Polym. Sci. Pol. Phys* 2006, *44*, (4), 756-763.

64. Dickinson, L. C.; Yang, H.; Chu, C. W.; Stein, R. S.; Chien, J. C. W. Limits to compatibility in poly(x-methylstyrene)/poly(2,6-dimethylphenylene oxide) blends by NMR. *Macromolecules* 1987, *20*, (8), 1757-1760.

65. McBrierty, V. J.; Douglass, D. C.; Kwei, T. K. Compatibility in blends of poly(methyl methacrylate) and poly(styrene-co-acrylonitrile). 2. An NMR study. *Macromolecules* 1978, *11*, (6), 1265-1267.

66. Aso, Y.; Yoshioka, S.; Miyazaki, T.; Kawanishi, T.; Tanaka, K.; Kitamura, S.; Takakura, A.; Hayashi, T.; Muranushi, N. Miscibility of nifedipine and hydrophilic polymers as measured by ^{1}H-NMR spin–lattice relaxation. *Chem. Pharm. Bull.* 2007, *55*, (8), 1227-1231.

67. Pham, T. N.; Watson, S. A.; Edwards, A. J.; Chavda, M.; Clawson, J. S.; Strohmeier, M.; Vogt, F. G. Analysis of amorphous solid dispersions using 2D solid-

state NMR and ^{1}H T_1 relaxation measurements. *Mol. Pharmaceutics* 2010, *7*, (5), 1667-1691.

68. Litvinov, V. M.; Guns, S.; Adriaensens, P.; Scholtens, B. J. R.; Quaedflieg, M. P.; Carleer, R.; Van den Mooter, G. Solid state solubility of miconazole in poly[(ethylene glycol)-g-vinyl alcohol] using hot-melt extrusion. *Mol. Pharmaceutics* 2012, *9*, (10), 2924-2932.

69. Aso, Y.; Yoshioka, S.; Otsuka, T.; Kojima, S. The physical stability of amorphous nifedipine determined by isothermal microcalorimetry. *Chem. Pharm. Bull.* 1995, *43*, 300-3.

70. Ishida, H.; Wu, T.; Yu, L. Sudden rise of crystal growth rate of nifedipine near T_g without and with polyvinylpyrrolidone. *J. Pharm. Sci.* 2007, *96*, (5), 1131-1138.

71. Aso, Y.; Yoshioka, S. Molecular mobility of nifedipine–PVP and phenobarbital–PVP solid dispersions as measured by ^{13}C-NMR spin-lattice relaxation time. *J. Pharm. Sci.* 2006, *95*, (2), 318-325.

72. Marsac, P. J.; Konno, H.; Taylor, L. S. A comparison of the physical stability of amorphous felodipine and nifedipine systems. *Pharm. Res.* 2006, *23*, 2306-2316.

73. Fung, B. M.; Khitrin, A. K.; Ermolaev, K. An improved broadband decoupling sequence for liquid crystals and solids. *J. Magn. Reson.* 2000, *142*, (1), 97-101.

74. Barich, D. H.; Gorman, E. M.; Zell, M. T.; Munson, E. J. 3-Methylglutaric acid as a ^{13}C solid-state NMR standard. *Solid State Nucl. Mag.* 2006, *30*, (3–4), 125-129.

75. Apperley, D. C.; Forster, A. H.; Fournier, R.; Harris, R. K.; Hodgkinson, P.; Lancaster, R. W.; Rades, T. Characterisation of indomethacin and nifedipine using variable-temperature solid-state NMR. *Magn. Reson. Chem.* 2005, *43*, (11), 881-892.

76. Gunn, E.; Guzei, I. A.; Cai, T.; Yu, L. Polymorphism of nifedipine: crystal structure and reversible transition of the metastable β polymorph. *Cryst. Growth Des.* 2012, *12*, (4), 2037-2043.

77. Oksanen, C. A.; Zografi, G. Molecular mobility in mixtures of absorbed water and solid poly(vinylpyrrolidone). *Pharm. Res.* 1993, *10*, (6), 791-799.

78. Sperger, D. M.; Fu, S.; Block, L. H.; Munson, E. J. Analysis of composition, molecular weight, and water content variations in sodium alginate using solid-state NMR spectroscopy. *J. Pharm. Sci.* 2011, *100*, (8), 3441-3452.

79. Grooff, D.; De Villiers, M. M.; Liebenberg, W. Thermal methods for evaluating polymorphic transitions in nifedipine. *Thermochim. Acta* 2007, *454*, (1), 33-42.

80. Yani, Y.; Chow, P. S.; Tan, R. B. H. Molecular simulation study of the effect of various additives on salbutamol sulfate crystal habit. *Mol. Pharmaceutics* 2011, *8*, (5), 1910-1918.

81. Gao, Y.; Olsen, K. W. Molecular dynamics of drug crystal dissolution: dimulation of acetaminophen Form I in water. *Mol. Pharmaceutics* 2013, *10*, (3), 905-917.

82. Taylor, L. S.; Zografi, G. Spectroscopic characterization of interactions between PVP and indomethacin in amorphous molecular dispersions. *Pharm. Res.* 1997, *14*, 1691-1698.

83. Rumondor, A. C. F.; Marsac, P. J.; Stanford, L. A.; Taylor, L. S. Phase behavior of poly(vinylpyrrolidone) containing amorphous solid dispersions in the presence of moisture. *Mol. Pharmaceutics* 2009, *6*, (5), 1492-1505.

84. Miyoshi, T.; Takegoshi, K.; Hikichi, K. High-resolution solid-state 13C nuclear magnetic resonance study of a polymer complex: poly(methacrylic acid)/poly(ethylene oxide). *Polymer* 1996, *37*, (1), 11-18.

85. Miyoshi, T.; Takegoshi, K.; Hikichi, K. High-resolution solid state 13C n.m.r. study of the interpolymer interaction, morphology and chain dynamics of the poly(acrylic acid)/poly(ethylene oxide) complex. *Polymer* 1997, *38*, (10), 2315-2320.

86. Miyoshi, T.; Takegoshi, K.; Terao, T. Dynamic alternation between inter- and intra-polymer hydrogen bonds in a polymer complex as studied by solid-state ^{13}C 2D exchange NMR. *Macromolecules* 1999, *32*, (26), 8914-8917.

87. Xiang, T.-X.; Anderson, B. D. Molecular dynamics simulation of amorphous indomethacin. *Mol. Pharmaceutics* 2012, *10*, (1), 102-114.

88. Xiang, T.-X.; Anderson, B. D. Molecular dynamics simulation of amorphous indomethacin–poly(vinylpyrrolidone) glasses: Solubility and hydrogen bonding interactions. *J. Pharm. Sci.* 2013, *102*, (3), 876-891.

89. Kaneniwa, N.; Otsuka, M.; Hayashi, T. Physicochemical characterization of indomethacin polymorphs and the transformation kinetics in ethanol. *Chem. Pharm. Bull.* 1985, *33*, (8), 3447-3455.

90. Bielecki, A.; Burum, D. P. Temperature dependence of ^{207}Pb MAS spectra of solid lead nitrate. An accurate, sensitive thermometer for variable-temperature MAS. *J. Magn. Reson. Ser. A* 1995, *116*, (2), 215-220.

91. Herzfeld, J.; Berger, A. E. Sideband intensities in NMR spectra of samples spinning at the magic angle. *J. Chem. Phys.* 1980, *73*, (12), 6021-6030.

92. Eichele, K. *HBA 1. 7. 3*, Universität Tübingen: 2012.

93. Kistenmacher, T. J.; Marsh, R. E. Crystal and molecular structure of an antiinflammatory agent, indomethacin, 1-(p-chlorobenzoyl)-5-methoxy-2-methylindole-3-acetic acid. *J. Am. Chem. Soc.* 1972, *94*, (4), 1340-1345.

94. Chen, X.; Morris, K. R.; Griesser, U. J.; Byrn, S. R.; Stowell, J. G. Reactivity differences of indomethacin solid forms with ammonia gas. *J. Am. Chem. Soc.* 2002, *124*, (50), 15012-15019.

95. Masuda, K.; Tabata, S.; Kono, H.; Sakata, Y.; Hayase, T.; Yonemochi, E.; Terada, K. Solid-state ^{13}C NMR study of indomethacin polymorphism. *Int. J. Pharm.* 2006, *318*, (1–2), 146-153.

96. Sperger, D. M. Solid-State NMR Analysis of Excipients and Drug-Excipient Interactions in the Amorphous State. Ph.D., University of Kansas, Lawrence, KS, 2010.

97. Zell, M. T.; Padden, B. E.; Paterick, A. J.; Hillmyer, M. A.; Kean, R. T.; Thakur, K. A. M.; Munson, E. J. Direct observation of stereodefect sites in semicrystalline poly(lactide) using ^{13}C solid-state NMR. *J. Am. Chem. Soc.* 1998, *120*, (48), 12672-12673.

98. Fortier-McGill, B.; Toader, V.; Reven, L. ^{1}H solid state NMR study of poly(methacrylic acid) hydrogen-bonded complexes. *Macromolecules* 2012, *45*, (15), 6015-6026.

99. Fortier-McGill, B.; Toader, V.; Reven, L. ^{13}C MAS NMR study of poly(methacrylic acid)–polyether complexes and multilayers. *Macromolecules* 2014, *47*, (13), 4298-4307.

100. Crowley, K. J.; Zografi, G. Cryogenic grinding of indomethacin polymorphs and solvates: Assessment of amorphous phase formation and amorphous phase physical stability. *J. Pharm. Sci.* 2002, *91*, (2), 492-507.

101. Ando, S.; Ando, I.; Shoji, A.; Ozaki, T. Intermolecular hydrogen-bonding effect on ^{13}C NMR chemical shifts of glycine residue carbonyl carbons of peptides in the solid state. *J. Am. Chem. Soc.* 1988, *110*, (11), 3380-3386.

102. Gu, Z.; McDermott, A. Chemical shielding anisotropy of protonated and deprotonated carboxylates in amino acids. *J. Am. Chem. Soc.* 1993, *115*, (10), 4282-4285.

103. Gu, Z.; Zambrano, R.; McDermott, A. Hydrogen bonding of carboxyl groups in solid-state amino acids and peptides: comparison of carbon chemical shielding, infrared frequencies, and structures. *J. Am. Chem. Soc.* 1994, *116*, (14), 6368-6372.

104. Potrzebowski, M. J.; Schneider, C.; Tekely, P. Hydrogen bonding pattern in N-benzoyl(-dl-)-l-phenylalanines as revealed by solid-state NMR spectroscopy. *Chem. Phys. Lett.* 1999, *313*, (3–4), 569-574.

105. Zaugg, N. S.; Paul Steed, S.; Woolley, E. M. Intermolecular hydrogen bonding of acetic acid in carbon tetrachloride and benzene. *Thermochim. Acta* 1972, *3*, (5), 349-354.

106. Borschel, E. M.; Buback, M. Dimerization of carboxylic acids in solution up to high pressures and temperatures. 3. acetic acid. *Zeitschrift für Naturforschung A* 1988, *43*, (3), 207.

107. Semmler, J.; Irish, D. E. Estimation of the enthalpy of dimerization of acetic acid from raman spectral measurements over the temperature range 25 to 275°C. *J. Mol. Liq.* 1990, *46*, (0), 1-6.

108. Maréchal, Y., *The Hydrogen Bond and the Water Molecule : The Physics and Chemistry of Water, Aqueous and Bio Media*. Amsterdam; Boston, 2007.

109. Yoshioka, S.; Aso, Y.; Kojima, S. Dependence of the molecular mobility and protein stability of freeze-dried gamma-globulin formulations on the molecular weight of dextran. *Pharm. Res.* 1997, *14*, (6), 736-741.

110. Aso, Y.; Yoshioka, S.; Kojima, S. Relationship between the crystallization rates of amorphous nifedipine, phenobarbital, and flopropione, and their molecular mobility as measured by their enthalpy relaxation and ^{1}H NMR relaxation times. *J. Pharm. Sci.* 2000, *89*, (3), 408-416.

111. Bhardwaj, S. P.; Suryanarayanan, R. Molecular mobility as an effective predictor of the physical stability of amorphous trehalose. *Mol. Pharmaceutics* 2012.

112. Shamblin, S. L.; Zografi, G. Enthalpy relaxation in binary amorphous mixtures containing sucrose. *Pharm. Res.* 1998, *15*, (12), 1828-1834.

113. Hancock, B. C.; Shamblin, S. L.; Zografi, G. Molecular mobility of amorphous pharmaceutical solids below their glass transition temperatures. *Pharm. Res.* 1995, *12*, (6), 799-806.

114. Shamblin, S. L.; Tang, X.; Chang, L.; Hancock, B. C.; Pikal, M. J. Characterization of the time scales of molecular motion in pharmaceutically important glasses. *J. Phys. Chem. B* 1999, *103*, (20), 4113-4121.

115. Liu, J.; Rigsbee, D. R.; Stotz, C.; Pikal, M. J. Dynamics of pharmaceutical amorphous solids: The study of enthalpy relaxation by isothermal microcalorimetry. *J. Pharm. Sci.* 2002, *91*, (8), 1853-1862.

116. Andronis, V.; Zografi, G. Molecular mobility of supercooled amorphous indomethacin, determined by dynamic mechanical analysis. *Pharm. Res.* 1997, *14*, (4), 410-414.

117. Andronis, V.; Zografi, G. The molecular mobility of supercooled amorphous indomethacin as a function of temperature and relative humidity. *Pharm. Res.* 1998, *15*, (6), 835-842.

118. Bhardwaj, S. P.; Suryanarayanan, R. Use of dielectric spectroscopy to monitor molecular mobility in glassy and supercooled trehalose. *J. Phys. Chem. B* 2012, *116*, (38), 11728-11736.

119. Masuda, K.; Tabata, S.; Sakata, Y.; Hayase, T.; Yonemochi, E.; Terada, K. Comparison of molecular mobility in the glassy state between amorphous indomethacin and salicin based on spin-lattice relaxation times. *Pharm. Res.* 2005, *22*, (5), 797-805.

120. Schaefer, J.; Stejskal, E. O.; Buchdahl, R. Magic-angle ^{13}C NMR analysis of motion in solid glassy polymers. *Macromolecules* 1977, *10*, (2), 384-405.

121. Zemke, K.; Chmelka, B. F.; Schmidt-Rohr, K.; Spiess, H. W. Conformational exchange near the glass transition: two-dimensional carbon-13 NMR study of atactic polypropylene. *Macromolecules* 1991, *24*, (26), 6874-6876.

122. Schmidt-Rohr, K.; Kulik, A. S.; Beckham, H. W.; Ohlemacher, A.; Pawelzik, U.; Boeffel, C.; Spiess, H. W. Molecular nature of the β relaxation in poly(methyl methacrylate) investigated by multidimensional NMR. *Macromolecules* 1994, *27*, (17), 4733-4745.

123. Schmidt-Rohr, K.; Spiess, H. W. Nature of nonexponential loss of correlation above the glass transition investigated by multidimensional NMR. *Phys. Rev. Lett.* 1991, *66*, (23), 3020-3023.

124. Schaefer, D.; Spiess, H. W. Two-dimensional exchange nuclear magnetic resonance of powder samples. IV. Distribution of correlation times and line shapes in the intermediate dynamic range. *J. Chem. Phys.* 1992, *97*, (11), 7944.

125. States, D. J.; Haberkorn, R. A.; Ruben, D. J. A two-dimensional nuclear overhauser experiment with pure absorption phase in four quadrants. *J. Magn. Reson.* 1982, *48*, (2), 286-292.

126. Schantz, S.; Maunu, S. L. Temperature dependence of segmental mobility in poly(ethylene oxide) complexed with Ba(ClO4)2: a Carbon-13 NMR study. *Macromolecules* 1994, *27*, (23), 6915-6921.

127. Schantz, S.; Hoppu, P.; Juppo, A. M. A solid-state NMR study of phase structure, molecular interactions, and mobility in blends of citric acid and paracetamol. *J. Pharm. Sci.* 2009, *98*, (5), 1862-1870.

128. Baird, J. A.; Van Eerdenbrugh, B.; Taylor, L. S. A classification system to assess the crystallization tendency of organic molecules from undercooled melts. *J. Pharm. Sci.* 2010, *99*, (9), 3787-3806.

129. Tang, X. C.; Pikal, M. J.; Taylor, L. S. A spectroscopic investigation of hydrogen bond patterns in crystalline and amorphous phases in dihydropyridine calcium channel blockers. *Pharm. Res.* 2002, *19*, (4), 477-483.

130. Aso, Y.; Yoshioka, S.; Kojima, S. Explanation of the crystallization rate of amorphous nifedipine and phenobarbital from their molecular mobility as measured by

^{13}C nuclear magnetic resonance relaxation time and the relaxation time obtained from the heating rate dependence of the glass transition temperature. *J. Pharm. Sci.* 2001, *90*, (6), 798-806.

131. Aso, Y.; Yoshioka, S.; Kojima, S. Molecular mobility-based estimation of the crystallization rates of amorphous nifedipine and phenobarbital in poly(vinylpyrrolidone) solid dispersions. *J. Pharm. Sci.* 2004, *93*, (2), 384-391.

132. Bhugra, C.; Rambhatla, S.; Bakri, A.; Duddu, S. P.; Miller, D. P.; Pikal, M. J.; Lechuga-Ballesteros, D. Prediction of the onset of crystallization of amorphous sucrose below the calorimetric glass transition temperature from correlations with mobility. *J. Pharm. Sci.* 2007, *96*, (5), 1258-1269.

133. Shamblin, S. L.; Zografi, G. The effects of absorbed water on the properties of amorphous mixtures containing sucrose. *Pharm. Res.* 1999, *16*, (7), 1119-1124.

134. Konno, H.; Taylor, L. S. Ability of different polymers to inhibit the crystallization of amorphous felodipine in the presence of moisture. *Pharm. Res.* 2008, *25*, (4), 969-978.

135. Patel, D. D.; Joguparthi, V.; Wang, Z.; Anderson, B. D. Maintenance of supersaturation I: indomethacin crystal growth kinetic modeling using an online second-derivative ultraviolet spectroscopic method. *J. Pharm. Sci.* 2011, *100*, (7), 2623-41.

136. Alonzo, D. E.; Zhang, G. G.; Zhou, D.; Gao, Y.; Taylor, L. S. Understanding the behavior of amorphous pharmaceutical systems during dissolution. *Pharm Res* 2010, *27*, (4), 608-18.

137. Sharma, V.; Khan, M. S. Prodrugs and mutual prodrugs: synthesis of some new pyrazolone and oxadiazole analogues of a few non-steroidal anti-inflammatory drugs. *Pharmazie* 2003, *58*, (2), 99-103.

138. Trask, A. V.; Shan, N.; Jones, W.; Motherwell, W. D. S. Indomethacin methyl ester. *Acta Crystallogr. Sect. E* 2004, *60*, (4), o508-o509.

139. Crowley, K. J.; Zografi, G. Water vapor absorption into amorphous hydrophobic drug/poly(vinylpyrrolidone) dispersions. *J. Pharm. Sci.* 2002, *91*, (10), 2150-2165.

140. Kothari, K.; Ragoonanan, V.; Suryanarayanan, R. Influence of molecular mobility on the physical stability of amorphous pharmaceuticals in the supercooled and glassy states. *Mol. Pharmaceutics* 2014, *11*, (9), 3048-3055.

141. Trasi, N. S.; Taylor, L. S. Effect of polymers on nucleation and crystal growth of amorphous acetaminophen. *CrystEngComm* 2012, *14*, (16), 5188-5197.

142. Mistry, P.; Mohapatra, S.; Gopinath, T.; Vogt, F. G.; Suryanarayanan, R. Role of the strength of drug–polymer interactions on the molecular mobility and crystallization inhibition in ketoconazole solid dispersions. *Mol. Pharmaceutics* 2015.

Vita

Xiaoda Yuan

EDUCATION

University of Kentucky, Lexington, KY
Ph.D. in Pharmaceutical Sciences, expected Dec 2015
Dissertation title: A molecular-level view of the physical stability of amorphous solid dispersions.

University of Illinois at Urbana-Champaign, Champaign, IL
M.S. in Food Science and Human Nutrition, Oct 2009
Thesis title: Investigation of the relationship between the critical relative humidity and the glassy to rubbery transition in polydextrose.

Purdue University, West Lafayette, IN
B.S. with Distinction in Biological and Food Process Engineering, Aug 2007

PROFESSIONAL EXPERIENCE

Research Assistant - University of Kentucky, College of Pharmacy,	Aug 2010 - Aug 2015
Pharmaceutical Development Intern - Alkermes, Plc. Waltham, MA	Nov 2012 - Feb 2013
Pharmaceutical Development Intern - Pfizer, Inc. Groton, CT	Jun 2010 - Aug 2010
Teaching Assistant - University of Kentucky, College of Pharmacy,	Aug 2009 - Jun 2010

HONORS AND AWARDS

National Institute of Pharmaceutical Technology and Education Travel Award	2015
Peter G. Glavinos Jr. Ph.D. Graduate Student Travel Award	2014
North American Thermal Analysis Society Student Sponsorship	2013
Experimental NMR Conference Student Travel Stipend	2013
Henry J. and Marjorie Atchison Becker Endowed Fellowship	2007 - 2009
John B. Greiner Scholarship	2006
Elsie L. Gruel Scholarship	2006
FutraGene Honor Program Scholarship	2005

LEADERSHIP AND SERVICE

- American Association of Pharmaceutical Scientists (AAPS), UK student chapter officer 2010 - 2012
- Volunteering Activities:
  - Krannert Center for the Performing Arts, Urbana, IL 2007 - 2009
  - Community service, San Juan, TX 2008
  - Hurricane Katrina relief, New Orleans, LA 2007

PUBLICATIONS

1. **Yuan, X.**, Sperger, D. and Munson, E. J. Investigating miscibility and molecular mobility of nifedipine-PVP amorphous solid dispersions using solid-state NMR spectroscopy. *Molecular Pharmaceutics.* 2014, 11(1): 329-337.
2. **Yuan, X.**, Carter, B.P. and Schmidt, S. J. Determining the critical relative humidity at which the glassy to rubbery transition occurs in polydextrose using an automatic water vapor sorption instrument. *Journal of Food Science*, 2011, 76(1): 78-89.
3. Yao, W., Yu, X., Lee,JW., **Yuan, X.** and Schmidt, S. J. Measuring the deliquescence point of crystalline sucrose as a function of temperature using a new automatic isotherm generator. *International Journal of Food Properties*. 2011, 14(4): 882-893.
4. **Yuan, X.** Investigation of the relationship between the critical relative humidity and the glassy to rubbery transition in polydextrose. *(*MS thesis*).* 2009. *Urbana-Champaign , IL .: University of Illinois at Urbana-Champaign.*

PRESENTATIONS

1. **Yuan, X.** and Munson, E. J. Quantitative insights of hydrogen bonding interactions of indomethacin with PVP and PVP/VA using ^{13}C solid-state NMR spectroscopy. *Midwest Organic Solid-State Chemistry Symposium (MOSSCS).* June 2015. West Lafayette, IN. (Talk)
2. **Yuan, X.** and Munson, E. J. Quantitative insights of hydrogen bonding interactions of indomethacin with PVP and PVP/VA using ^{13}C solid-state NMR spectroscopy. *National Institute for Pharmaceutical Technology and Education (NIPTE).* April 2015. Washington, DC. (Poster)
3. **Yuan, X.** and Munson, E. J. Molecular interactions and dynamics of indomethacin-PVP amorphous solid dispersion using SSNMR spectroscopy. *AAPS Annual Meeting and Exposition.* Nov 2014. San Diego, CA. (Poster)
4. **Yuan, X.** and Munson, E. J. Characterizing hydrogen bonding interactions in amorphous solid dispersions using solid-state NMR spectroscopy. *Small Molecule NMR Conference (SMASH).* Sep 2014. Atlanta, GA. (Poster)
5. **Yuan, X.** and Munson, E. J. Investigating molecular interactions of indomethacin and

PVP in amorphous solid dispersions using SSNMR spectroscopy. *AAPS Annual Meeting and Exposition.* Nov 2013. San Antonio, TX. (Poster)

6. **Yuan, X.** and Munson, E. J. Miscibility and molecular mobility of amorphous solid dispersions of nifedipine and polyvinylpyrrolidone. *41st Annual Conference of North American Thermal Analysis Society (NATAS).* Aug 2013. Bowling Green, KY. (Poster)
7. **Yuan, X.** and Munson, E. J. Molecular interactions of amorphous indomethacin and PVP in solid dispersions. *45th Annual Pharmaceutics Graduate Student Research Meeting (PGSRM).* June 2013. Iowa City, IA. (Podium talk)
8. **Yuan, X.** and Munson, E. J. Investigating miscibility and molecular mobility of amorphous solid dispersions using SSNMR spectroscopy. *Experimental NMR Conference (ENC).* April 2013. Pacific Grove, CA. (Poster)
9. **Yuan, X.** and Munson, E. J. Investigating the miscibility and molecular mobility of amorphous solid dispersions of nifedipine and PVP. *AAPS Annual Meeting and Exposition.* Oct 2012. Chicago, IL. (Poster)
10. **Yuan, X.**, Sperger, D. M. and Munson, E. J. Characterizing the miscibility and molecular mobility of amorphous solid dispersions. *AAPS Annual Meeting and Exposition.* Oct 2011. Washington, DC. (Poster)
11. Polizzi, M. **Yuan, X.** and Hancock, B. Direct measurement of the unconfined yield stress of moderately compressed pharmaceutical powders. *AAPS Annual Meeting and Exposition.* Oct 2011. Washington, DC. (Poster)
12. **Yuan, X.**, Sperger, D. M. and Munson, E. J. Characterization of the miscibility of amorphous solid dispersion of nifedipine and PVP. *Midwest Organic Solid-State Chemistry Symposium (MOSSCS).* June 2011. Charleston, IL. (Talk)
13. **Yuan, X.**, Sperger, D. M. and Munson, E. J. Characterization of the miscibility of amorphous solid dispersion of nifedipine and PVP. *43rd Annual Pharmaceutics Graduate Student Research Meeting (PGSRM).* June 2011. Madison, WI. (Podium talk)
14. **Yuan, X.**, Schmidt, A. R. and Schmidt, S. J. Investigating the use of automatic water vapor sorption instruments for the determination of the critical relative humidity at which the glassy to rubbery transition occurs in amorphous food materials. *Institute of Food Technologists Annual Meeting and Food Expo.* June 2009. Anaheim, CA. (Poster)